XERRA

# Manawatū-Whanganui: Lake water quality monitoring by satellite remote sensing

APRIL 2020

# Contents

# Acronyms

| | |
|---|---|
| AOP | Apparent optical properties |
| CIE | International Commission on Illumination |
| CDOM | Coloured dissolved organic matter |
| DOC | Dissolved organic carbon |
| DoD | Department of Defense |
| EnMAP | Environmental Mapping and Analysis Program |
| ESA | European Space Agency |
| ETM+ | Enhanced Thematic Mapper Plus |
| FENZ | Freshwaters of New Zealand |
| FU | Forel-Ule colour system |
| ha | Hectare (10,000 $m^2$) |
| HysIS | Hyperspectral Imaging Satellite |
| ID | Identification |
| IOCG | The International Ocean-Colour Coordinating Group |
| IOP | Inherent optical properties |
| LakeSPI | Lake submerged plant indicators |
| MERIS | Medium Resolution Imaging Spectrometer |
| MfE | Ministry for the Environment |
| MODIS | Moderate Resolution Imaging Spectroradiometer |
| MSI | Multispectral Instrument |
| NASA | National Aeronautics and Space Administration |
| NDVI | Normalised difference vegetation index |
| NIWA | National Institute of Water and Atmospheric Research |
| nm | Nanometers |
| NOAA | National Oceanic and Atmospheric Administration |
| NPS-FM | National Policy Statement for Freshwater Management |
| NTU | Nephelometric turbidity units |
| OAC | Optically active constituents |
| OLCI | Ocean and Land Colour Instrument |
| OLI | Operational Land Imager |
| PACE | Plankton, Aerosol, Cloud, Ocean Ecosystem |
| PC | Phycocyanin |
| PRISMA | Precursore Iperspettrale della Missione Applicativa |
| SD | Secchi depth |
| SeaDAS | SeaWiFS Data Analysis System |
| SOE | State of the Environment |
| SWIR | Short wave infrared |
| TOA | Top of the atmosphere |
| TSS | Total suspended solids |
| USA | United States of America |
| USGS | United States Geological Survey |
| UTC | Coordinated universal time |
| VIIRS | Visible Infrared Imaging Radiometer Suite |

# Executive summary

There are 226 lakes in the Manawatū-Whanganui region. Due to time and cost limitations, Horizons Regional Council currently monitors only 15 of these lakes using discrete water quality sampling by boat or helicopter.

This report was commissioned by Horizons Regional Council to describe the scientific and technical feasibility of using satellite remote sensing to monitor more lakes at improved temporal and spatial scales.

The report concludes that satellites can provide reliable monitoring of over 50 lakes in the region at better-than-monthly frequency.

The primary attributes that can be estimated from satellite data include algal concentration (chlorophyll *a*), suspended particulate matter, water clarity, water colour, floating algae and macrophytes. The detection of cyanobacteria blooms is possible, but will require careful ground validation.

The advantage of satellite remote sensing lies in efficiently obtaining states and trends of important water quality attributes for a regionally representative number of lakes. Combined with established in situ observation programmes, satellites can provide reliable monitoring at more frequent intervals, over more lakes, and for lower cost. Additionally, satellites can map the spatial variation in water quality across a lake, which may reveal important blooms that are missed by point-based sampling.

The fundamental limitations of satellite monitoring of water quality attributes include the requirement for a cloudless view when the picture is taken and that satellites only directly observe the surface layer of the water.

Satellite-derived water quality attributes can match in situ samples with 70-90% accuracy. The uncertainty is due to a combination of factors including measurement error, temporal offset and an effect of different spatial scale of the measurement.

Horizons Regional Council is well-positioned to exploit the benefits of cost-effective satellite observations for lake monitoring due to the Council's ongoing data collection and the availability of historical in situ data, which enables calibration of satellite-based retrieval algorithms. Further accuracy improvements can be achieved with targeted in situ observations and bio-optical characterisation of water bodies.

However, this endeavour will require collaboration with external expertise. The calibration and validation of algorithms for water quality attribute retrieval and the automated processing of satellite data requires specialist knowledge and skills. Our experience is that a partnership such as this could lead to greater confidence around

satellite-based accuracy, opening the door for more streamlined reporting.

Xerra has a track record of being a reliable partner and the mandate, as a regional research institute, to facilitate the use of Earth observation data for the stewardship of New Zealand's natural resources and the prosperity and sustainability of our economy. We have the scientific and software design and development expertise to work with you to develop an easy-to-use, effective satellite remote sensing platform for lake monitoring built on the findings of this report.

# 1. Introduction

The Horizons Regional Council has statutory environmental monitoring requirements, including commitments arising from the National Policy Statement for Freshwater Management (NPS-FM), (Ministry for the Environment (MfE) 2015) and State of the Environment (SOE) reporting.

However, lakes, large rivers and estuaries pose a challenge for monitoring programmes due to their size, number and accessibility. To meet an increasing demand for more comprehensive monitoring (e.g., related to swimmable lakes and rivers (MfE 2017)), cost-effective tools that are capable of capturing various temporal and spatial scales are required.

Remote sensing by satellite-borne sensors can address this challenge by autonomously observing environmental data at synoptic space and time scales (Alikas et al. 2015). These observations can support established programmes (e.g., regional environmental monitoring and swimmability testing) by directing ground-based sampling.

Xerra Earth Observation Institute Limited (Xerra) was commissioned by Horizons Regional Council to evaluate the feasibility of lake water quality monitoring using satellite remote sensing. The scientific and technical feasibility of using remote sensing for the routine monitoring of lake water quality hinges on the responses to two key questions:

1. Which key water quality attributes can be measured by satellites?
2. How many lakes can be observed using satellites, and at what frequency?

This report focuses on the technical issues related to the suitability of satellite remote sensing to deliver data that will enhance the monitoring programmes currently in place.

## 1.1 Structure of this report

This report is organised into five sections, followed by references and appendices. The first section is the introduction.

In Section 2, we identify the key water quality attributes that can be measured by satellites by reviewing literature pertinent to the use of remote sensing for water quality monitoring. We outline the current satellite and sensor technologies, define the water quality parameters which are observable using remote sensing platforms, and review which sensors are most suitable for the retrieval of individual parameters from lakes at a regional scale. We also describe different algorithms used to estimate water quality parameters from satellite imagery in terms of their error and validation statistics.

We illustrate this using case studies, which highlight the accuracy that can be achieved with current remote sensing technologies for estimating water quality parameters.

In Section 3, we quantify the number of lakes that can be observed using satellites and estimate the frequency of observations. To do this, we present the results of a spatial analysis on the size and shape of lakes in the Manawatū-Whanganui region. This section is supported by Appendix A and B, which show the lakes that are visible from space at 30 m pixel resolution in the region. We also provide imagery of these lakes to demonstrate their spatial scales relative to satellite-sensor pixel size, respectively. Finally, we present a reliable estimate of the number of clear satellite images that can be expected every month of the year, for each lake.

Section 4 discusses practical aspects of designing and implementing a framework for satellite monitoring of lake water quality. We determine how much in situ data is available for calibration and validation of satellite estimates and we show preliminary chlorophyll *a* estimates for lakes Wiritoa and Pauri. We then demonstrate how satellite imagery provides the ability to interpret changes in lake water quality in the context of catchment scale processes. Finally, data processing requirements are summarised and an argument is made for automated retrieval, processing and reporting.

The main conclusions of the report are followed by references and appendices. In Appendix A, we list the lakes visible from space at 30 m pixel resolution in the Manawatū-Whanganui region. In Appendix B, we show air photos and satellite images of these lakes to demonstrate their spatial scales relative to satellite-sensor pixel size. Appendix C shows four years of water colour data for the lakes listed in Appendix A.

# 2. Key water quality attributes measurable from space

This section answers the question: What water quality related parameters can be measured with remote sensing? We describe the challenges of monitoring water quality at the regional level and outline how remote sensing may provide opportunities to support existing monitoring programmes.

We also provide a succinct literature review summarising the state-of-the-art of water quality remote sensing applications and provide a number of case studies from our previous work (e.g., Lehmann et al. 2019; Allan et al. 2015; Hicks et al. 2013).

## 2.1 The challenges of conventional water quality monitoring

The Manawatū-Whanganui region contains 226 standing water bodies (lakes[1]) larger than 1 ha in surface area, of which 49 are named (Table 1 (below), Freshwaters of New Zealand (FENZ) geo-database, Leathwick 2010).

Due to time and cost, the Ministry for the Environment State of the Environment (SOE) monitoring provides, usually, every two months, seasonal or annual sampling. This infrequency limits a decision maker's ability to detect trends in water quality and important ecological processes occurring at weekly and monthly time scales.

Furthermore, due to access, time and cost, conventional monitoring can only measure a small fraction of the region's surface water resources. This sparsity limits a decision maker's ability to uncover and address water quality issues across the region.

[1] While these standing water bodies may not be lakes by definition, the term "lake" is used in this report to refer to these water bodies, for convenience.

Table 1: Named lakes in the Manawatū-Whanganui region. Lakes that are part of SOE monitoring or NIWA's macrophyte assessment, Lake Submerged Plant Indicators (LakeSPI), are indicated by a check mark. Lake identity (ID) is taken from the FENZ geo-database, Leathwick 2010.

| Lake name | Lake ID | SOE monitoring | LakeSPI |
|---|---|---|---|
| Lake Moawhango | 18610 | | |
| Lake Horowhenua | 4345 | ✓ | ✓ |
| Lake Otamangakau | 21383 | | ✓ |
| Lake Papaitonga | 1974 | | ✓ |
| Kaitoke Lake | 18936 | | |
| Lake Wiritoa | 18934 | ✓ | ✓ |
| Crater Lake | 20844 | | |
| Mangahao Upper No 1 Reservoir | 4342 | | |
| Lake Pauri | 18933 | ✓ | ✓ |
| Pukepuke Lagoon | 5042 | ✓ | ✓ |
| Lake Kaikokopu | 5014 | | |
| Lake Heaton | 13446 | ✓ | ✓ |
| Lake Namunamu | 19624 | | ✓ |
| Marron Reservoirs a | 18023 | | |
| Lake Alice | 13456 | ✓ | ✓ |
| Turitea Dams b | 4926 | | |
| Mangahao Lower No 2 Reservoir | 4343 | | |
| Omanuka Lagoon | 5306 | ✓ | ✓ |
| Lake Koitata | 16901 | ✓ | ✓ |
| Tokomaru No 3 Reservoir | 476 | | |
| Lake Koputara | 5008 | ✓ | ✓ |
| Lake Westmere | 18951 | ✓ | ✓ |
| Lake Bernard | 13438 | | ✓ |

| | | | |
|---|---|---|---|
| Lake Dudding | 13447 | ✓ | ✓ |
| Lake Ngaruru | 19621 | | ✓ |
| Lake Poroa | 17286 | | ✓ |
| Lake Waipu | 16939 | ✓ | ✓ |
| Lake Virginia | 18957 | | |
| Lake William | 13437 | ✓ | ✓ |
| Lake Vipan | 13443 | | |
| Lake Rotokauwau | 17014 | | |
| Lake Te Whaiau | 21372 | | |
| Lake Maungaratanui | 20096 | | |
| Marron Reservoirs b | 18027 | | |
| Lake Rotokuru | 18609 | | |
| Lake Kohata | 17214 | ✓ | ✓ |
| Lake Herbert | 17363 | ✓ | ✓ |
| Lake Maungarataiti | 20094 | | ✓ |
| Karere Lagoon | 4509 | | |
| Lake Colenso (Kokopunui) | 34051 | | |
| Lake Hawkes | 20741 | | |
| Rotoataha Lake | 5955 | | |
| Turitea Dams a | 4925 | | |
| Lake Oraekomiko | 16932 | | |
| Lake Hickson | 13457 | | |
| Lake Otamataraha | 20673 | | ✓ |
| Lake Pounamu | 20239 | | |
| Ohinetonga Lagoon | 21313 | | |
| Mahangaiti Lake | 31749 | | |

## 2.2 The remote sensing opportunity

In contrast to conventional sampling methods, remote sensing provides an opportunity to 'remotely sample' water bodies at daily to weekly intervals. Furthermore, because of the spatial array of image pixels, remote sensing methods can map the spatial heterogeneity of water quality within a lake better than all but the most intense, boat-based sampling grids, and at comparatively small cost (Allan et al. 2015; Hicks et al. 2013).

As a result, remote sensing technologies have been applied to a number of inland water quality studies worldwide (see Section 2.8 *Case studies*). Continuous developments in satellite and sensor technologies, and research into parameter retrieval algorithms, will only increase the use of remote sensing methods for water quality monitoring in the future (Dekker & Hestir 2012; Matthews 2011; Palmer et al. 2015).

## 2.3 Fundamentals of remote sensing for water quality

Remote sensing provides a clear opportunity to address the challenges of conventional water quality monitoring. In this section we review the fundamental science used for retrieving water quality via remote sensing.

Water quality remote sensing relies on sunlight reflected by water and its constituents, and therefore we begin with a description of how light interacts with matter.

Light travelling through a medium, such as air or water, can be absorbed, reflected and scattered. The remotely sensed signal is the portion of the incoming solar radiation that is scattered back and reflected into a light sensing instrument (Figure 1).

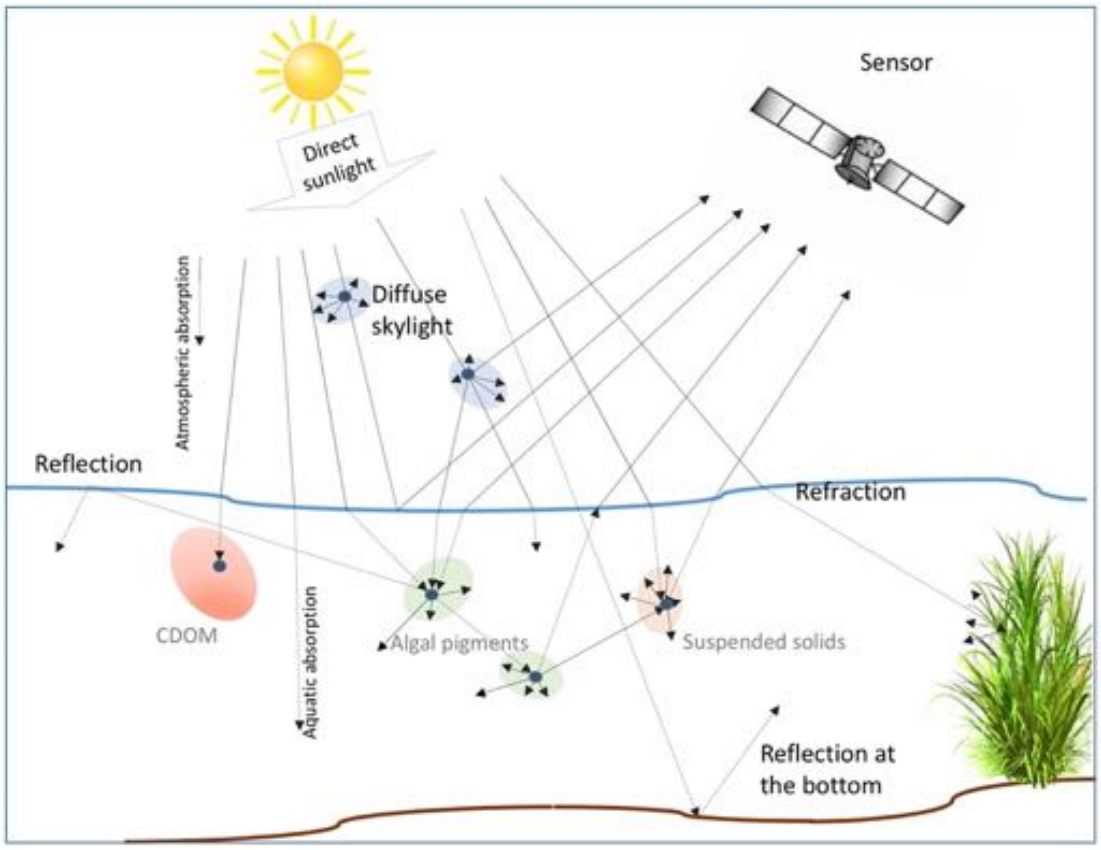


Figure 1: Light interactions through the atmosphere, water and substratum (After Dekker & Hestir, 2012).

There are a multitude of pathways by which light can reach the sensor. First, sunlight is both absorbed and scattered by the atmosphere. Some of this light reaches the line of sight of the sensor and therefore does not interact with the water. The light that reaches the water surface is a mixture of direct sunlight and diffuse light, i.e., light scattered by the atmosphere (Olmanson et al. 2015).

At the water surface, some light reflects back and may reach the sensor as sun glint. The portion of light that finally reaches below the air-water interface is then absorbed and scattered by water molecules and substances within the water (Kirk 1994). Again, only the portion of this light that is scattered back into the line of sight of the sensor and makes it back through the atmosphere can be measured by a satellite sensor.

In order to estimate the water's optical properties, the effect of atmospheric absorption and scattering has to be compensated for. Compensating for the atmosphere and sun glint, a process that is called atmospheric correction, results in an estimate of surface reflectance.

Surface reflectance is the ratio of the light exiting the water surface upwards over the incoming sunlight (Schott, 2007). The normalisation of the light upwelling from the water to downwelling sunlight accounts for variations in the intensity and spectral shape of the incoming solar radiation. It is important to note that all

light-related quantities are calculated across a range of wavelengths within the spectral band, which are specific to the design of the sensor.

Substances that alter the underwater light field are known as optically active constituents (OACs). OACs include the attributes that are related to water quality, such as algal pigments (chlorophyll *a* and phycocyanin), suspended particulate matter (TSS) and coloured dissolved organic matter (CDOM). These OACs have characteristic absorption and scattering properties which change the nature of the underwater light (Dekker & Hestir 2012, Mobley 1994).

Once the spectrum of light reflected and scattered from the water column (i.e., spectral reflectance) is determined by remote sensing, we can apply retrieval algorithms to derive concentrations of constituent matter within the water column, which provides an estimate of water quality (Seyhan & Dekker 1986).

Retrieval algorithms can be developed in a variety of ways, ranging from simple empirical relationships between in situ samples and radiance reflectance at certain wavelengths, through to spectral additive models based on radiative transfer theory.

Many algorithms have been developed and validated for individual sensors, however the majority of these were created specifically for ocean waters (‘Case 1’ waters) where the dominant OAC is chlorophyll *a* (Olmanson et al. 2015). Inland water bodies and estuaries are known as ‘complex’ or ‘Case 2’ waters where three or more constituents are normally present in a mixture (Matthews 2011).

The complexity of Case 2 signatures lies in the fact that different constituents can have reflectance or absorption peaks in the same area of the spectrum. For example, both chlorophyll *a* and TSS have a reflectance peak near 665 nanometers (nm), making it difficult to distinguish one from the other. As a result, Case 1 algorithms do not produce accurate results in Case 2 waters and, moreover, no single Case 2 algorithm exists which works well in all Case 2 waters. A detailed review of algorithms is given in Section 2.7 *Retrieval algorithms*.

Due to light extinction and scattering in the aquatic medium, most of the upwelling light comes from the surface layer of the water. Therefore, the depth to which the remotely-sensed information is attainable depends on water clarity, as it cannot resolve vertical variability in OACs.

## 2.4 Current state of satellite remote sensing of inland water quality parameters

Remote sensing of water quality parameters is carried out using a sensor for electromagnetic radiation in the visible range of the spectrum (approximately 400 to 750 nm) which is mounted on Earth-orbiting satellites.

Four main attributes of the sensor and its satellite platform determine the potential of remote sensing for monitoring water quality parameters: spatial resolution, spectral resolution, temporal resolution and swath size.

**Spatial resolution** refers to the pixel size on the ground of the image that is produced by a sensor. This parameter determines the size of the feature that can be accurately mapped using remote sensing (Dekker & Hestir 2012). A greater number of pixels within a water body means that the spatial variability of water quality can be determined with finer detail and that the water quality maps will have better resolution.

Moreover, the spatial resolution has a direct impact on the size of the water body that can be accurately analysed. In other words, it is important to obtain a water-only pixel in a part of the lake where the bottom can not be seen. Else, the radiometric signal will be mixed with reflectance from land and the lake bottom, which compromises the quality of the retrieved water quality metrics. As the shape of lakes and their bathymetry can be complicated, an area of pure water pixels should be identified for each body of water to be used in the analysis of satellite imagery.

Dekker & Hestir (2012) suggest that water body size should be at least 3 to 4 times the size of the pixel in order to obtain enough pure water pixels without signals from the surrounding banks and vegetation. For example, a sensor with 30 m spatial resolution, such as Landsat 7 and 8, could resolve a body of water of 120 by 120 m. Section 3 further discusses the limitations of sensor footprint for the visibility of water bodies in the Manawatū-Whanganui region.

**Spectral resolution** describes the number and width of spectral bands that can be recorded by a sensor (Olmanson et al. 2015). A spectral band is a range of wavelengths within the full spectrum of light over which the sensor responds with a signal. The width of the spectral band is important because the spectral signature of some water-borne constituents can overlap. Thus, the more numerous and thinner the bands, the better the chances are for separating constituents and obtaining individual water quality parameters.

A third sensor attribute is **temporal resolution**. Temporal resolution describes the time interval between time images of the same location are taken by a sensor (Matthews 2011). The temporal resolution of a particular satellite sensor depends on the return period of the satellite to the orbital path and the overlap of imaging swaths between adjacent paths. Satellites used for Earth observations have return periods ranging from one day to several weeks, with longer return periods meaning fewer images over a given duration of time.

The return period and time of a satellite overpass is crucial when planning field work to collect corresponding in situ samples, as these samples are required as near to the time of a satellite overpass as possible. Whether in situ samples can be usefully related to satellite observations depends on the temporal variability of the water environment (e.g., most studies suggest that an offset be no more than a few days

apart). Odermatt et al. (2010) found that images taken up to 5 days after in situ measurements were adequate for oligotrophic lakes, however estuary sites required sampling to be nearer to the time of the satellite overpass.

The fourth sensor attribute important in determining sensor feasibility is **swath size**, defined as the width of the sensor footprint on the ground. Many sensors sample a continuous track along the axis of satellite movement like a pushbroom. Thus, the swath size is the width of the sensor footprint perpendicular to the axis of movement.

Satellite orbits are typically designed so that adjacent orbital paths produce overlapping swaths to ensure gapless coverage (Figure 3). Swath size and overlap are important to consider in the design of routine monitoring applications for inland water bodies, as they determine how much of a region can be covered in a single overpass. A complete image of a region may have to be composed of several overpasses and often, there are several days between adjacent orbits.

This has implications when the objective is to compare simultaneous states of water bodies in the same region and also increases data processing requirements.

Typically, sensors with larger swath sizes are more suited for monitoring at the regional scale, but have a disadvantage in that greater spatial coverage comes at a cost of lower spatial resolution, i.e., larger pixels.

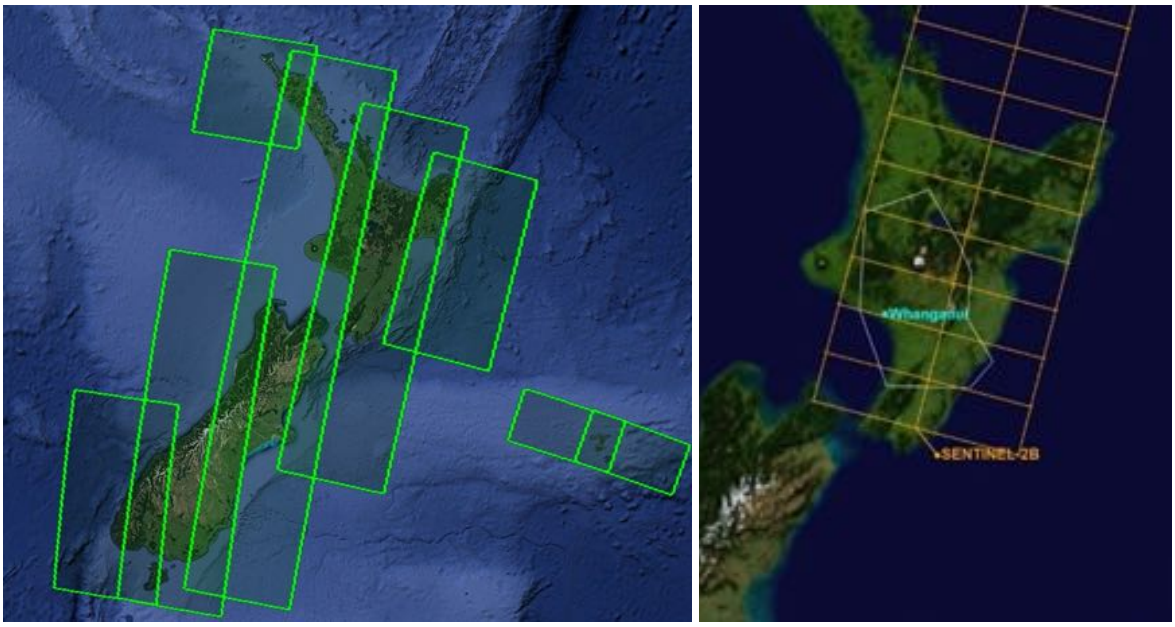


Figure 3: Left: Swaths of Sentinel-2 orbits covering New Zealand. Right: Position of Sentinel-2B on 1 January 2020 22:17:30 Coordinated Universal Time (UTC). The orange line shows the imaging swath covered on this north-south overpass.

Based on these sensor attributes, it is possible to determine which sensors are appropriate for satellite-based water quality monitoring.

Olmanson et al. (2015) suggest that regional scale inland water quality monitoring requires freely available imagery with a spatial resolution of 5 to 50 $m^2$ at no less than weekly intervals and suitable spectral bands.

### 2.4.1 Characteristics of current satellite sensors

The satellite sensors in orbit today cover a range of resolutions, return periods and spectral bands (Table 2, below). It is noted that this list includes the information to date, but may be incomplete or contain obsolete sensors at the time of reading. For example, the Medium Resolution Imaging Spectrometer (MERIS) sensor which has provided data for numerous inland water studies is not included in this list due to its decommissioning in May 2012.

Table 2: Current satellite/sensor pairs available for inland water quality retrieval with spatial, temporal and spectral characteristics. The number of spectral bands of each sensor within the range commonly used for water quality sensing is provided (additional spectral bands outside this range are not listed). Lifespan is the planned operational life of the satellite. A plus (+) indicates that satellites are still operational beyond their original operational expectancy. Minimum detectable water body size was calculated as four times the pixel footprint (Dekker & Hestir 2012).

| Satellite (Operator) | Sensor | Revisit (days) | Spatial resolution (m)** | Number of spectral bands* | Lifespan (years) | Minimum water body area (ha) |
|---|---|---|---|---|---|---|
| Landsat 7 (NASA/USGS) | ETM+ | 16 | 30 | 4 | 1999-2004+ | 1.4 |
| Landsat 8 (NASA/USGS) | OLI | 16 | 15 | Pan*** | 2013-2023 | 1.4 |
| | | | 30 | 5 | | |
| Terra and Aqua (NASA) | MODIS | 1 | 250 | 2 | 1999-2008+ | 1600 |
| | | | 500 | 2 | | |
| | | | 1000 | 9 | | |
| Suomi NPP (NASA/NOAA /DoD) | VIIRS | 0.5 | 750 | 7 | 2011-2016 | |
| Sentinel-2a and 2b (ESA) | MSI | 5 | 10 | 4 | a: 2015-2023 b: 2017-2024 | 0.64 |
| | | | 20 | 4 | | |
| Sentinel-3a and 3b (ESA) | OLCI | 1-2 | 300 | 21 | a: 2016-2025 b: 2017 - 2025 | 144 |

*In the spectral range 400-1000 nm
**Spatial resolution may vary between spectral bands
***Pan: one single band (panchromatic band 8, 500-680 nm)
See *Acronyms* for further details of satellite and operator names.

Table 2 summarises the currently available satellite-sensor pairs. Landsat Operational Land Imager (OLI) and Sentinel-2 Multispectral Instrument (MSI) provide high spatial resolution, but at the expense of lower spectral resolution and broad spectral bands. Broad spectral bands mean that individual OACs cannot be easily retrieved (see discussion in Allan et al. 2015).

The narrow spectral bands of Moderate Resolution Imaging Spectroradiometer (MODIS), Ocean and Land Colour Instrument (OLCI) and MERIS provide sufficient spectral resolution to enable the application of semi-analytical algorithms which simultaneously estimate chlorophyll *a*, TSS and CDOM (Olmanson et al. 2011). However, the spatial resolution of these sensors precludes many smaller lakes from observation.

Some investigators have attempted to circumvent the resolution trade-off by pansharpening, a data-fusion technique to merge images of high spectral resolution with images of high spatial resolution (Ashraf et al. 2008; Chang et al. 2015). This technique could be considered for small, high-priority water bodies.

Sensor technology is continually under development and significant advances are expected from hyperspectral satellite missions. Successful hyperspectral satellites have already been launched by India (Hyperspectral Imaging Satellite (HysIS), launched November 2018), Italy (PRecursore IperSpettrale della Missione Applicativa (PRISMA), launched March 2019) and China (four Zhuhai-1 satellites, launched September 2019), although their data has not yet been made available for outside users. Germany's Environmental Mapping and Analysis Program (EnMAP) is set to launch in 2020 and the Plankton, Aerosol, Cloud, ocean Ecosystem (PACE) mission (USA) has entered the critical design phase. Whether early hyperspectral satellite data is suitable for lake monitoring remains to be seen, as spatial resolution and light sensitivity may not be sufficient to resolve small and dark targets.

In summary, inland waters are a difficult target for satellite remote sensing applications. Sensors that are designed for water (e.g., OLCI and MODIS) by virtue of their spectral resolution and light sensitivity have coarse spatial resolution while sensors for land (MSI and OLI) lack important spectral bands. Arguably, Landsat 8 OLI, Sentinel-2 MSI and some sensors on privately operated satellites are the only choice for small lakes.

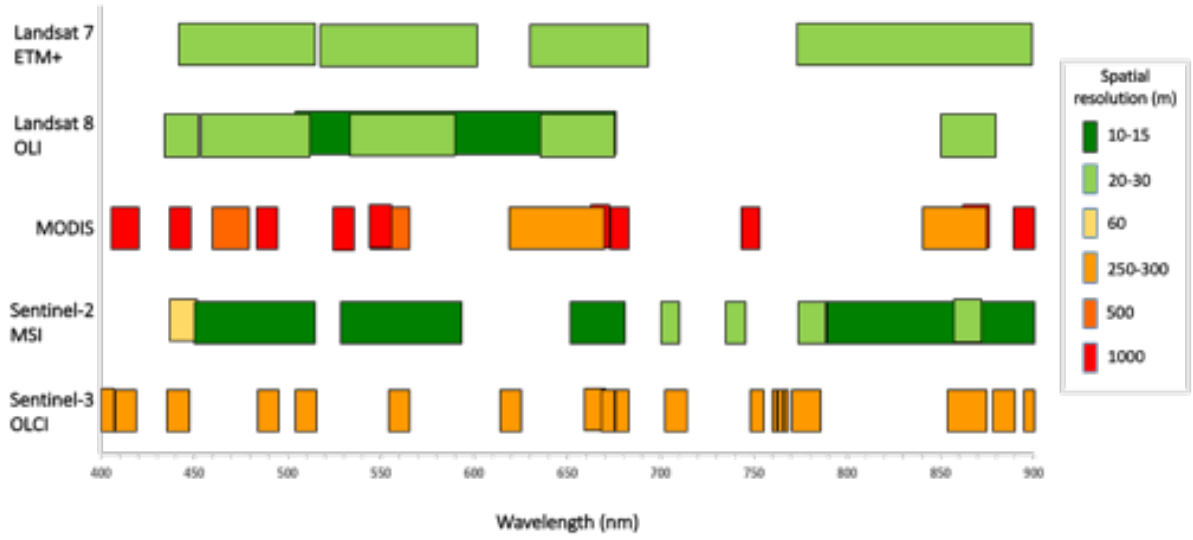


Figure 4: Comparison of the spatial and spectral resolution of existing satellite sensors.

### 2.4.2 Other sensor platforms

Sensors akin to those mounted on satellites can also be used in situ, from the ground or on airborne platforms.

Handheld and stationary sensors retrieve optical measurements from a water body at a small spatial scale, (millimetres to metres) which can provide very detailed optical information for a particular site, but are inefficient at providing data across wider scales. Tan et al. (2015) recommend using handheld spectrometers in conjunction with in situ sampling to accurately and conveniently measure the spectral signature of smaller rivers and streams. This would require field visits much like current monitoring regimes, though the empirical relationship found between these could be used to enhance algorithms developed for multispectral satellite or airborne sensors that are limited by spectral resolution (Tan et al. 2015).

Airborne platforms are often optimal for monitoring small water bodies as they have high spatial resolution and can employ newer or larger hyperspectral sensors (Julian et al. 2013; Matthews 2011; Tan et al. 2015; Torgersen et al. 2001). In addition, the sensors are flown at low altitudes reducing the need for atmospheric correction when applying water quality retrieval algorithms (Matthews 2011).

Olmanson et al. (2013) found that airborne hyperspectral sensors could adequately predict water quality in large rivers, however the low-altitude flight paths again result in swath sizes too small for the complete capture of larger water bodies. Moreover, recurring flights are difficult to schedule for regular monitoring intervals, making it difficult to assess temporal trends.

Finally, the large cost of both the sensors and air time may exceed operational budgets for regional-scale routine monitoring purposes (Julian et al. 2013; Matthews 2011; Tan et al. 2015).

## 2.5 Observable water quality constituents

In Section 2.4, we evaluated which sensors are best-suited for operational water quality monitoring. In this section, we summarise the extent to which various water quality attributes can be measured by remote sensing. We specifically focus on three OACs: chlorophyll *a* and phycocyanin, coloured dissolved organic matter (CDOM), and total suspended solids (TSS). Several additional water quality attributes are discussed, including: turbidity, water clarity (Secchi depth), water colour, and surface scums/macrophytes.

Inland waters contain mixtures of OACs whose combined spectral absorption and scattering characteristics result in the observed spectral reflectance spectra.

Figure 5 shows reflectance spectra from three lakes, each determined by a distinct complement of OACs.

The reflectance spectrum of the oligotrophic Lake Taupō is dominated by absorption characteristics of water which produces highest reflection in the blue range of the spectrum (400-500 nm).

Lake Rotoehu has a strong reflectance peak in the green range of the spectrum (around 550 nm) indicating that phytoplankton pigments are dominating the optical characteristics in this eutrophic lake.

The reflectance spectrum of Lake Rotomanuka is lower than that of the other lakes with a maximum in the red end of the spectrum (700 nm). In this peat lake, CDOM absorbs much of the light, especially in the blue and green regions of the spectrum, making the water appear dark and brown.

Finally, the increase of reflection in Lake Rotomanuka in the range 750 to 800 nm is likely caused by light scattered by suspended particulate matter.

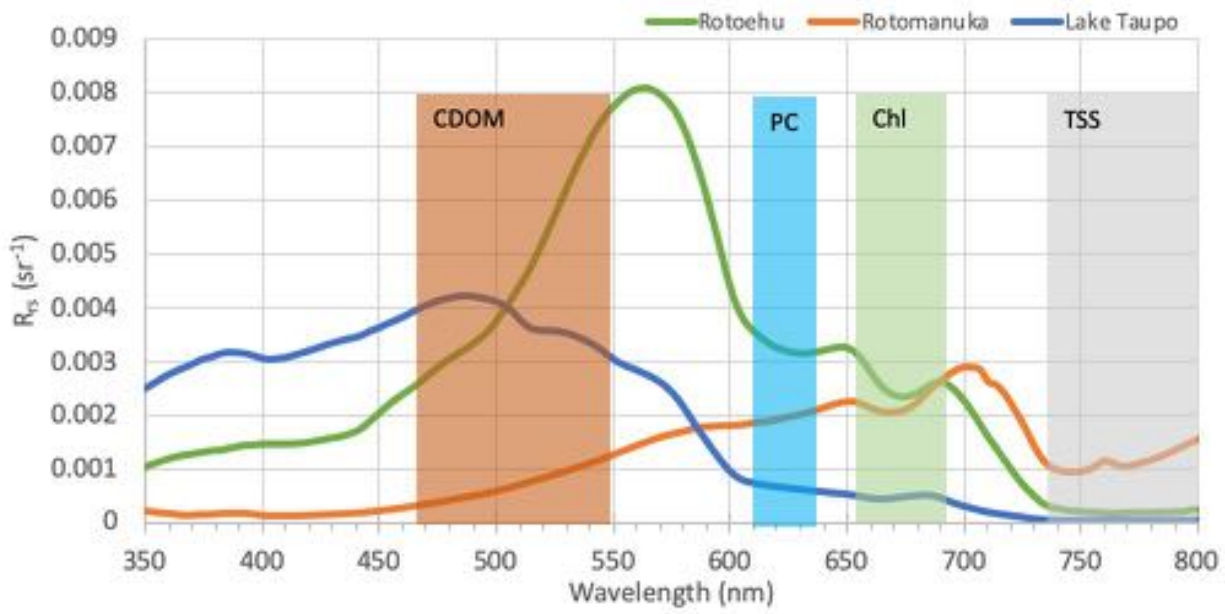


Figure 5: Reflectance spectra ($R_{rs}$) for a eutrophic lake (Lake Rotoehu), a peat lake (Lake Rotomanuka) and a clear oligotrophic lake (Lake Taupo) with coloured bars indicating regions of the spectrum often used to detect water quality constituents such as chlorophyll *a* (Chl), coloured dissolved organic matter (CDOM), phycocyanin (PC) and total suspended solids (TSS) (Reflectance spectra courtesy of the University of Waikato).

To measure these reflectance spectra, multispectral remote sensing radiometers are designed to estimate the reflectance in strategic spectral regions, thus enabling the characterisation of the relative height of the peaks and troughs in the spectrum.

The spectral responses of two satellite sensors (MSI on Sentinel-2 and OLCI on Sentinel-3) are superimposed on lake reflectance spectra in Figure 6. This illustrates that the narrower bands of OLCI are better suited to characterise the nuances of aquatic reflectance spectra than the broad bands of MSI (Gitelson et al. 2008; Olmanson et al. 2015).

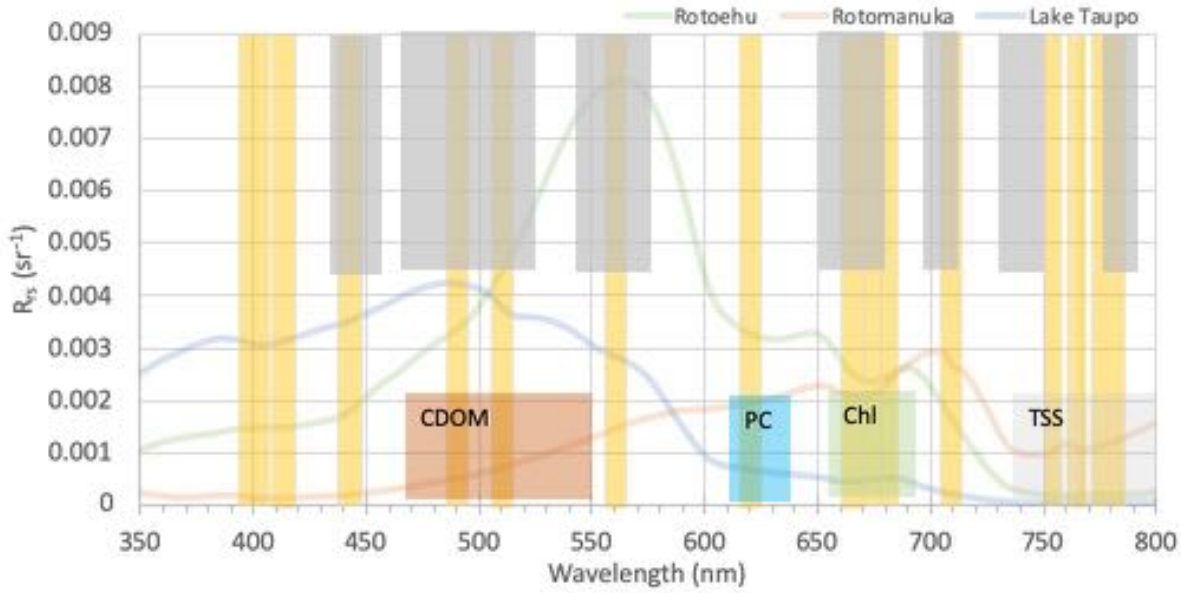


Figure 6: Wave bands of Sentinel-2 MSI (grey boxes) and Sentinel-3 OLCI (yellow boxes) superimposed on reflectance spectra from three lakes and the spectral regions affected by OACs as in Figure 5.

Indeed, the spectral and spatial characteristics of these sensors (Table 2) means that lake water quality remote sensing is challenging, because sensors whose spectral response is optimised for water (MODIS and OLCI) have lower spatial resolution, thus restricting the size of lakes that can be resolved. Therefore, many inland water studies have used data from sensors optimised for terrestrial applications (Landsat Enhanced Thematic Mapper Plus (ETM+) and OLI as well as Sentinel-2 MSI). Limitations of using the terrestrial sensors include a reduced ability to distinguish chlorophyll *a* from TSS and a reduced ability to detect cyanobacteria using the phycocyanin signal.

In Sections 2.5.1–2.5.6, we describe the specific challenges related to the retrieval of individual water quality components (i.e. chlorophyll *a* and phycocyanin, CDOM, TSS, turbidity, Secchi depth, water colour, and surface scums/macrophytes).

### 2.5.1 Chlorophyll *a* and phycocyanin

The photosynthetic pigment chlorophyll *a* (found in algae) and the accessory pigment, phycocyanin (found in cyanobacteria), are indicative of phytoplankton and cyanobacterial biomass, respectively (Dekker & Hestir 2012). High concentrations of chlorophyll *a* can signify nuisance algal blooms, high nutrient levels, and increased

trophic status, while high phycocyanin concentrations can indicate the presence of often harmful or toxic cyanobacterial blooms (Dekker & Hestir 2012).

Chlorophyll *a* concentrations <30 microgram per litre (mg $m^{-3}$) have been successfully retrieved using a strong absorbance trough at 440 nm, while chlorophyll *a* concentrations >30 mg $m^{-3}$ have been retrieved using both a peak at 560 nm and the ratio of the absorbance trough near 660 nm with the reflectance peak at 700 nm (refer to Figure 6 for reflectance spectra) (Allan, 2008; Matthews, 2011; Odermatt et al. 2012; Olmanson et al. 2013).

Inclusion of the peak at 700 nm has proven highly successful in a number of studies on lakes, rivers and estuaries ($r^2$ > 0.8) as CDOM absorption in this region is minimal, aiding in the distinction between these two co-occurring constituents (Matthews 2011; Olmanson et al. 2013).

It should be noted that the exact location and width of these spectral peaks and troughs differ depending on the species of phytoplankton present as well as their physiological state (Allan 2014), which may add an error to the retrieval of chlorophyll concentration from reflectance.

Phycocyanin has a strong absorption peak at 620 nm, often detectable by sensors with narrow bands. This spectral region falls within a gap in Landsat sensor wavebands (Matthews 2011; Olmanson et al. 2015), however, successful retrieval estimates have been obtained using MERIS imagery. Simis et al. (2005) and Gomez et al. (2011) both found close relationships of phycocyanin ($r^2$ = 0.94 – 0.97) using MERIS imagery to both in situ samples and fluorometry measurements, respectively.

### 2.5.2 Coloured dissolved organic matter (CDOM)

CDOM is comprised of coloured humic and fulvic acids which originate from the breakdown of both allochthonous and autochthonous organic matter, also known as yellow-substance, gelbstoff or gilvin, and is often visible in water as brownish or tea-like colouration (Matthews 2011; Vant 2015). As such, CDOM concentrations can be indicative of the organic matter and aquatic carbon content of water (Dekker & Hestir, 2012) as well as potentially providing an indication of dissolved organic carbon (DOC) concentration, although these correlations require further development (Brezonik et al. 2015).

CDOM is often a major constituent in peat lakes (Allan 2008; Davies-Colley & Vant 1987) and it is the main light absorbing constituent in many rivers under normal flow conditions, with concentrations increasing after storm events, which flush humics from the catchment (Julian et al. 2013). Due to the strong absorbance characteristics of CDOM, it is often difficult to derive from reflectance signatures because it appears similar to clear, deep water (Dornhofer & Oppelt 2016). However, many studies have used the strong absorption peak at 440 nm or the ratio of both

sensitive bands below 600 nm and normalisation bands above 600 nm to retrieve CDOM estimates (Matthews 2011; Odermatt et al. 2012) (Figure 5).

### 2.5.3 Total suspended solids (TSS)

Total suspended solids (TSS) include all particles suspended in water which do not pass through a 0.2 µm filter. According to this definition TSS is comprised of a wide variety of material, such as mineral or inorganic particles, detritus, phytoplankton cells and animal matter. Especially in shallow lakes, TSS can include considerable amounts of detritus and inorganic mineral particles resuspended from the bottom.

While its detailed optical characteristics depend on the absorption and scattering properties of the various constituents (Vant 2015), scattering by the suspended mineral fraction causes a reflection peak between 510 – 550 nm and in the infrared range of the spectrum, i.e. above 700 nm (Allan 2008). The reflectance peak between 510 and 550 nm is successfully used to derive TSS when these are below 30 mg $L^{-1}$, but at higher TSS concentrations, reflectance above 800 nm is used due to superimposition by the optical properties of chlorophyll *a* at 550 nm (Olmanson et al. 2013).

Often in the technical literature, variables related to TSS are defined and used in remote sensing applications, e.g., suspended sediment, suspended particles, suspended matter or non-volatile suspended solids. This makes it difficult to compare and contrast TSS-related results in detail. In this review, several operational definitions for TSS-related variables may be reported.

### 2.5.4 Turbidity

Turbidity is a measure of water clarity related to light absorbed and scattered by all OACs. Turbidity is a useful measure of light availability under water and is therefore related to many ecosystem processes (Dekker & Hestir 2012). Due to the strong influence of suspended solids on water clarity, reflectance at 700 nm is most often used to derive turbidity from remotely sensed signals (Figure 6) (Hicks et al. 2013).

### 2.5.5 Secchi depth

Secchi depth (SD) is a measure of water clarity in the vertical direction. Like turbidity, it is a function of scattering and absorption caused by all OACs. It has been successfully correlated to OACs, especially to chlorophyll *a* concentrations in the open ocean. Due to its relationship with water clarity it can be related to the depth of the euphotic zone, i.e. the depth to which net positive rates of photosynthesis occur. Remote sensing has been shown to produce very good estimates of Secchi depth in

several studies, most often using the ratio of peaks at 500 nm and 610 nm (Figure 7) (Allan 2008; Hicks et al. 2013; Olmanson et al. 2015; Zhao et al. 2011; Zhao et al. 2014).

### 2.5.6 Water colour

The colour of water as perceived by a human observer is intuitively associated with its suitability for consumption, quality for food collection, fitness for recreation, and aesthetic value, making it arguably one of the oldest water quality attributes. Colour is similar to water clarity (e.g., Secchi depth) in that it integrates across several routinely measured attributes as well as being a useful attribute in itself.

The main constituents that give water a colour other than blue are phytoplankton pigments, suspended particulate matter and coloured dissolved organic matter (IOCCG 2006). Thus, water perceived in hues of green, yellow, and brown are fundamentally linked to concentrations of chlorophyll *a*, TSS and other optically active constituents.

Determination of water colour does not require knowledge of inherent optical properties and can therefore be unequivocally determined from spectral observations such as those made by optical satellite sensors. It is therefore a good choice for first implementations of satellite monitoring applications.

### 2.5.7 Surface scums and macrophytes

A final water quality attribute relates to surface scums. Surface scums, such as those produced by buoyant algal blooms and macrophytes floating at the surface or suspended just below the surface, can effectively shield the water column from observation by satellite sensors. On the other hand, the detection of surface scums and macrophytes by satellite sensors may be useful in its own right.

Surface vegetation can be qualitatively distinguished from open water using the reflectance signal at red or near infrared wavelengths. This is known as the ‘red-edge method’. Water efficiently absorbs light at these wavelengths and therefore appears nearly black in, for example, band 5 of MSI (centered at 704 nm), while vegetation at the surface reflects some light at this wavelength. Several methods have been developed involving single-band reflectances or simple functions of multiple bands (see summary in Liang et al. 2017).

Complications of the red-edge method arise in highly turbid waters where the water-leaving signal in the red may not be zero. Dogliotti et al. (2018) used the floating algal index, which makes use of the strong signal in the infrared part of the spectrum. They combined this with conditions set on the red band in order to avoid misclassifying highly turbid waters. Conditions were also added on the CIE L*a*b*

colour space[2] coordinates to confirm the visually 'green' pixels as floating vegetation. Using this method, they were able to map floating mats of water hyacinth in turbid waters in a river in Lower Amazonia, Brazil, using MSI, OLI and Aqua/MODIS data.

Simple red-band reflectance methods can not discriminate between floating algae such as cyanobacteria scum and macrophytes. To study the differential distribution of these two indicators of eutrophication in Lake Taihu, China, Lian et al. (2017) developed an index using MODIS data at 250 m spatial resolution. Their index was based on a blue, a green, and a shortwave infrared band to separate waters with cyanobacterial scums from those dominated by aquatic macrophytes, as well as a turbid water index to avoid interference from high turbid waters typical of shallow lakes.

## 2.6 Retrieval of water quality constituents

The main steps required in obtaining estimates of water body constituents from remote sensing imagery are (summarised from Dekker & Hestir 2012):

1. Access the raw satellite data;
2. Process the data to correct for atmospheric effects;
3. Identify water body and isolate water-only pixels; and
4. Apply algorithms for the retrieval of water quality information.

### 2.6.1 Access the raw satellite data

The first step involves the acquisition of this satellite imagery, which can usually be downloaded from the operators' website or file service. The pre-processing steps can range from simple to complex depending on the corrections applied to the image.

The spectral shape of light at the top of the atmosphere (TOA), i.e., at the sensor, is a function of the optical properties of aerosols and clouds. Up to 90% of sensor-reaching light can be a result of atmospheric scattering and absorption (e.g., Allan et al. 2015). Therefore, the majority of studies employ atmospheric correction methods and cloud cover assessments that aim to remove atmospheric effects, resulting in water-leaving radiance or water-leaving reflectance.

Additionally, satellite data are provided by vendors at varying processing levels. At the processing level used for water quality assessment, the data are already

[2] A perceptually uniform color space which expresses color as three values: *L** (lightness) *a** (green to red) and *b** (blue to yellow).

georectified with information on the quality of the georectification relative to control points provided in the metadata.

### 2.6.2 Atmospheric correction

The second step is atmospheric correction. The most common atmospheric correction methods are either image-based or based on radiative transfer theory.

Image-based correction methods rely solely on the information provided in the satellite image and involve the use of either dark or light pixels as an estimate of the atmospheric signal to be subtracted from the TOA measurement (Allan et al. 2011).

Alternatively, methods based on radiative transfer theory attempt to model the atmosphere's optical properties based on current conditions. These methods are often preferred due to their flexibility in being able to model atmospheric complexities over inland waters such as changes in elevation and adjacency effects (Allan et al. 2015; Campbell et al. 2011). One popular approach is the "Second simulation of a satellite signal in the solar spectrum" (the 6sv model of Vermote et al. 1997)

These methods require an accurate record of the atmospheric conditions present during satellite image capture. Such information can be difficult to obtain and may have to be estimated, although more recent satellite sensors such as MODIS now collect concurrent atmospheric data that can be used for correction (Allan 2014).

While radiative transfer modelling aims for a more accurate correction, numerous atmospheric parameters are often estimated, which can create considerable uncertainty in the result (Allan et al. 2011). Some studies found that non-atmospherically corrected empirical methods produced similar if not more accurate results than atmospherically corrected semi-analytical algorithms in Minnesota lakes (e.g., Olmanson et al. 2011). This suggests that it is possible to get atmospheric correction wrong with detrimental effects for the parameter retrieval.

Related to atmospheric correction is the detection and mapping of clouds within the image, which occlude water targets and can introduce error in the results. Thus, cloud masks are often applied to remove pixels disguised or contaminated by clouds (Olmanson et al. 2008; Allan 2014).

Cloud detection methods can be automated, as successfully demonstrated by Hicks et al. (2013) and Allan (2014). To improve these assessments, newer sensors include bands specifically positioned for cloud detection such as the new short wave infrared (SNIR) band on Landsat 8 (Roy et al. 2014) and two SWIR bands on Sentinel-2 (Olmanson et al. 2015).

In addition to meteorological clouds, wildfires and storms over desert areas pose challenges to the retrieval of surface reflectance, as these produce highly absorbing

aerosols which atmospheric correction algorithms relying on the dark pixel method cannot identify and account for (Frouin et al. 2019).

As a result, the water reflectance in such cases will typically be underestimated, leading to an overestimation of water quality constituents such as chlorophyll concentration. The Australian bushfires burning between December 2019 and February 2020 produced atmospheric aerosols visible by the naked eye and detectable in satellite imagery (Figure 7).

A search for images in which the Manawatū-Whanganui region was affected by aerosols from the Australian bushfires yielded few results. In other words, the distance to the fire, variability of atmospheric transport and coincident cloud-free coverage of the region appear to have minimised the probability of impacting satellite images in this region. However, this case illustrates the sensitivity of water quality retrievals to atmospheric conditions and stresses the need to assess the results critically.

Figure 7: Sentinel-3 OLCI image from 2 February 2020 (New Zealand date) showing diffuse aerosols from the Australian bushfires over the lower North Island and over the Tasman Sea.

Lehmann et al. (2018) found that the atmospherically corrected Landsat OLI data available from USGS was suitable for first applications of retrieval algorithms and similar conclusions were made with MSI data provided by ESA (unpublished). It is therefore recommended that the design of water quality monitoring applications starts with established atmospheric corrections and their suitability is evaluated at the validation stage.

### 2.6.3 Isolate water pixels

After atmospheric compensation and cloud removal, step three involves the removal of all non-water pixels, in addition to those contaminated by light reflected from the bottom of the lake or stray light from the surrounding land. This is usually done by first masking terrestrial pixels from the image and, second, analysing the data to detect spectral signatures typical for scattering from the bottom or edges of the lake.

### 2.6.4 Apply water quality retrieval algorithms

Finally, the fourth, and arguably the most important step, is to apply algorithms for the retrieval of water quality parameters. Given the optical complexity and heterogeneity of inland waters, rigorous algorithm development and testing is required to find suitable approaches for a range of sites, conditions and constituent concentrations.

To date, no operational algorithm exists that is generally applicable to complex inland waters (Palmer et al. 2015; Politi et al. 2015), unlike open ocean algorithms, which are operational and widely applicable. In Section 2.7, we review the most common retrieval algorithms for inland water quality.

The uncertainty in satellite-derived estimates is partly due to uncertainty in atmospheric and aquatic optical characteristics which are a component of the measurement error inherent in any analytical method. Also contributing to this variability is the discrepancy between the spatial scale of the measurements: The satellite signal is a spatially integrated measurement, both across a depth horizon (tens of centimeters to meters) and the pixel size (tens to hundreds of meters). The satellite measurement is therefore representative of a larger area of the lake while the in situ sample is really only valid for the singular sampling location. Finally, there is usually a time difference between samples used for validation of satellite retrieval accuracy and and changes in attributes over this time period will increase the error.

## 2.7 Retrieval algorithms

Retrieval algorithms are used to estimate the concentration of a water quality parameter from the spectral water-leaving radiance measured by a sensor. Commonly-used algorithms generally fit into two categories, empirical or semi-analytical (The International Ocean-Colour Coordinating Group (IOCCG) 2006; Olmanson et al. 2015).

Empirical algorithms describe the statistical relationships between spectral band reflectance and in situ water quality samples. They can be viewed as a black box approach, which requires little understanding of radiative transfer.

The semi-analytical approach, on the other hand, aims to use radiative transfer theory to estimate parameter concentrations based on spectral absorption and scattering by OACs. Figure 8 illustrates the fundamental difference between empirical and semi-analytical algorithms, where IOP refers to inherent optical properties and TOA refers to top-of-atmosphere.

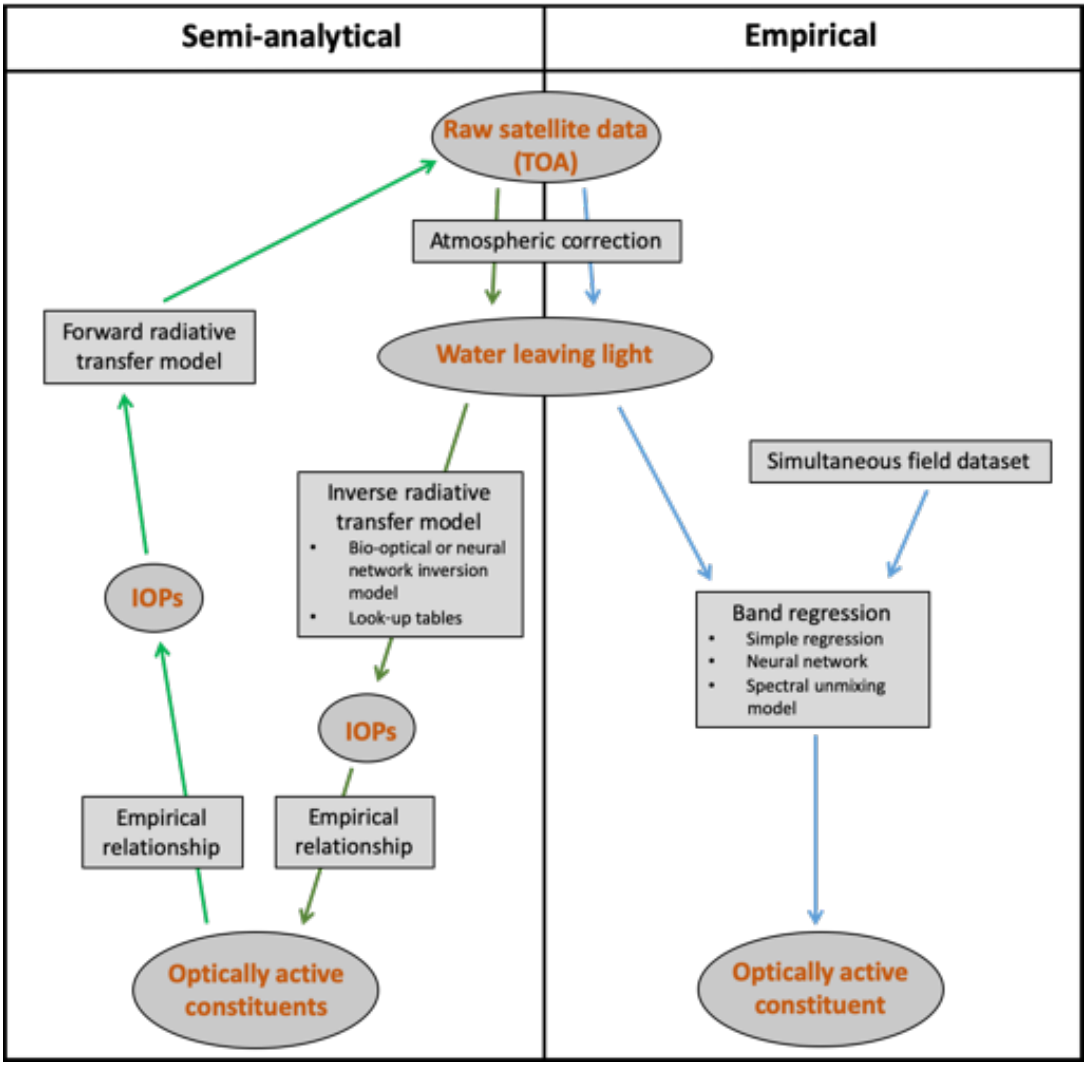


Figure 8: Generalised flow chart of common constituent retrieval methods, from satellite data at the top of the atmosphere (TOA) to OAC concentration (bottom of the chart). IOP (inherent optical properties) are the spectral absorption and scattering characteristics of OACs

The major difference between the types of algorithms for end-users is the scale of possible application. Empirical algorithms are generally applicable only to the water body and the specific sensor for which they were created, while semi-analytical algorithms should be more generally applicable to a range of water bodies and concentrations (Allan et al. 2015). Sections 2.71 and 2.7.2 provide a review of recent advances in the application of both types of algorithms.

### 2.7.1 Empirical algorithms

Empirical algorithms require in situ data on each water quality variable in order to determine a statistical relationship between the reflectance of spectral bands and the concentration of constituents at the time of image capture (Dornhofer & Oppelt 2016; Olmanson et al. 2015). The resulting algorithm returns a site and time-specific estimate of a single constituent, calibrated with in situ data points that can then be applied to each pixel in the image (Matthews 2011). These methods most commonly utilise one of three different approaches: empirical band regressions, spectral unmixing models and semi-empirical neural network models (Dornhofer & Oppelt 2016).

Empirical band regression uses either atmospherically corrected, i.e., water-leaving signal, or the raw satellite TOA signal regressed with in situ data. A successful example for this kind of algorithm is the estimation of Secchi depth (SD, units of metre) from Landsat imagery (Kloiber et al. 2002). SD is calculated using the ratio of Landsat bands 1 and 3 in the linear equation:

$$Ln(SD) = a(TM1/TM3) + b(TM1) + c$$

where TM1 and TM3 are the mean band reflectance values of pixels within a given distance of measured in situ locations (Zhao et al. 2011) and a, b, and c are constants estimated by regression. This algorithm has been successful in many complex water bodies, particularly the '10,000 Lakes' region of Minnesota ($r^2$ = 0.71 – 0.96 for 280 samples ranging from 0.1 to 9.8 m) as reported by Olmanson et al. (2011). Generally, algorithms incorporating three bands have better accuracy in more complex waters than two-band algorithms (Lyu et al. 2015).

Spectral unmixing models are particularly useful in optically complex waters where OACs co-occur and their constituent signatures overlap. For example, the spectral signatures of CDOM, TSS and chlorophyll *a* share peaks near 440 nm, 560 nm, 660 nm and 700 nm, respectively, rendering the simple band regression problematic. The method is a multivariate regression technique in which the known spectra of pure chlorophyll *a*, CDOM and TSS are combined such that their sum reproduces the observed spectrum (Allan 2008; Tyler et al. 2006; Zhang et al. 2014). Zhang et al. (2014) used a four-endmember spectral decomposition model to retrieve chlorophyll *a* concentrations in Lake Taihu—a shallow, eutrophic lake in China. Tyler et al. (2006) carried out a retrospective analysis of chlorophyll *a* concentrations in Lake Balaton, a large shallow lake in Europe, using a spectral mixing model which was significantly correlated with in situ chlorophyll *a* samples above 10 mg $m^{-3}$ ($r^2$ = 0.95, 12 samples). Allan (2008) applied a linear spectral unmixing model to Landsat images of the Waikato region in order to obtain chlorophyll *a* estimates. Given the optical complexity of many Waikato lakes, a spectral unmixing approach was chosen and applied to Landsat 7 Enhanced Thematic Mapper Plus (ETM+) images.

Another approach uses a neural network model to determine which satellite bands are most strongly correlated with the retrieved water-leaving radiance before applying a band regression (Dornhofer & Oppelt 2016). Matthews (2011) found that this approach improves the strength of the correlation, and if applied to atmospherically corrected data, can reduce errors associated with atmospheric scattering. Due to the additional neural network step, Matthews (2011) termed this approach semi-empirical.

While often correlating well with in situ data, the major disadvantage of using empirical methods is that the resultant equations are strictly only valid within the temporal and spatial ranges of data used to build the models. The further the algorithm is applied across time or space, the greater the chance to encounter atmospheric and water-related conditions outside the initial range, leading to errors associated with the predictions (Allan 2008; Matthews 2011).

Specifically, these models have been found to be unreliable in water bodies with particularly high or low concentrations of constituents, suggesting that non-linear relationships exist at the extremes (Chang et al. 2015). Further, empirical algorithms lack the ability to retrieve more than one parameter and are often unable to discriminate between covariant constituents (Matthews 2011). These disadvantages have been attributed to a shift in focus towards the development of analytical and semi-analytical algorithms (Chang et al. 2015).

### 2.7.2 Semi-analytical algorithms

Analytical algorithms use purely theoretical methods to estimate constituents, while semi-analytical methods strike a balance between the use of physical theory and the inclusion of in situ data (Olmanson et al. 2015). A major advantage for analytical and semi-analytical algorithms, as compared with empirical algorithms, is their ability to retrieve multiple constituents simultaneously using one algorithm (Matthews 2011). Semi-analytical algorithms are based on fundamental optical principles and often forward or inverse models to approximate the equation of radiative transfer.

Forward models predict the spectral signature of water-leaving radiance based on the water column constituents and benthic reflectance, and inverse models predict the concentration of OACs based on the water's spectral reflectance (Matthews 2011; Dekker & Hestir 2012).

Semi-analytical methods require knowledge of the specific optical properties of the water being studied, including inherent optical properties (IOPs) or apparent optical properties (AOPs), as well as in situ measurements for calibration and validation. IOPs, most importantly scattering and absorption, are properties of the water medium and independent of the surrounding light field (Dekker & Hestir 2012). These coefficients include scattering and absorption contributions from phytoplankton, CDOM, non-algal particles and pure water. AOPs, on the other hand, include

properties such as reflectance, and depend on the IOPs and the characteristics of the underwater light field (Wang et al. 2016).

Semi-analytical algorithms can be time consuming and costly to develop, although many satellite sensor organisations now supply companion algorithms developed for use specifically with particular sensors. For example, NASA provides free data processing software for MODIS (SeaWiFS Data Analysis System (SeaDAS)) as well as offering specific algorithms. However, the local application of these to coastal waters in Canterbury has not been overly successful (Schwarz et al. 2010).

Similarly, ESA offers a MERIS Case-2 bio-optical algorithm that has been applied to inland waters with limited success (Matthews et al. 2010; Odermatt et al. 2010). However, Keith et al. (2014) retrieved successful chlorophyll *a* estimates from estuaries in the United States using the algorithm ($r^2$ = 0.84 - 0.87).

The transferability of semi-analytical algorithms between sensors that share similar waveband locations and widths is another potential way to reduce the time and cost of algorithm development. Augusto-Silva et al. (2014) applied three bio-optical algorithms originally developed for MERIS imagery to simulated output expected from the Sentinel-3 sensor and found that two of the three algorithms were successfully transferable.

The main disadvantages associated with semi-analytical algorithms include the larger data requirements, the sensitivity to errors arising from atmospheric correction and the error accrued from the estimation of IOPs (Matthews 2011).

Allan (2014) identified the need for local IOP data in order to successfully develop regional bio-optical models, avoiding the uncertainty in using literature values and non-local data. A number of researchers have addressed the errors associated with IOP estimates by measuring site-specific IOPs and conducting bio-optical modelling. More details on bio-optical sampling can be found in Belzile et al. (2014), Gallegos et al. (2008) and Wang et al. (2016). However, bio-optical variability over time and between water bodies can result in poor performance when semi-analytical algorithms are used to extrapolate beyond the observational data set (Politi et al. 2015).

This means that no single bio-optical algorithm is likely to be applicable to all water bodies in a region or to neighbouring water bodies of different trophic levels. The high initial cost associated with the development of an algorithm is another disadvantage in addition to modelling errors. This is in part due to the collection and analysis of in situ samples for calibration, although there is expected to be little cost associated with the ongoing use of a validated algorithm and further in situ measurements should not be required (Dekker & Hestir 2012).

### 2.7.3 Recommended way forward

In summary, there has been much discussion in the literature regarding the comparative applicability and feasibility of empirical vs. semi-analytical algorithms for the retrieval of inland water quality parameters, and all algorithms described have individual disadvantages. For example empirical algorithms lack wider applicability (Odermatt et al. 2012), while bio-optical algorithms may not be applicable to all lake types and trophic levels (Politi et al. 2015; Lyu et al. 2015).

In conclusion, it is most effective to begin with the calibration and validation of empirical methods in the initial design of water quality monitoring programmes, because field observations of traditional water quality attributes are available. The preliminary data analysis shown below illustrates that an uncalibrated algorithm is already capable of estimating realistic concentrations.

Sentinel-2a MSI captured a predominantly cloud-free image of the Manawatū-Whanganui region on the 9th January 2020 (New Zealand standard time). An uncalibrated algorithm for chlorophyll *a* (Mishra and Mishra 2012) was applied to this image (Figure 9), which estimates concentrations around 20 mg $m^{-3}$ in lakes Pauri and Wiritoa. The maps also show that there is variability of chlorophyll *a* within lakes. This variability appears to be associated with nearshore pixels, which suggests that further effort should be dedicated to excluding pixels overlapping with the shoreline and those over shallow water.


Figure 9: Lakes Wiritoa and Pauri in a Sentinel-2 MSI image from 9 January 2020. Data over water was processed to show the concentration of chlorophyll *a* (mg $m^{-3}$) using an established algorithm not yet calibrated for these lakes.

## 2.8 Case studies

We have thus far described the satellites and sensors, the observable water quality

constituents, and the retrieval algorithms that are used to estimate water quality. This section summarises pertinent applications of remote sensing for water quality parameters in lakes, focussing specifically on New Zealand studies.

### 2.8.1 Rotorua lakes and Lake Taupō

A first case study involves lake monitoring in the Rotorua lakes and Lake Taupō. Allan et al. (2011) derived simple empirical relationships between remote sensing reflectances of Landsat 7 ETM+ wavebands and chlorophyll *a*, Secchi depth and turbidity, measured in situ in 12 lakes in the Bay of Plenty region and Lake Taupō (Waikato region). In situ samples from regular monitoring programmes were chosen, which fell within two days of two satellite overpasses (24 January 2002 and 23 October 2002). Satellite pixels closest to the sampling locations were used.

The approach of the study was to compare the goodness of fit of in situ water quality parameters with reflectances at the satellite wavebands (and also commonly used band ratios), and to test the sensitivity of the relationships to two types of atmospheric correction. The authors found that all in situ variables could be related to one of the remotely-sensed spectral bands using one of two atmospheric correction methods (Pearson correlation coefficients, between r = 0.84 and r = 0.98).

The scatter plot in Figure 10 shows that log-transformed chlorophyll *a* concentrations can be derived using band 3 reflectance of Landsat 7, ETM+ and data pooled from all lakes and both image-capture dates (Figure 11). This relationship appears to hold over three orders of magnitude of chlorophyll *a* concentration.

The results suggest that remote sensing may be used to observe lake water quality parameters at the regional scale across a wide range of trophic states simultaneously.

One of the caveats of this study is that there was no single best retrieval algorithm for each variable, but the optimal method varied unpredictably depending on the date of the satellite overpass. This suggests that there is significant temporal variability in the dominant OACs affecting which retrieval algorithm to use, and that further ground truthing is needed.

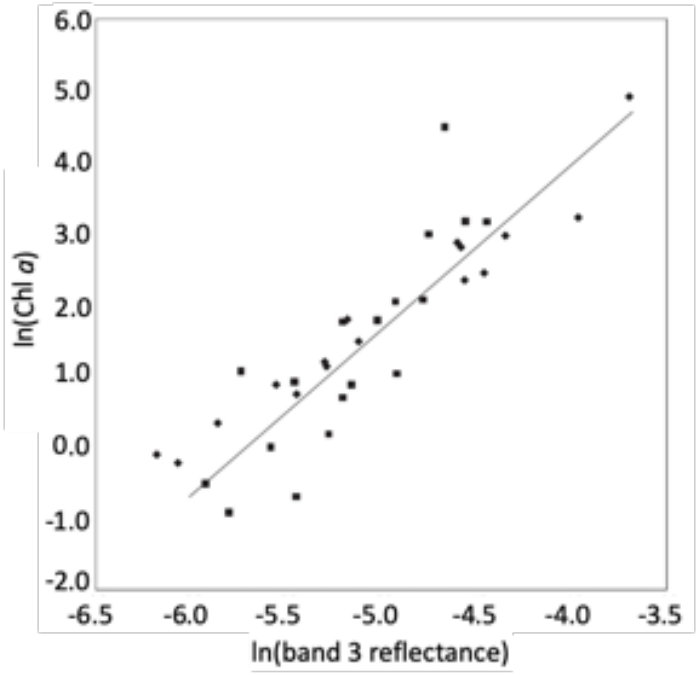


Figure 10: The empirical retrieval algorithm recommended by Allan et al. (2011) is a linear regression of log-transformed chlorophyll *a* concentration against log-transformed reflectance of ETM+ band 3 using 6sv atmospheric correction, $r^2$= 0.80.

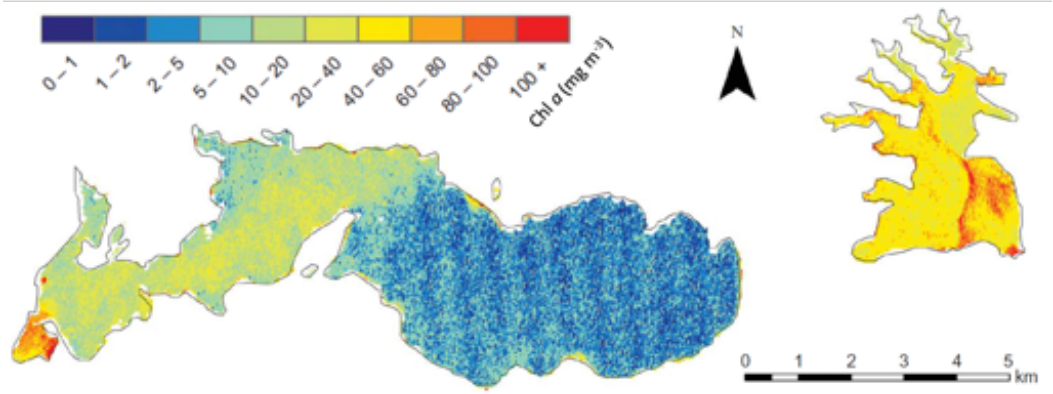


Figure 11: Chlorophyll *a* concentrations (mg $m^{-3}$) estimated for Lake Rotoiti (left) and Lake Rotoehu (right) by Landsat 7 ETM+ for 24 January 2002 using the regression shown in the scatterplot above. (Allan et al. 2011).

## 2.8.2 Waikato lakes

A second case study is focused on the Waikato region and covering lakes of similar size to those found in the Manawatū-Whanganui region. Hicks et al. (2013) used Landsat 7 ETM+ imagery to predict TSS, Secchi depth and turbidity in 34 Waikato lakes (including Lakes Waikare, Whangape, Waahi, Rotomanuka, Gin, Rotopiko, Rotokauri, Ngaroto, Maratoto, and Hakanoa) over a 10-year period (2000 – 2009). The authors developed regression relationships between in situ measurements and spectral reflectance over multiple lakes to find an overall relationship specific to the Waikato region that can be applied to local unmonitored lakes lacking in situ data.

Reflectance intensity in Band 4 from Landsat images at the locations of in situ samples were regressed against measured TSS in mg $L^{-1}$ ($r^2$ = 0.94), turbidity in nephelometric turbidity units (NTU; $r^2$ = 0.92) and measured Secchi depth ($r^2$ = 0.67). These empirical relationships were then used to hindcast water clarity predictions for the images without in situ measurements. Secchi depth was the most poorly predicted variable, most likely due to the interference of CDOM and suspended sediment (e.g., Allan 2008).

Image pre-processing, including atmospheric correction,cloud detection and masking, was automated and applied to 53 images over 10 years. The results showed clear spatial variation within lakes which would have been missed in localised manual sampling (Figure 12). For example, the three in situ sampling points in Lake Waikare shown in the 9 Sep 2001 image did not sample the suspended sediment plume at the southern end of the lake that appears to have originated from flood waters of the Matahuru Stream (see Hicks et al. 2013 for more detail).

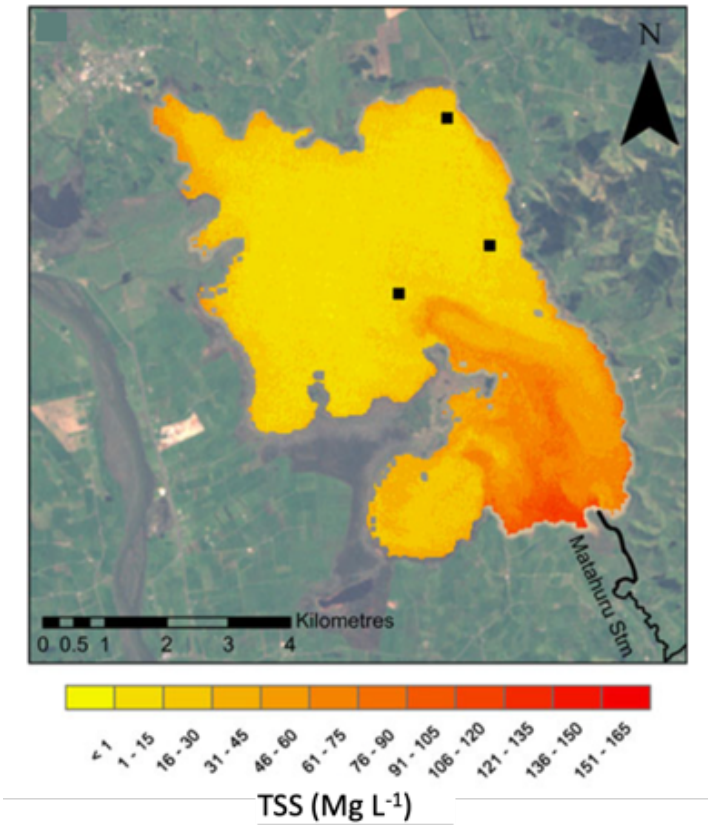


Figure 12: Estimated TSS (mg $L^{-1}$) in Lake Waikare on 9 September 2001 showing spatial variability and how in situ samples (black squares) can miss discharge plume from the Matahuru stream (Hicks et al. 2013).

### 2.8.3 Lake Ellesmere

A third case study investigated water quality in Lake Ellesmere. Allan (2014) used MODIS band 1 reflectance data to estimate suspended particle concentrations in

Lake Ellesmere, which is a large shallow turbid coastal lagoon (Figure 13). Semi-analytical and empirical algorithms were derived to determine spatial and temporal variations in suspended particles in the lake. Both algorithms predicted suspended particles similarly, but the semi-analytical model had the advantage of being applicable to different satellite sensors, spatial locations, and suspended particles concentration ranges.

When compared to literature values of error in TSS estimation, this error is of a similar magnitude (e.g., 18 and 22% for MODIS Terra and Aqua 250 m resolution data respectively, in extremely turbid Gironde estuary, France (Doxaran et al. 2009)). This study suggested that the semi-analytical model used to estimate suspended particles can be applied over the existing archive and future images of the MODIS sensor for the purposes of environmental monitoring.

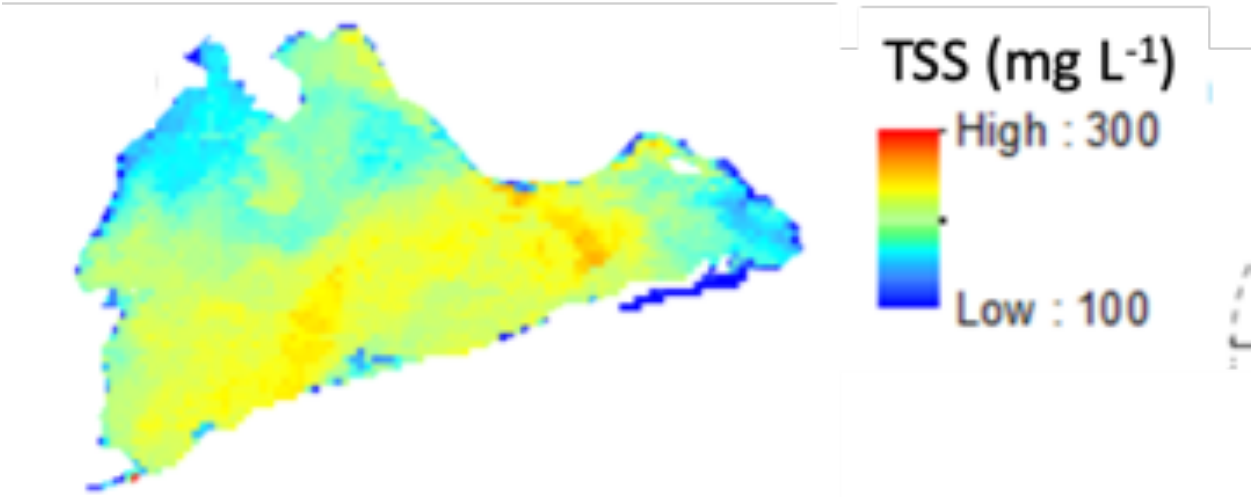


Figure 13: MODIS estimated suspended mineral concentrations on 1 March 2007 (Allan 2014).

### 2.8.4 Rotorua lakes

A fourth case study is the long-term analysis of the Rotorua lakes. Lehmann et al. (2019) demonstrated the power of the long-term data archive of satellite imagery by analysing 18 years of Landsat-derived water clarity (Secchi disk depth) in lakes in the Bay of Plenty region (Figure 13). Several trends were statistically significant and towards clearer water, and only one lake showed significantly decreasing water clarity.

Because the model was developed with regional applicability, the investigators were able to provide water clarity time series not only for the eight lakes which had a history of in situ sampling, but also for another 15 lakes, which are not routinely monitored. The availability of two decades of data for all of New Zealand enables such an analysis for all lakes in the country if a satisfactory algorithm for water quality attributes can be determined for the area of interest.

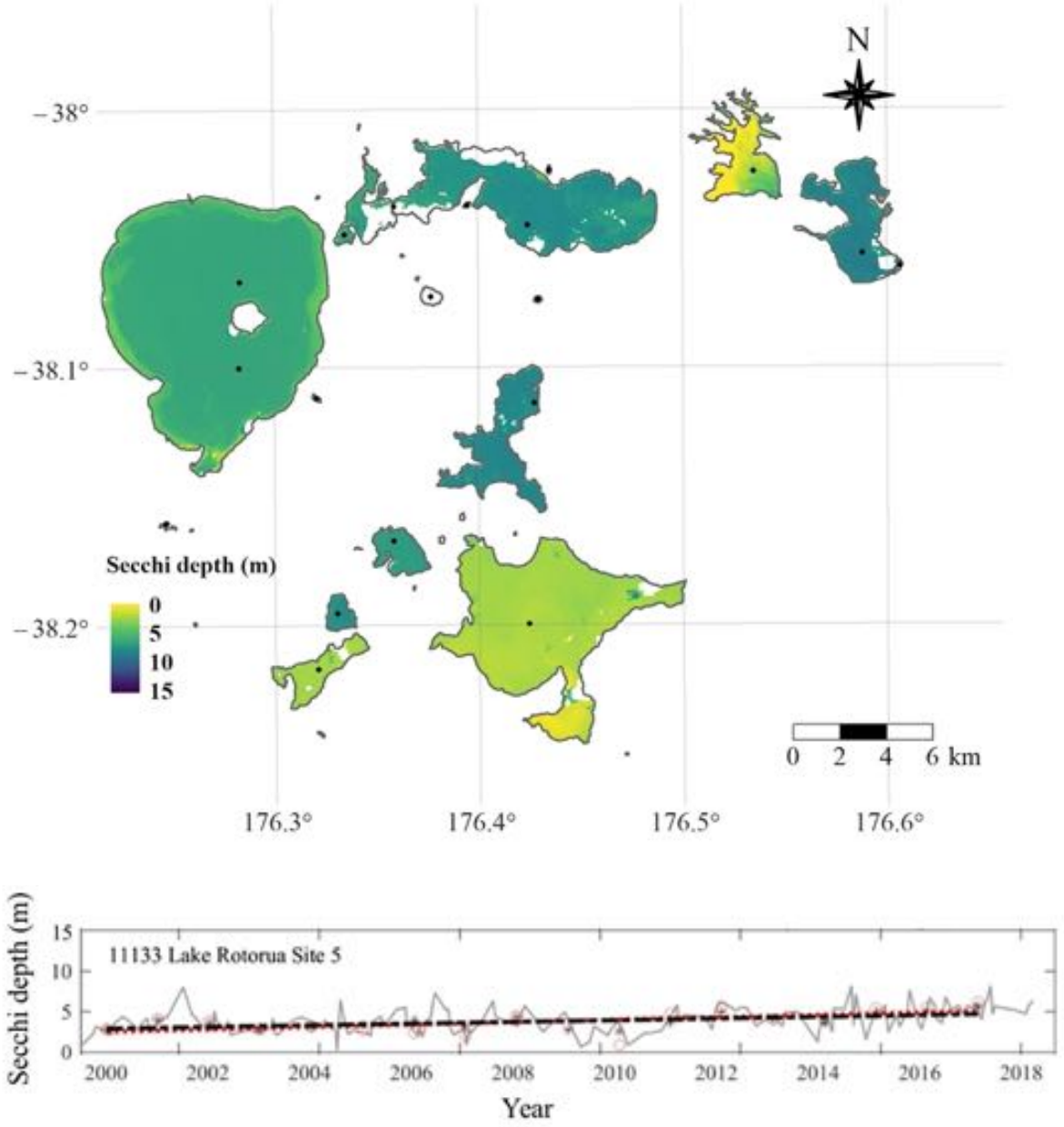


Figure 14: (Top) Secchi depth in the Rotorua lakes derived from a Landsat 8 OLI image taken on 28 January 2018. Black dots indicate sampling sites monitored via the Bay of Plenty water quality monitoring programme. (Bottom) Time series of satellite-derived Secchi depth in Lake Rotorua. Grey lines connect all available observations. Red dotted lines are linear fits through the summer averages (red circles) and black dashed lines are linear fits through the annual averages (black asterisks).

### 2.8.5 All New Zealand lakes

A final case study deals with monitoring all New Zealand lakes above 1 hectare (ha, 10,000 $m^{-2}$) in area which could be resolved in Landsat imagery. Lehmann et al. (2018) published the first comprehensive assessment of lake water colour in New Zealand based on four years of satellite observations. The researchers found that New Zealand's lakes span close to the full global range of possible water colours; some lakes have a stable blue or yellow colour, while others show very strong

variability related to seasonal and episodic events which may be driven by agriculture, forestry, invasive species and climate change.

Water colour lends itself as an intuitive water quality attribute that can be measured from all lakes without knowledge of the optical water type. In addition, it is a promising attribute for outreach and citizen science purposes as it is easy to communicate and can be measured using simple devices on the ground.

New Zealand lake colours for August 2016 are shown in Figure 15. Figure 16 shows water colour data for Lake Dudding as an example for a practical water colour monitoring application. This analysis was performed according to Lehmann et al. (2018); Appendix C contains plots for the other lakes in the region.

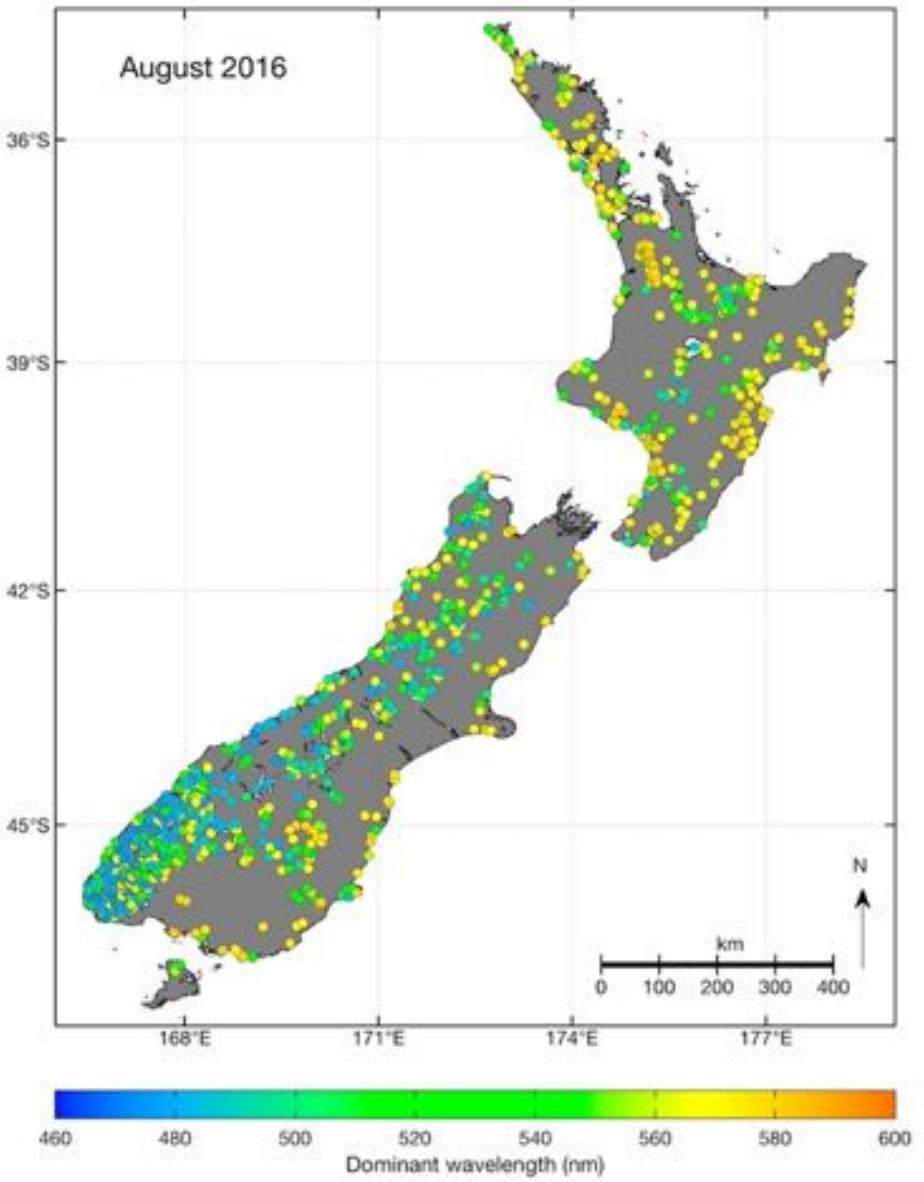


Figure 15: Colour of 1486 lakes determined from Landsat 8 satellite images taken in August 2016. Colour is expressed as dominant wavelength, an intensification of the colour as perceived by the human eye.

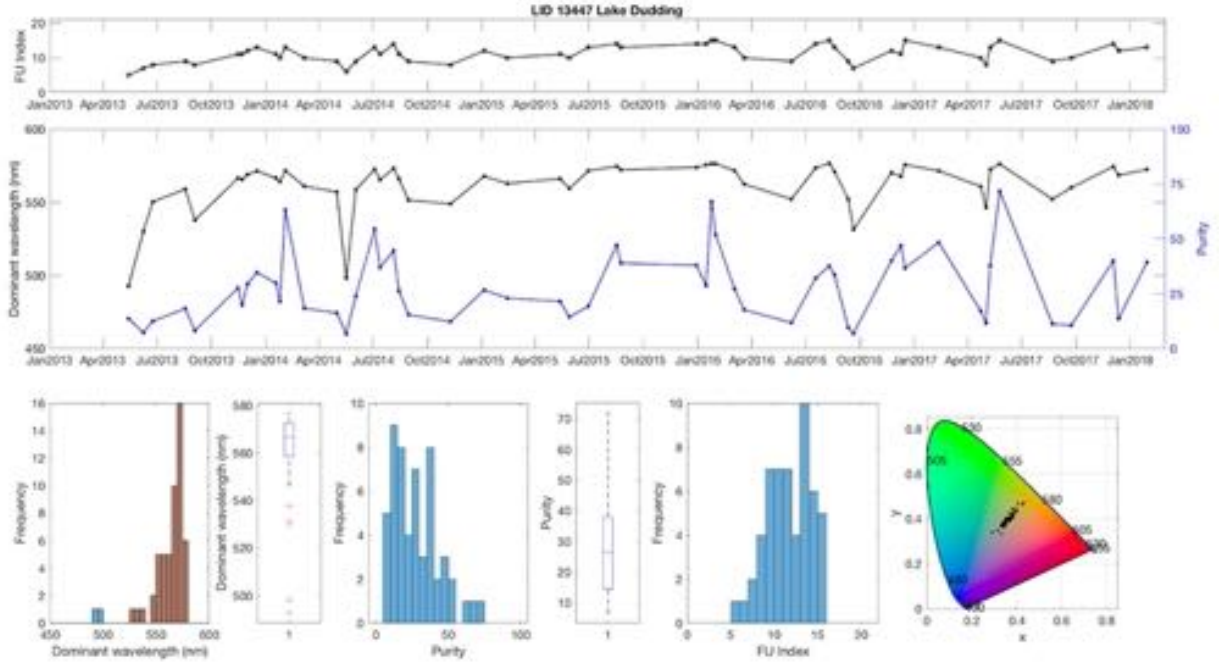


Figure 16: Four years of colour data from Lake Dudding determined from Landsat 8 OLI data according to Lehmann et al. (2018). Time series (top two panels) as well as location in the colour space (horseshoe-shaped plot in the bottom right) are shown. Histograms and box plots assist in detecting pollution or a bloom event. FU index: Water colour in the Forel-Ule colour system; dominant wavelength: intensification of the colour as perceived by the human eye in units of nanometers (nm); x and y are chromaticity coordinates of the standard colorimetric system of the Commission Internationale de l'Éclairage (CIE 1932). LID: FENZ lake ID. Appendix C contains plots for the other lakes in the region.

# 3. Number of lakes and frequency of satellite observations

In principle, a water body is suitable for remote sensing if the surface area is large enough to include water-only pixels and deep enough to preclude interference from bottom reflection. In practice, this depends on the size and shape of the water body, the characteristics of its bathymetry, and its water clarity.

Furthermore, a consideration for large lakes may be whether they lie fully within the swath width of a satellite sensor, such that the entire water body can only be mapped in consecutive overpasses (Figure 3).

Finally, feasibility of reliable monitoring depends on the occurrence of clouds and the frequency of overpasses of the satellite.

This section provides information on the extent to which lakes of the Manawatū-Whanganui region are visible by the remote sensing satellites that are considered in this study.

## 3.1 Manawatū-Whanganui lakes visible from space

There are 226 water bodies greater than 1 ha classified as lakes in the Manawatū-Whanganui region (Figure 17) according to the Freshwater Ecosystems New Zealand geo-database (FENZ geo-database, Leathwick 2010). Effectively, the remotely visible area is reduced by extending the shoreline inwards by the width of a satellite pixel (e.g., 10 m, 30 m or 300 m, depending on satellite resolution) to avoid contamination of the upwelling radiance by signals from the shoreline and the bottom.


Figure 17: Lakes greater than 1 ha in the Manawatū-Whanganui. Lakes currently monitored by Horizons Regional Council are shown in red. Lakes marked with dots have been found to contain a large enough area of open water to yield usable data at 30 m pixel size characteristic of the Landsat multispectral imagers. Lakes without black dots are too small for open water pixels at 30 m resolution.

For example, Figure 18 illustrates that Lake Dudding is large enough to yield water-only pixels using 30 m spatial resolution (Landsat OLI pixels), but not at 300 m MODIS or OLCI resolution. Using a semi-automated approach, we found that 57 lakes in the region had enough open water for reliable retrieval of water quality estimates at 30 m pixel size characteristic of the Landsat multispectral instruments (Lehmann et al. 2018). These 57 lakes are identified in Figure 17. Appendix A contains the list of FENZ lake IDs and lake names, where available, and Appendix B shows maps of the lakes for illustration of the spatial scales.

The number of observable lakes can be increased using sensors with higher spatial resolution, such as MSI (Sentinel-2, 10-20 m) or commercial sensors (e.g., Airbus Pléiades, 2 m). These higher-resolution sensors provide significant opportunities to map more water bodies as well as spatial patterns within lakes, such as patchy algal blooms and point sources of contamination. All but the three largest lakes of the region (Lakes Moawhango, Horowhenua and Otamangakau) are too small to be resolved by sensors with better spectral resolution, such as OLCI (Sentinel-3) and MODIS.

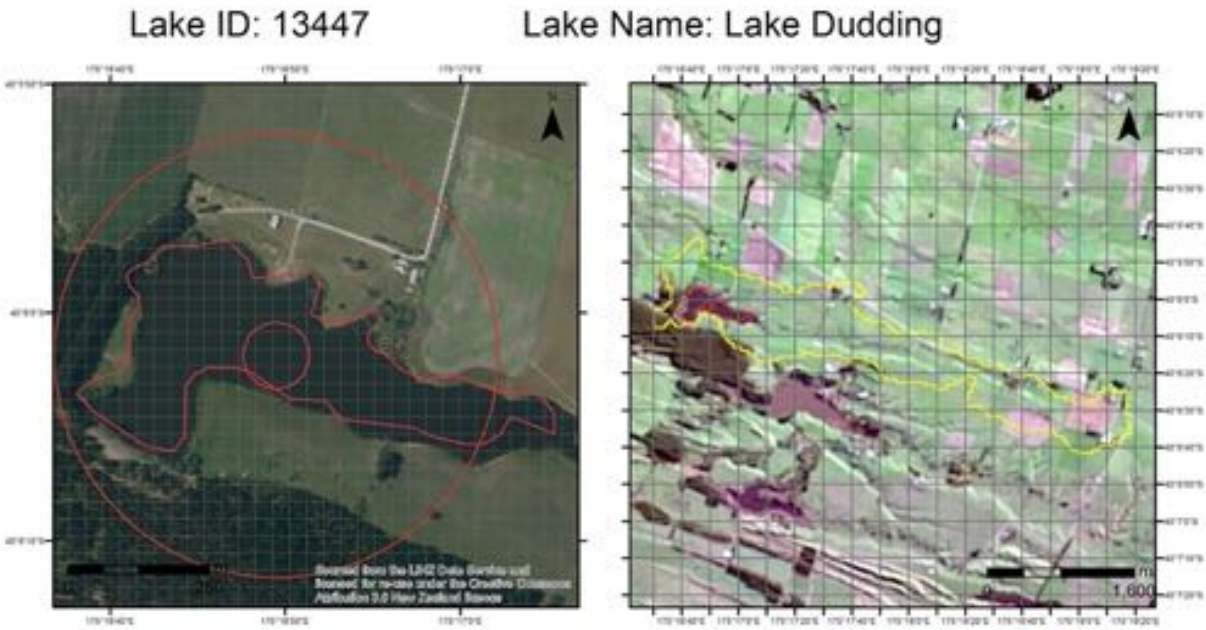


Figure 18: Example maps of Lake Dudding, which show the size and geometry of the lake for successful retrieval of satellite data. Left panel: Closeup of the lake with outlines provided in the FENZ geodatabase. The circles have diameters of 50 and 400 m, respectively, and are placed at the geometric center of each lake. Grid spacing is 30 m, showing pixel size characteristic of the Landsat multispectral instruments. Right panel: Lake and catchment outlines as provided in the FENZ geodatabase on a Landsat 8 OLI image. Maps for all other lakes visible from space are provided in Appendix B.

## 3.2 Expected frequency of satellite observations

We have shown how to calculate the minimum lake size that can be detected by sensors of varying spatial resolution. The next consideration is to determine whether a lake can be imaged at sufficient enough frequency.

The return periods of the satellite (Table 2) and site location within the overlapping image swaths determine the upper limit of the number of images that can be collected per month for a given lake. We use the term ‘upper limit’ because this does not account for the missed imaging opportunities due to obstruction by cloud cover.

The upper limit in image frequency varies from daily to twice per month for the sensors commonly used for water quality studies. For example, the Manawatū-Whanganui region is covered by three image swaths of the Sentinel-2 MSI sensor (Figure 3). As the constellation of the two Sentinel-2 satellites has a combined return period of five days, the theoretical image yield is two to three days at best in swath-overlapping areas and five days elsewhere.

As previously stated, cloud cover reduces the number of possible imaging opportunities and has to be taken into account when determining the feasibility of satellite monitoring. Cloud cover varies seasonally and within the region, so that lakes have different probabilities of being under a clear sky.

To estimate expected image yield for any lake during the months of the year, we used three years of daily percentage of clouds in the MOD06_L2 data product. This product has a resolution of 1 km and is produced from daily imagery from the MODIS Terra satellite taken at approximately 10:30 local time. Figure 19 shows the expected number of days in January with less than 20% cloud cover as an example. The orbits of most imaging satellites (e.g., Landsat 8 and Sentinel-2) pass over close to 10:30 in the morning; and we found that 20% cloud cover provides usable data over at least a portion of a lake, most of the time.

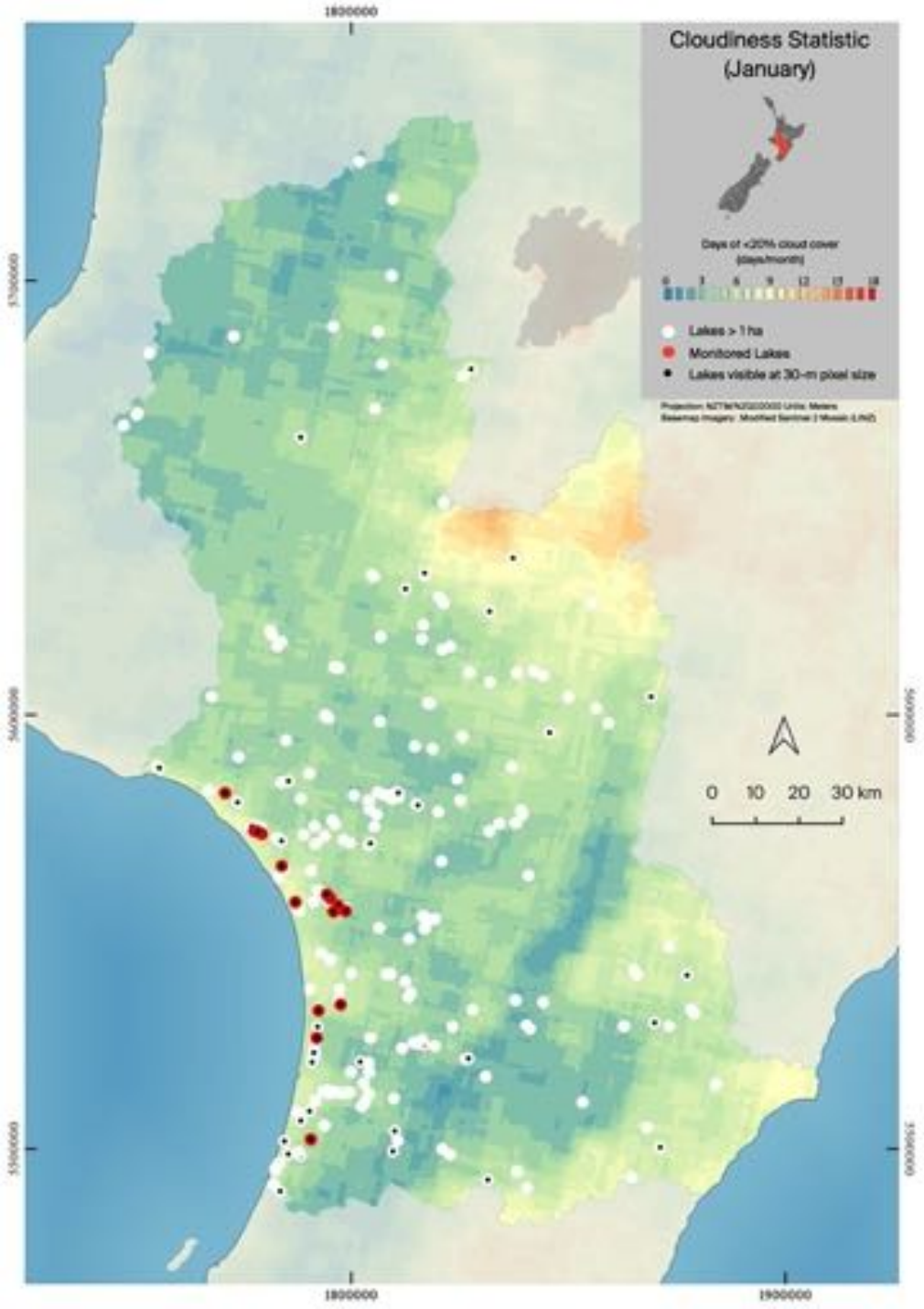


Figure 19: Expected number of days in January with less than 20 percent cloud fraction during the morning hours. Lakes currently monitored by Horizons Regional Council are shown in red. Lakes marked with dots have been found to be visible by at 30 m pixel size characteristic of the Landsat multispectral imagers, while those without dots would not be visible with 30 m pixel sizes.

By combining the theoretical image frequency and the cloud cover statistic, an expected image yield for Sentinel-2 MSI can be calculated for the entire region (Figure 20). Extracting the image yields at the location of each lake shows that most lakes are expected to be successfully imaged at least once per month using the Sentinel-2 pair of satellites (Table 3), although there may be some gaps during September to November.

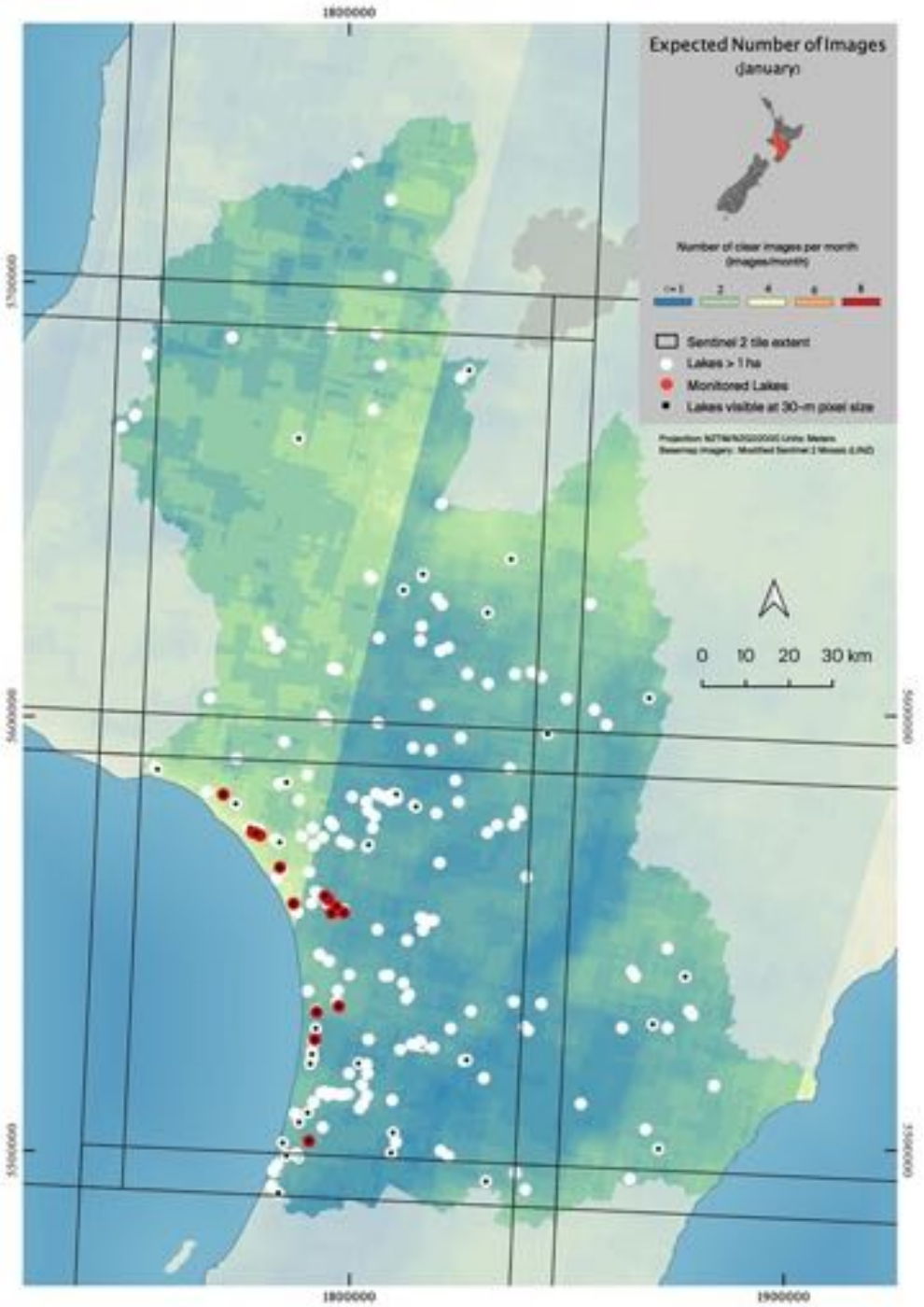


Figure 20: Expected number of clear images of Sentinel-2 in the Manawatū-Whanganui region for the month of January. The black grid on the map shows the area covered in individual downloadable MSI data files (image tiles); image tiles overlap by about 10 km. The diagonal discontinuity is due to overlap in adjacent satellite overpasses, causing a higher number of clear images per month.

Table 3: Expected number of images from Sentinel-2 MSI per year and for each month for currently monitored lakes. Most lakes can be imaged at least once per month (green cells). See Appendix for expected number of images per year for 57 lakes of the region.

| Name | Images per year | Images per month | | | | | | | | | | | |
|---|---|---|---|---|---|---|---|---|---|---|---|---|---|
| | | Jan | Feb | Mar | Apr | May | Jun | Jul | Aug | Sep | Oct | Nov | Dec |
| Lake Alice | 15.2 | 0.8 | 1 | 1.6 | 2 | 1.4 | 1.6 | 1.8 | 1.6 | 0.6 | 0.4 | 1 | 1.4 |
| Lake Dudding | 16.4 | 0.8 | 1 | 1.6 | 1.8 | 1.8 | 1.8 | 2 | 2 | 1 | 0.4 | 0.8 | 1.4 |
| Lake Heaton | 16.4 | 0.8 | 1 | 1.6 | 1.8 | 1.8 | 1.8 | 2 | 2 | 1 | 0.4 | 0.8 | 1.4 |
| Lake Herbert | 16.4 | 0.8 | 0.8 | 1.6 | 2 | 1.6 | 1.8 | 2 | 1.8 | 0.8 | 0.6 | 1 | 1.6 |
| L.Horowhenua | 13.8 | 1 | 1 | 1 | 1.4 | 1.4 | 1.2 | 1.2 | 1.4 | 1 | 0.6 | 1 | 1.6 |
| Lake Kohata | 36 | 3.2 | 2 | 3.2 | 4 | 3.2 | 3.2 | 3.2 | 4.4 | 2.4 | 1.2 | 2.4 | 3.6 |
| Lake Koitata | 40.4 | 2.8 | 2.8 | 4 | 4 | 3.6 | 3.6 | 4 | 4.4 | 2.8 | 2 | 2.4 | 4 |
| Lake Koputara | 17 | 1 | 0.8 | 1.6 | 1.6 | 1.6 | 1.6 | 2 | 1.6 | 1.2 | 0.8 | 1.4 | 1.8 |
| Lake Pauri | 17.6 | 1.4 | 1 | 1.6 | 2 | 1.6 | 1.6 | 1.8 | 2 | 1 | 0.6 | 1.2 | 1.8 |
| Lake Waipu | 36.8 | 2.4 | 2.8 | 3.6 | 4 | 3.2 | 3.2 | 3.6 | 4.4 | 2.4 | 1.2 | 2.4 | 3.6 |
| L. Westmere | 35.6 | 2.4 | 2.4 | 3.6 | 3.2 | 3.6 | 4 | 3.2 | 4.4 | 1.6 | 1.6 | 2 | 3.6 |
| Lake William | 16 | 0.8 | 1 | 1.6 | 2 | 1.8 | 1.8 | 1.8 | 1.6 | 0.8 | 0.6 | 0.8 | 1.4 |
| Lake Wiritoa | 36 | 2.8 | 2 | 3.2 | 4 | 3.2 | 3.6 | 3.2 | 4 | 2 | 1.6 | 2.8 | 3.6 |
| Omanuka L. | 16.4 | 1.2 | 1.2 | 1.6 | 1.8 | 1.2 | 1.6 | 1.8 | 1.8 | 1.2 | 0.6 | 1 | 1.4 |
| Pukepuke L. | 18.4 | 1.2 | 1.2 | 1.6 | 1.8 | 1.4 | 1.8 | 2 | 2 | 1.2 | 0.8 | 1.4 | 2 |

A similar analysis had been carried out previously for Landsat satellites, which have a return period of 16 days and also an area of swath overlap. While the image yield of the Landsat satellites is much lower, they have been imaging New Zealand regularly since 1999, providing a valuable archive for retrospective studies. This is illustrated in Section 4.

# 4. Practical implementation

In Sections 2 and 3, we described the theory related to remote sensing of lake water quality. We answered the following two questions: Which key water quality attributes can be measured by satellites? And, how many lakes can be observed and at what frequency?

In this section, we describe some practical considerations that Horizons Regional Council should consider when implementing a lake monitoring programme based on remote sensing.

## 4.1 Integrating in situ monitoring data with match-up images

A first practical consideration is how to integrate current and historical in situ data collected via existing monitoring programmes. This is critical to the success of remote sensing methods, because water quality parameter retrieval depends on ground truth measurements for calibration and validation. Ideally, a suite of in situ optical measurements in combination with measurements of chlorophyll *a*, TSS and CDOM are required to determine optical water types.

Horizons Regional Council has collected water quality monitoring data from 15 lakes at intervals from three to five months. Monitoring started at different times in different lakes, with the earliest start date of July 2013 (Lake Horowhenua) to the latest in March 2016 (Lake Westmere). Observed parameters relevant for calibration and validation of remote-sensing-retrieved attributes include Secchi depth, black disk depth, TSS (organic and inorganic), turbidity and chlorophyll *a*.

It is suggested to increase the frequency of sampling these attributes, enhance sensitivity of TSS measurements and add absorption measurements for the quantification of CDOM (Davies-Colley & Vant 1987). Chlorophyll *a* data from four example lakes from this monitoring is shown in Figure 20.

Existing in situ data can be readily integrated with satellite data, providing an opportunity to calibrate retrieval algorithms and backcast historical lake quality trends over decadal time scales.

This approach was taken by Lehmann et al. (2018), who analysed all satellite imagery collected over New Zealand by the Landsat satellites (Landsat 5, 7 and 8) and extracted cloud-free data over lakes up to January 2018. An illustration of the information gained over and above field-based sampling is provided in Figure 20, where the availability of cloud-free Landsat data is marked on the in situ chlorophyll *a* time series for four lakes.

Matched data, i.e., a cloud-free Landsat image within two days of the in situ sampling, was found to exist between two and ten times per year for each lake (Appendix 1). Table 4 lists the matching dates for these four lakes, as shown in Figure 20. Note that Landsat data from February 2018 onwards is not shown in this figure because it is based on work carried out previously.

Therefore, it is concluded that Horizons Regional Council is well-positioned to leverage its existing monitoring programme and data archive to deliver a marked increase in effectiveness, cost-efficiency and scale via satellite monitoring.

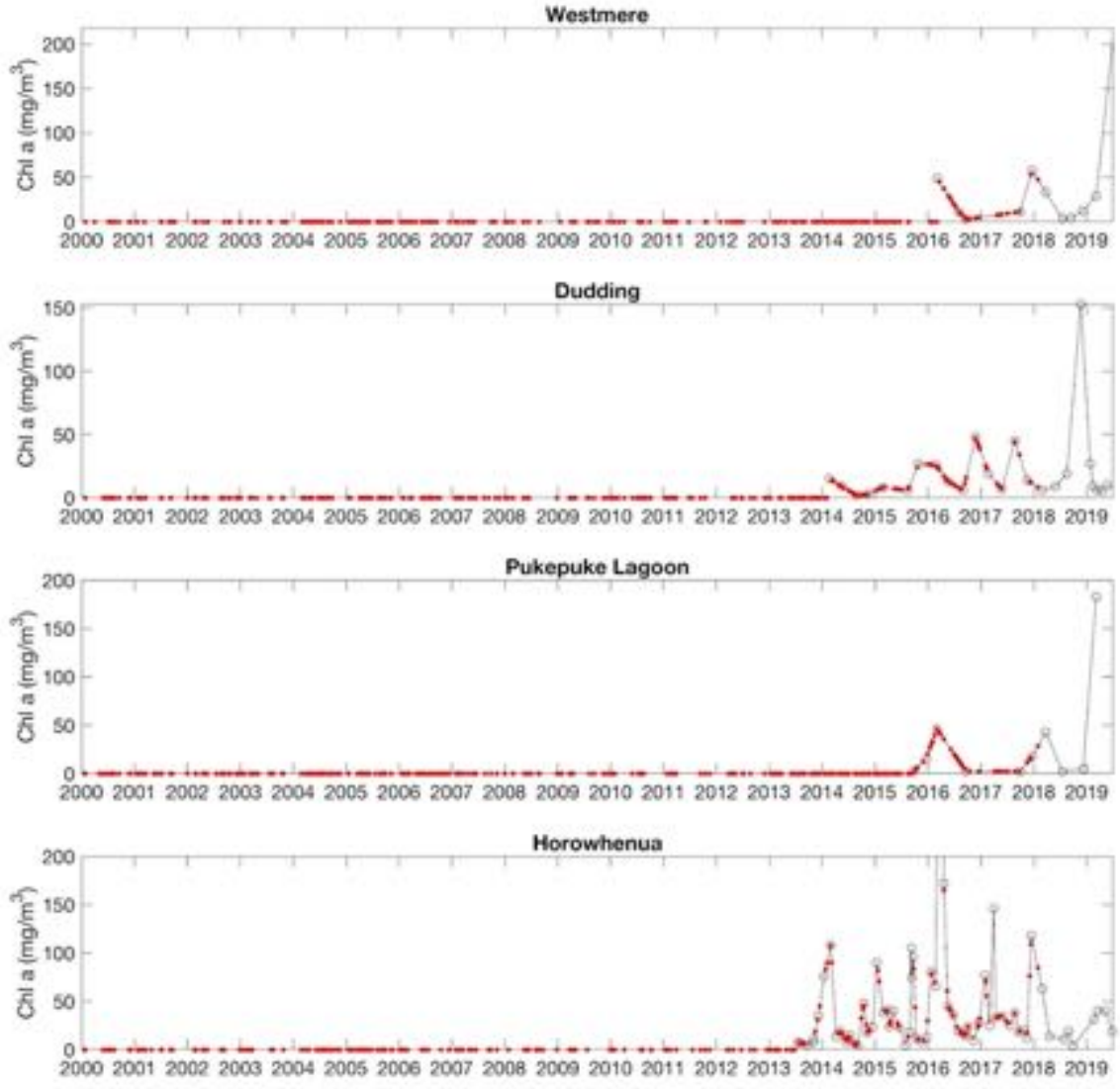


Figure 20: Chlorophyll *a* time series from water quality monitoring of four lakes by Horizons Regional Council, plotted as connected black circles. The red dots indicate the availability of Landsat satellite data. Note that the Landsat dots are placed on the line connecting the in situ data points or at zero and do not indicate an observed chlorophyll *a* concentration. Landsat images after January 2018 are available, but have not been analysed.

Table 4: Dates during which in situ samples fall within two days of a clear Landsat image for the four lakes shown in Figure 20. The number of matched observations for 56 other lakes within the Manawatū-Whanganui region are provided in Appendix A.

| Lake name | Date of in situ sampling | Date of Landsat image |
|---|---|---|
| Dudding | 28/08/14 | 29/08/14 |
| Dudding | 28/05/15 | 29/05/15 |
| Dudding | 24/11/16 | 23/11/16 |
| Dudding | 24/05/17 | 25/05/17 |
| Dudding | 23/08/17 | 22/08/17 |
| Horowhenua | 27/02/14 | 27/02/14 |
| Horowhenua | 5/08/14 | 5/08/14 |
| Horowhenua | 14/10/14 | 16/10/14 |
| Horowhenua | 7/11/14 | 9/11/14 |
| Horowhenua | 25/03/15 | 25/03/15 |
| Horowhenua | 19/04/16 | 21/04/16 |
| Horowhenua | 23/06/16 | 24/06/16 |
| Horowhenua | 4/10/16 | 5/10/16 |
| Horowhenua | 22/08/17 | 22/08/17 |
| Horowhenua | 15/11/17 | 17/11/17 |
| Westmere | 3/03/16 | 3/03/16 |
| Westmere | 2/08/16 | 2/08/16 |
| Westmere | 21/09/16 | 20/09/16 |
| Pukepuke L. | 3/03/16 | 3/03/16 |
| Pukepuke L. | 2/08/16 | 2/08/16 |

## 4.2 Coordinating ground sampling with satellite overpasses

Satellites make repeated observations over a large area of interest. For Sentinel-2, the entire Manawatū-Whanganui is imaged every five days. Clearly, in situ monitoring teams can not ground truth every overpass, nor do they need to.

Furthermore, it is impractical to wait until a suitable cloud-free observation has been received to deploy field teams for ground-truthing, as this would be an inefficient use of personnel, equipment and resources.

Instead, existing in situ monitoring schedules should be coordinated in order to align with known satellite overpasses and predicted weather windows (e.g., limited cloud). This increases the chances of obtaining in situ water samples for direct comparison with satellite-derived estimates, while not adding any additional burden to existing field operations.

The schedules of satellite overpasses are predictable and can often be looked up online. Images are usually available for download within hours of acquisition but may take up to a day or more.

For lakes in the Manawatū-Whanganui region, Sentinel-2 and Landsat 8 are the satellites of choice due the spatial resolution of their instruments on the order of tens of meters.

The acquisition plans for Sentinel-2 a and b are provided as respective KML files for 10 to 15 day periods on an ESA website[3]. These files can be opened in Google Earth and provide data acquisition areas and times in UTC. In addition, ESA also provides the mobile app *Copernicus Sentinel*[4], which allows determination of recent and near-future overpass information for the whole fleet of Copernicus satellites. Finally, Sentinel-2 overpasses can be predicted simply by adding multiples of 5 days to a known date of an image of the area of interest.

Landsat 5 and 8 have a revisit period of 16 days, respectively, and the time of data acquisition of a specific area of interest can be looked up on a USGS website[5]. Adding multiples of 16 days to a known date of an image of the area of interest can also be used to predict future overpasses.

It is important to note that dates and times of satellite overpasses are given in Coordinated Universal Time (UTC), which, for practical purposes, is the same as Greenwich Mean Time (GMT). The satellites discussed in this report all have an acquisition pass at the same time of day, usually late morning at local time.

[3] https://sentinel.esa.int/web/sentinel/missions/sentinel-2/acquisition-plans
[4] https://itunes.apple.com/it/app/esa-sentinel/id1036738151?mt=8 and https://play.google.com/store/apps/details?id=esa.sentinel&hl=it
[5] https://landsat.usgs.gov/landsat_acq

For practical purposes, any field samples taken on the same day as a satellite image are considered matchups. However, the suitability of samples to serve as matchups depends on the local scale of variability to the measured property and thus the matchup window may be reduced or extended.

For example, chlorophyll concentration may be stable over weeks during winter and increase markedly from day to day during spring; and shallow lakes may be sensitive to wind-driven resuspension of bottom particles within hours. Therefore, the assumptions of representativeness of a sample taken at a certain time that applies to in situ samples also applies to remotely sensed attributes.

As a rule of thumb, images taken between a day before and a day after the in situ samples are often considered matchups. The matchup time window is commonly assessed during algorithm development and should be stated in comparisons of remotely versus in situ observations.

## 4.3 Providing additional insight through catchment-scale context

A second practical consideration and opportunity when using remote sensing for lake water quality monitoring is the ability to interpret changes in lake water quality in the context of catchment scale processes.

Land applications are illustrated using the image from March 2018 in a map of the normalised difference vegetation index (NDVI) (Figure 21, left panel). This index measures the health and density of vegetation using the red and near infrared channels from a multispectral sensor (Chuvieco 2016). Much of the region in this map has NDVI > 0.5 suggesting healthy and dense vegetation. In contrast, urban areas, water and shorelines have low NDVI. Some fields or paddocks also show low NDVI suggestive of grazing, tilling or spraying activities.

Observing the temporal change in vegetation is possible by comparing NDVI between images, e.g., spring (November 2017) to summer (March 2018). NDVI in much of that region did not change significantly, and most of the change that did occur indicates vegetation growth over the summer (Figure 21, right panel). This information is valuable to interpret changes in lake water quality in the context of catchment scale processes. Grazing, logging and habitat restoration all have NDVI signatures and may point towards pressures that drive lake water quality.

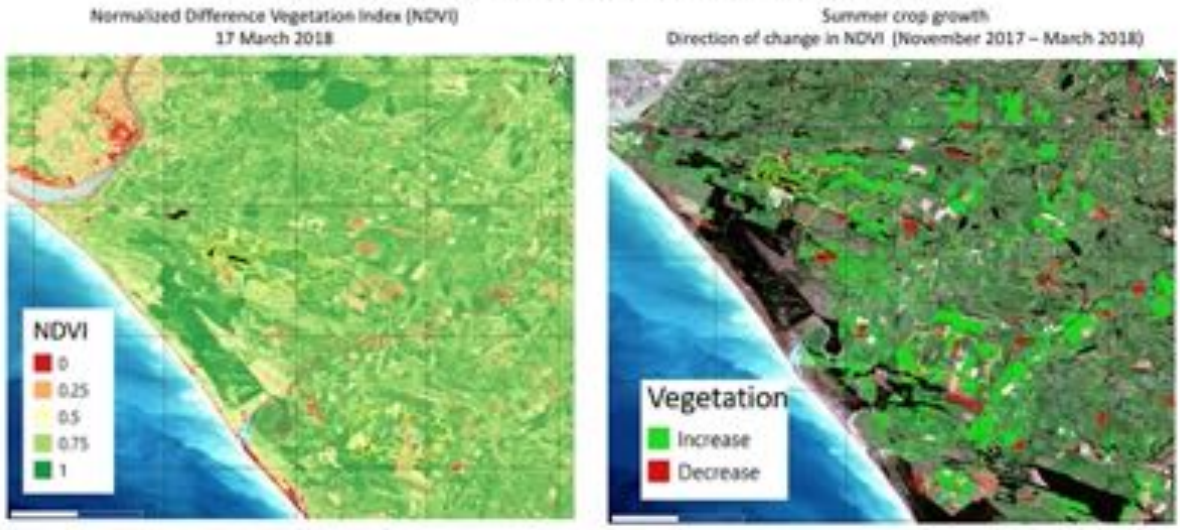


Figure 21: (Left) Normalised difference vegetation index (NDVI) of the region south of Whanganui. (Right) True colour rendering of the region with areas highlighted which have undergone an increase or decrease, respectively, in vegetation between November 2017 and March 2018.

## 4.4 Automated processing of satellite data

A final practical consideration is how to automate the processing of large volumes of satellite data to provide timely water quality attributes.

Satellite data is collected regularly and made available to users through well-developed file servers. Water quality products suitable for lake monitoring, however, are not included in the data, therefore further processing is needed.

The data processing tasks required for environmental monitoring were listed in Section 2.6. This processing is a technical task which requires the handling and management of large data sets and experience in spatial analysis. Two approaches can be taken: manual and automated processing.

Manual image-by-image processing can be performed by point-and-click navigation of software based on graphical user interfaces, but the effort involved makes it poorly suited to operational monitoring, and the choice of tools depends on various factors, including the data source.

Automated processing leverages routine collection, distribution and analysis of satellite data via application programming interfaces. Automated methods are therefore efficient and cost-effective, returning dividends beyond the initial investment in setup.

Ideally, such an automated processing engine sits in the centre of an efficient, scalable, and cost-effective framework for operational monitoring of lake water quality (Figure 22).

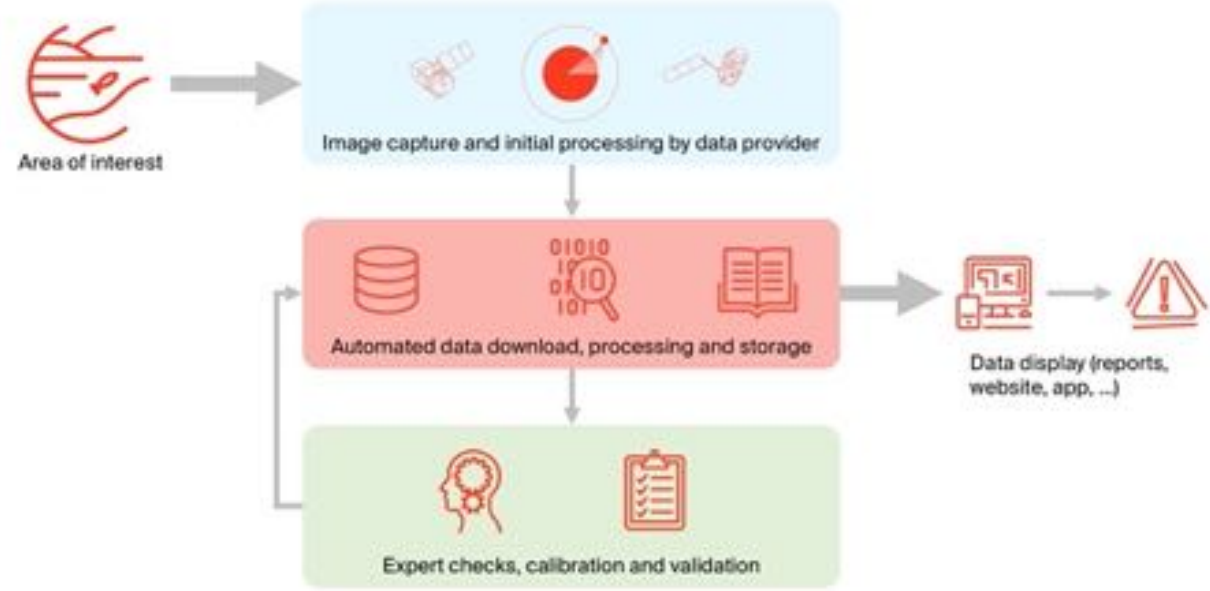


Figure 22: Automation of the download and processing of satellite data (red shaded area in the middle) is the central component of the framework for operational monitoring of lake water quality. The output can be designed to meet specific needs such as alerting to algal blooms or long-term monitoring.

Our discussion of the practical implementation of lake water quality monitoring in this section can be summarised as follows.

First, existing in situ data can be readily integrated with satellite data, providing an opportunity to calibrate retrieval algorithms and backcast historical lake water quality trends over decadal time scales.

Second, satellite imagery provides the synoptic perspective to interpret changes in lake water quality in the context of catchment scale processes.

And finally, automated methods are now possible, which make satellite monitoring efficient and cost effective, returning dividends beyond the initial investment in setup.

These considerations indicate that Horizons Regional Council is well-positioned to realise the full potential of satellite observations, if financial planning provides consideration for expert consultation and software development.

# 5. Conclusion

**Satellite monitoring of lakes provides reliable states and trends of water quality from more lakes, at a higher frequency and at greater spatial fidelity, compared to what is feasible using ground-based methods.**

This report investigated the feasibility of using satellite remote sensing for monitoring lake water quality in the Manuwatū-Whanganui region.

This feasibility was evaluated by estimating how many lakes can reliably be resolved by available satellite sensors, and how much data can be expected, considering regional and seasonal cloud cover statistics.

In addition, the principles of remote sensing of water quality attributes were reviewed to illustrate the fundamental principles underlying the accuracy and uncertainty of satellite-based estimates.

The main conclusions from this report are:

1. **In the region, at least 57 lakes are large enough to be monitored by satellite.**

Of the 226 lakes in the Manawatū-Whanganui region, 57 have large enough open-water areas to be resolved by 30 m pixels typical of Landsat sensors.

Additional smaller lakes are likely visible in 10 m Sentinel-2 MSI resolution images.

All lakes currently included in the Horizons Regional Council water quality monitoring programme can be monitored.

2. **Better-than-monthly monitoring frequency is expected for most lakes.**

Satellite revisit periods and regional cloud cover statistics suggest that Sentinel-2 satellites will successfully image all lakes at least once per month with a few exceptions.

Some lakes are expected to yield up to four images per month during certain times of the year.

3. **Common water quality attributes can be predicted from satellite data.**

Attributes that are commonly derived from satellite data include chlorophyll *a*, suspended particulate matter, Secchi disk depth, water colour and turbidity. Several other observations, such as cyanobacteria blooms, macrophyte presence and floating algae can also be developed.

Additionally, satellites can map the spatial variation in water quality across a lake, which may reveal important blooms that are missed by point-based sampling. Visual images of the lake and catchment provide a wealth of intuitive information to experts and stakeholders.

4. **Satellite-derived water quality attributes can match in situ samples with 70-90% accuracy**

The accuracy of satellite estimates must be established using in situ observations. Depending on the water type and the availability of data for calibration, good prediction accuracies can be obtained with sufficient investment which are best facilitated through close partnership between councils and a research organisation.

Despite high accuracies, satellite-based data are not yet accepted by the Ministry for the Environment State of the Environment Reporting. We hope that subsequent collaboration could lead to greater confidence around satellite-based monitoring accuracy, opening the door to better and more streamlined reporting to statutory monitoring requirements.

5. **Automation of data processing makes satellite monitoring efficient and cost-effective**

Satellite data are routinely collected and are accessible using application programming interfaces. Significant processing is required to derive water quality attributes, which can be automated in the cloud or dedicated desktop machines to produce end-user products.

In conclusion, Horizons Regional Council is well-positioned to leverage its existing monitoring programme and data archive to deliver a marked increase in effectiveness, cost-efficiency and scale using satellite monitoring.

# References


Alikas, K., Kangro, K., Randoja, R., Philipson, P., Asukull, E., Pisek, J., & Reinart, A. (2015). Satellite-based products for monitoring optically complex inland waters in support of EU Water Framework Directive. International Journal of Remote Sensing, 36(17), 4446-4468.

Allan, M. G. (2008). Remote Sensing of Water Quality in Rotorua and Waikato Lakes. MSc thesis, University of Waikato, Hamilton, New Zealand.

Allan, M. G. (2014). Remote sensing, numerical modelling and ground truthing for analysis of lake water quality and temperature. PhD thesis, University of Waikato, Hamilton, New Zealand.

Allan, M. G., Hamilton, D. P., Hicks, B., & Brabyn, L. (2015). Empirical and semi-analytical chlorophyll *a* algorithms for multi-temporal monitoring of New Zealand lakes using Landsat. Environmental Monitoring and Assessment, 187(6), 364.

Ashraf, S., Brabyn, L., & Hicks, B. (2008). Evaluating remote sensing data classification techniques for mapping freshwater habitats: Trial application in the Tongariro River delta, Lake Taupo. CBER Contract Report 87. Centre for Biodiversity and Ecology Research, University of Waikato, Hamilton, New Zealand. 33p.

Augusto-Silva, P. B., Ogashawara, I., Barbosa, C. C. F., de Carvalho, L. A. S., Jorge, D. S. F., Fornari, C. I., & Stech, J. L. (2014). Analysis of MERIS reflectance algorithms for estimating chlorophyll a concentration in a Brazilian reservoir. Remote Sensing, 6(12), 11689-11707.

Chang, N. B., Imen, S., & Vannah, B. (2015). Remote sensing for monitoring surface water quality status and ecosystem state in relation to the nutrient cycle: A 40-year perspective. Critical Reviews in Environmental Science and Technology, 45(2), 101-166.

Chuvieco, E. (2016). Fundamentals of satellite remote sensing. (Second ed.). Boca Raton: CRC Press.

CIE. Commission Internationale de l'Éclairage Proceedings; Cambridge University Press: Cambridge, UK, 1932.

Davies-Colley, R. J., & Vant, W. N. (1987). Absorption of light by yellow substance in fresh-water lakes. Limnology and Oceanography, 32(2), 416-425.

Dekker, A. G., & Hestir, E. L. (2012). Evaluating the Feasibility of Systematic Inland Water Quality Monitoring with Satellite Remote Sensing. CSIRO: Water for a Healthy Country National Research Flagship.

Dogliotti, A., Gossn, J., Vanhellemont, Q., Ruddick, K. (2018). Detecting and quantifying a massive invasion of floating aquatic plants in the río de la plata turbid waters using high spatial resolution ocean color imagery. Remote Sensing 10 (7), 1140.

Dornhofer, K., & Oppelt, N. (2016). Remote sensing for lake research and monitoring - Recent advances. Ecological Indicators, 64, 105-122.

Frouin, R. J., B. A. Franz, A. Ibrahim, K. Knobelspiesse, Z. Ahmad, B. Cairns, J. Chowdhary, H. M. Dierssen, J. Tan, O. Dubovik, X. Huang, A. B. Davis, O. Kalashnikova, D. R. Thompson, L. A. Remer, E. Boss, O. Coddington, P.-Y. Deschamps, B.-C. Gao, L. Gross, O. Hasekamp, A. Omar, B. Pelletier, D. Ramon, F. Steinmetz and P.-W. Zhai (2019). Atmospheric Correction of Satellite Ocean-Color Imagery During the PACE Era. Frontiers in Earth Science 7: 145.

Gitelson, A. A., Dall'Olmo, G., Moses, W., Rundquist, D. C., Barrow, T., Fisher, T. R., Gurlin, D., & Holz, J. (2008). A simple semi-analytical model for remote estimation of chlorophyll a in turbid waters: Validation. Remote Sensing of Environment, 112(9), 3582-3593.

Gomez, J. A. D., Alonso, C. A., & Garcia, A. A. (2011). Remote sensing as a tool for monitoring water quality parameters for Mediterranean Lakes of European Union water framework directive (WFD) and as a system of surveillance of cyanobacterial harmful algae blooms (SCyanoHABs). Environmental Monitoring and Assessment, 181(1-4), 317-334.

Hicks, B. J., Stichbury, G. A., Brabyn, L. K., Allan, M. G., & Ashraf, S. (2013). Hindcasting water clarity from Landsat satellite images of unmonitored shallow lakes in the Waikato region, New Zealand. Environmental Monitoring and Assessment, 185(9), 7245-7261.

Julian, J. P., Davies-Colley, R. J., Gallegos, C. L., & Tran, T. V. (2013). Optical water quality of inland waters: A landscape perspective. Annals of the Association of American Geographers, 103(2), 309-318.

Kirk, J. T. O. (1994). Light & Photosynthesis in Aquatic Ecosystems. (2 ed.). Cambridge: Cambridge University Press.

Leathwick, J. W.-G. (2010). Freshwater Ecosystems of New Zealand (FENZ) Geodatabase Version One - User Guide. NIWA, Wellington.

Lehmann, M. K., Nguyen, U., Muraoka, K., & Allan, M. G. (2019). Regional trends in remotely sensed water clarity over 18 years in the Rotorua Lakes, New Zealand. New Zealand Journal of Marine and Freshwater Research, 1-23.

Lehmann, M. K., Nguyen, U., Allan, M., & van der Woerd, H. (2018). Colour Classification of 1486 Lakes across a Wide Range of Optical Water Types. Remote Sensing, 10(8).

Liang, Q.; Zhang, Y.; Ma, R.; Loiselle, S.A.; Li, J.; Hu, M. A (2017) MODIS-Based Novel Method to Distinguish Surface Cyanobacterial Scums and Aquatic Macrophytes in Lake Taihu. Remote Sensing, 9, 133.

Matthews, M. W. (2011). A current review of empirical procedures of remote sensing in inland and near-coastal transitional waters. International Journal of Remote Sensing, 32(21), 6855-6899.

Mishra, S., Mishra, D. R. (2012). Normalized difference chlorophyll index: A novel model for remote estimation of chlorophyll-a concentration in turbid productive waters. Remote Sensing of Environment 117, 394–406.

MfE. (2015). A Draft Guide to Attributes in Appendix 2 of the National Policy Statement for Freshwater Management 2014. Ministry for the Environment, Wellington.

MfE. (2017). National Policy Statement for Freshwater Management 2014 (amended 2017). Ministry for the Environment.

Mobley, C. D. (1994). Light and Water: Radiative Transfer in Natural Waters. San Diego: Academic Press.

Odermatt, D., Giardino, C., & Heege, T. (2010). Chlorophyll retrieval with MERIS Case-2-Regional in perialpine lakes. Remote Sensing of Environment, 114(3), 607-617.

Odermatt, D., Gitelson, A., Brando, V. E., & Schaepman, M. (2012). Review of constituent retrieval in optically deep and complex waters from satellite imagery. Remote Sensing of Environment, 118, 116-126.

Olmanson, L. G., Brezonik, P. L., & Bauer, M. E. (2011). Evaluation of medium to low resolution satellite imagery for regional lake water quality assessments. Water Resources Research, 47.

Olmanson, L. G., Brezonik, P. L., & Bauer, M. E. (2015). Remote sensing for regional lake water quality assessment: Capabilities and limitations of current and upcoming satellite systems. In T. Younos & T. E. Parece (Eds.), Advances in Watershed Science and Assessment (pp. 111-140).

Palmer, S. C. J., Kutser, T., & Hunter, P. D. (2015). Remote sensing of inland waters: Challenges, progress and future directions. Remote Sensing of Environment, 157, 1-8.

Politi, E., Cutler, M. E. J., & Rowan, J. S. (2015). Evaluating the spatial transferability and temporal repeatability of remote-sensing-based lake water quality retrieval algorithms at the European scale: a meta-analysis approach. International Journal of Remote Sensing, 36(11), 2995-3023.

Roy, D. P., Wulder, M. A., Loveland, T. R., Woodcock, C. E., Allen, R. G., Anderson, M. C., Helder, D., Irons, J. R., Johnson, D. M., Kennedy, R., Scambos, T., Schaaf, C. B., Schott, J. R., Sheng, Y., Vermote, E. F., Belward, A. S., Bindschadler, R., Cohen, W. B., Gao, F., Hipple, J. D., Hostert, P., Huntington, J., Justice, C. O., Kilic, A., Kovalskyy, V., Lee, Z. P., Lymbumer, L., Masek, J. G., McCorkel, J., Shuai, Y., Trezza, R., Vogelmann, J., Wynne, R. H., & Zhu, Z. (2014). Landsat-8: Science and product vision for terrestrial global change research. Remote Sensing of Environment, 145, 154-172.

Rudorff, C. M., Novo, E. M. L. M., & Galvao, L. S. (2006). Spectral mixture analysis for water quality assessment over the Amazon floodplain using Hyperion/EO-1 Images. Revista Ambi-Agua, 1(2), 65-79.

Schott, J. R. (2007). Remote sensing: the image chain approach. Oxford University Press.

Seyhan, E., & Dekker, A. (1986). Application of remote sensing techniques for water quality monitoring. Hydrobiological Bulletin, 20(1), 41-50.

Simis, S. G. H., Peters, S. W. M., & Gons, H. J. (2005). Remote sensing of the cyanobacterial pigment phycocyanin in turbid inland water. Limnology and Oceanography, 50(1), 237-245.

Tan, J., Cherkauer, K. A., & Chaubey, I. (2015). Using hyperspectral data to quantify water-quality parameters in the Wabash River and its tributaries, Indiana. International Journal of Remote Sensing, 36(21), 5466-5484.

Torgersen, C. E., Faux, R. N., McIntosh, B. A., Poage, N. J., & Norton, D. J. (2001). Airborne thermal remote sensing for water temperature assessment in rivers and streams. Remote Sensing of Environment, 76(3), 386-398.

Vant, W. N., & Davies-Colley, R. J. (1984). Factors affecting clarity of New-Zealand lakes. New Zealand Journal of Marine and Freshwater Research, 18(3), 367-377.

Vermote, E. F., Tanre, D., Deuze, J. L., Herman, M., & Morcrette, J. J. (1997). Second simulation of the satellite signal in the solar spectrum, 6S: An overview. IEEE Transactions on Geoscience and Remote Sensing, 35(3), 675-686.

# Appendix A

## Lakes visible from space at 30 m pixel resolution

Of the 226 lakes in the Manawatū-Whanganui region, 57 have been found to be visible in satellite data with at least 30 m spatial resolution (Lehmann et al 2018). These lakes are listed below with pertinent information taken from the FENZ geodatabase (Leathwick 2010). The number of satellite images that could be collected per year was calculated using monthly cloud cover statistics and orbit characteristics of the Sentinel-2 satellite constellation. *Landsat matchups* is the number of in situ samples collected at each lake within two days of a clear Landsat image (for the 15 lakes in the Horizons lake monitoring programme).

| Lake ID | Name | Type | Area (ha) | Elevation (m) | Max. depth (m) | Images per year | Landsat matchups |
|---|---|---|---|---|---|---|---|
| 476 | Tokomaru No 3 Reservoir | Dam | 9.5 | 357.6 | 23.7 | 8.4 | |
| 869 | | Aeolian | 5.3 | 10.0 | 2.9 | 17 | |
| 871 | | Aeolian | 4.0 | 10.0 | 2.9 | 16.8 | |
| 877 | | Aeolian | 2.4 | 18.7 | 3.0 | 13.6 | |
| 1962 | | Aeolian | 4.3 | 15.2 | 2.8 | 17.4 | |
| 1972 | | | 2.0 | 20.0 | 7.6 | 16.2 | |
| 1974 | Lake Papaitonga | Aeolian | 51.5 | 19.7 | 6.8 | 13.2 | |
| 4342 | Mangahao Upper No 1 Reservior | Dam | 19.5 | 373.4 | 35.2 | 7.8 | |
| 4345 | Lake Horowhenua | Aeolian | 304.0 | 19.9 | 1.8 | 13.8 | 10 |
| 4358 | | Aeolian | 2.5 | 20.0 | 2.9 | 16.4 | |
| 4365 | | Aeolian | 1.9 | 20.0 | 2.9 | 16 | |
| 4380 | | | 10.0 | 11.3 | 0.0 | 16.8 | |
| 4486 | | Aeolian | 9.7 | 10.4 | 2.9 | 17 | |
| 4560 | | Dam | 1.9 | 290.7 | 26.2 | 14.8 | |
| 4913 | | Dam | 2.1 | 19.2 | 3.3 | 12.4 | |
| 4926 | Turitea Dams b | Dam | 11.4 | 185.3 | 27.1 | 8.2 | |
| 5008 | Lake Koputara | Aeolian | 9.4 | 10.0 | 2.9 | 17 | 4 |
| 5014 | Lake Kaikokopu | Aeolian | 14.7 | 10.2 | 3.0 | 17.2 | |

| | | | | | | | |
|---|---|---|---|---|---|---|---|
| 5042 | Pukepuke Lagoon | Aeolian | 17.9 | 10.2 | 3.0 | 18.4 | 2 |
| 5306 | Omanuka Lagoon | Aeolian | 11.0 | 28.9 | 3.4 | 16.4 | 4 |
| 5610 | | Dam | 1.6 | 119.6 | 21.5 | 17.8 | |
| 5955 | Rotoataha Lake | Riverine | 2.7 | 336.3 | 30.0 | 13.2 | |
| 13437 | Lake William | Aeolian | 6.8 | 105.8 | 11.8 | 16 | 2 |
| 13438 | Lake Bernard | Aeolian | 8.0 | 79.4 | 23.4 | 16 | |
| 13443 | Lake Vipan | Aeolian | 6.7 | 80.0 | 8.4 | 16.8 | |
| 13446 | Lake Heaton | Aeolian | 14.4 | 97.2 | 11.7 | 16.4 | |
| 13447 | Lake Dudding | Aeolian | 7.8 | 91.8 | 19.7 | 16.4 | 5 |
| 13456 | Lake Alice | Aeolian | 11.9 | 116.3 | 9.1 | 15.2 | 3 |
| 16901 | Lake Koitata | Aeolian | 9.6 | 18.0 | 3.6 | 40.4 | 4 |
| 16939 | Lake Waipu | Aeolian | 7.0 | 20.3 | 7.0 | 36.8 | 2 |
| 17014 | Lake Rotokauwau | Aeolian | 6.6 | 88.8 | 11.7 | 32.4 | |
| 17214 | Lake Kohata | Aeolian | 5.2 | 47.9 | 6.6 | 36 | 2 |
| 17286 | Lake Poroa | Riverine | 7.1 | 357.6 | 27.1 | 28.8 | |
| 17363 | Lake Herbert | Aeolian | 4.7 | 95.5 | 9.3 | 16.4 | 3 |
| 18023 | Marron Reservoirs a | Dam | 12.3 | 236.8 | 22.1 | 14.8 | |
| 18027 | Marron Reservoirs b | Dam | 6.1 | 245.1 | 21.1 | 14.6 | |
| 18606 | | Peat | 1.5 | 820.0 | 15.1 | 25.2 | |
| 18608 | | Volcanic | 7.2 | 697.5 | 17.8 | 16.8 | |
| 18609 | Lake Rotokuru | Volcanic | 5.8 | 714.0 | 9.9 | 17 | |
| 18610 | Lake Moawhango | Dam | 485.8 | 851.8 | 47.7 | 16.6 | |
| 18933 | Lake Pauri | Aeolian | 19.2 | 57.6 | 7.9 | 17.6 | 6 |
| 18934 | Lake Wiritoa | Aeolian | 21.8 | 51.1 | 28.9 | 36 | 6 |
| 18936 | Kaitoke Lake | Aeolian | 25.3 | 15.8 | 14.0 | 36 | |
| 18951 | Lake Westmere | Aeolian | 8.1 | 96.2 | 23.4 | 35.6 | 3 |
| 18957 | Lake Virginia | Aeolian | 7.0 | 59.4 | 16.2 | 34.4 | |
| 19140 | | Peat | 3.8 | 114.5 | 23.9 | 30.8 | |
| 19621 | Lake Ngaruru | Riverine | 7.8 | 157.8 | 24.1 | 14.4 | |
| 19624 | Lake Namunamu | Riverine | 12.9 | 200.2 | 22.8 | 14.6 | |
| 19921 | | Dam | 2.2 | 280.3 | 9.7 | 26.4 | |
| 20094 | Lake Maungarataiti | Landslide | 4.1 | 239.3 | 26.0 | 14.4 | |
| 20096 | Lake Maungaratanui | Landslide | 6.3 | 260.8 | 23.8 | 15 | |
| 20693 | | | 2.8 | 648.4 | 0.0 | 14.4 | |
| 20720 | | Volcanic | 2.9 | 574.4 | 17.6 | 24.8 | |

| | | | | | | | |
|---|---|---|---|---|---|---|---|
| 20741 | Lake Hawkes | Landslide | 3.1 | 392.7 | 23.9 | 30.8 | |
| 21383 | Lake Otamangakau | Aeolian | 156.3 | 607.3 | 32.6 | 15.2 | |
| 31847 | | Dam | 3.2 | 378.4 | 12.2 | 16.8 | |
| 34051 | Lake Colenso (Kokopunui) | Landslide | 3.5 | 721.1 | 18.4 | 11.2 | |

# Appendix B

## Maps of lakes visible from space at 30 m pixel resolution

Maps of 57 lakes with open water areas large enough to accommodate 30 m pixels.

Left panel: Closeup of the lake with outlines provided in the FENZ geodatabase. The reference circles have diameters of 50 and 400 m respectively and are placed at the geometric center of each lake.

Due to the scale, some figures do not show the larger circle. Furthermore, due to the irregular shape of some lakes, the geometric center may not be a good location for data retrieval.

Grid spacing is 30 m. Right panel: Lake and catchment outlines as provided in the FENZ geodatabase on a Landsat 8 OLI image.

Lake ID: 476 Lake Name: Tokomaru No 3 Reservoir

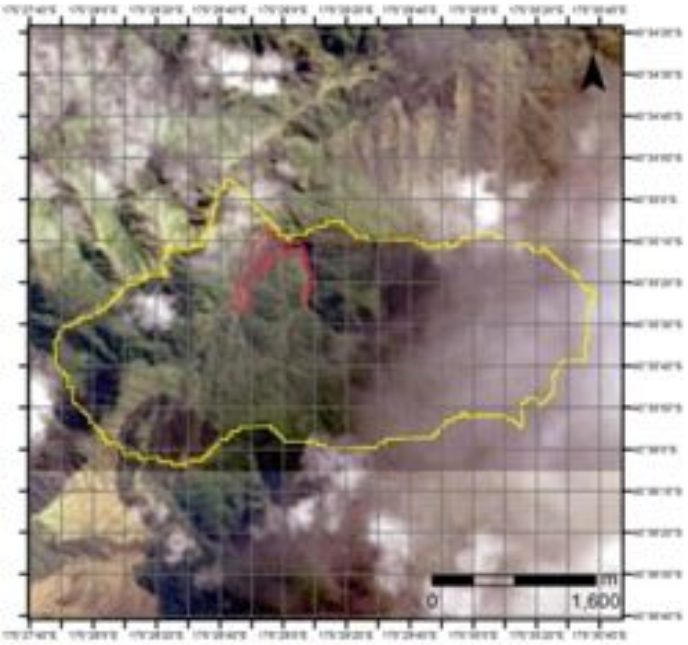


Lake ID: 869 Lake Name:

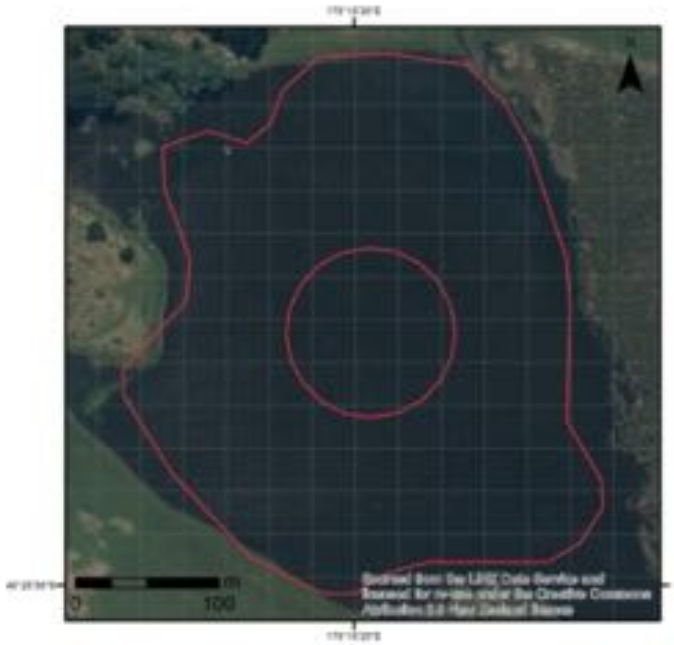


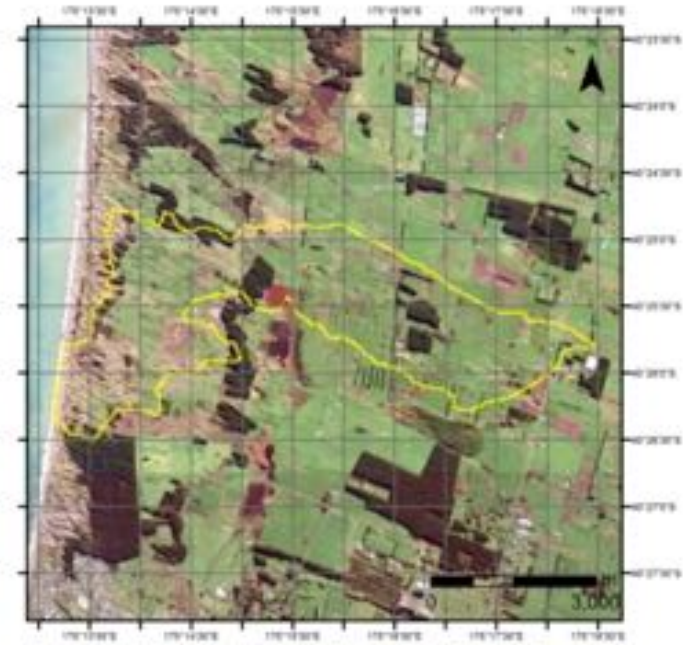

Lake ID: 871

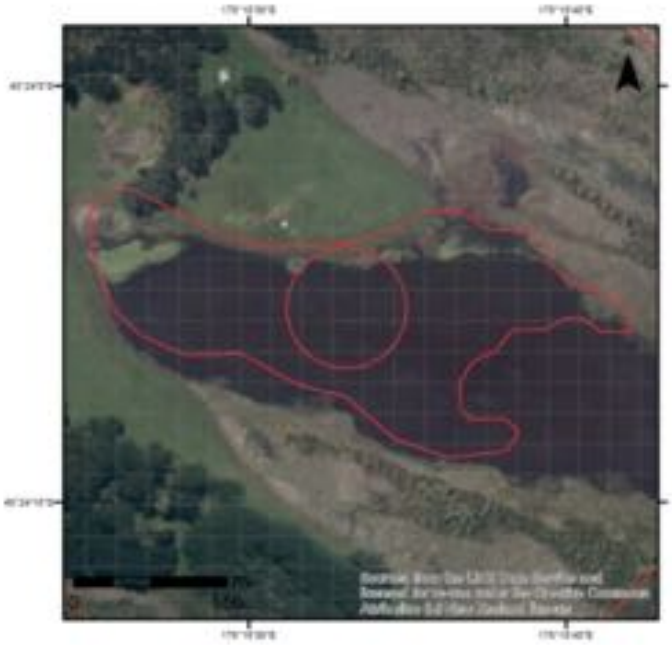

Lake Name:

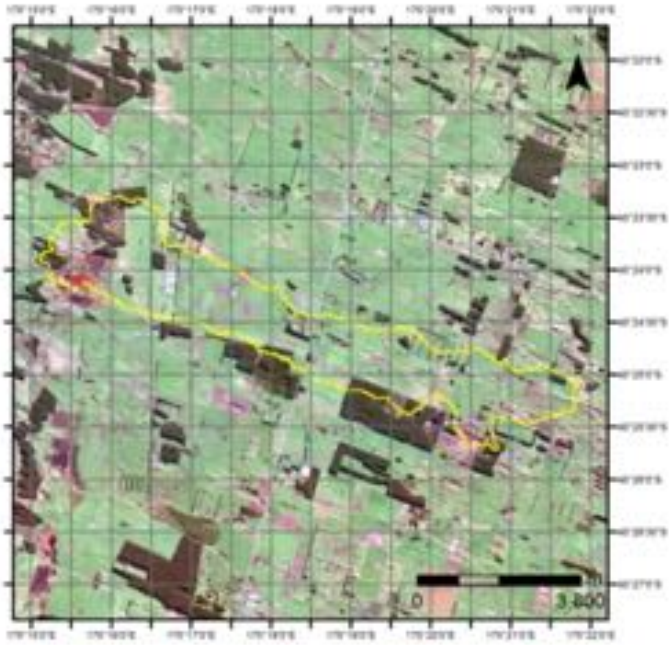

Lake ID: 877

Lake Name:

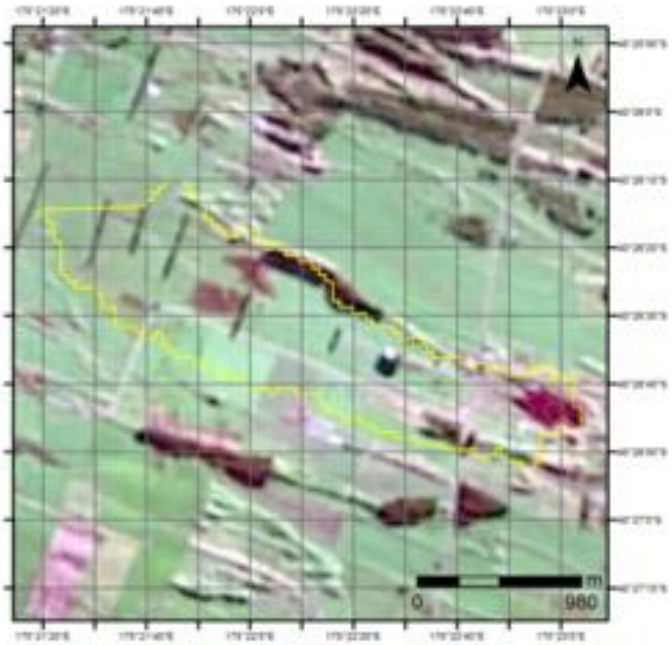

Lake ID: 1962

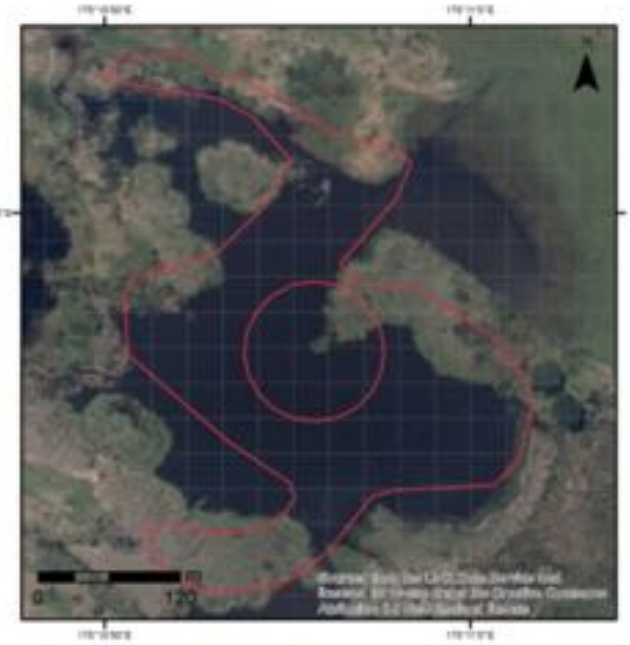


Lake Name:

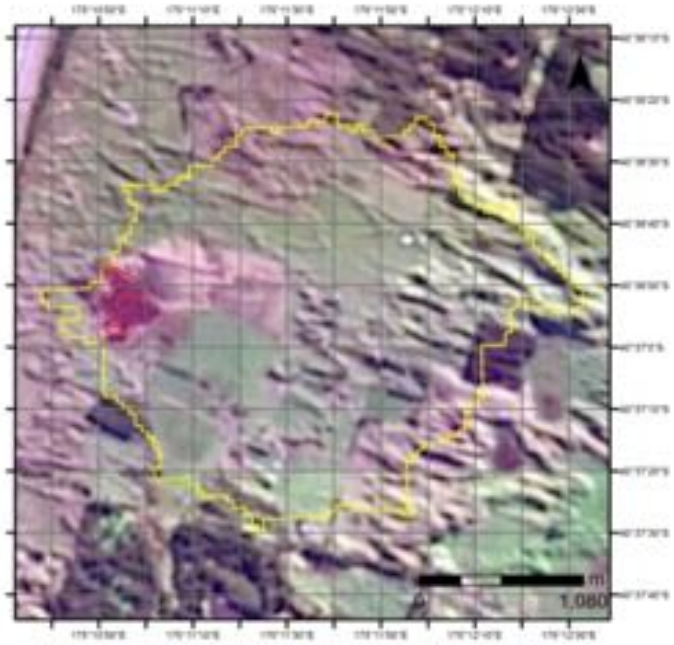


Lake ID: 1972

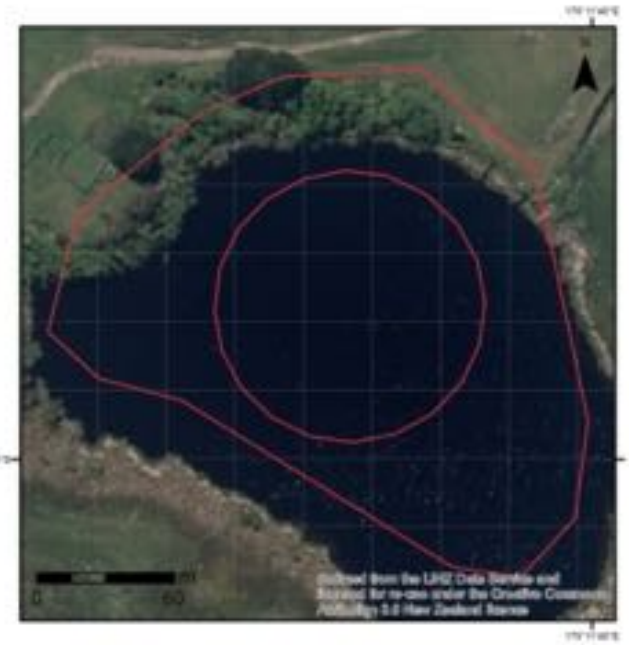


Lake Name:

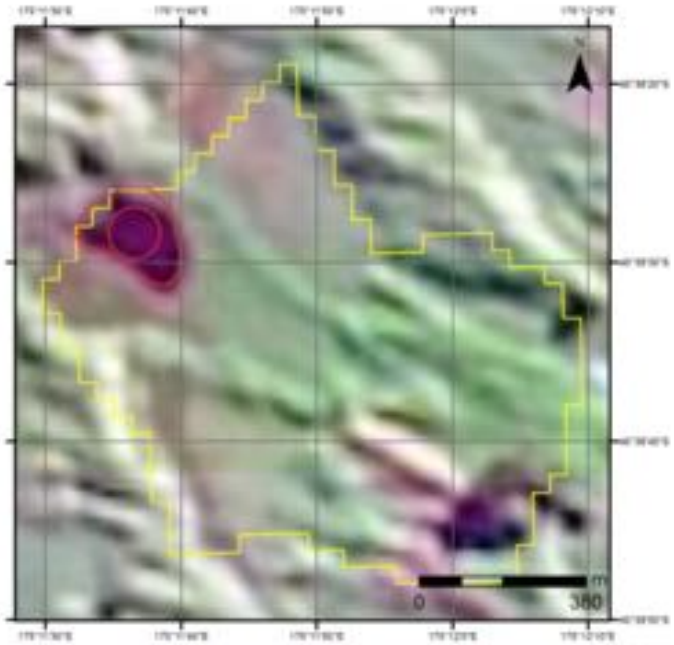

Lake ID: 1974 Lake Name: Lake Papaitonga

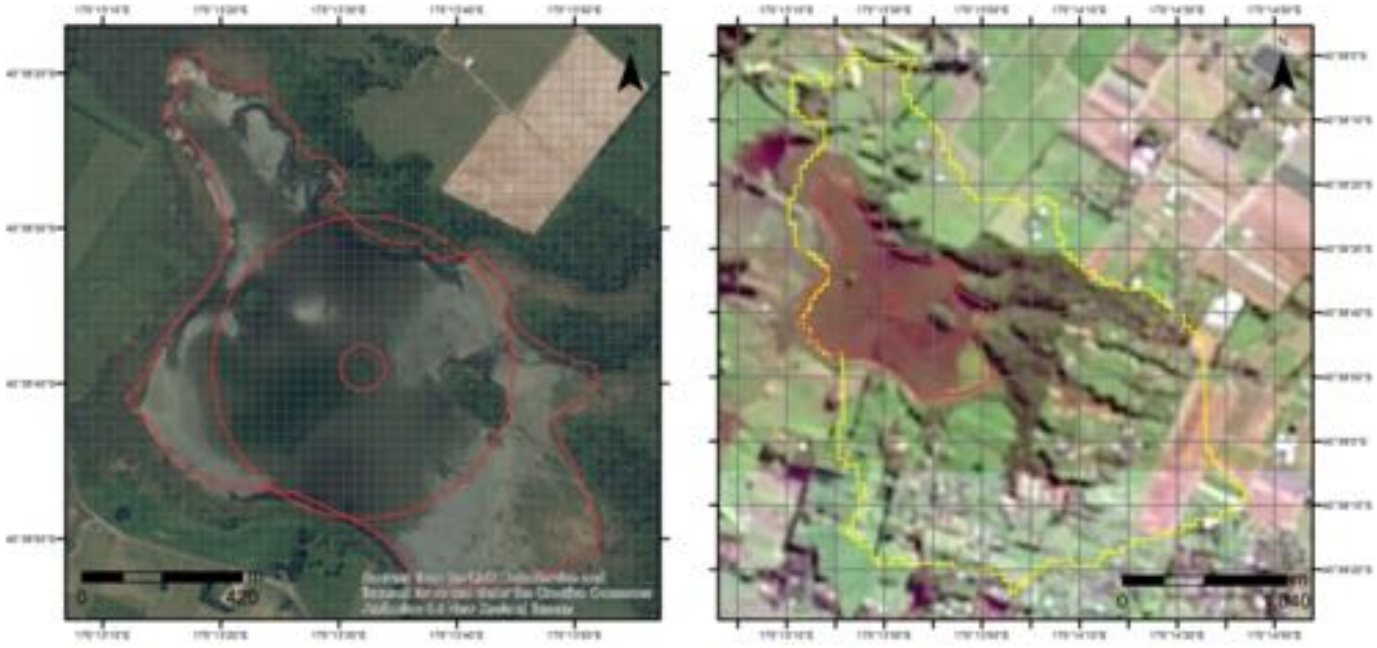

Lake ID: 4342 Lake Name: Mangahao Upper No 1 Reservior

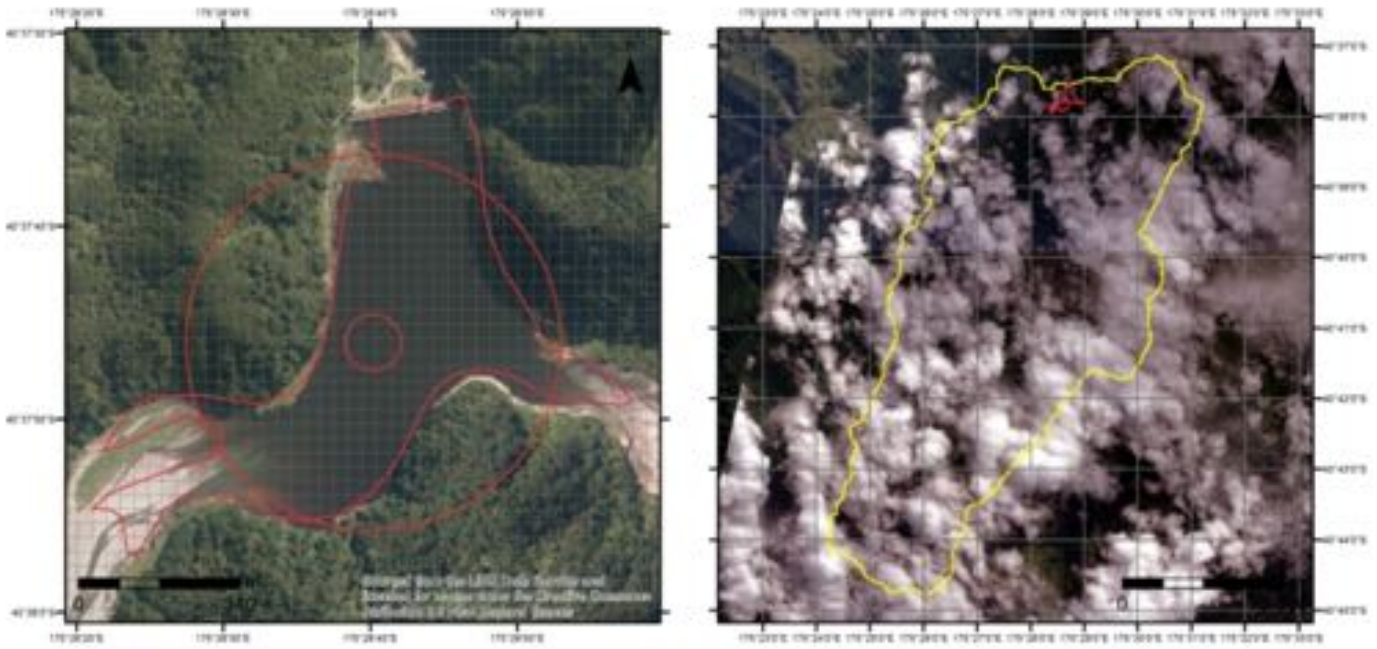

Lake ID: 4345 Lake Name: Lake Horowhenua


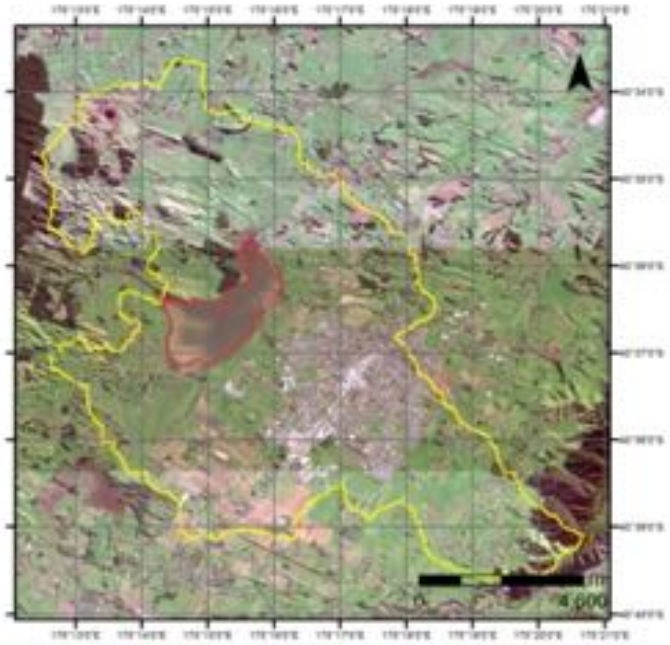


Lake ID: 4358 Lake Name:

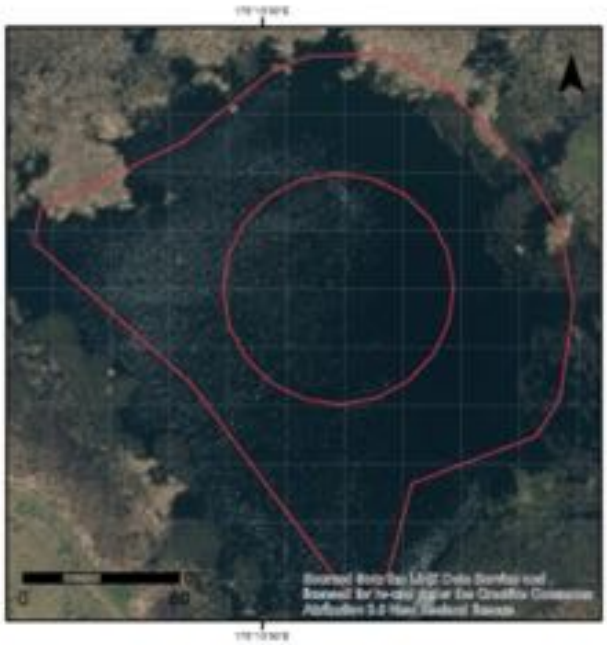


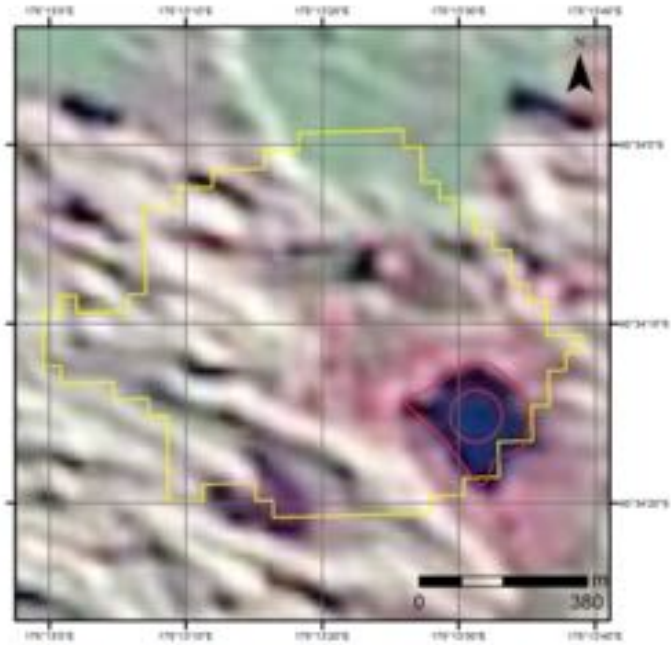

Lake ID: 4365

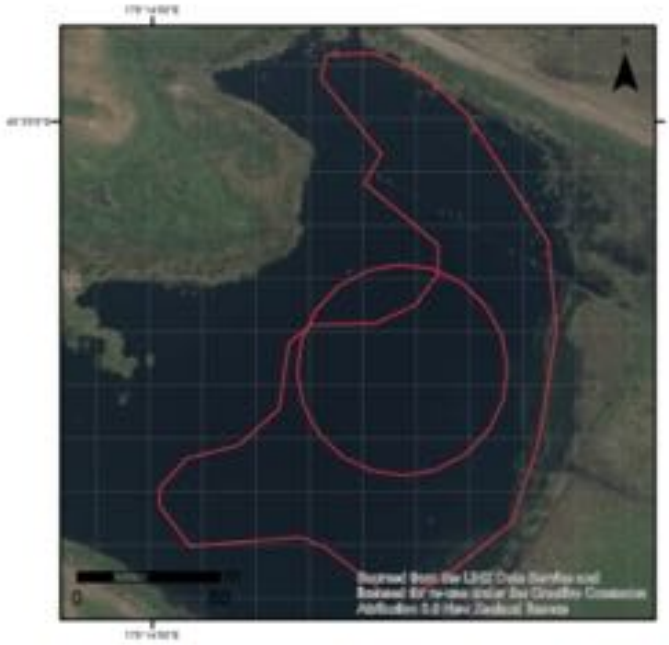

Lake Name:

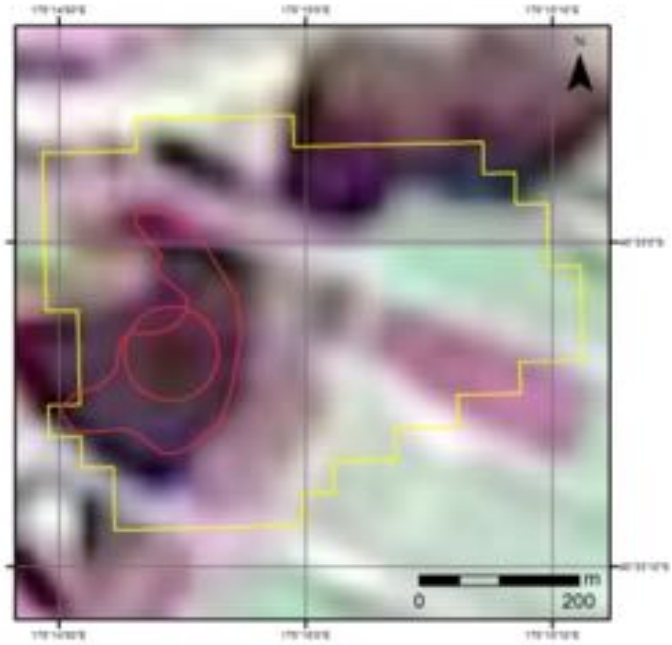


Lake ID: 4380

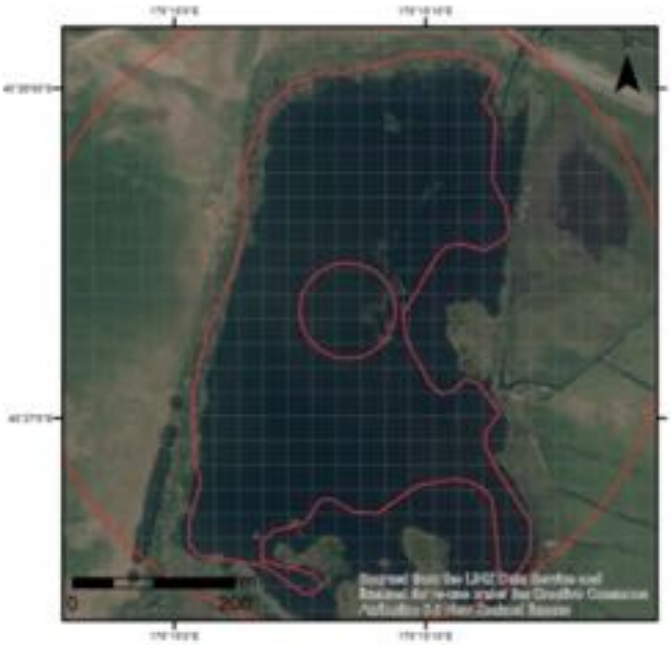

Lake Name:

Lake ID: 4486

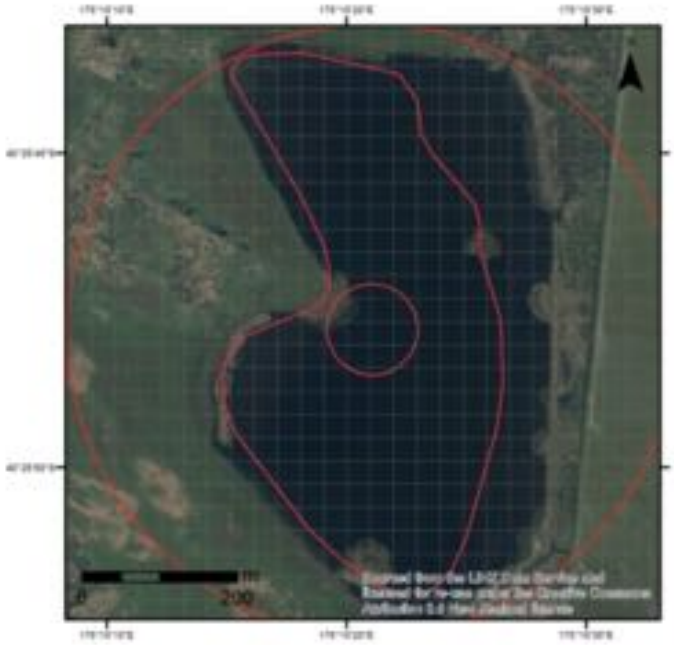


Lake Name:

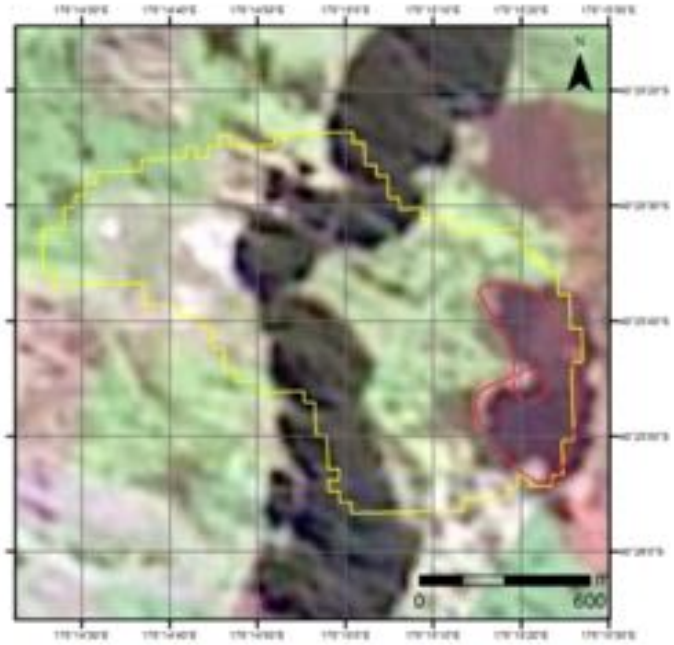


Lake ID: 4560

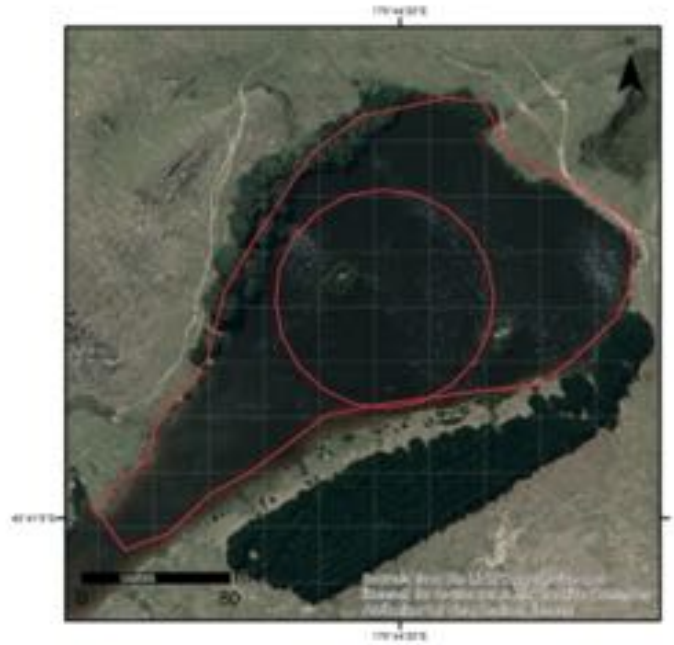


Lake Name:

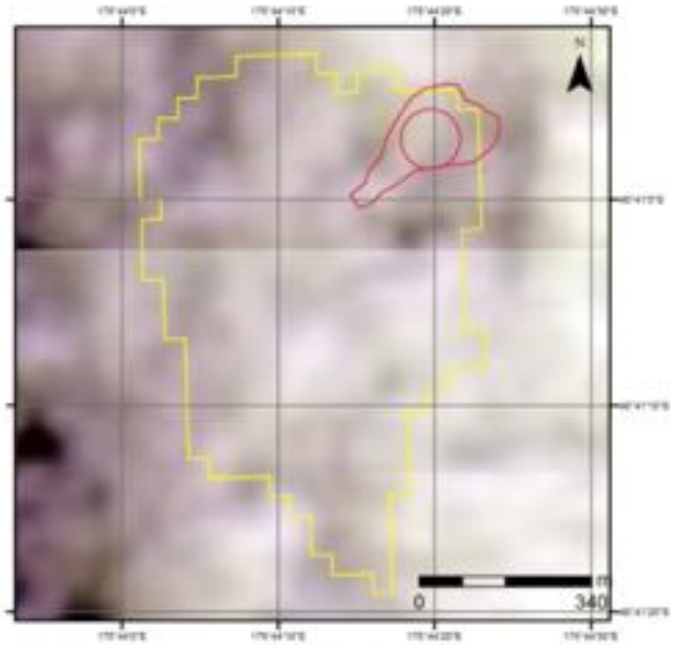

Lake ID: 4913


Lake Name:

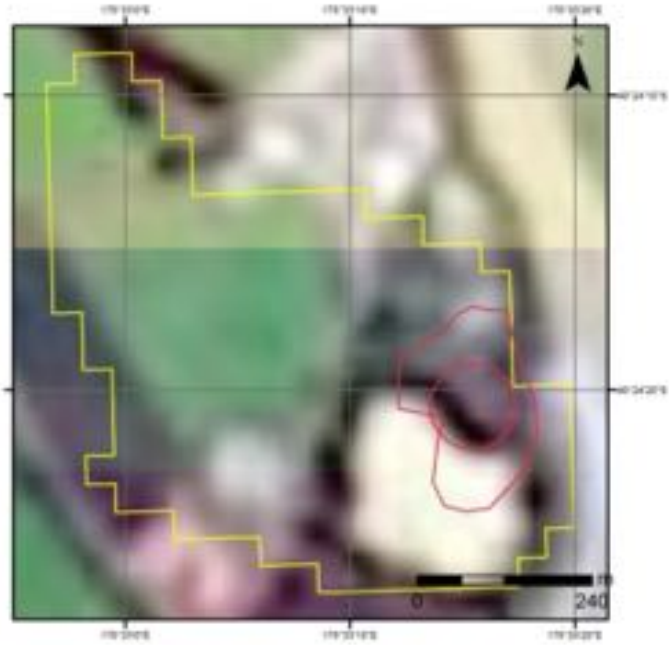


Lake ID: 4926

Lake Name: Turitea Dams b

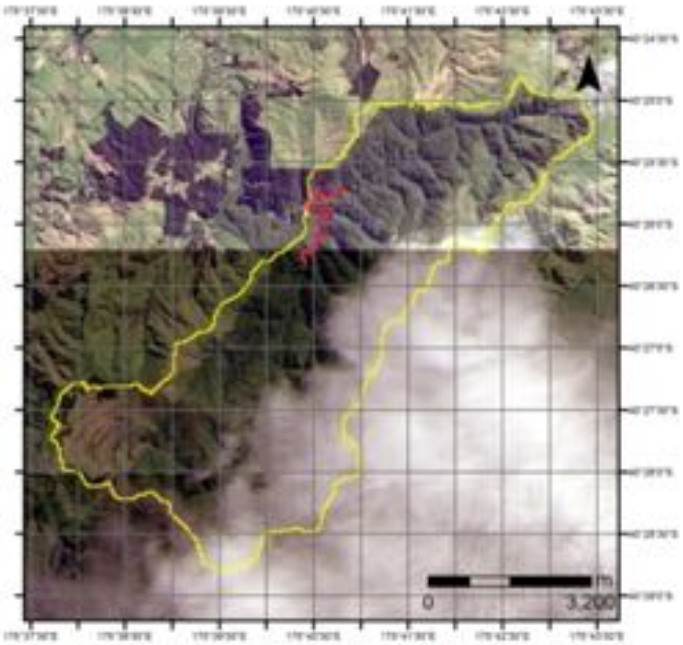

Lake ID: 5008 Lake Name: Lake Koputara

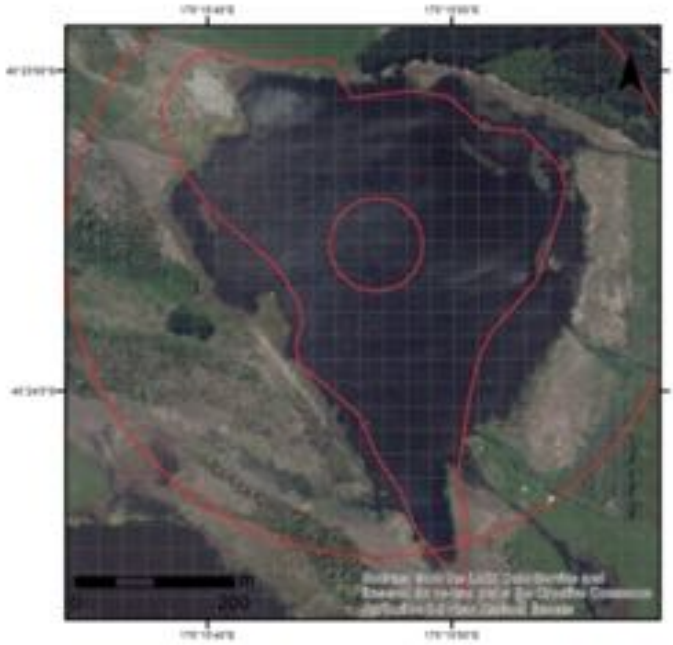

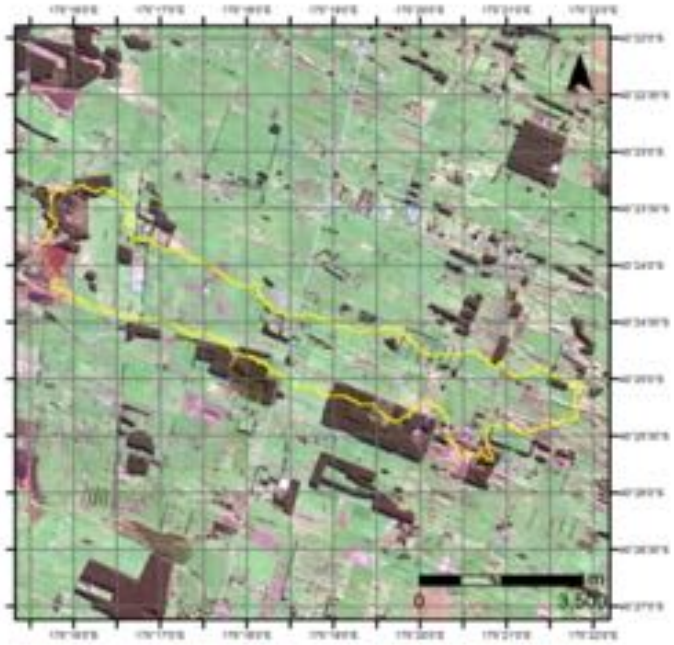

Lake ID: 5014 Lake Name: Lake Kaikokopu

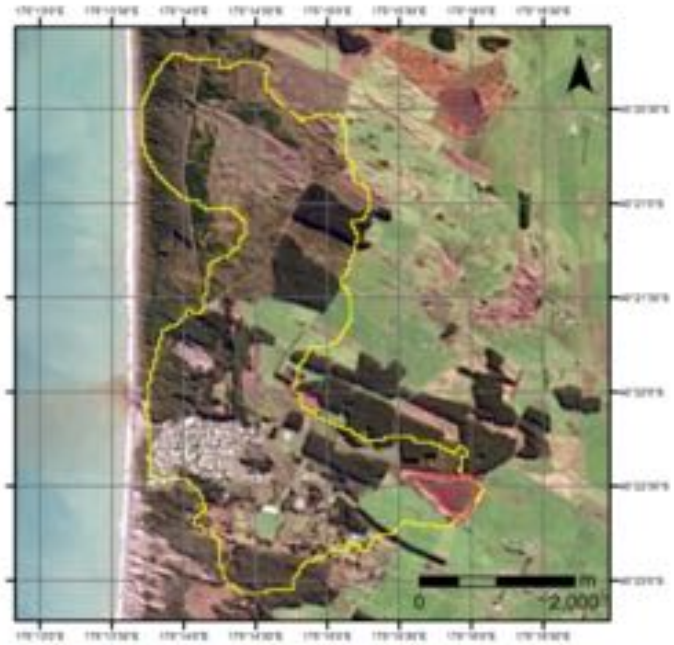

Lake ID: 5042 Lake Name: Pukepuke Lagoon

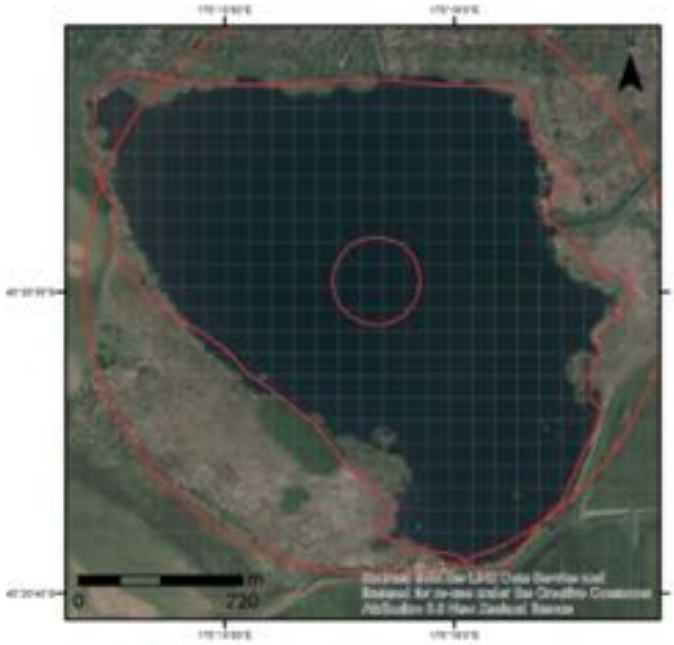


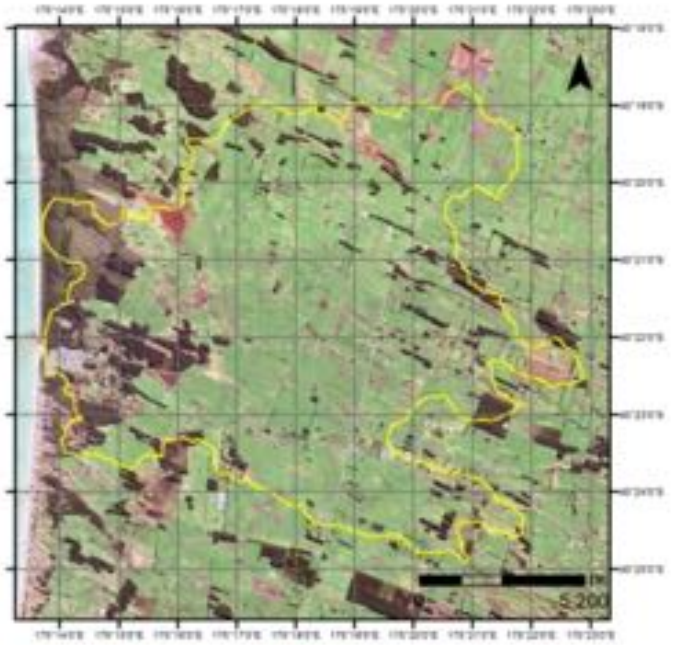


Lake ID: 5306 Lake Name: Omanuka Lagoon

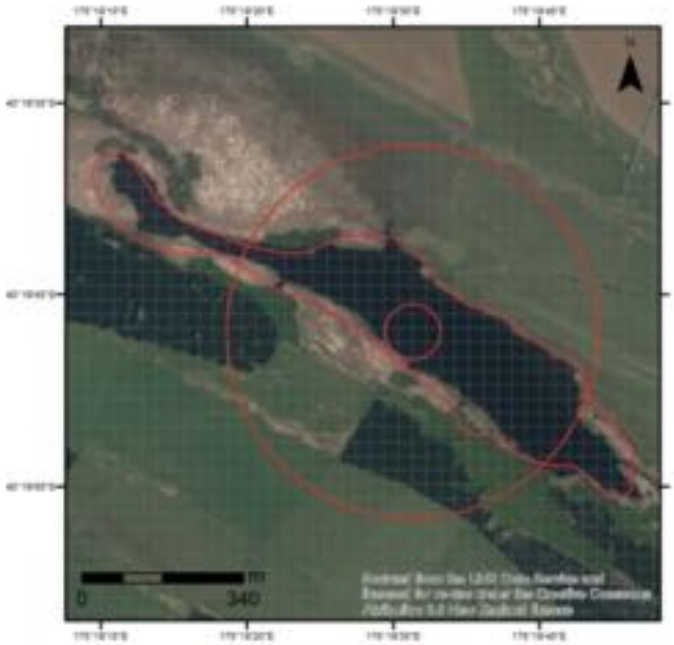


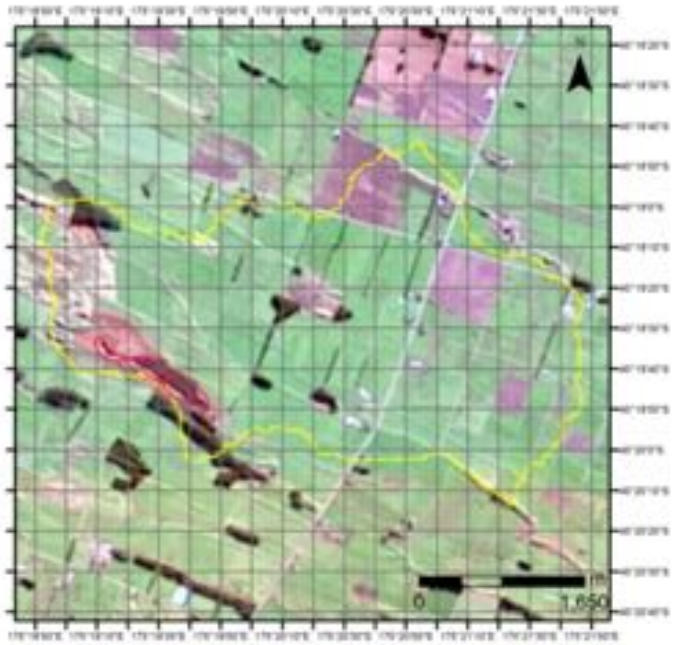

Lake ID: 5610

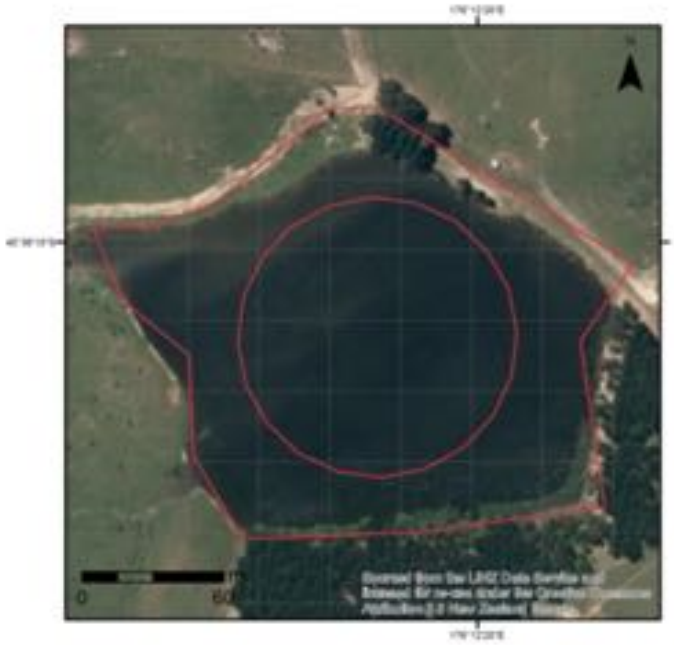

Lake Name:

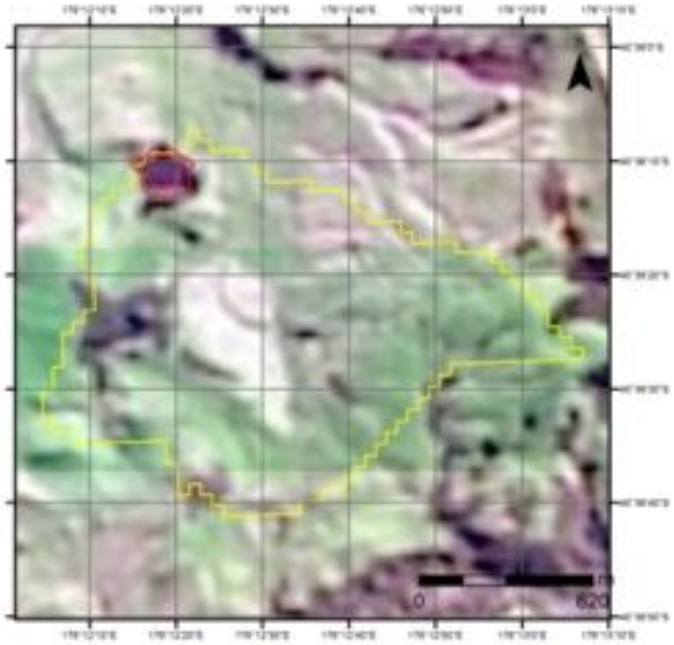

Lake ID: 5955

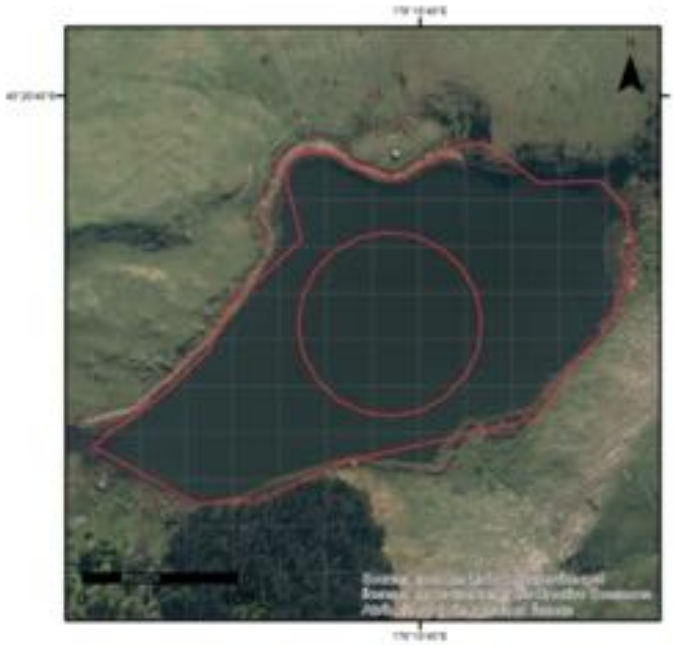

Lake Name: Rotoataha Lake

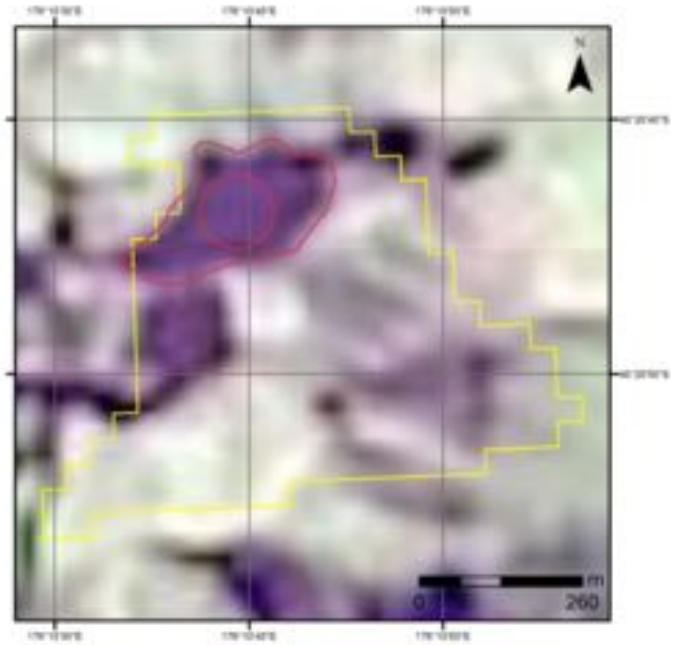

Lake ID: 13437 Lake Name: Lake William

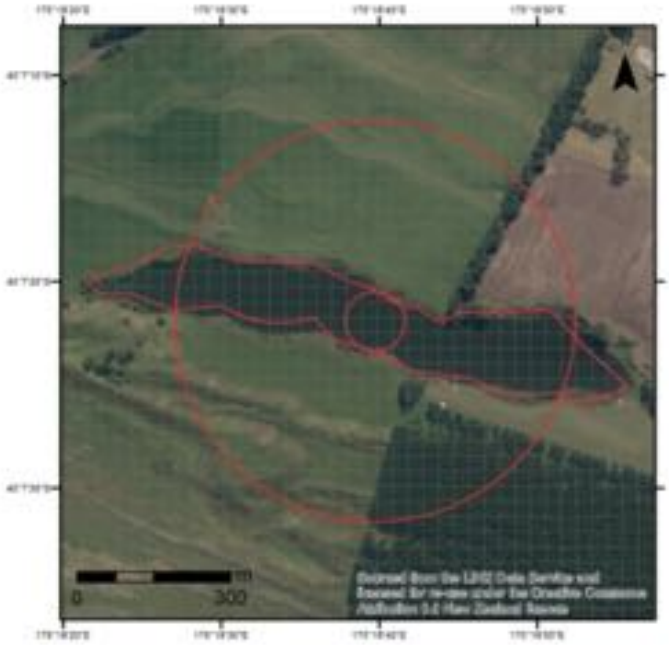


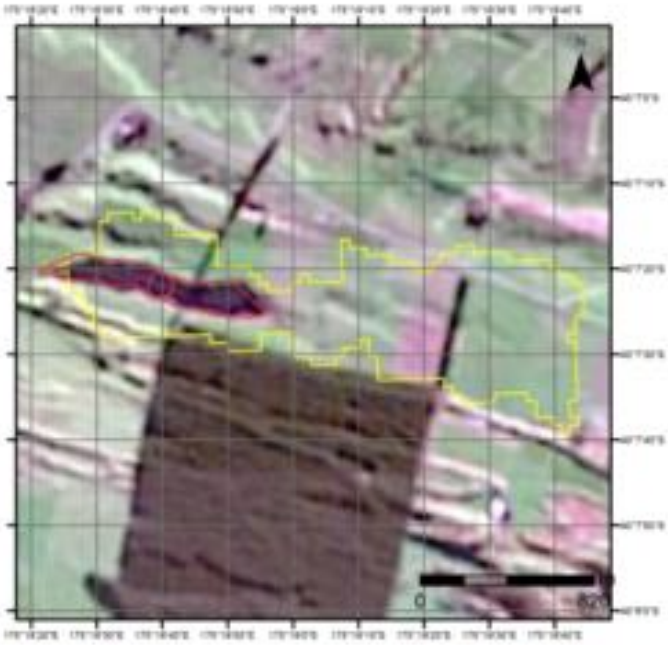


Lake ID: 13438 Lake Name: Lake Bernard

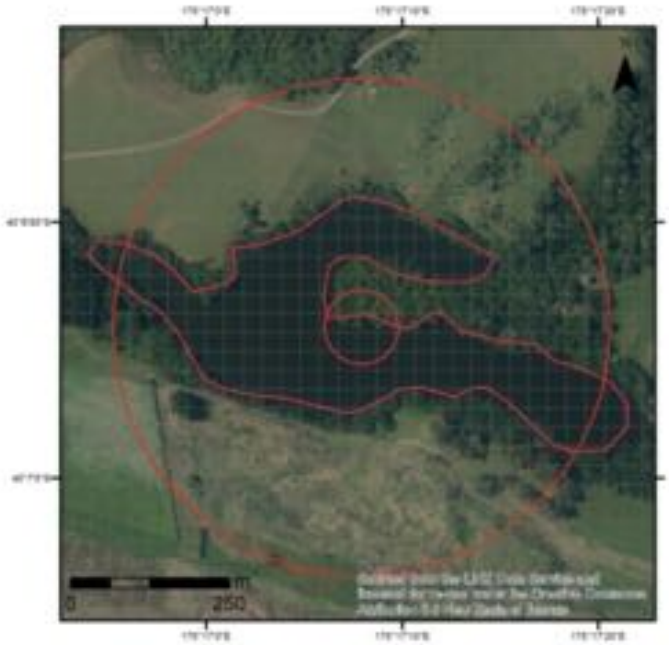


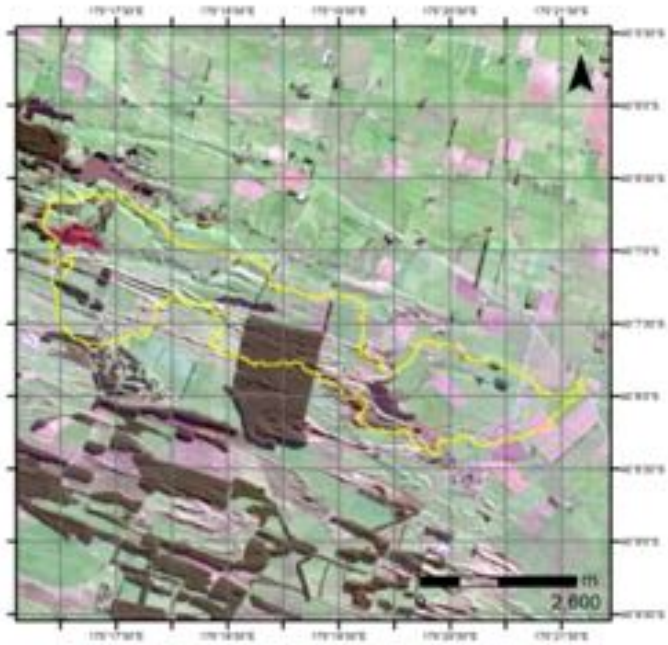

Lake ID: 13443 Lake Name: Lake Vipan

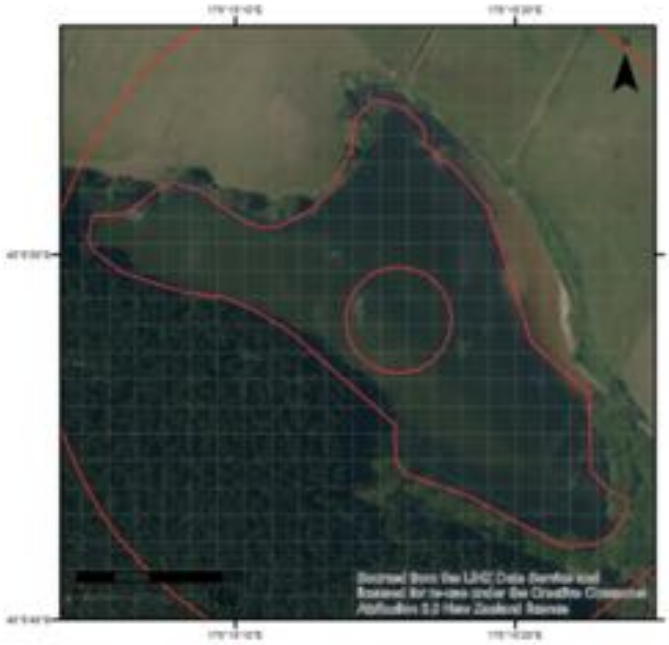

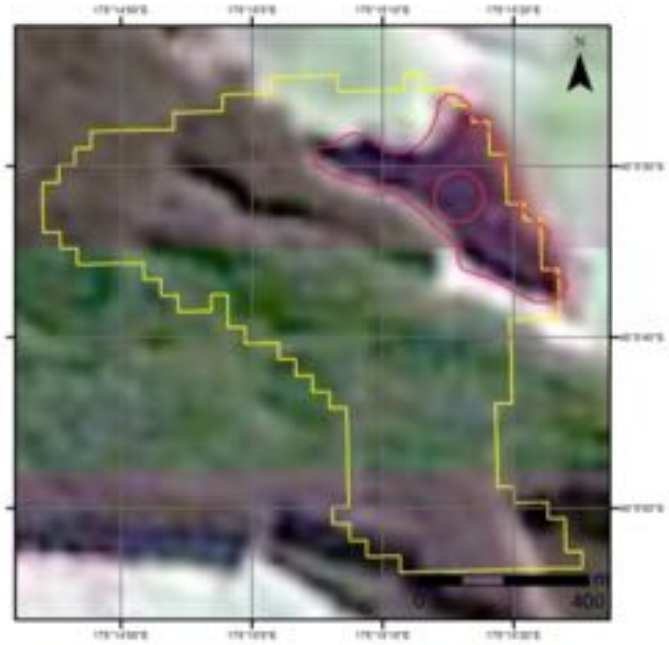


Lake ID: 13446 Lake Name: Lake Heaton


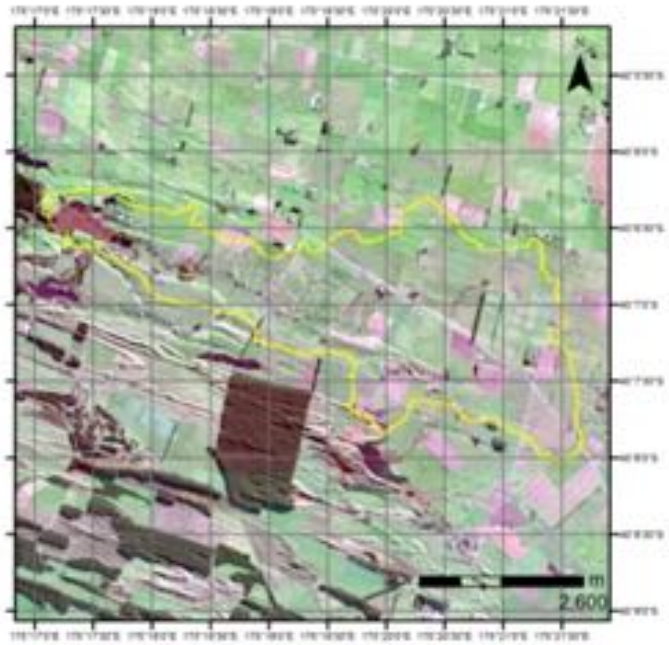

Lake ID: 13447 Lake Name: Lake Dudding

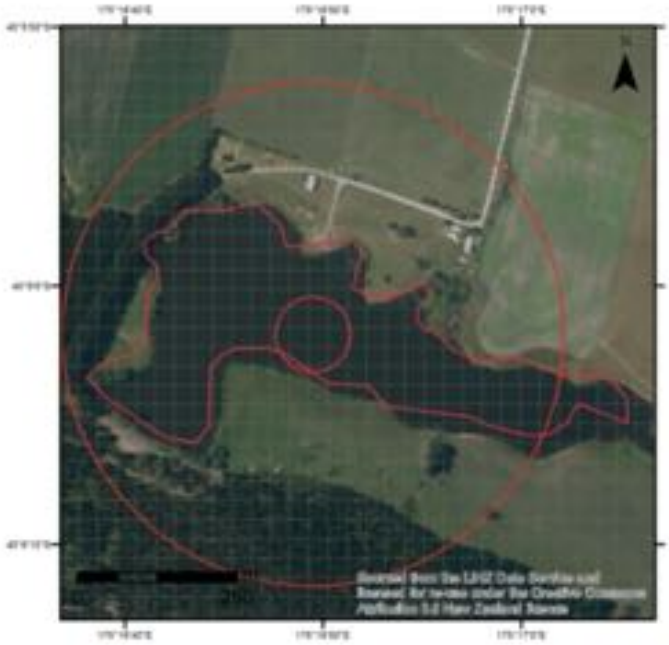

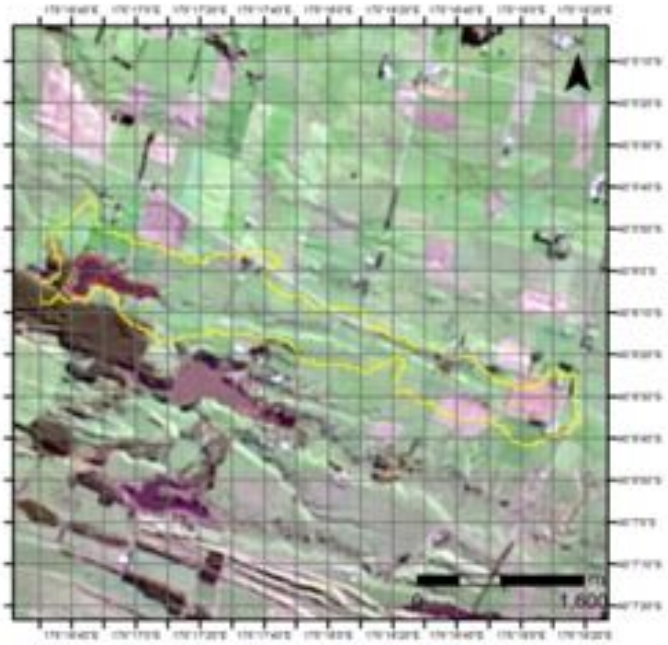


Lake ID: 13456 Lake Name: Lake Alice

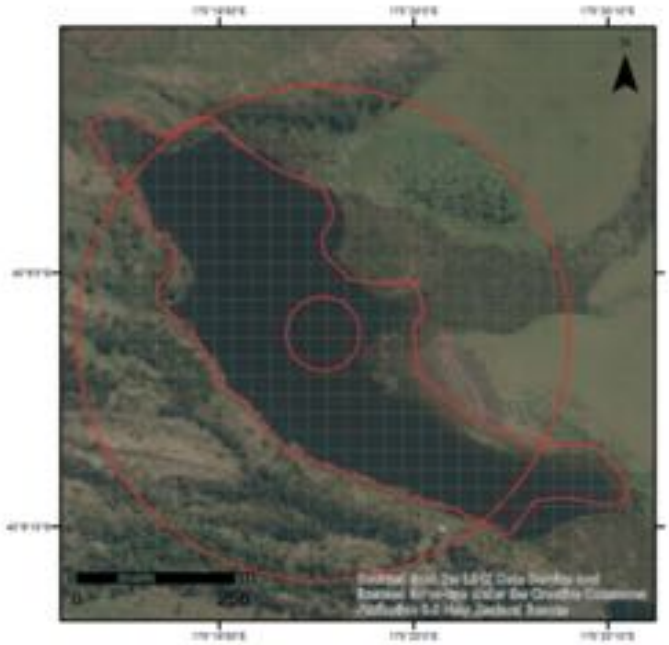

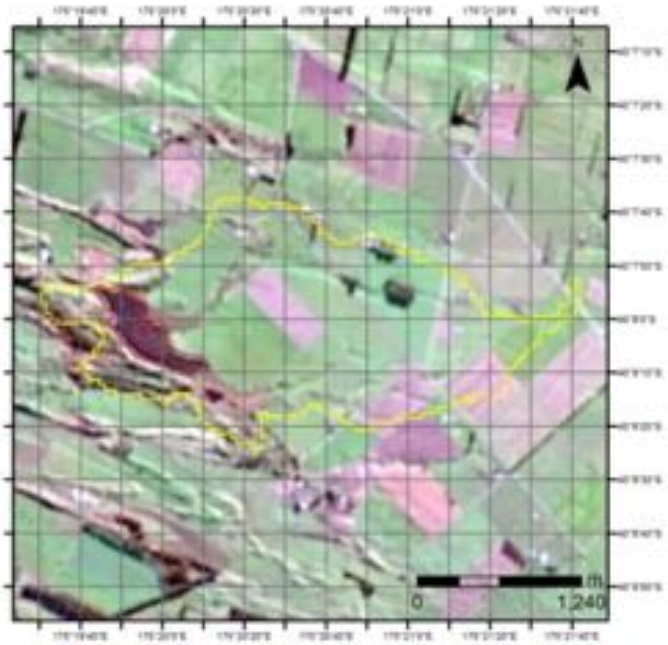

Lake ID: 16901 Lake Name: Lake Koitata

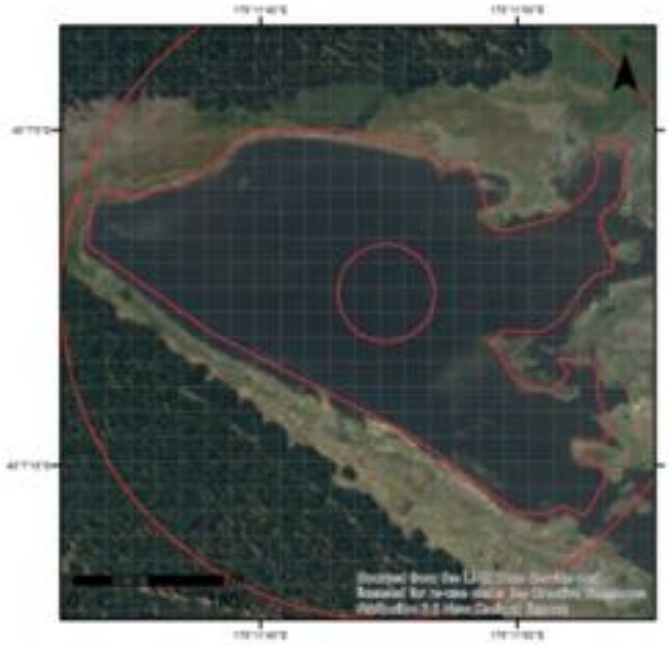

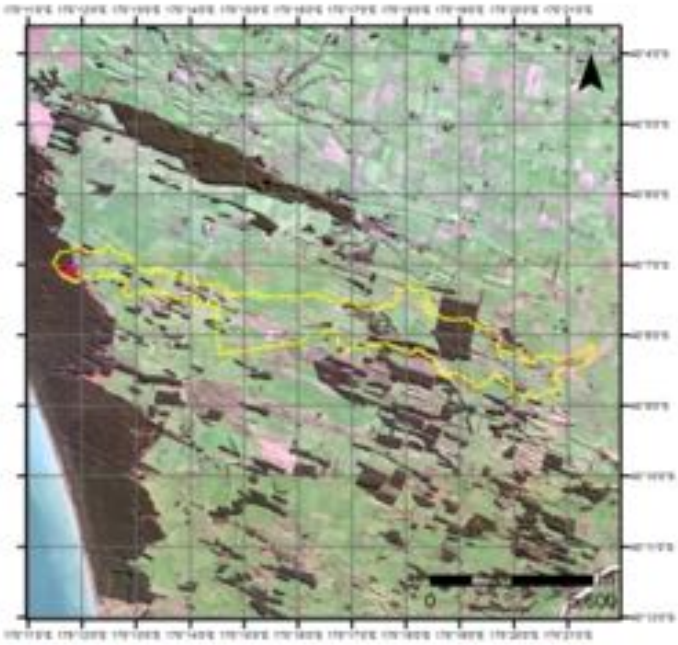

Lake ID: 16939 Lake Name: Lake Waipu

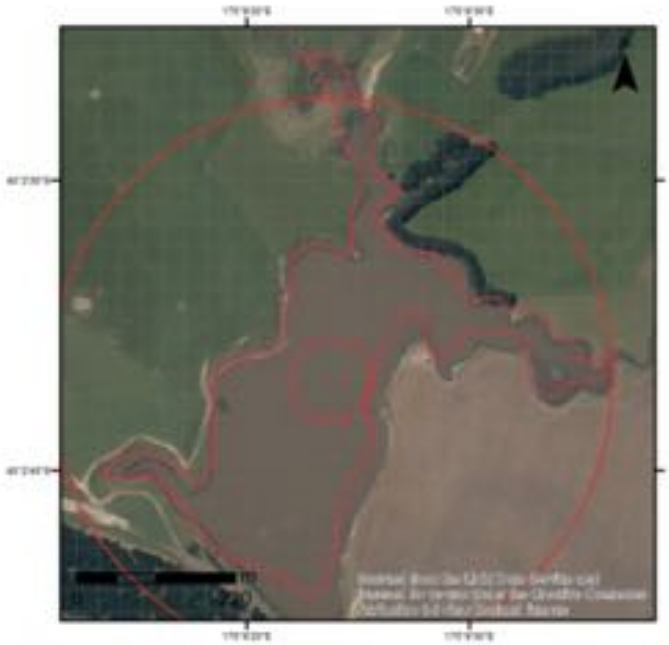

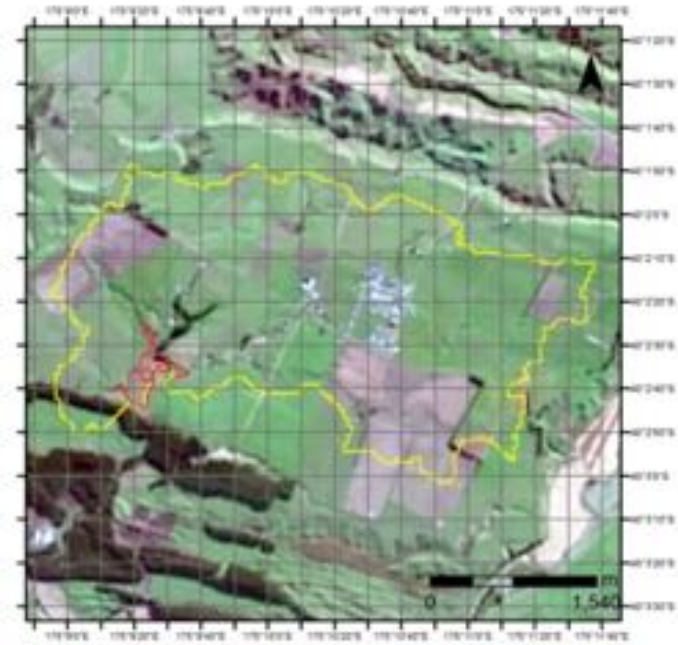

Lake ID: 17014 Lake Name: Lake Rotokauwau

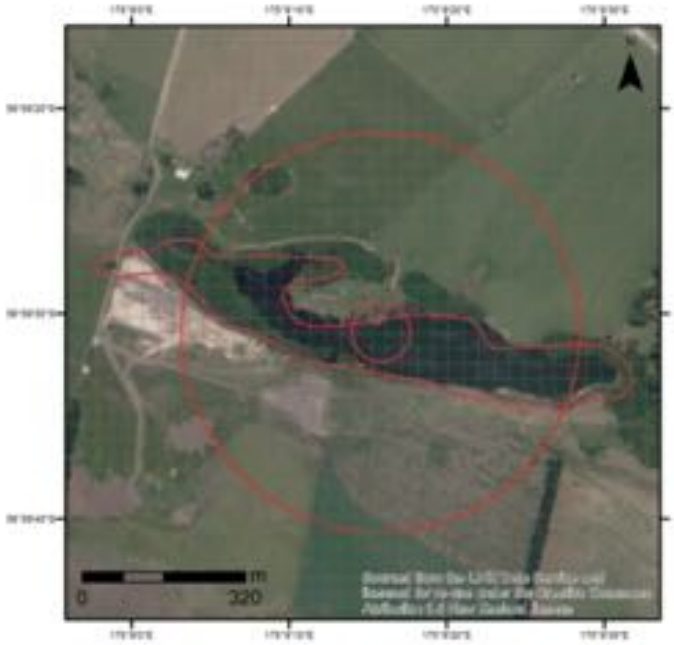


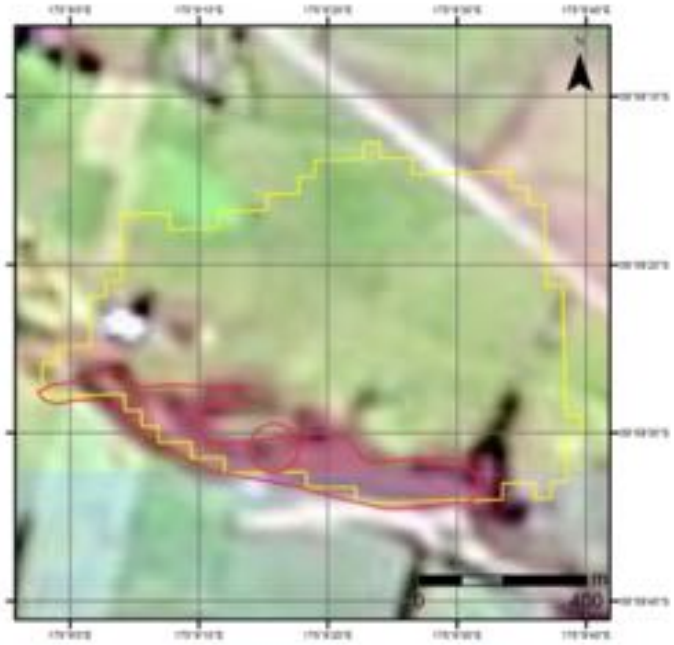


Lake ID: 17214 Lake Name: Lake Kohata

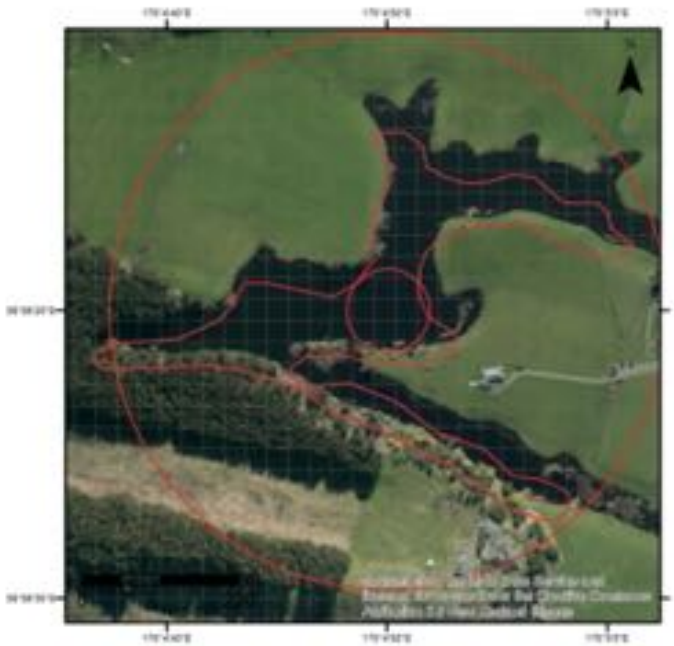

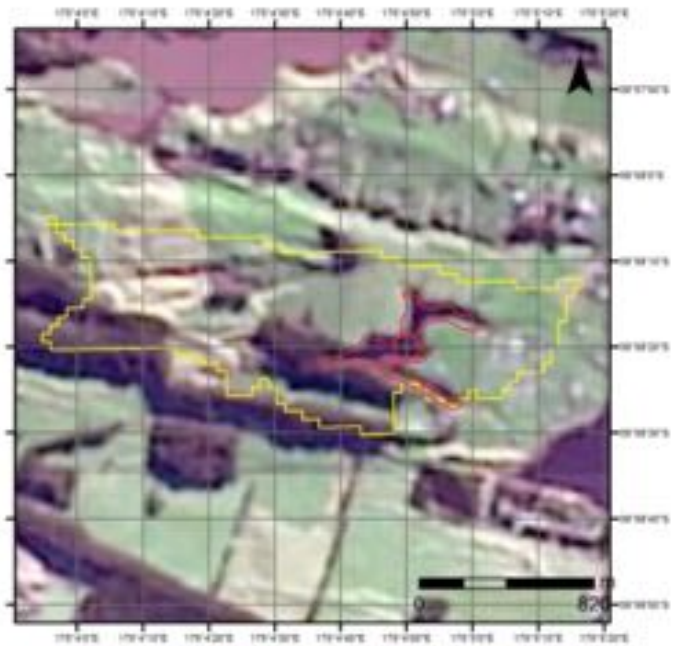

Lake ID: 17286

Lake Name: Lake Poroa


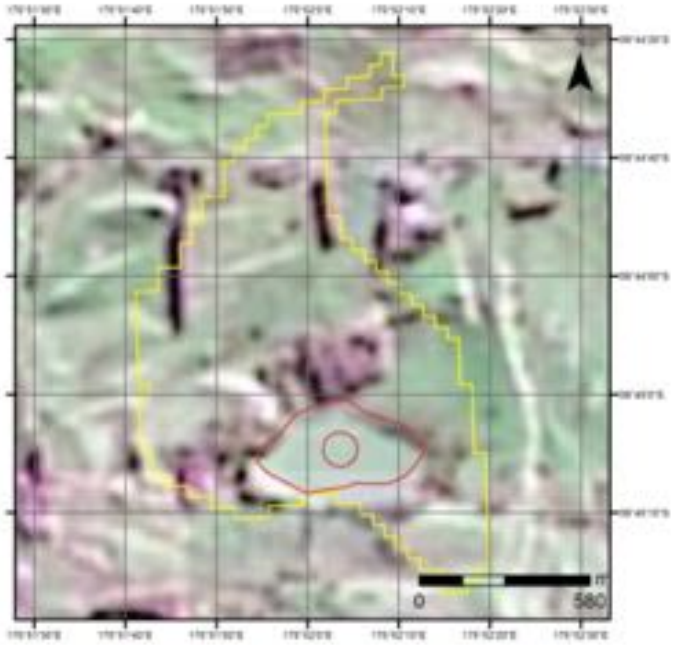


Lake ID: 17363

Lake Name: Lake Herbert


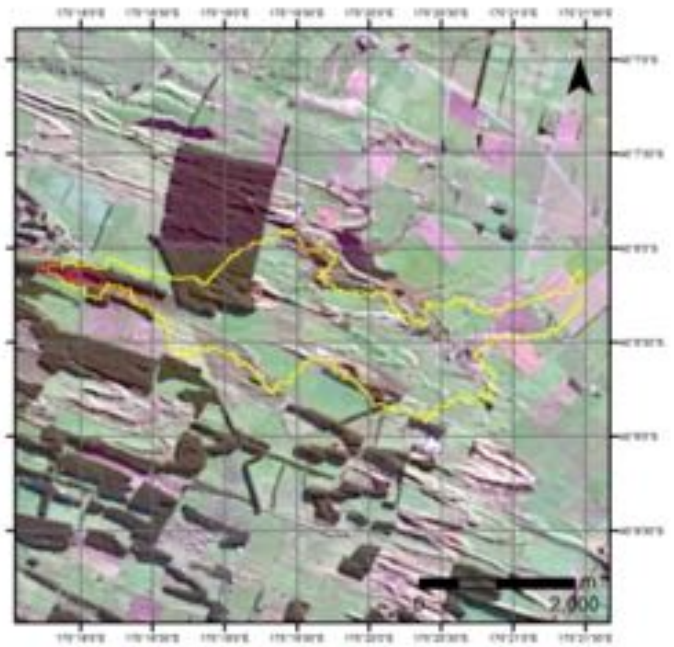

Lake ID: 18023 Lake Name: Marron Reservoirs a

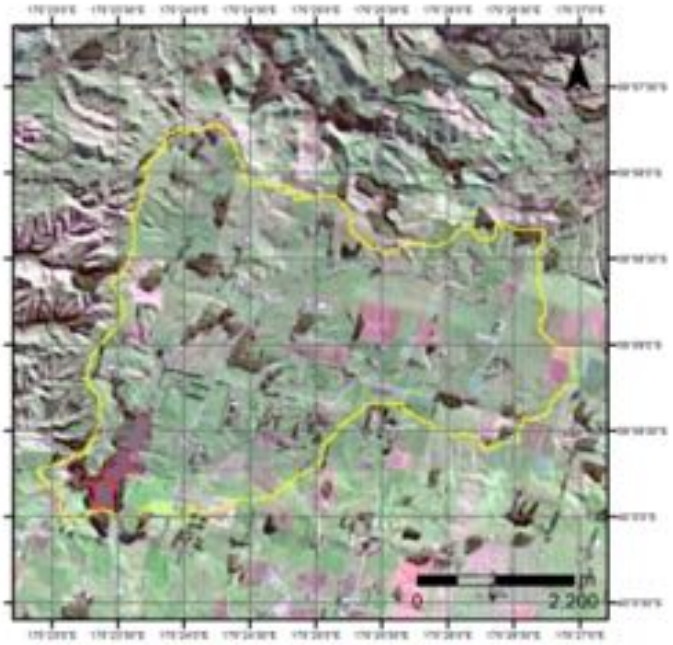

Lake ID: 18027 Lake Name: Marron Reservoirs b

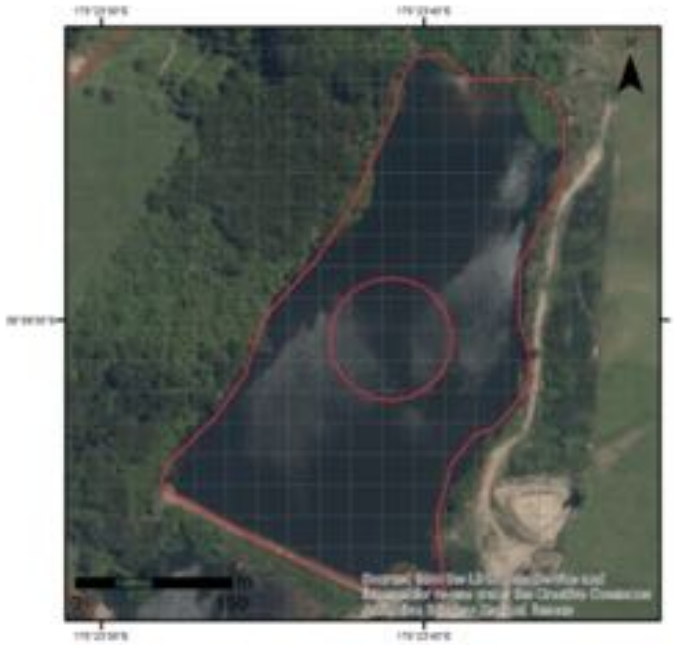

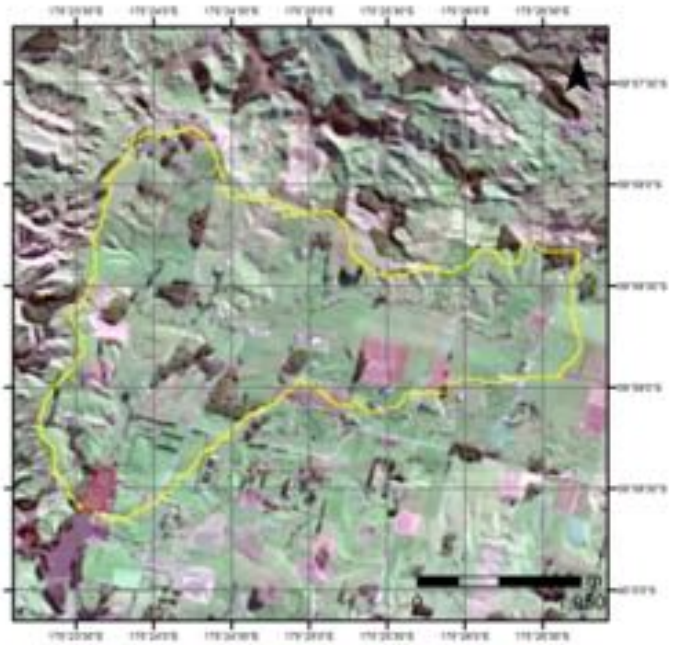

Lake ID: 18606

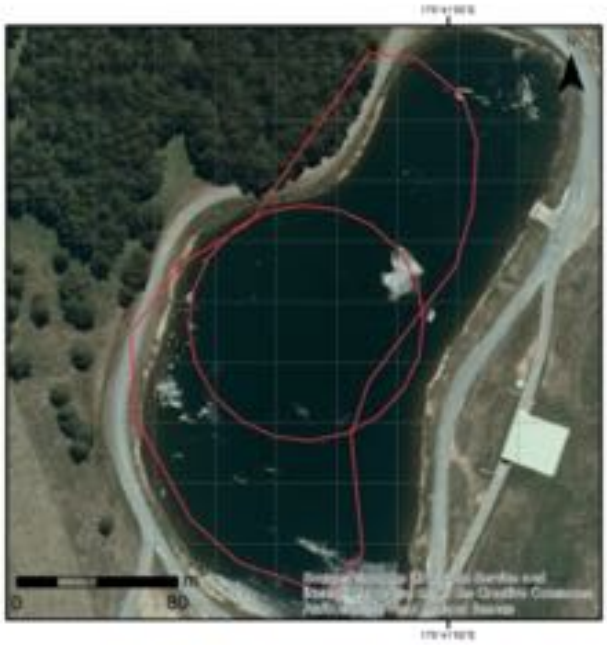


Lake Name:

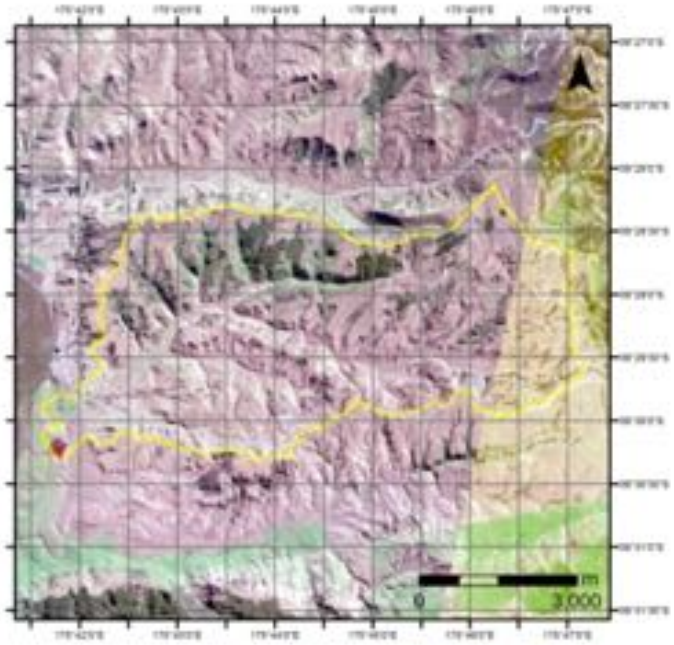


Lake ID: 18608

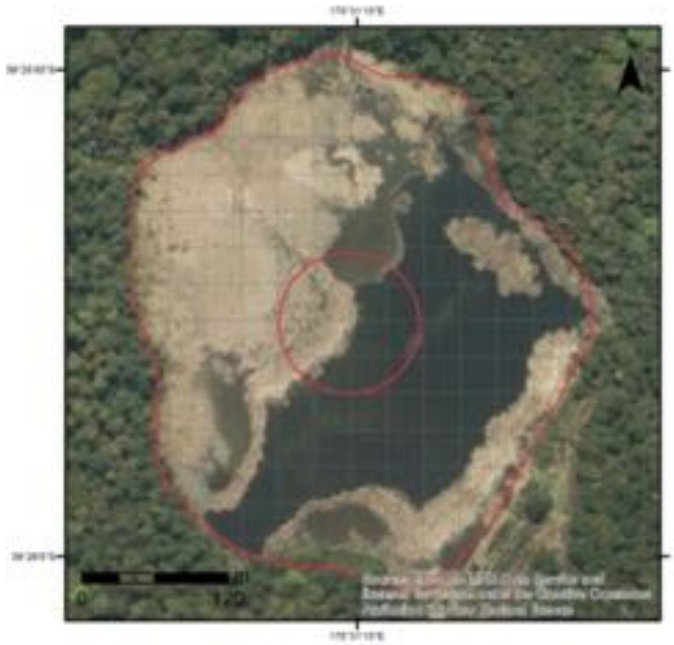


Lake Name:

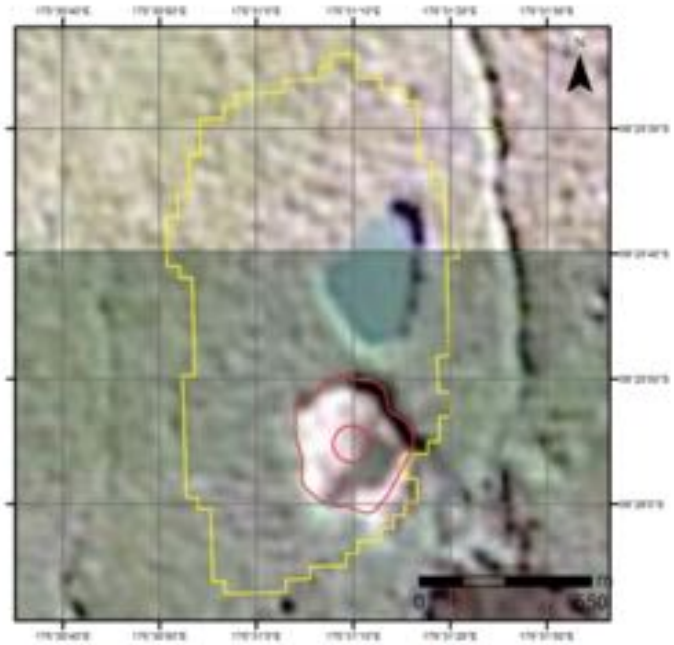

Lake ID: 18609 Lake Name: Lake Rotokuru

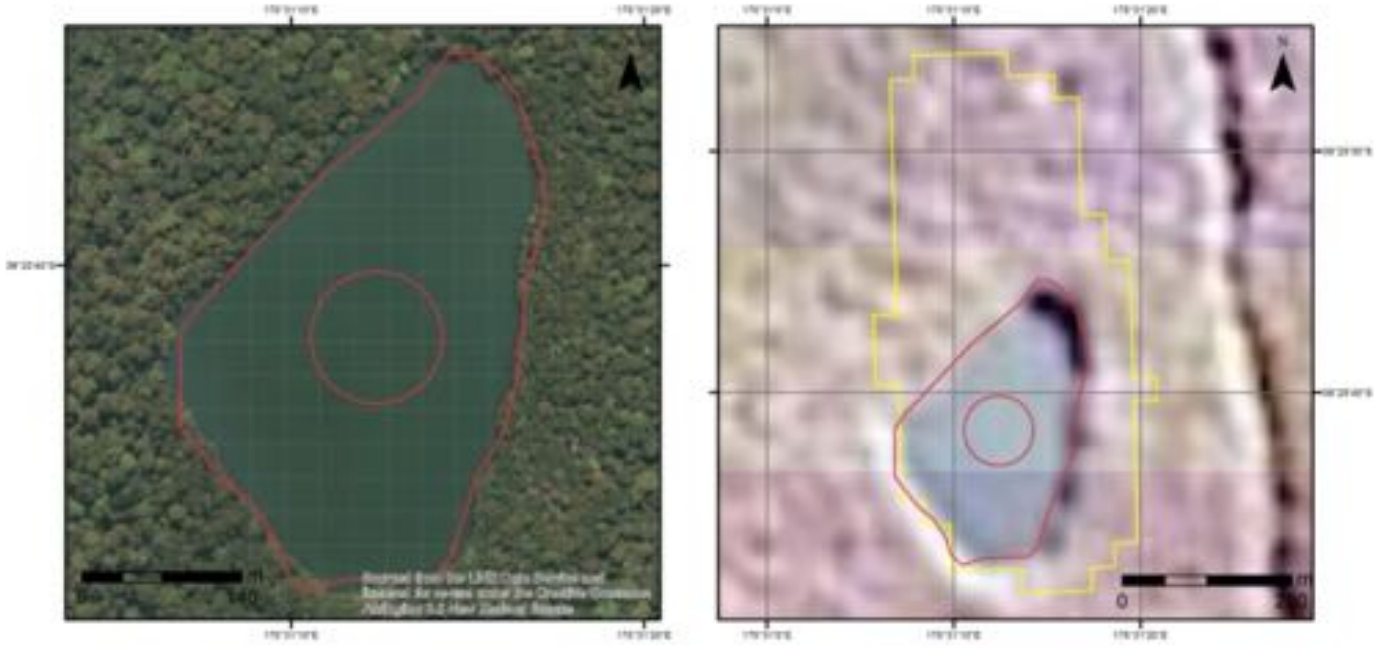

Lake ID: 18610 Lake Name: Lake Moawhango

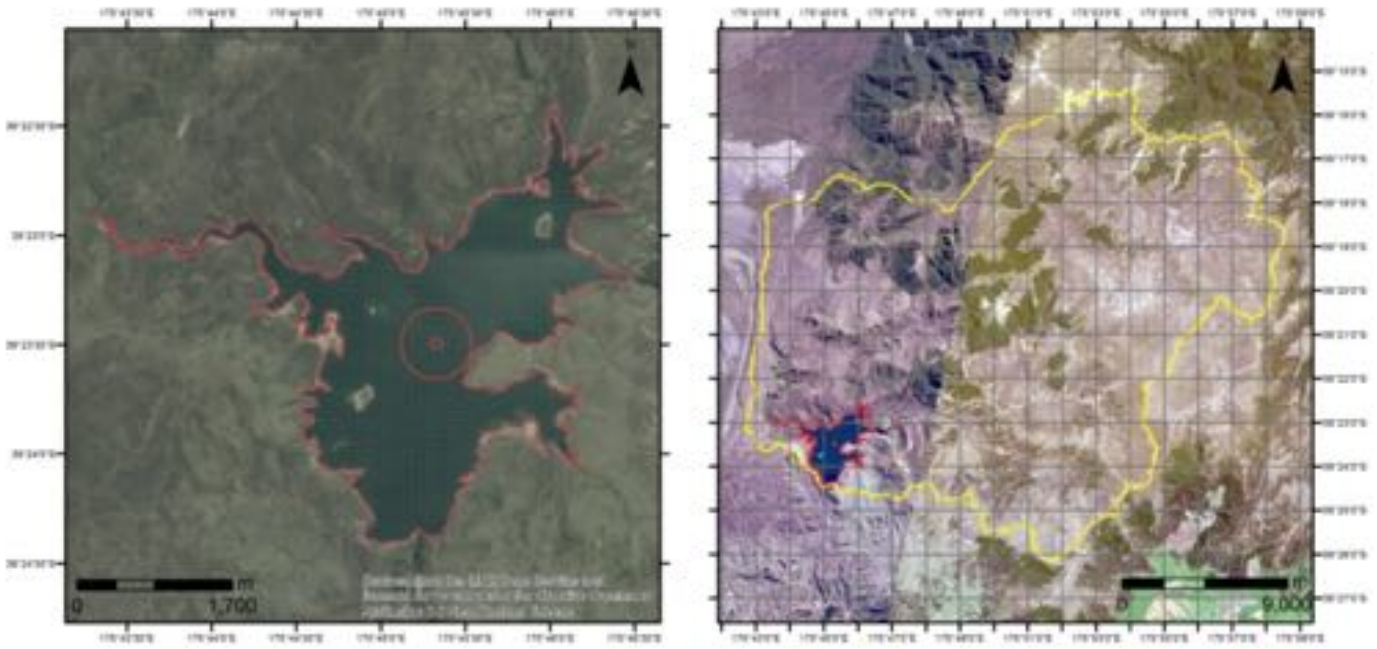

Lake ID: 18933 Lake Name: Lake Pauri

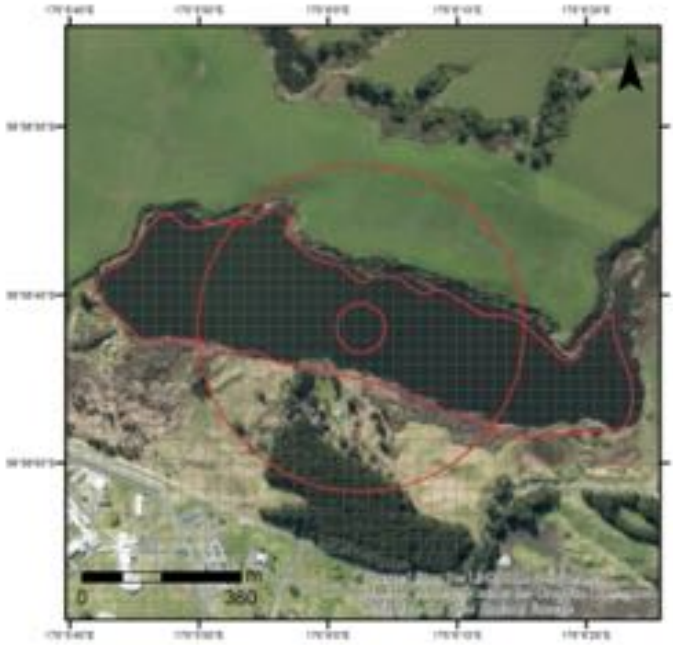


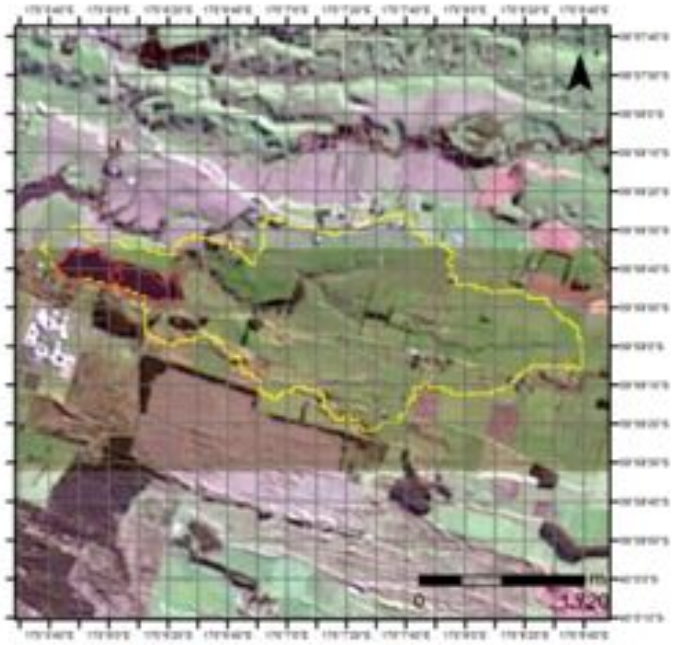


Lake ID: 18934 Lake Name: Lake Wiritoa


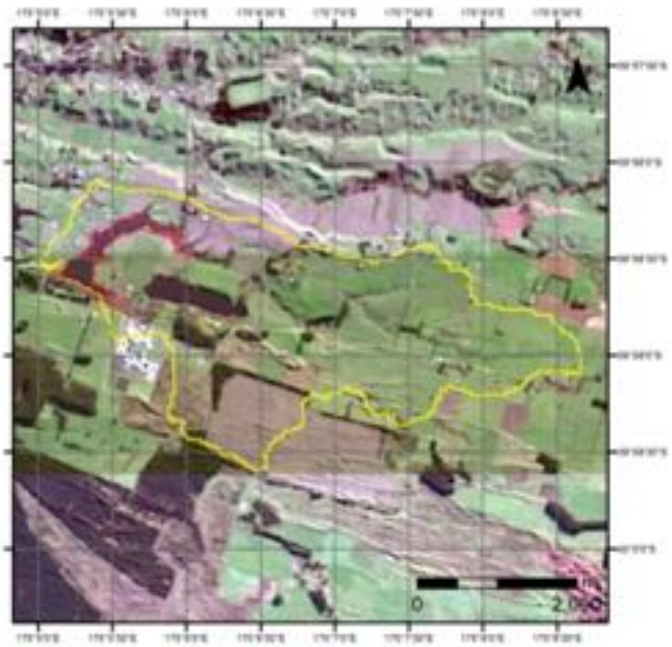

Lake ID: 18936 Lake Name: Kaitoke Lake


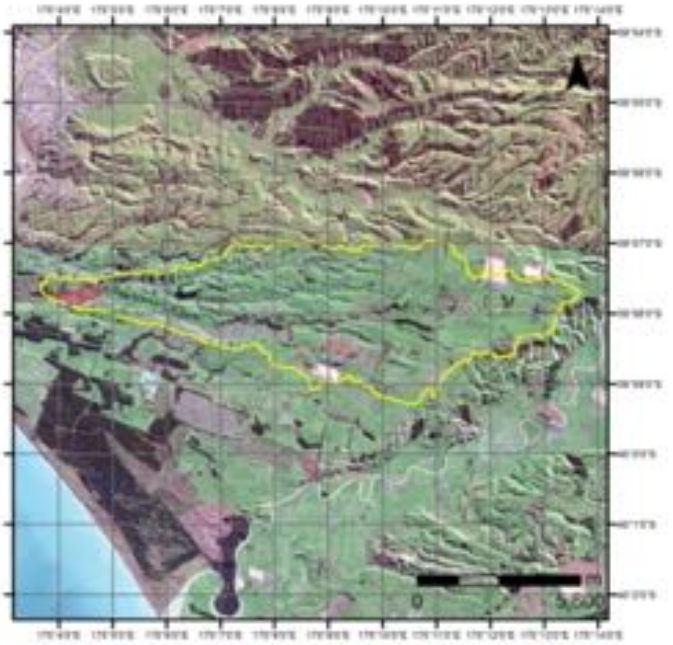


Lake ID: 18951 Lake Name: Lake Westmere

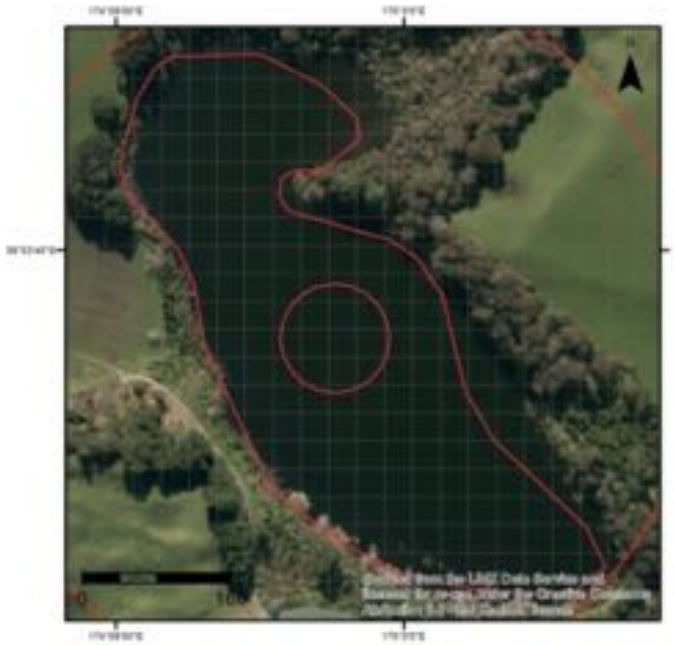


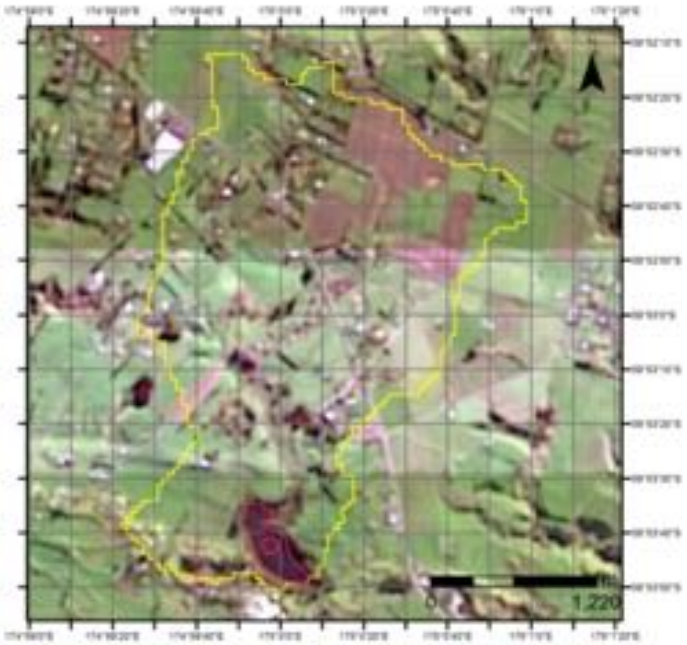

Lake ID: 18957

Lake Name: Lake Virginia

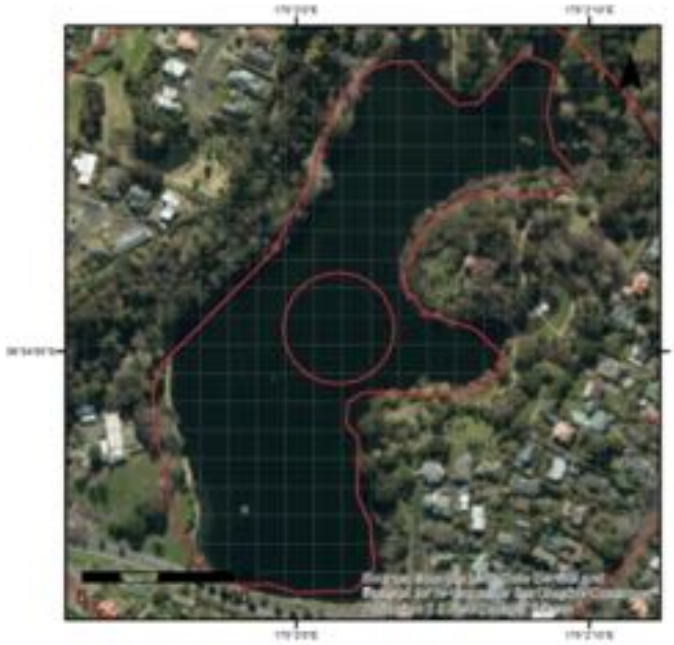

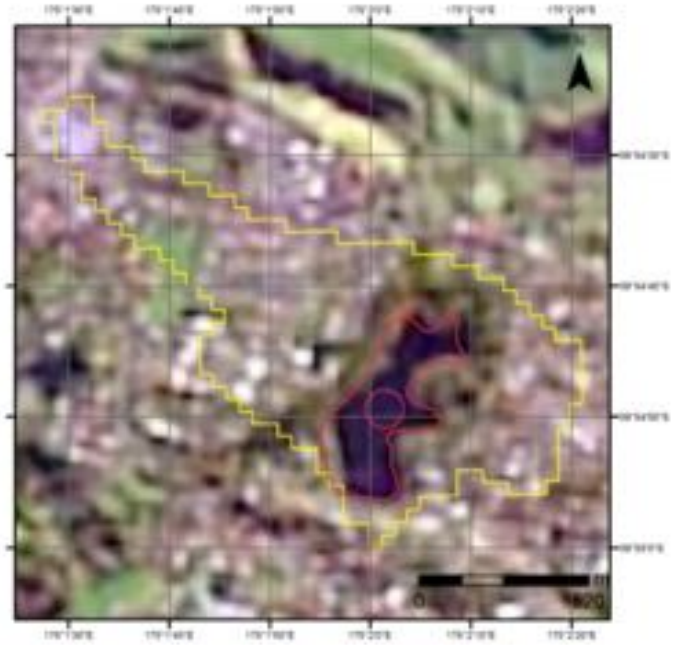

Lake ID: 19140

Lake Name:

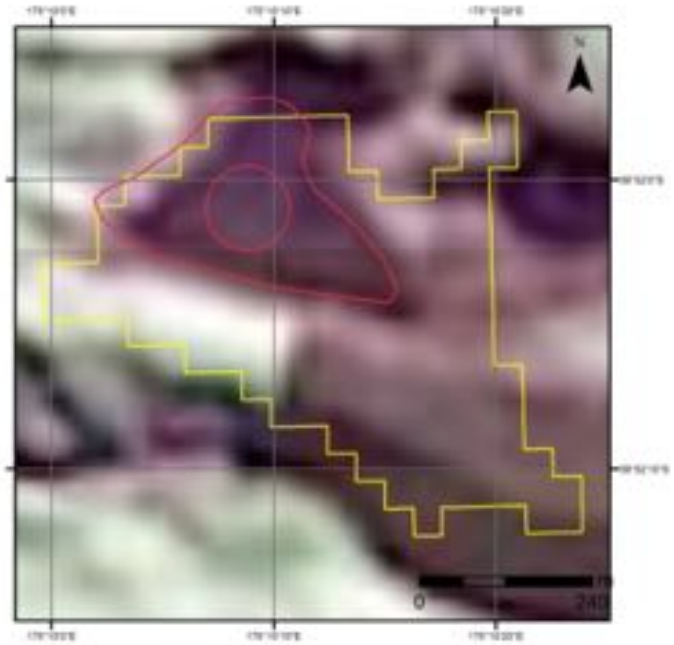

Lake ID: 19621 Lake Name: Lake Ngaruru

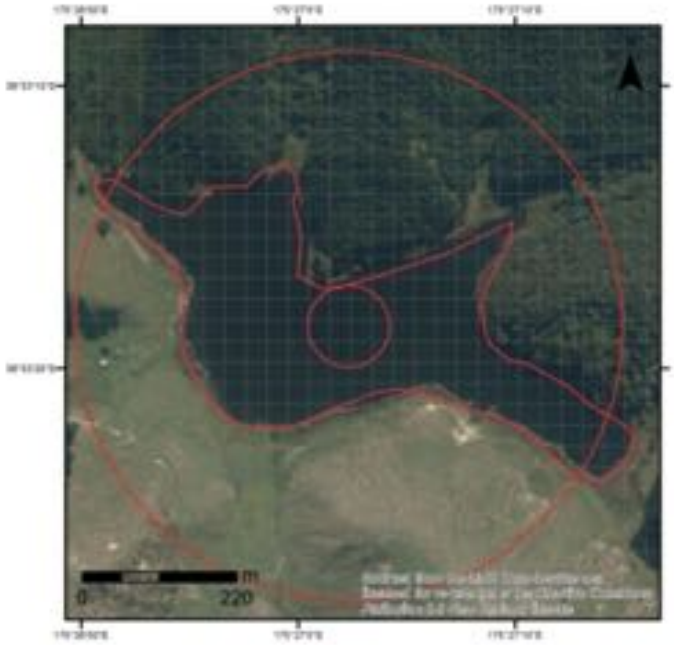


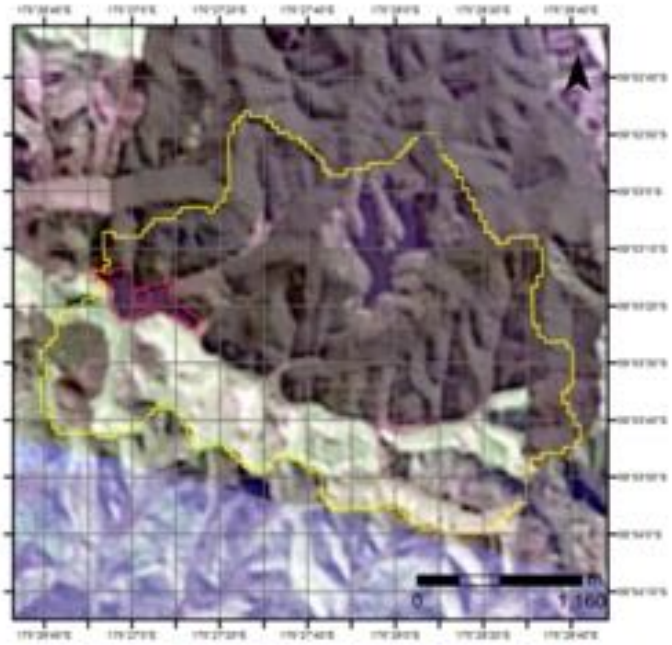


Lake ID: 19624 Lake Name: Lake Namunamu

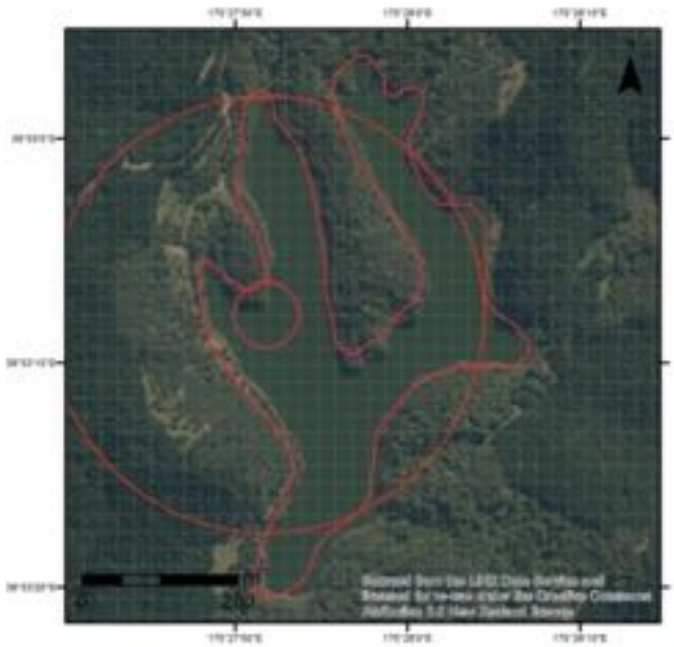


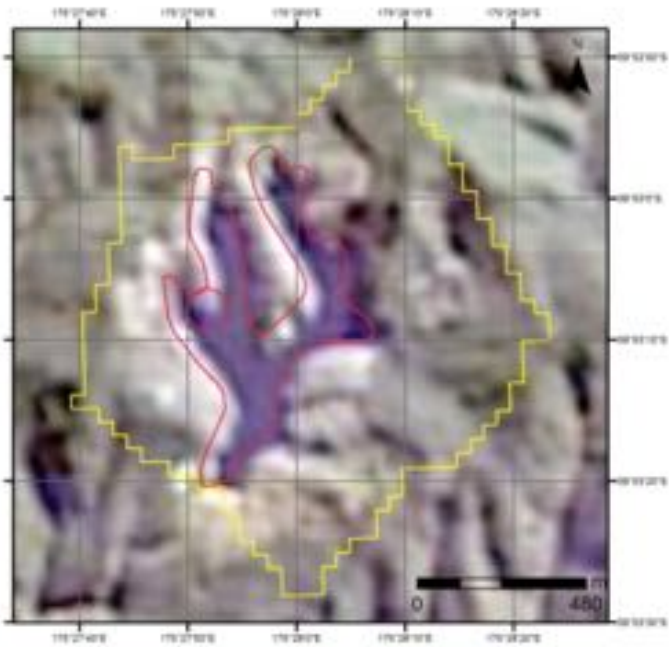

Lake ID: 19921

Lake Name:

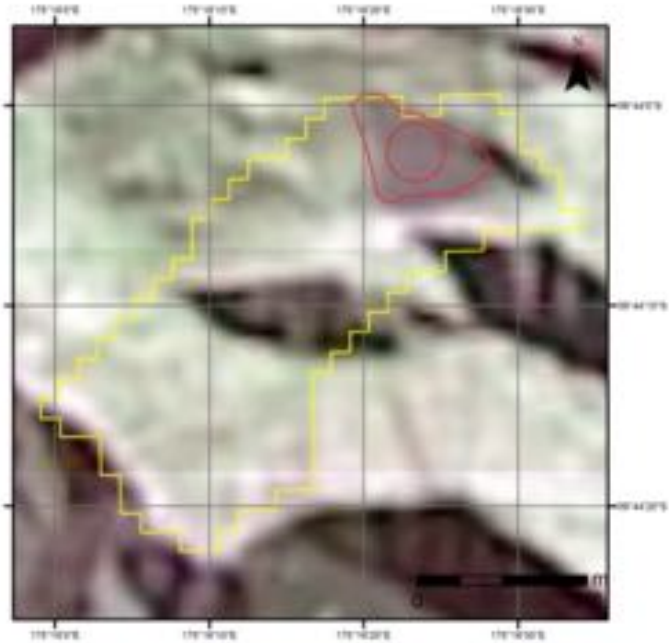

Lake ID: 20094

Lake Name: Lake Maungaratiti

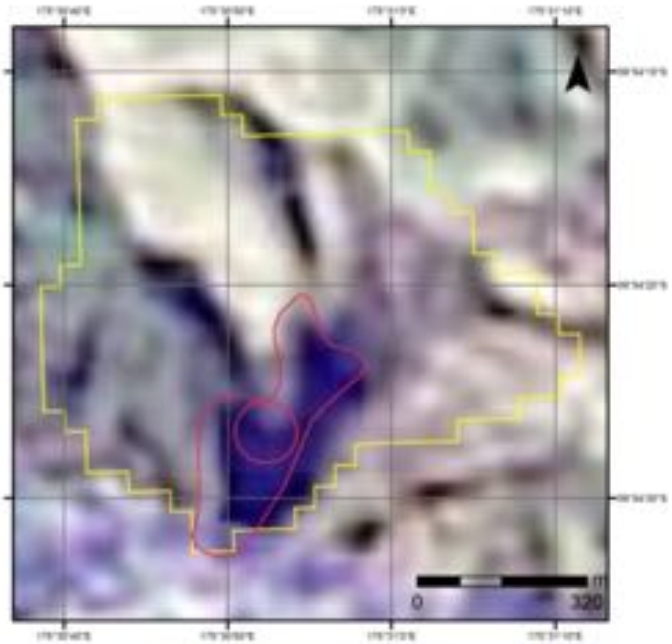

Lake ID: 20096 Lake Name: Lake Maungaratanui

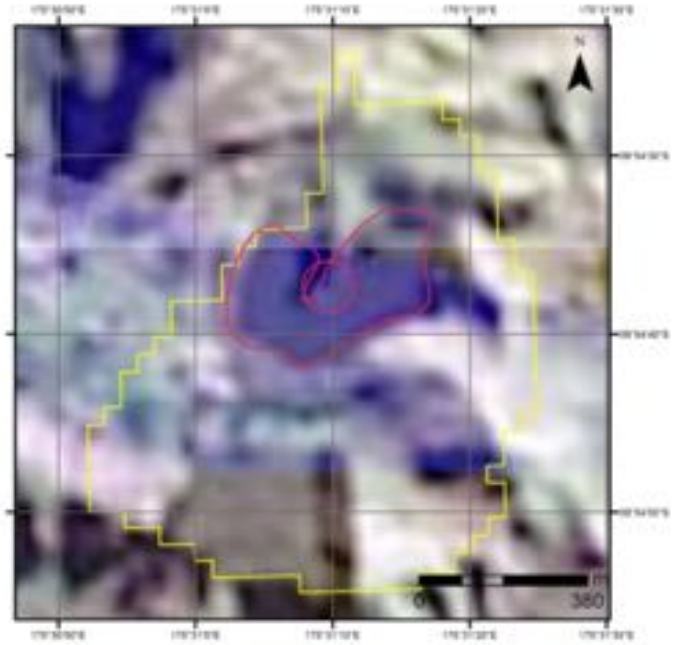

Lake ID: 20693 Lake Name:

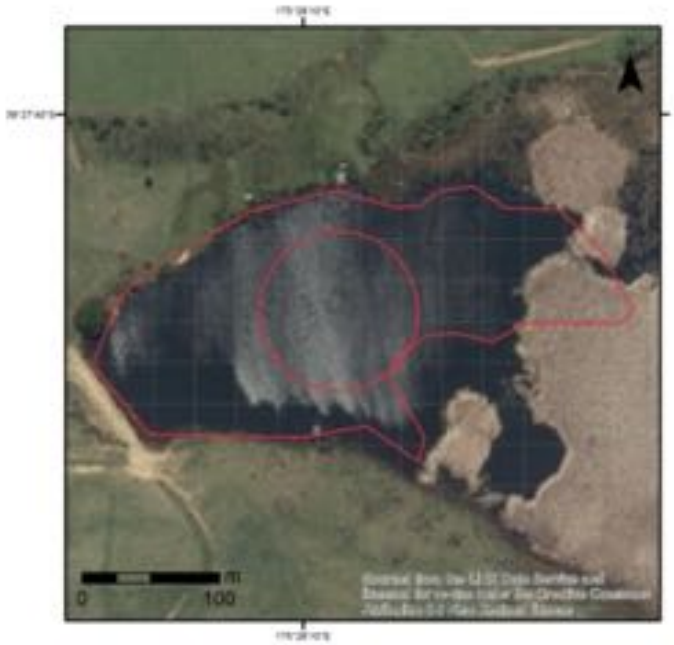

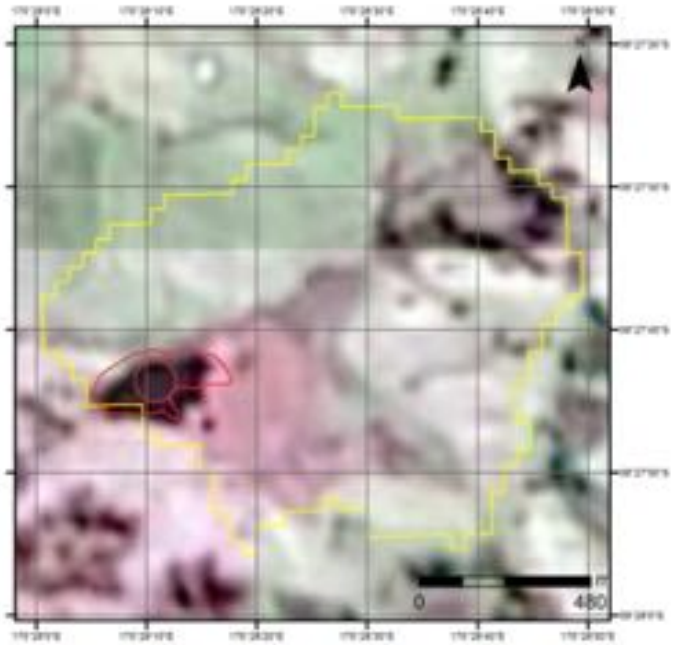

Lake ID: 20720

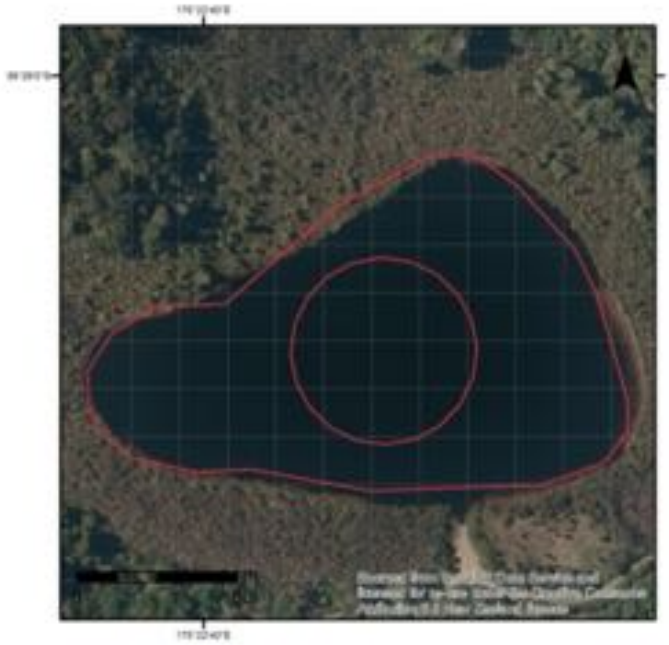

Lake Name:

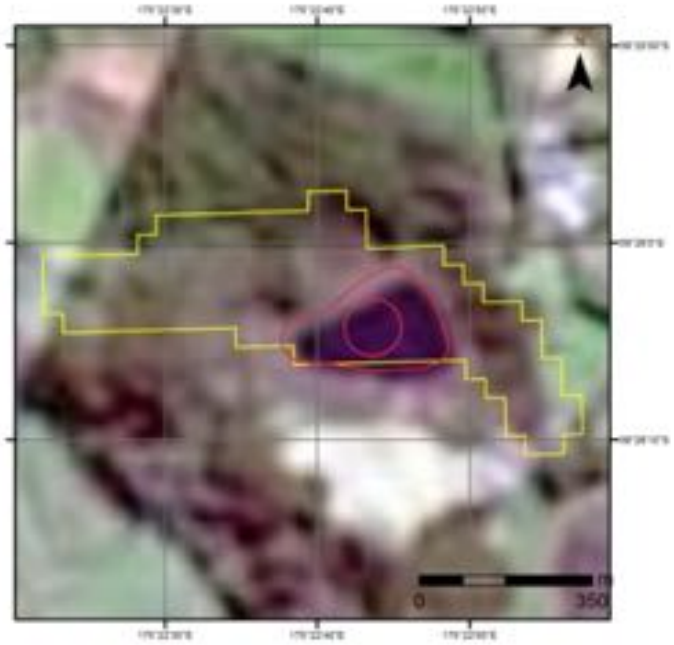


Lake ID: 20741

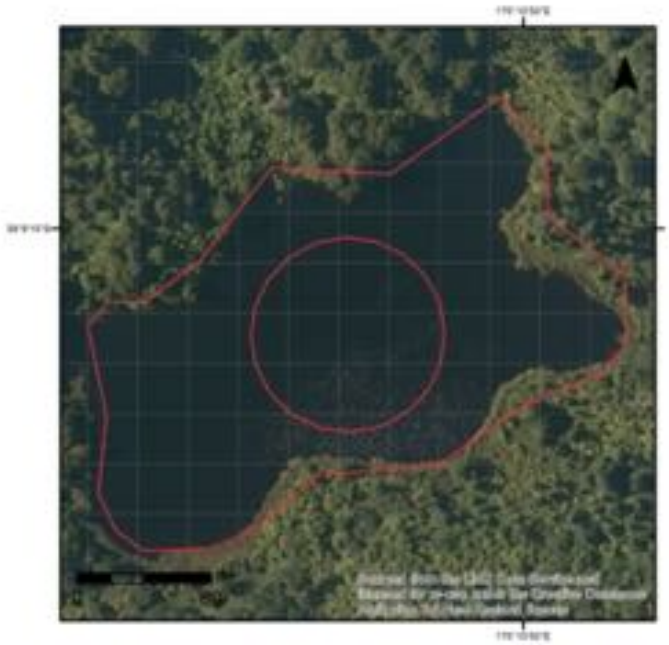

Lake Name: Lake Hawkes

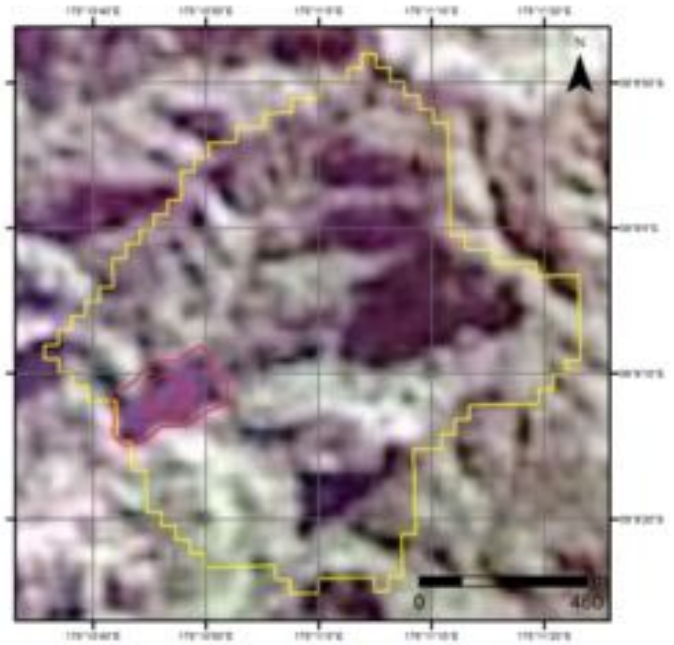

Lake ID: 21383 Lake Name: Lake Otamangakau


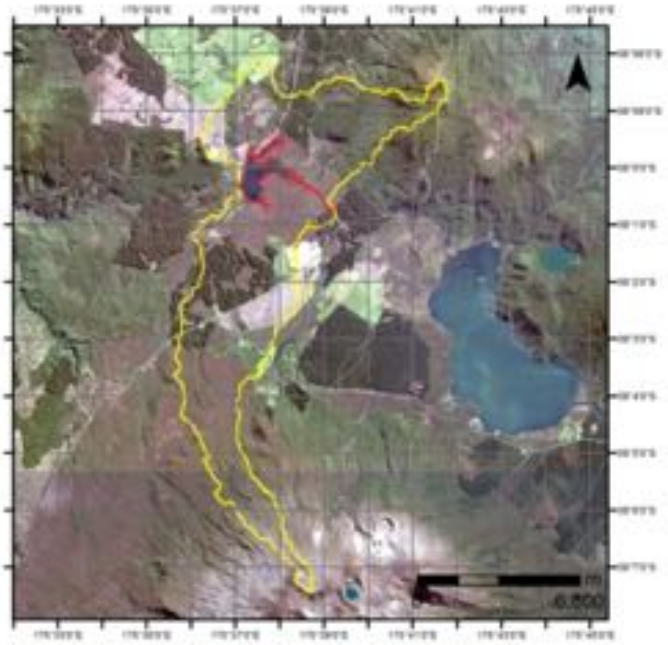


Lake ID: 31847 Lake Name:

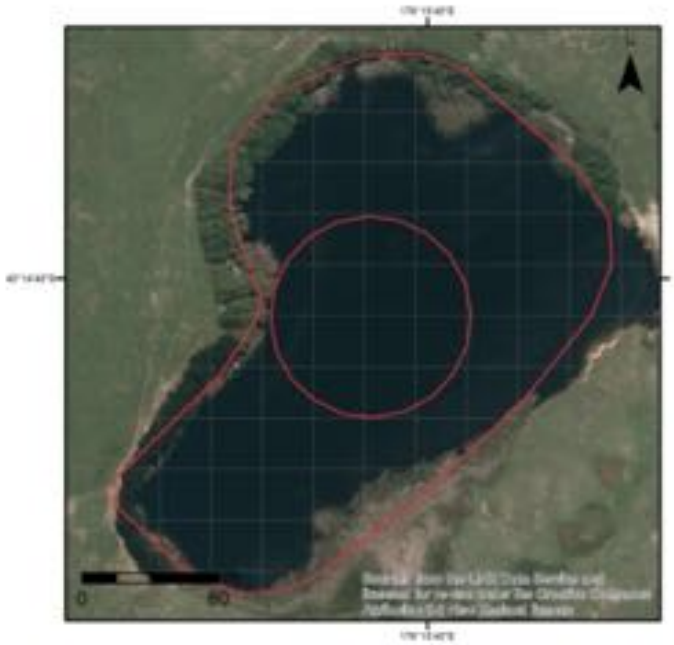


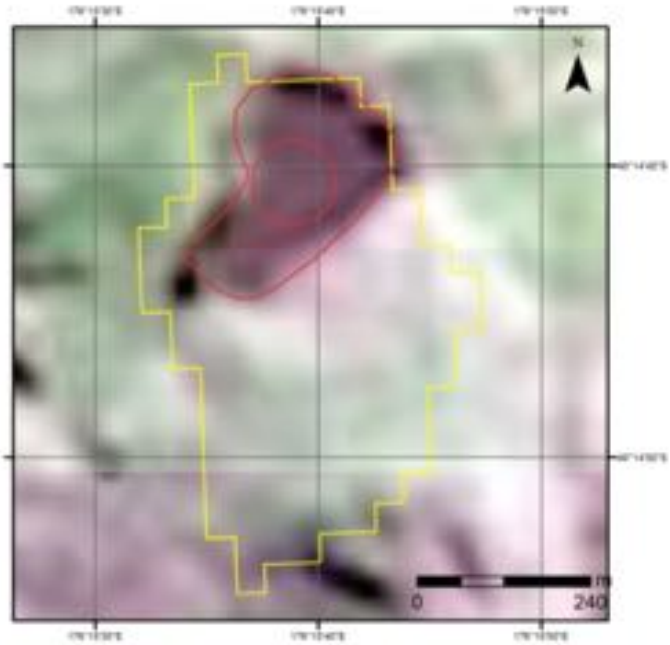

Lake ID: 34051 Lake Name: Lake Colenso (Kokopunui)

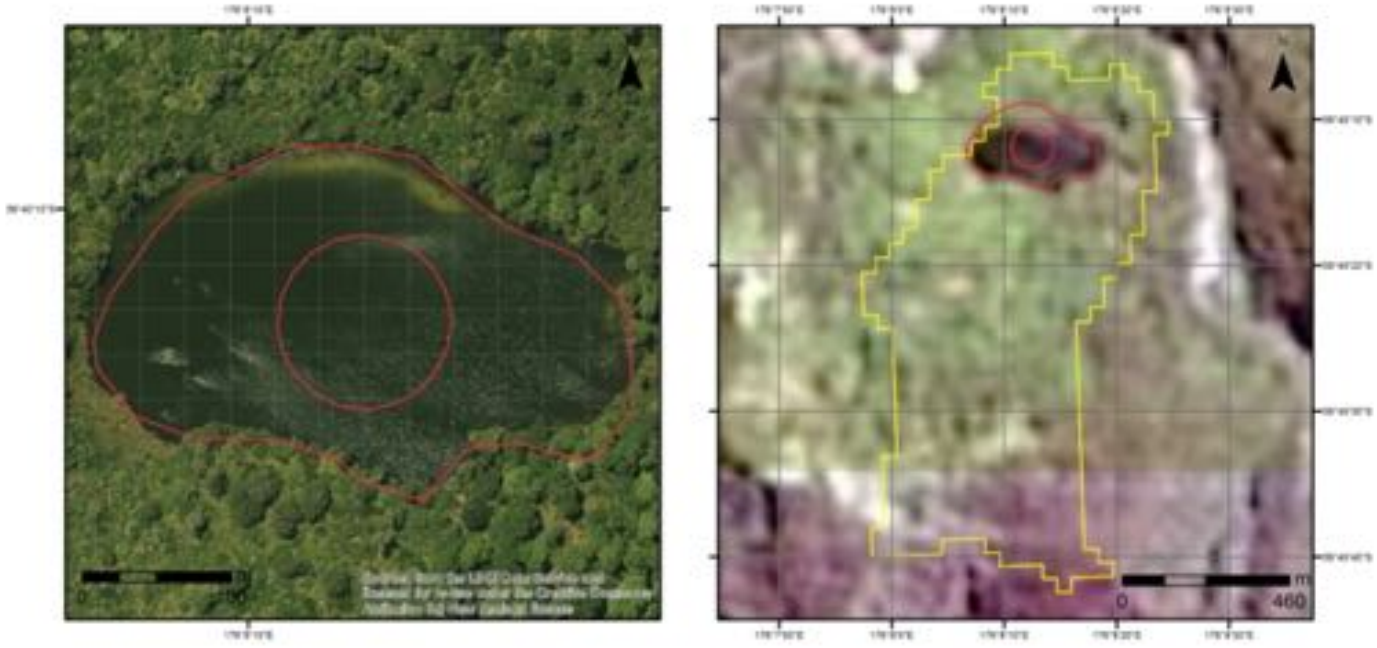

# Appendix C

## Water colour time series for lakes

Four years of colour data for 57 lakes from Landsat 8 OLI data according to Lehmann et al. (2018). Time series (top two panels) as well as location in the colour space (horseshoe-shaped plot in the bottom right) are shown.

Histograms and box plots assist in detecting pollution or bloom event.

FU index: Water colour in the Forel-Ule colour system; dominant wavelength: intensification of the colour as perceived by the human eye in units of nanometers (nm); x and y are chromaticity coordinates of the standard colorimetric system of the Commission Internationale de l'Éclairage (CIE 1932). LID: FENZ lake ID.

Further details are provided in Section 2.8.5.

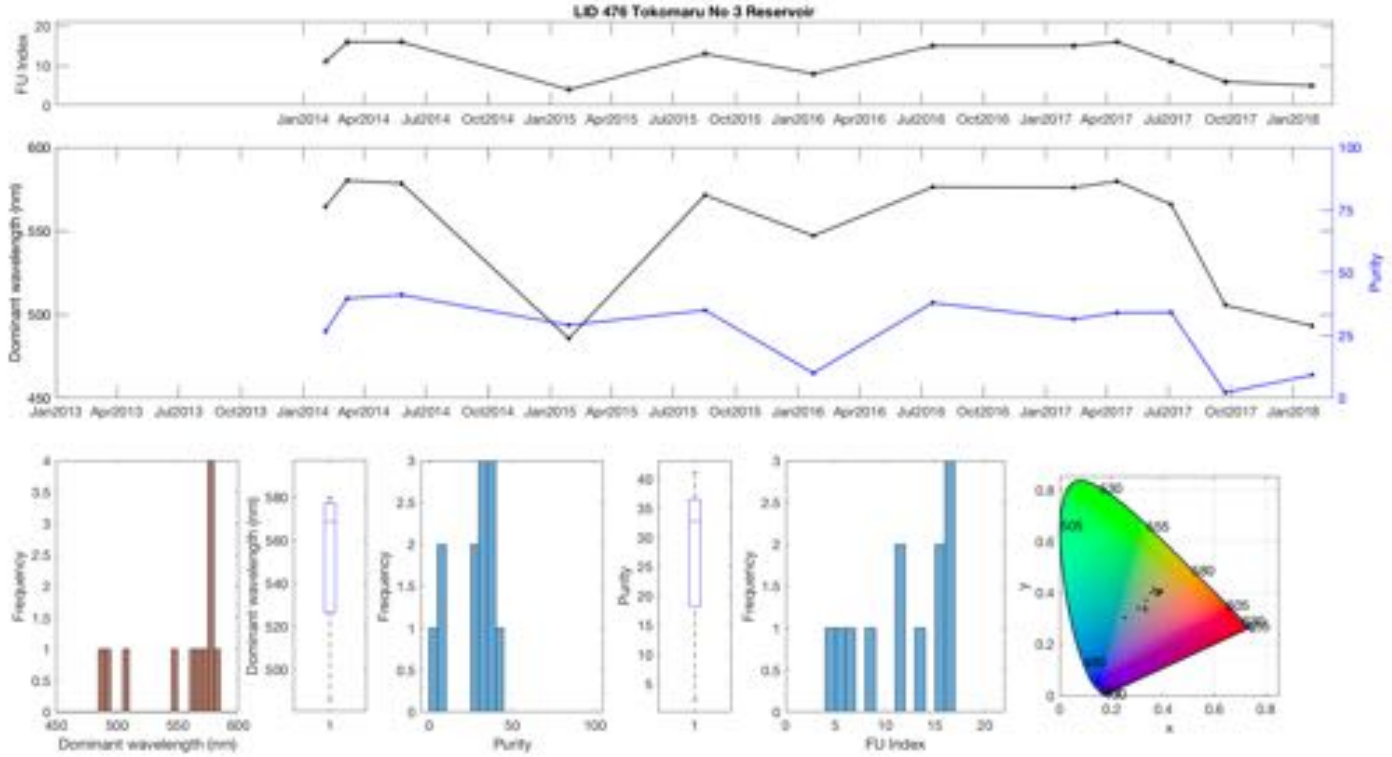
LID 476 Tokomaru No 3 Reservoir
FU Index
Dominant wavelength (nm)
Purity
Frequency
Dominant wavelength (nm)
Frequency
Purity
Purity
Frequency
FU Index
y
x

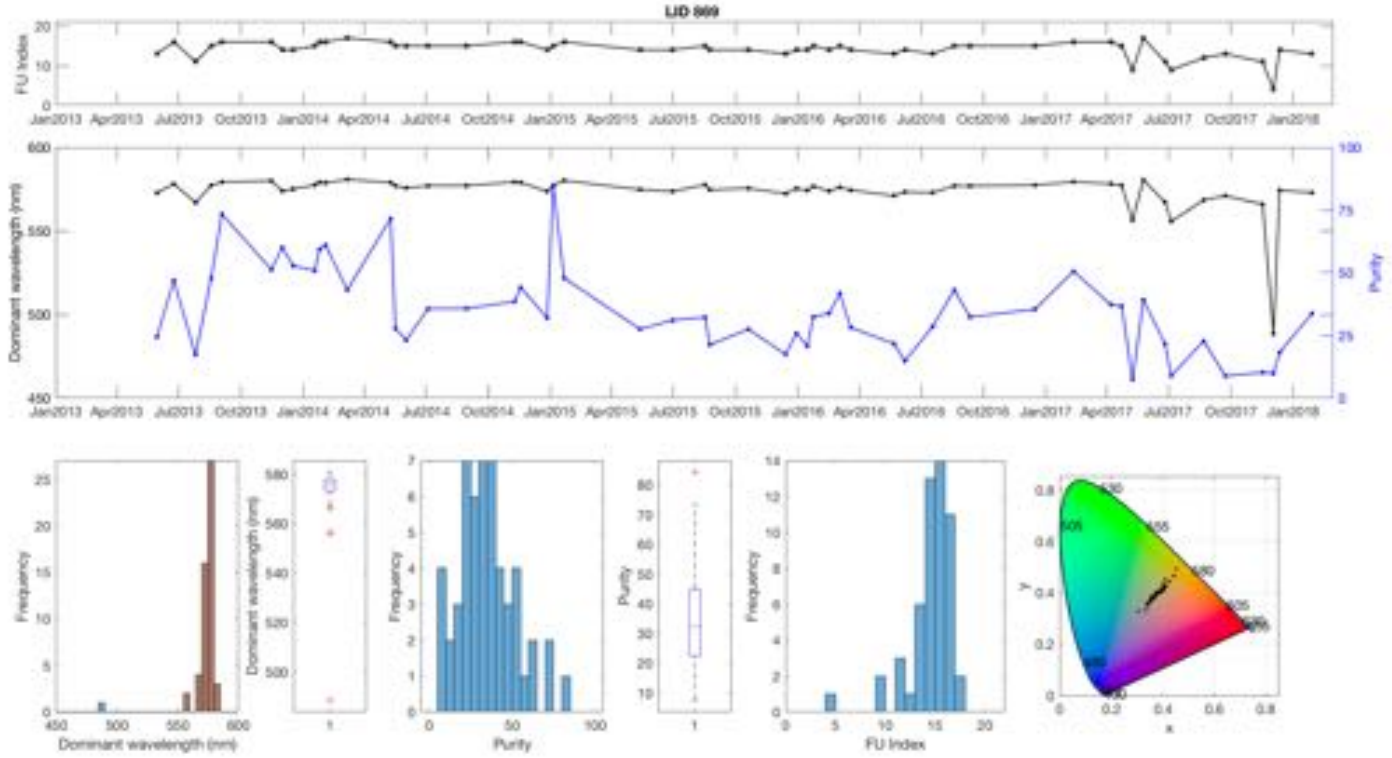
LID 869
FU Index
Dominant wavelength (nm)
Purity
Frequency
Dominant wavelength (nm)
Frequency
Purity
Purity
Frequency
FU Index
y
x

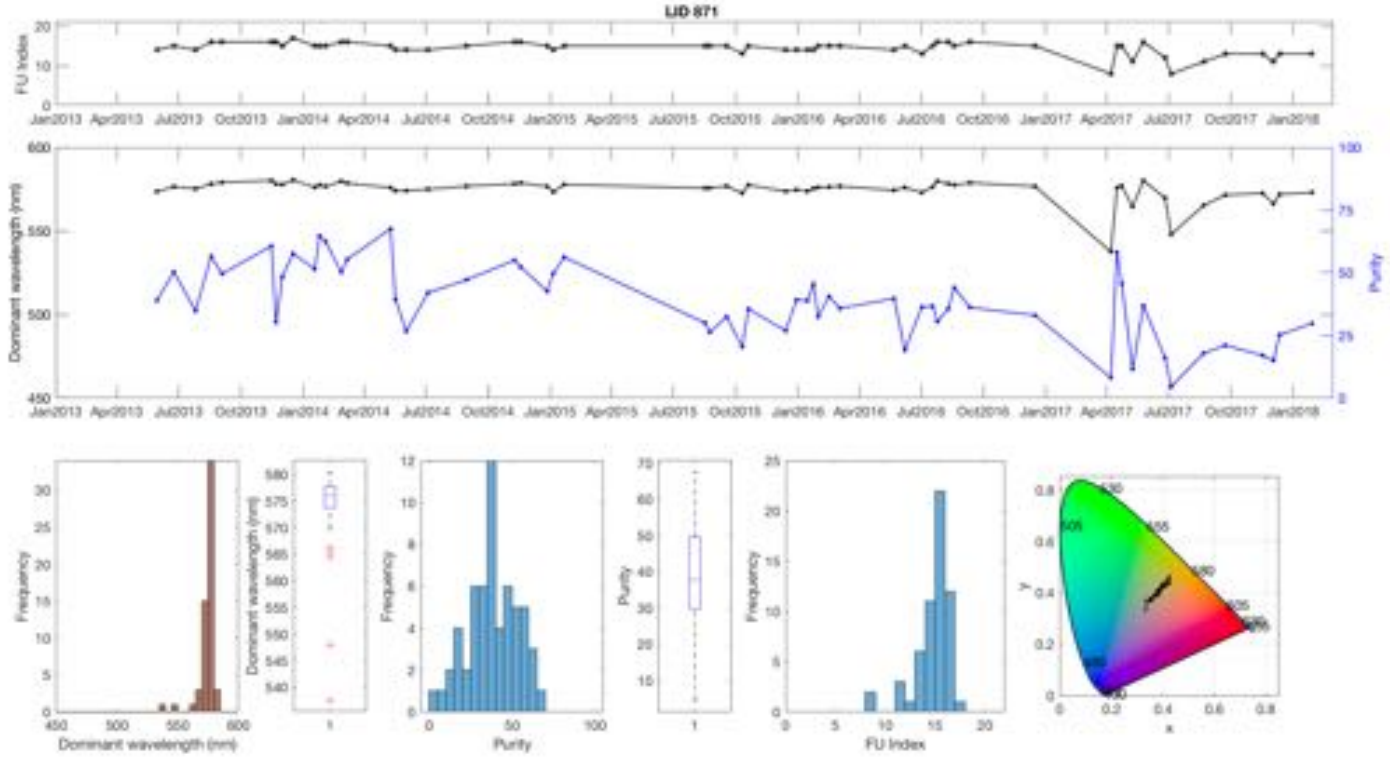
LID 871
FU Index
Dominant wavelength (nm)
Purity
Frequency
Dominant wavelength (nm)
Purity
FU Index
y
x

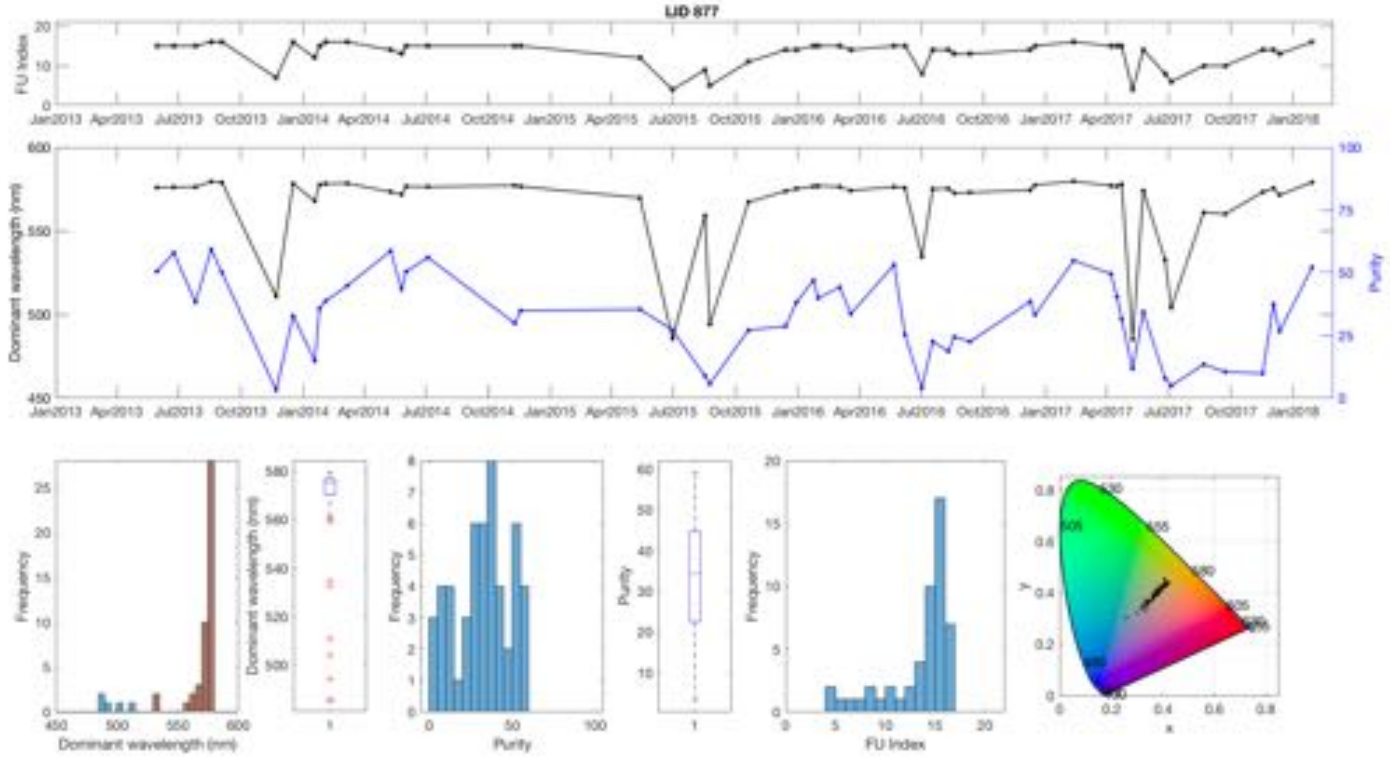
LID 877
FU Index
Dominant wavelength (nm)
Purity
Frequency
Dominant wavelength (nm)
Purity
FU Index
y
x

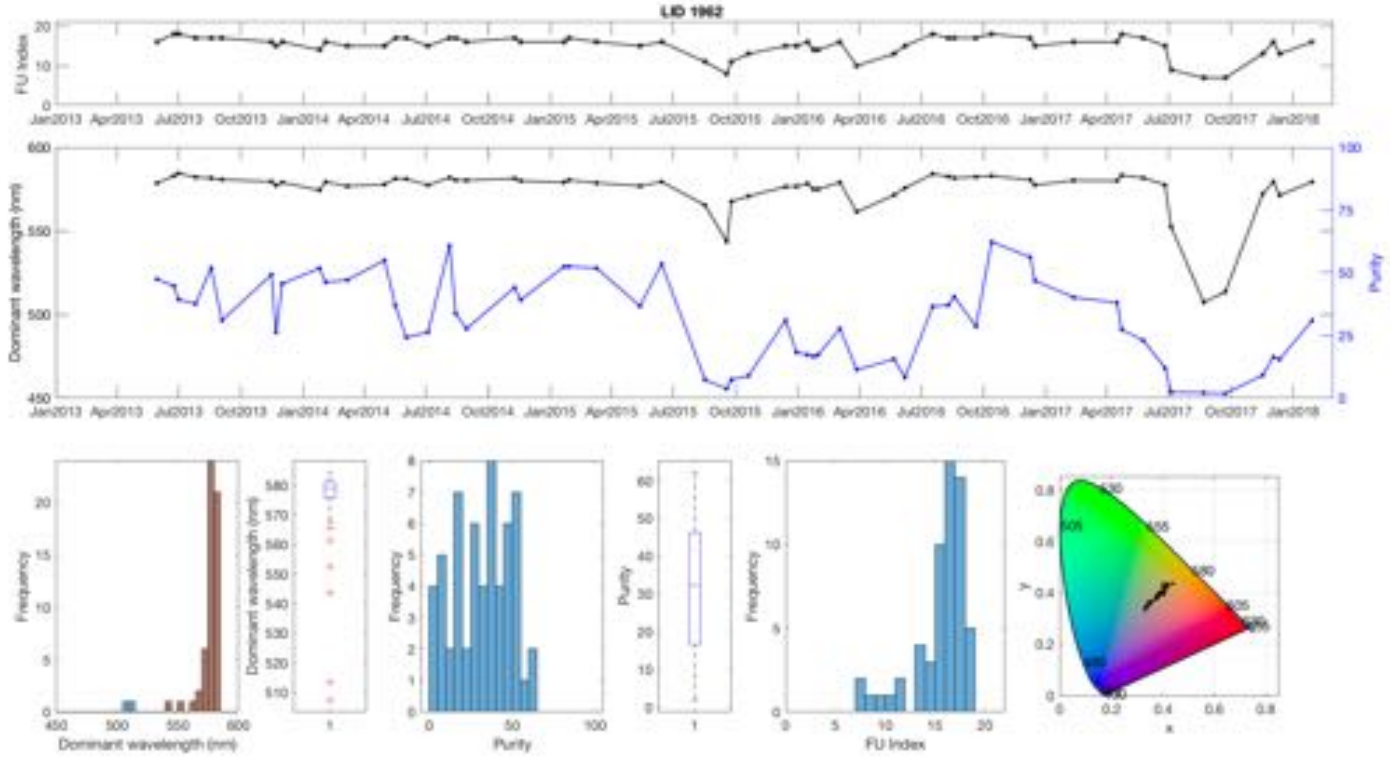
LID 1962
FU Index
Dominant wavelength (nm)
Purity
Frequency
Dominant wavelength (nm)
Purity
Frequency
Purity
Frequency
FU Index
y
x

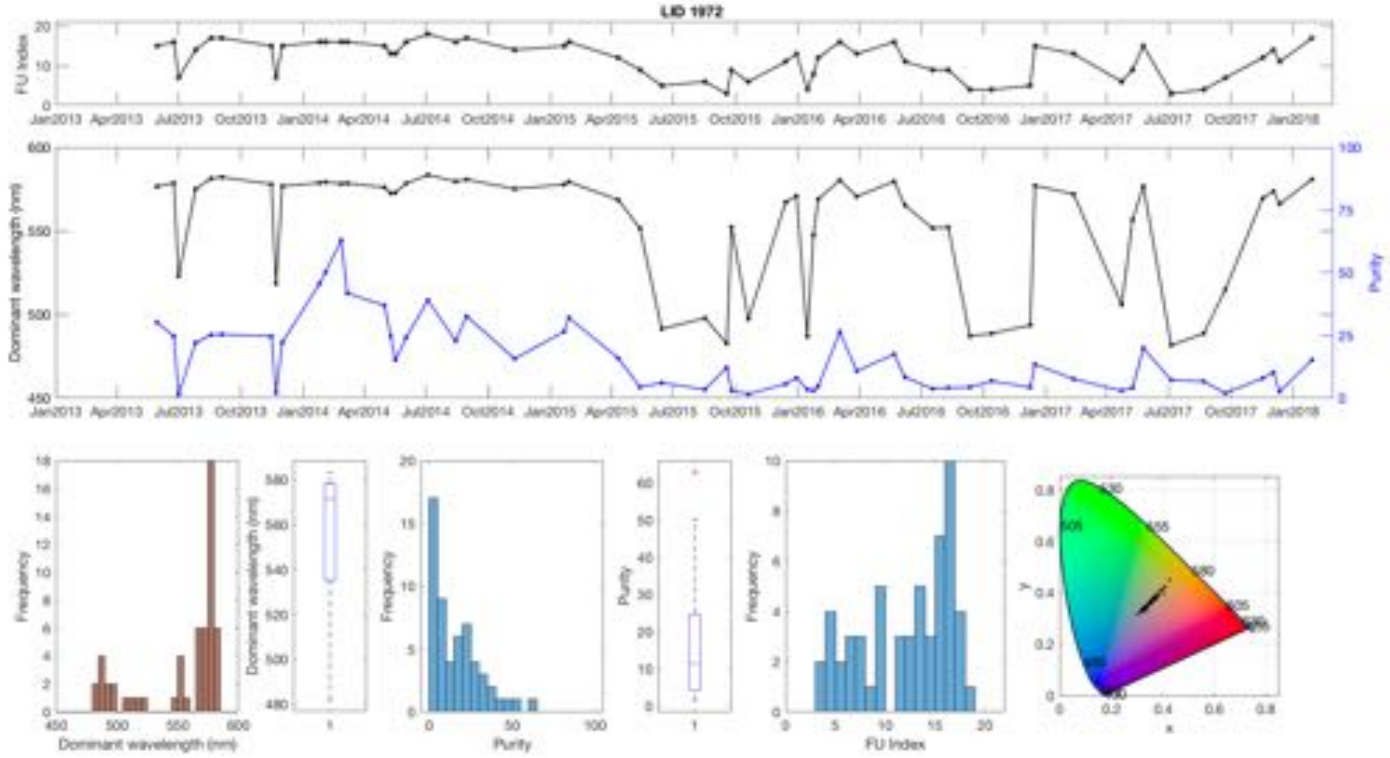
LID 1972
FU Index
Dominant wavelength (nm)
Purity
Frequency
Dominant wavelength (nm)
Purity
Frequency
Purity
Frequency
FU Index
y
x

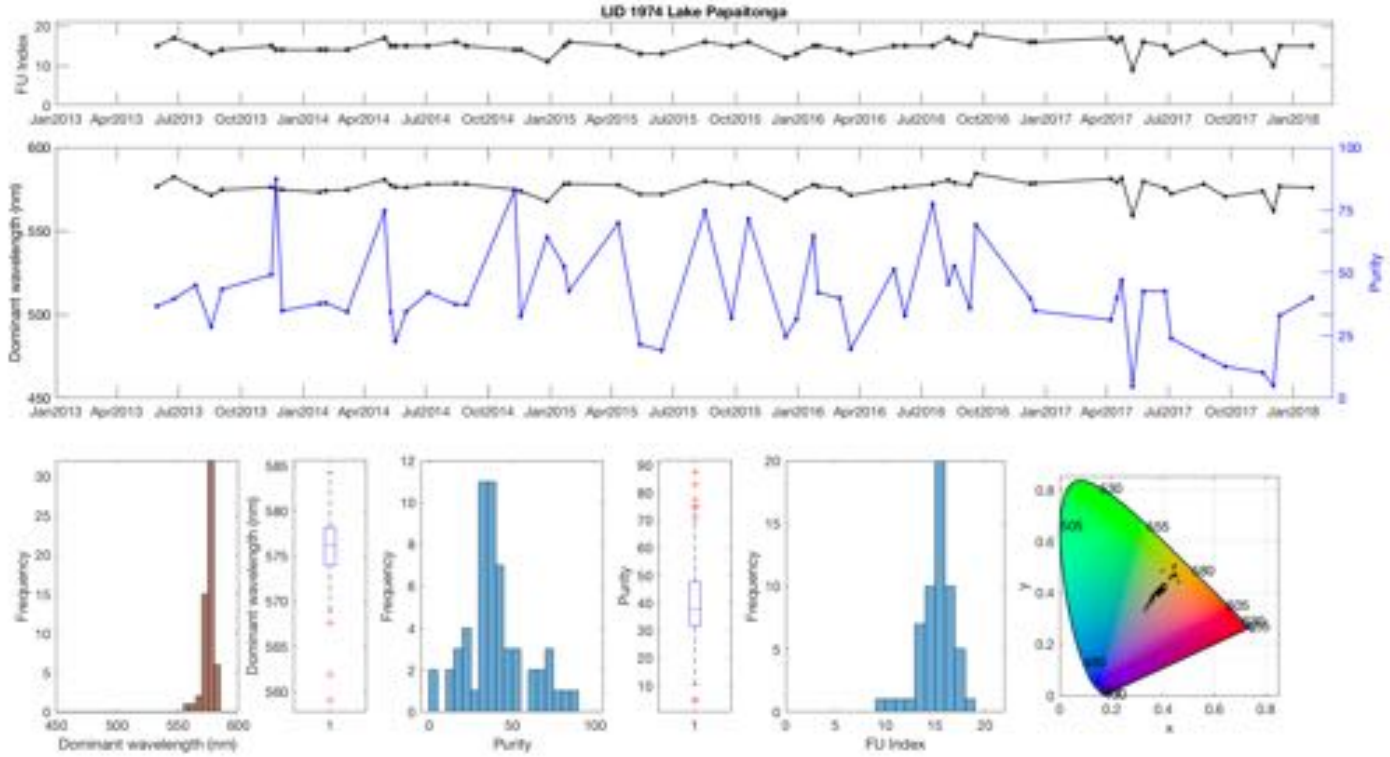
LID 1974 Lake Papaitonga
FU Index
Dominant wavelength (nm)
Purity
Frequency
Dominant wavelength (nm)
Frequency
Purity
Purity
Frequency
FU Index
y
x

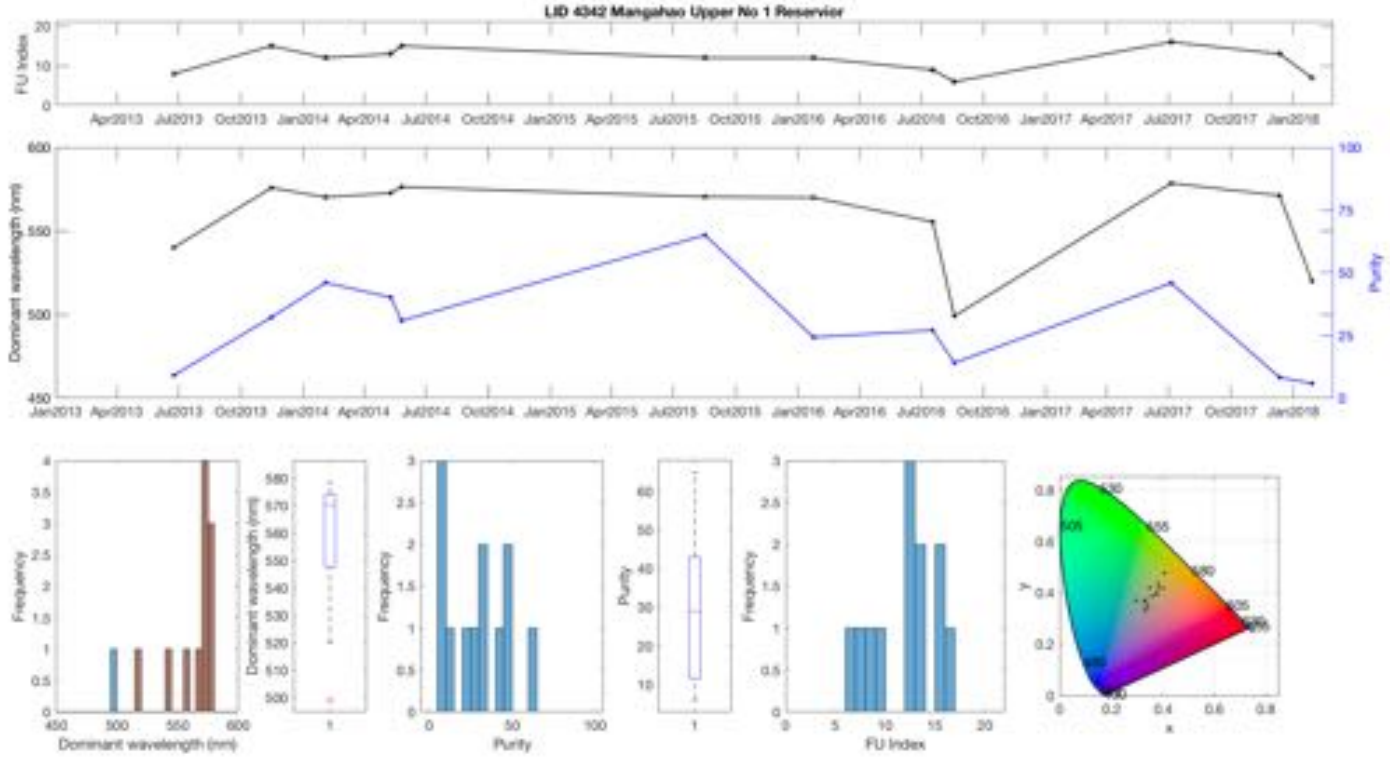
LID 4342 Mangahao Upper No 1 Reservior
FU Index
Dominant wavelength (nm)
Purity
Frequency
Dominant wavelength (nm)
Frequency
Purity
Purity
Frequency
FU Index
y
x

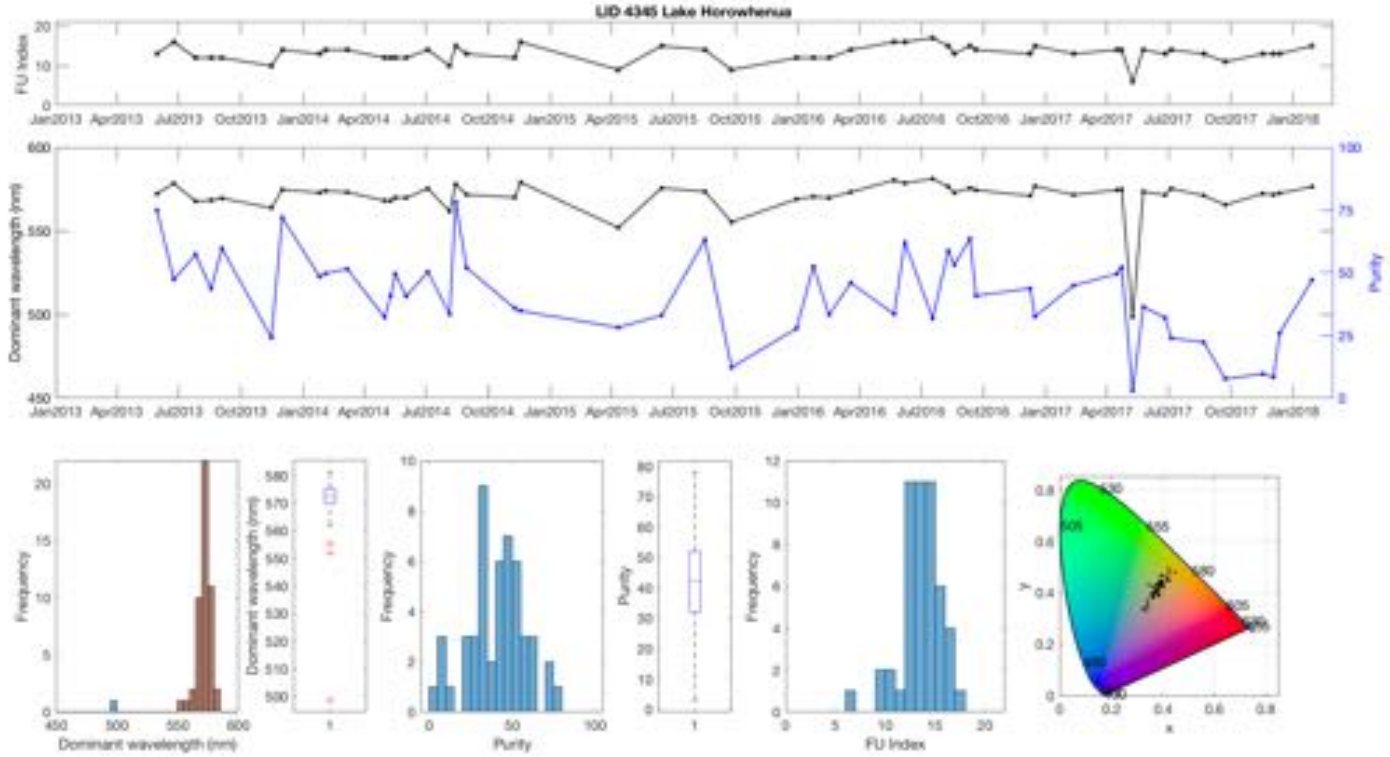
LID 4345 Lake Horowhenua
FU Index
Dominant wavelength (nm)
Purity
Frequency
Dominant wavelength (nm)
Purity
Frequency
Purity
Frequency
FU Index
y
x

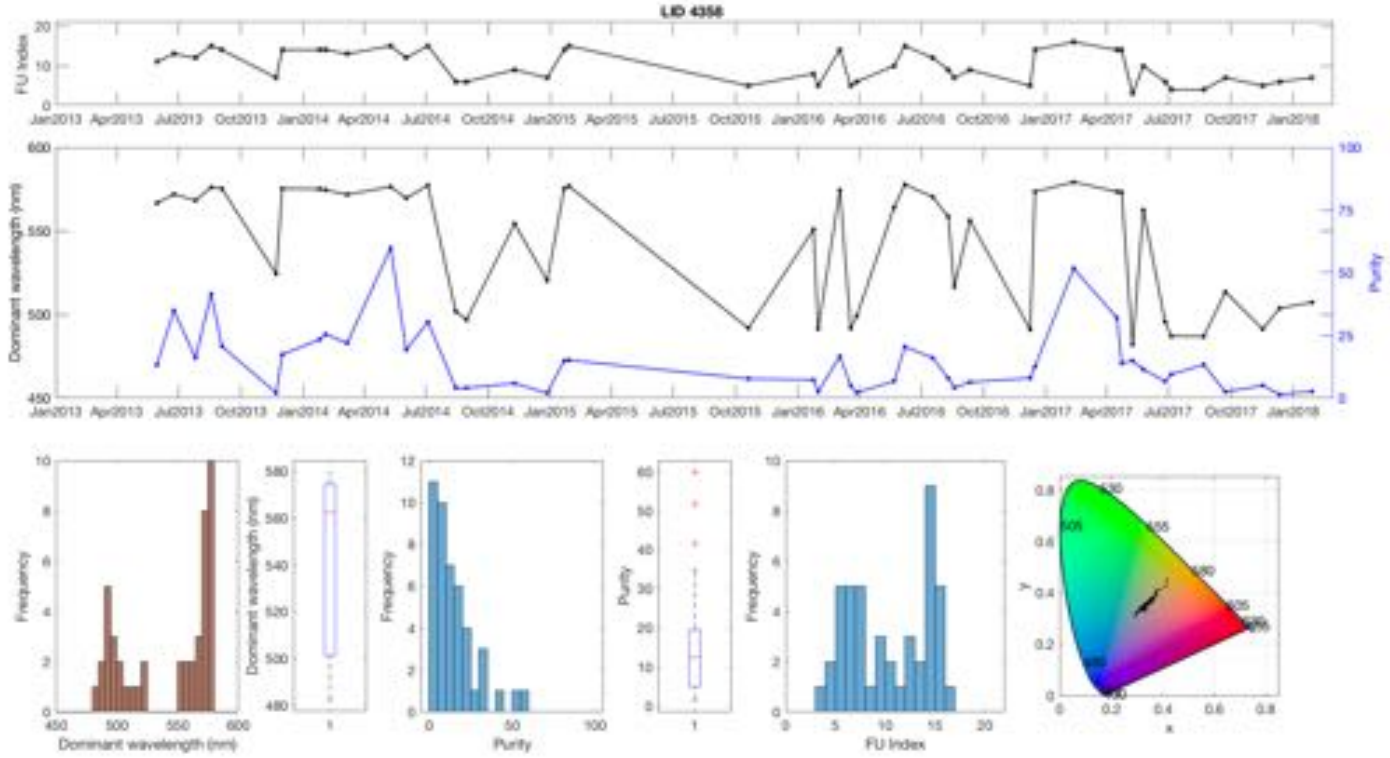
LID 4358
FU Index
Dominant wavelength (nm)
Purity
Frequency
Dominant wavelength (nm)
Purity
Frequency
Purity
Frequency
FU Index
y
x

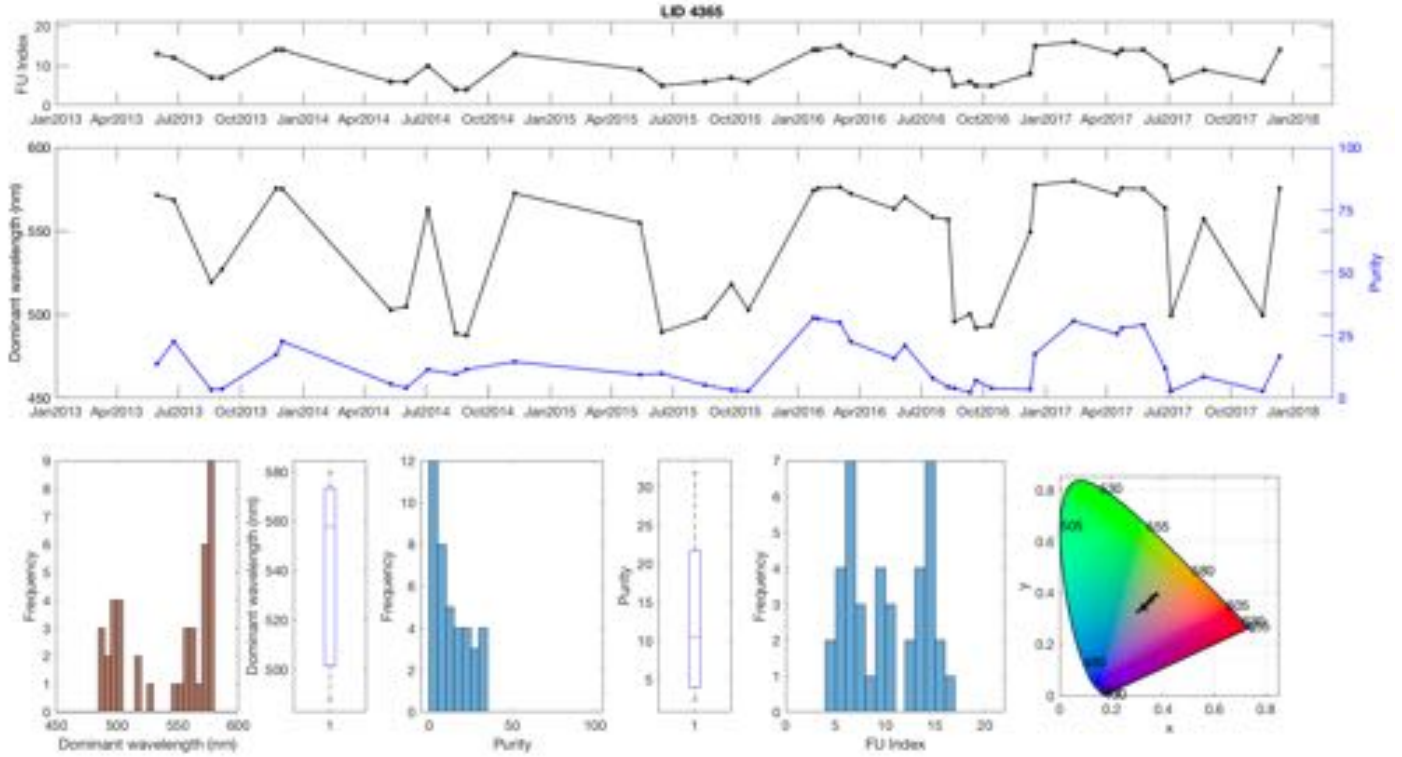
LID 4365
FU Index
Dominant wavelength (nm)
Purity
Frequency
Dominant wavelength (nm)
Purity
Frequency
Purity
Frequency
FU Index
y
x

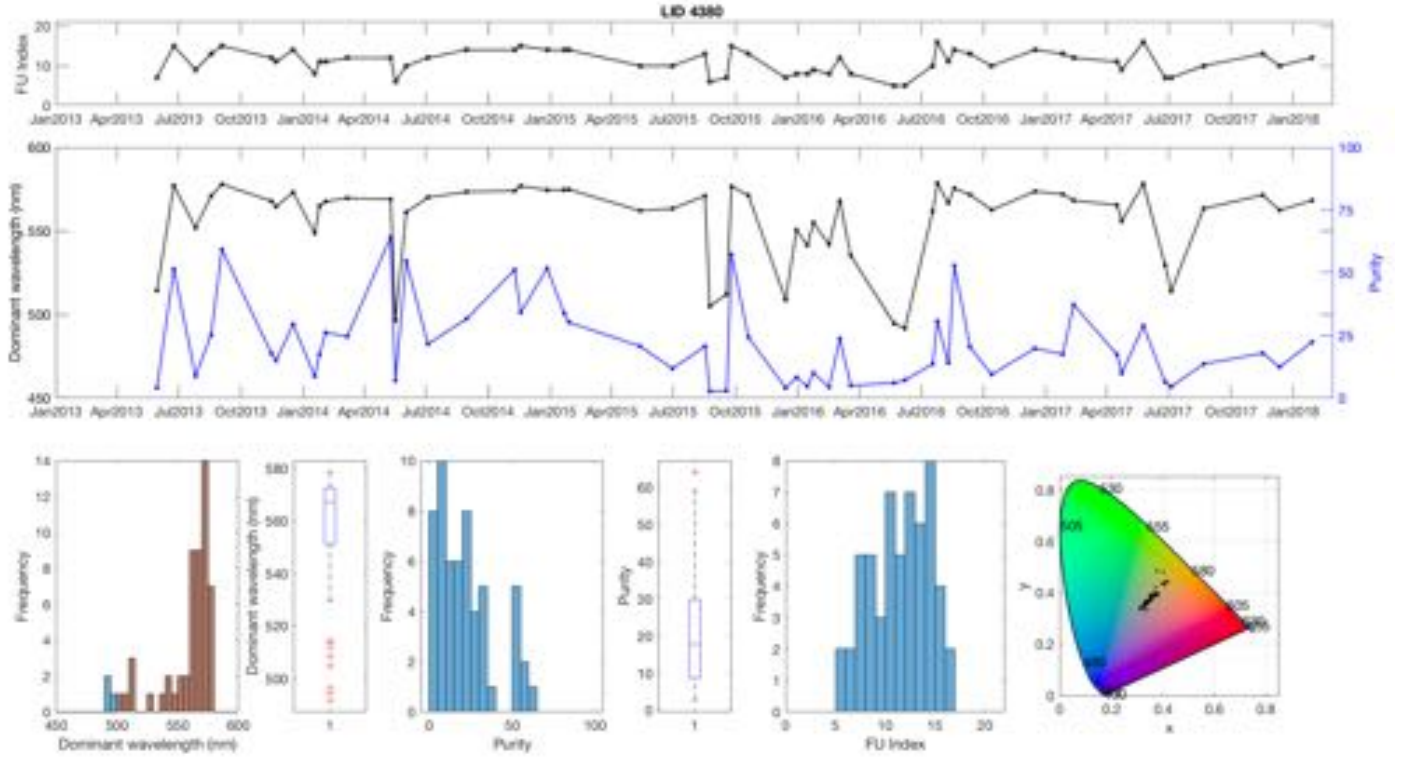
LID 4380
FU Index
Dominant wavelength (nm)
Purity
Frequency
Dominant wavelength (nm)
Purity
Frequency
Purity
Frequency
FU Index
y
x

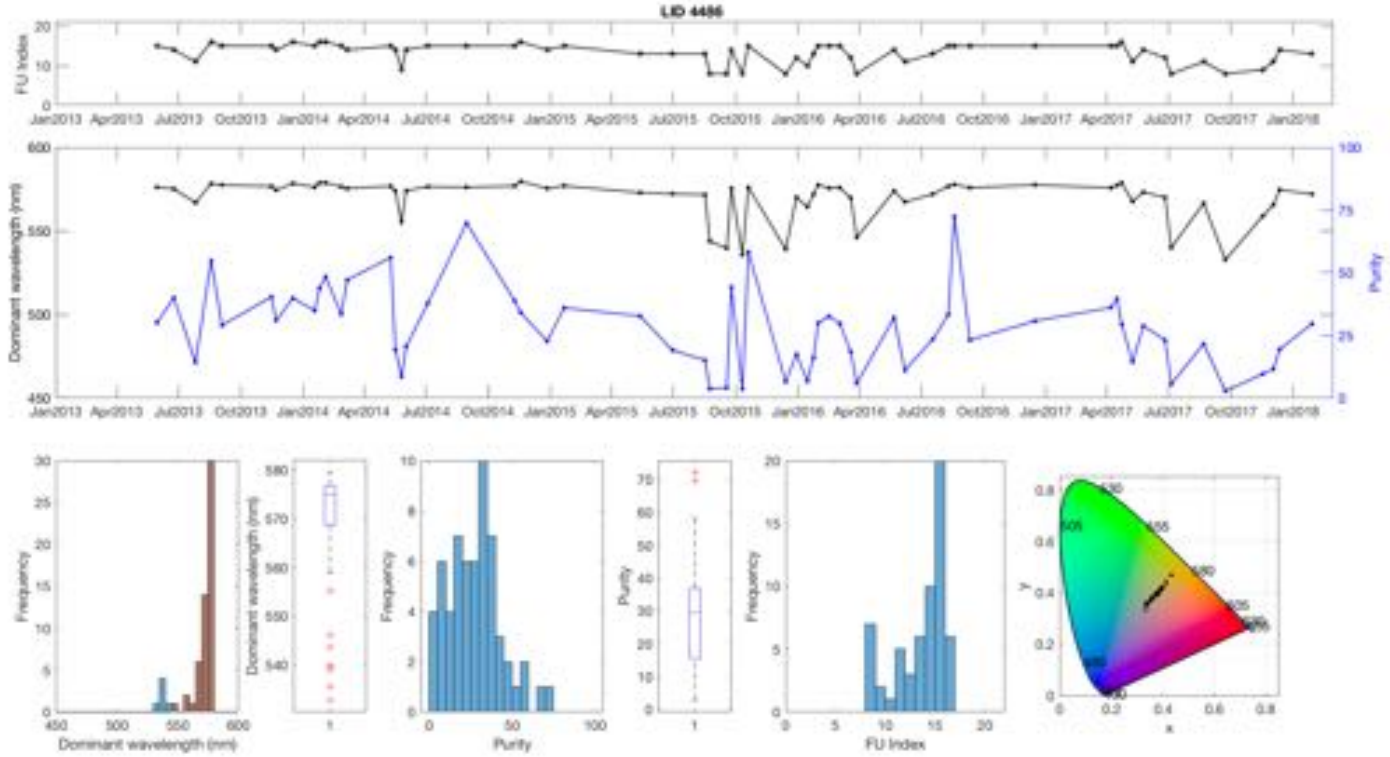
LID 4486
FU Index
Dominant wavelength (nm)
Purity
Frequency
Dominant wavelength (nm)
Purity
Frequency
Purity
Frequency
FU Index
y
x

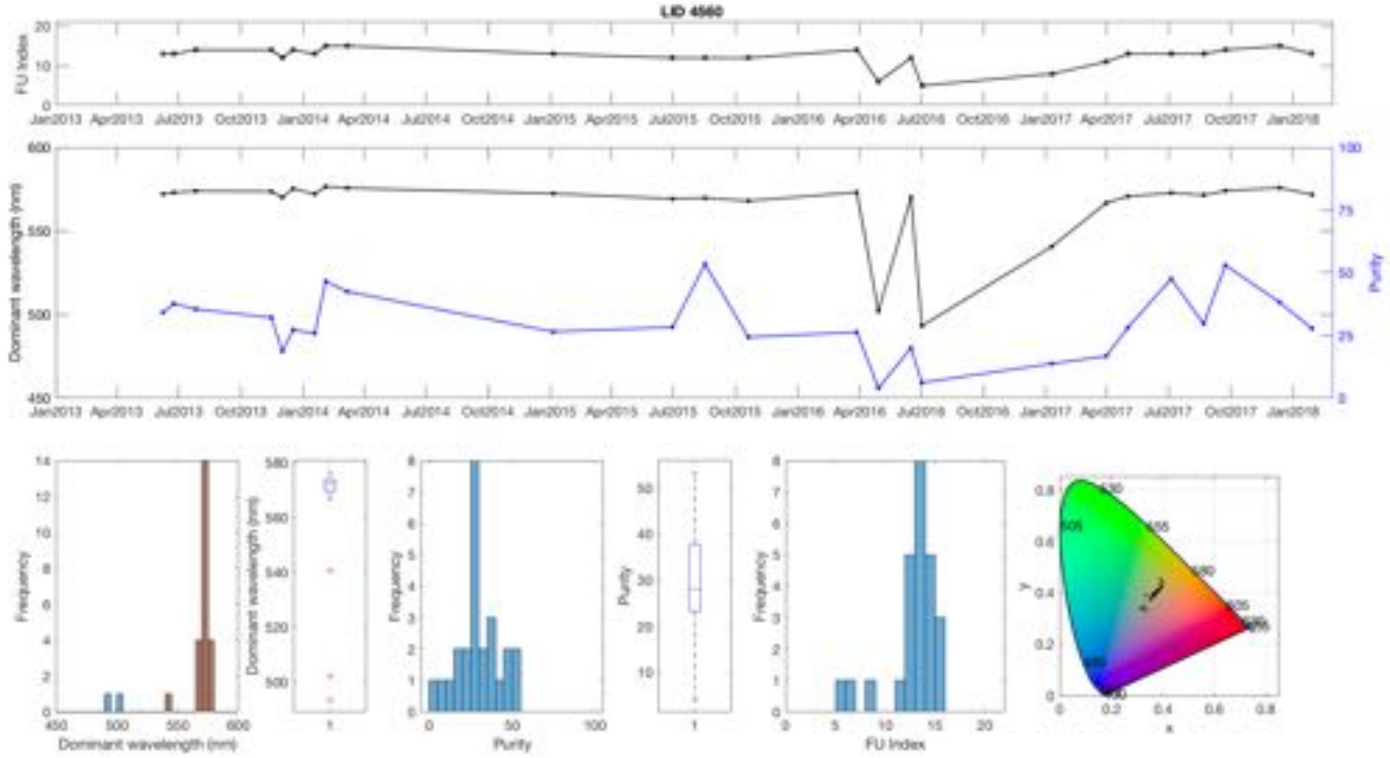
LID 4560
FU Index
Dominant wavelength (nm)
Purity
Frequency
Dominant wavelength (nm)
Purity
Frequency
Purity
Frequency
FU Index
y
x

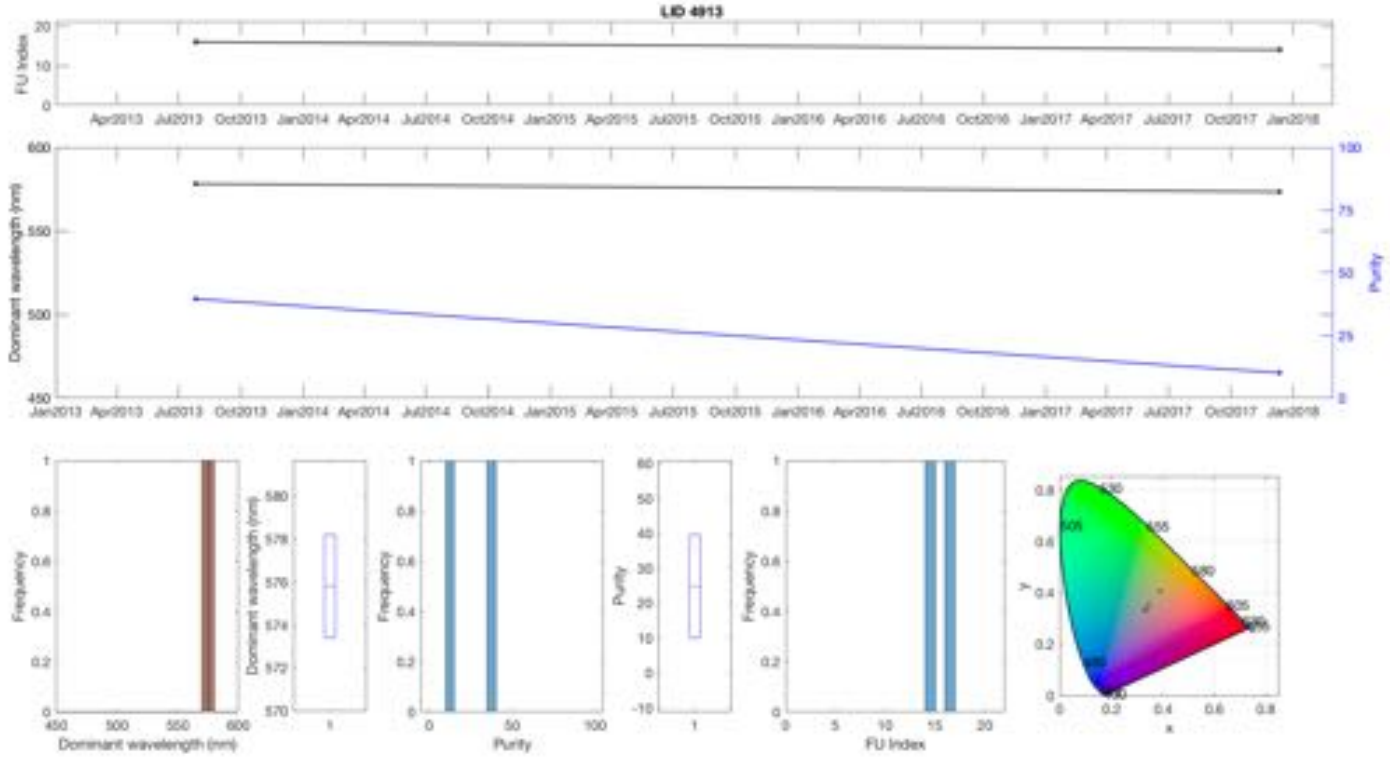
LID 4913
FU Index
Dominant wavelength (nm)
Purity
Frequency
Dominant wavelength (nm)
Purity
FU Index
x
y

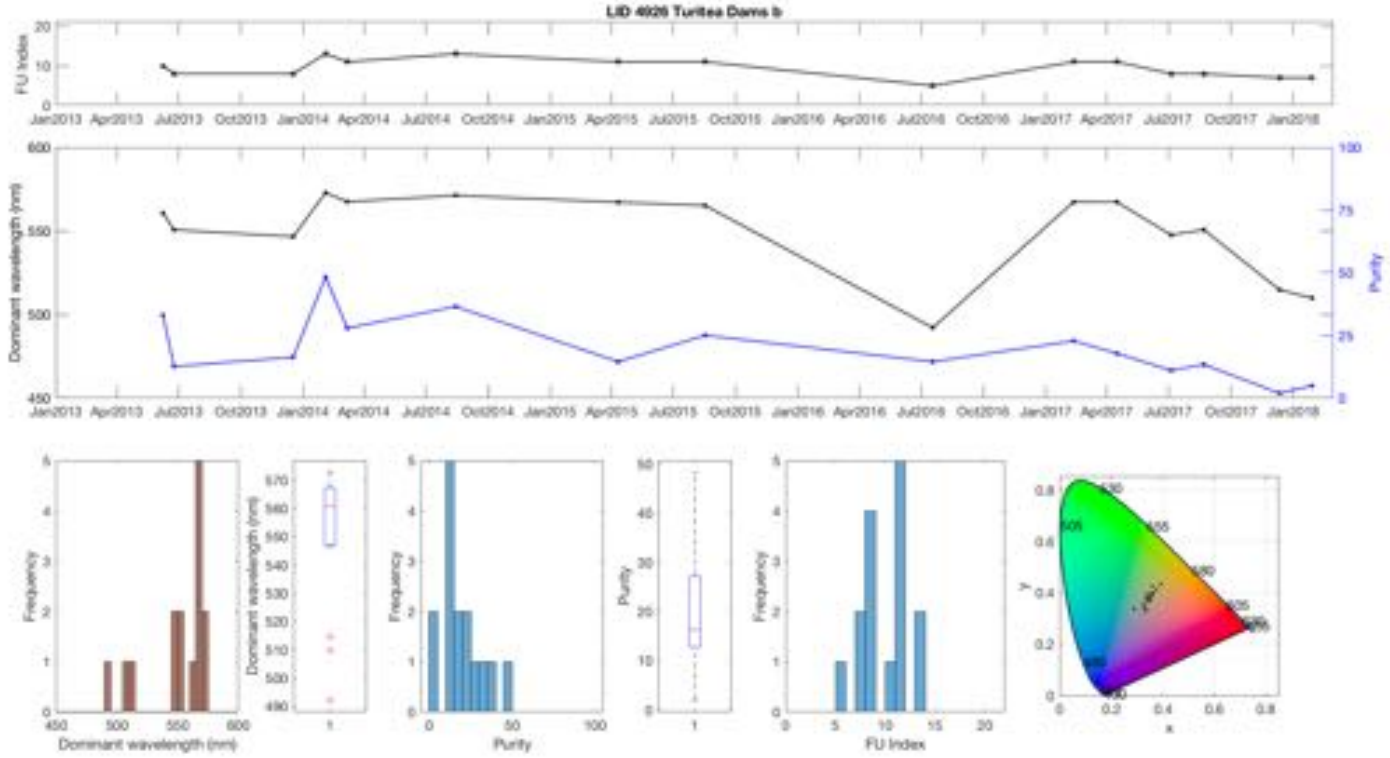
LID 4926 Turitea Dams b
FU Index
Dominant wavelength (nm)
Purity
Frequency
Dominant wavelength (nm)
Purity
FU Index
x
y

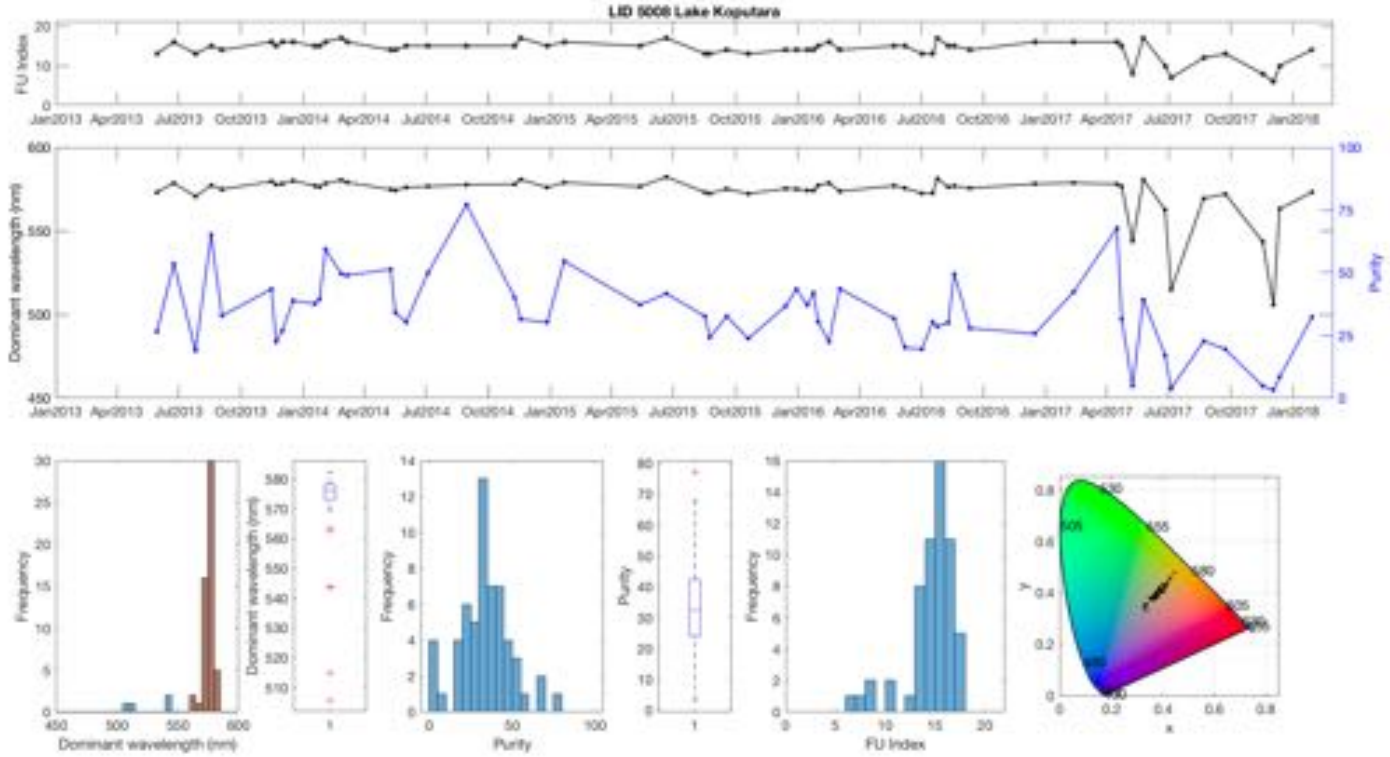
LID 5008 Lake Koputara
FU Index
Dominant wavelength (nm)
Purity
Frequency
Dominant wavelength (nm)
Purity
Frequency
Purity
Frequency
FU Index
y
x

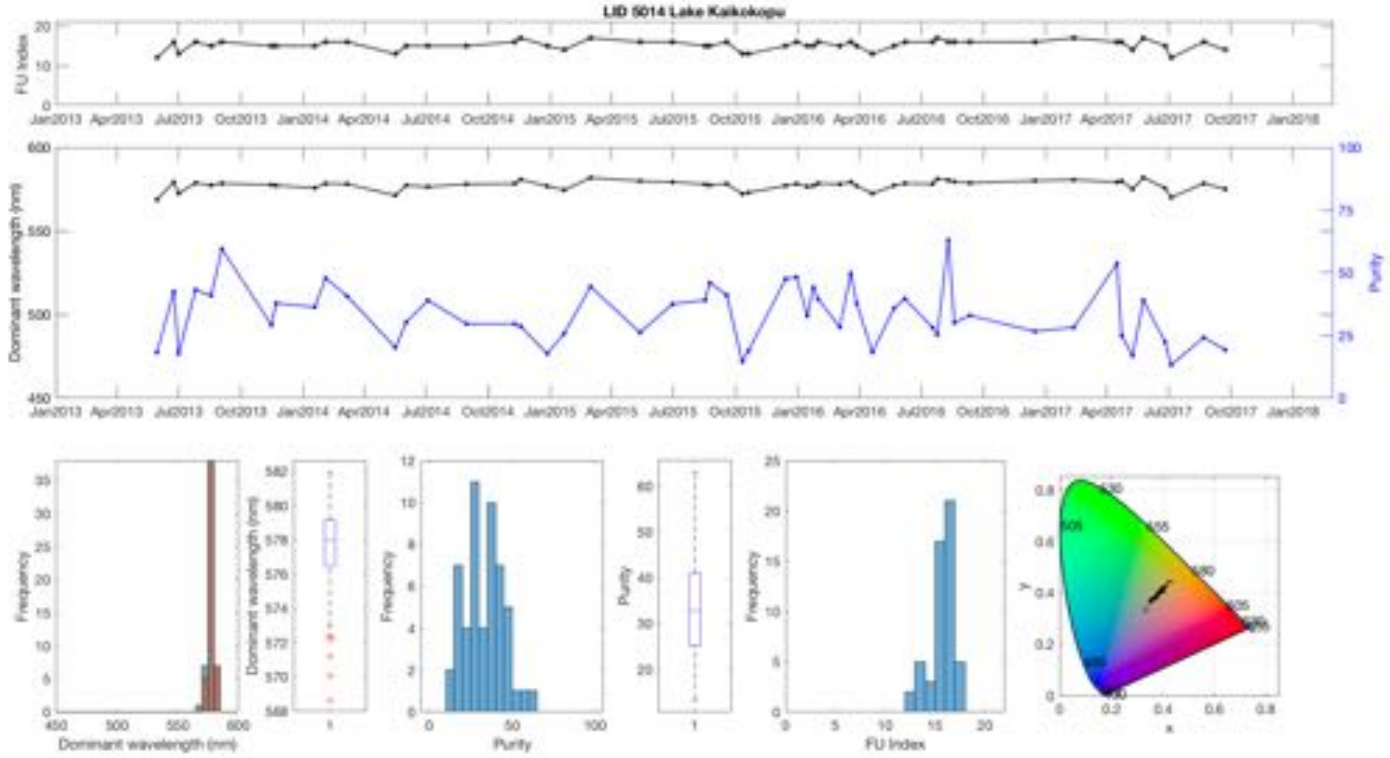
LID 5014 Lake Kaikokopu
FU Index
Dominant wavelength (nm)
Purity
Frequency
Dominant wavelength (nm)
Purity
Frequency
Purity
Frequency
FU Index
y
x

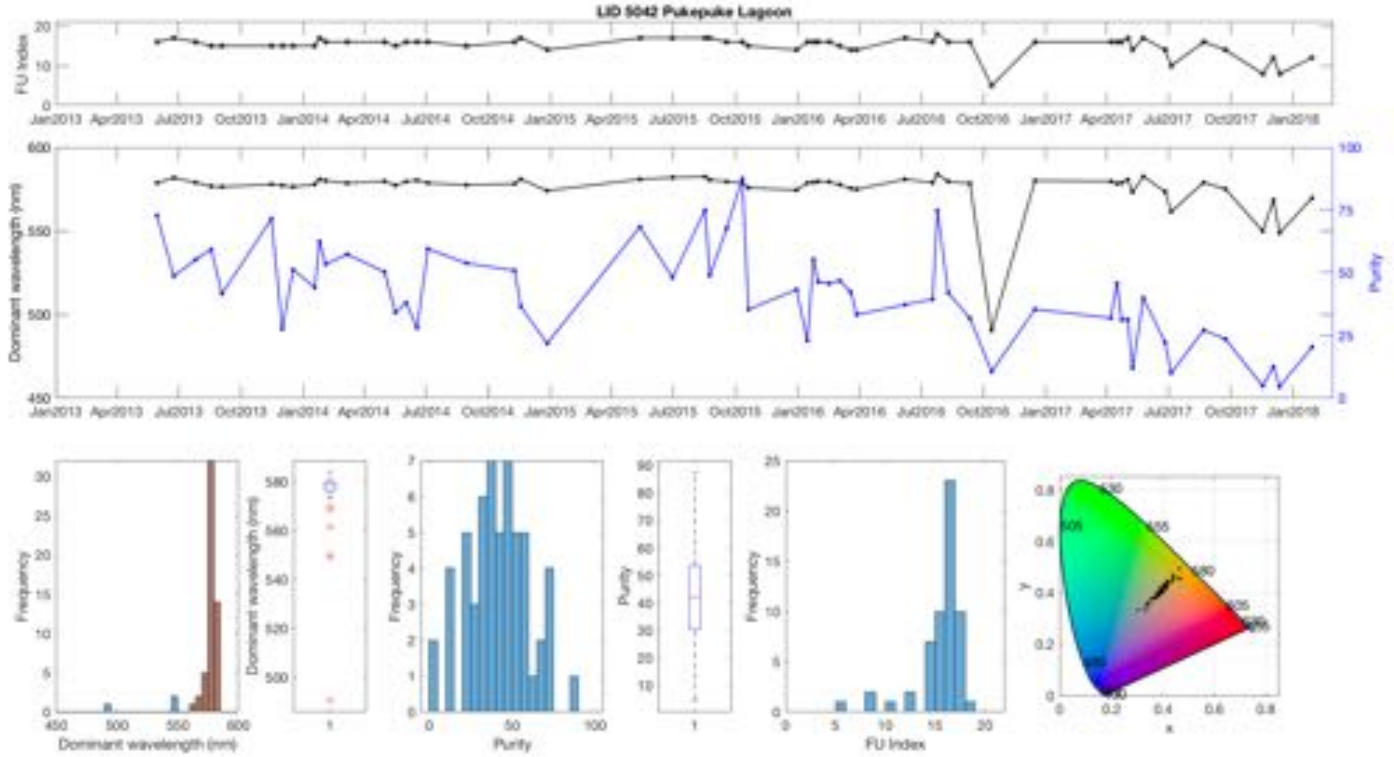
LID 5042 Pukepuke Lagoon
FU Index
Dominant wavelength (nm)
Purity
Frequency
Dominant wavelength (nm)
Purity
Frequency
Purity
Frequency
FU Index
y
x

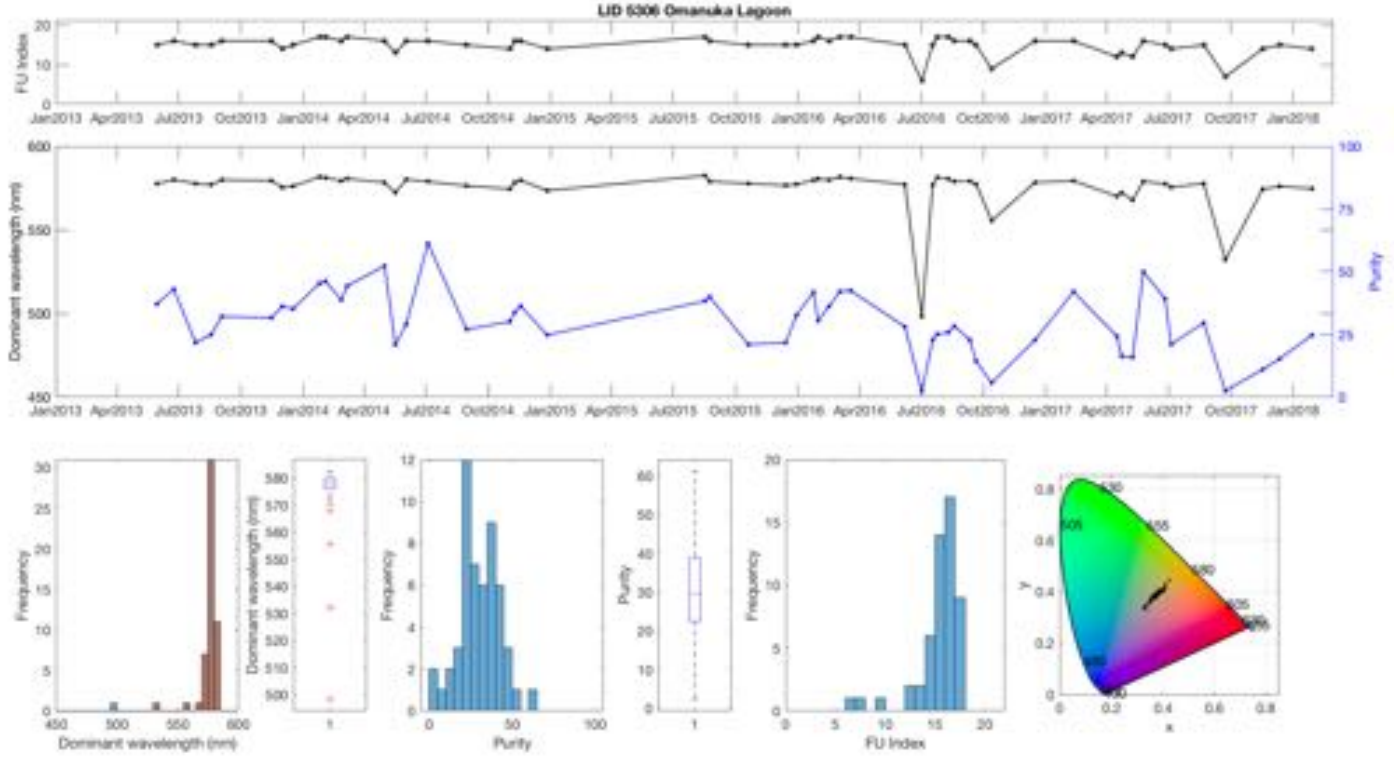
LID 5306 Omanuka Lagoon
FU Index
Dominant wavelength (nm)
Purity
Frequency
Dominant wavelength (nm)
Purity
Frequency
Purity
Frequency
FU Index
y
x

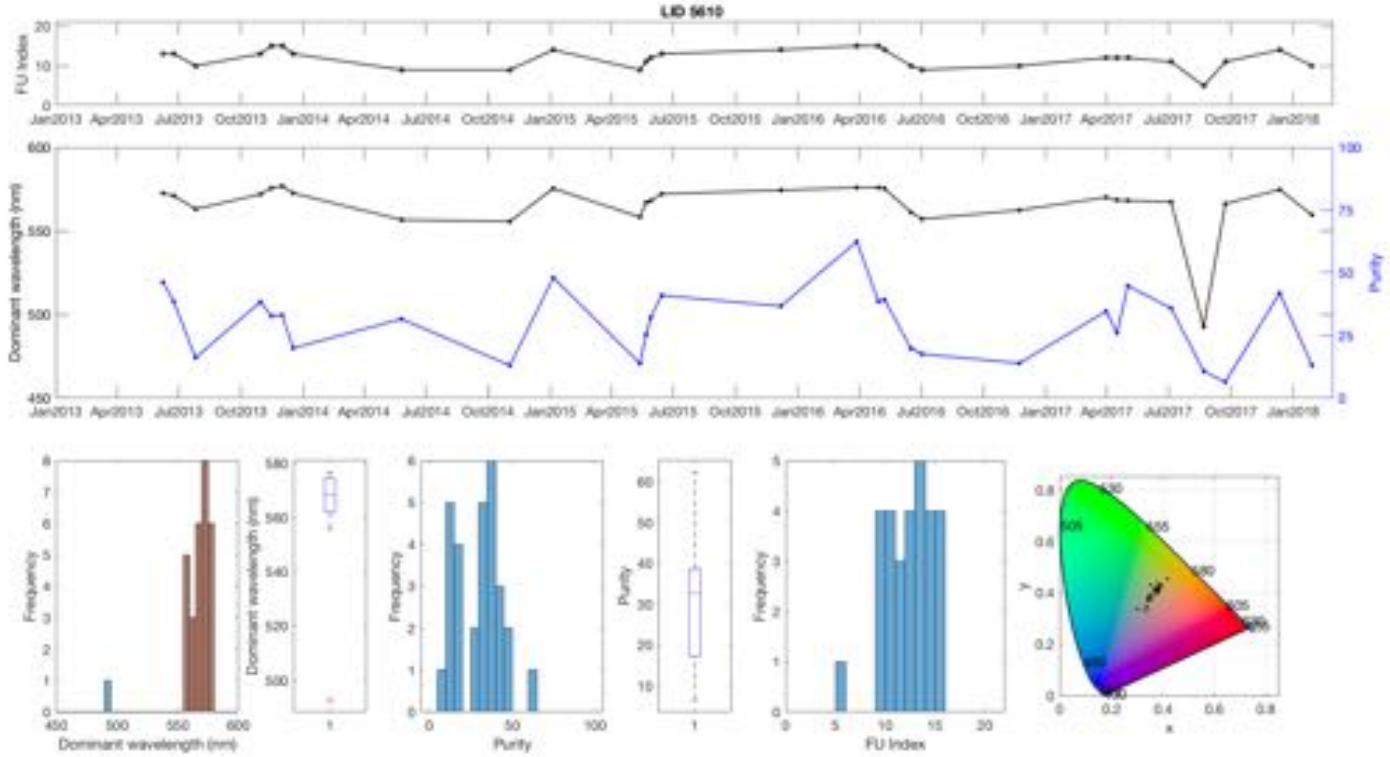
LID 5610
FU Index
Dominant wavelength (nm)
Purity
Frequency
Dominant wavelength (nm)
Purity
Frequency
Purity
Frequency
FU Index
y
x

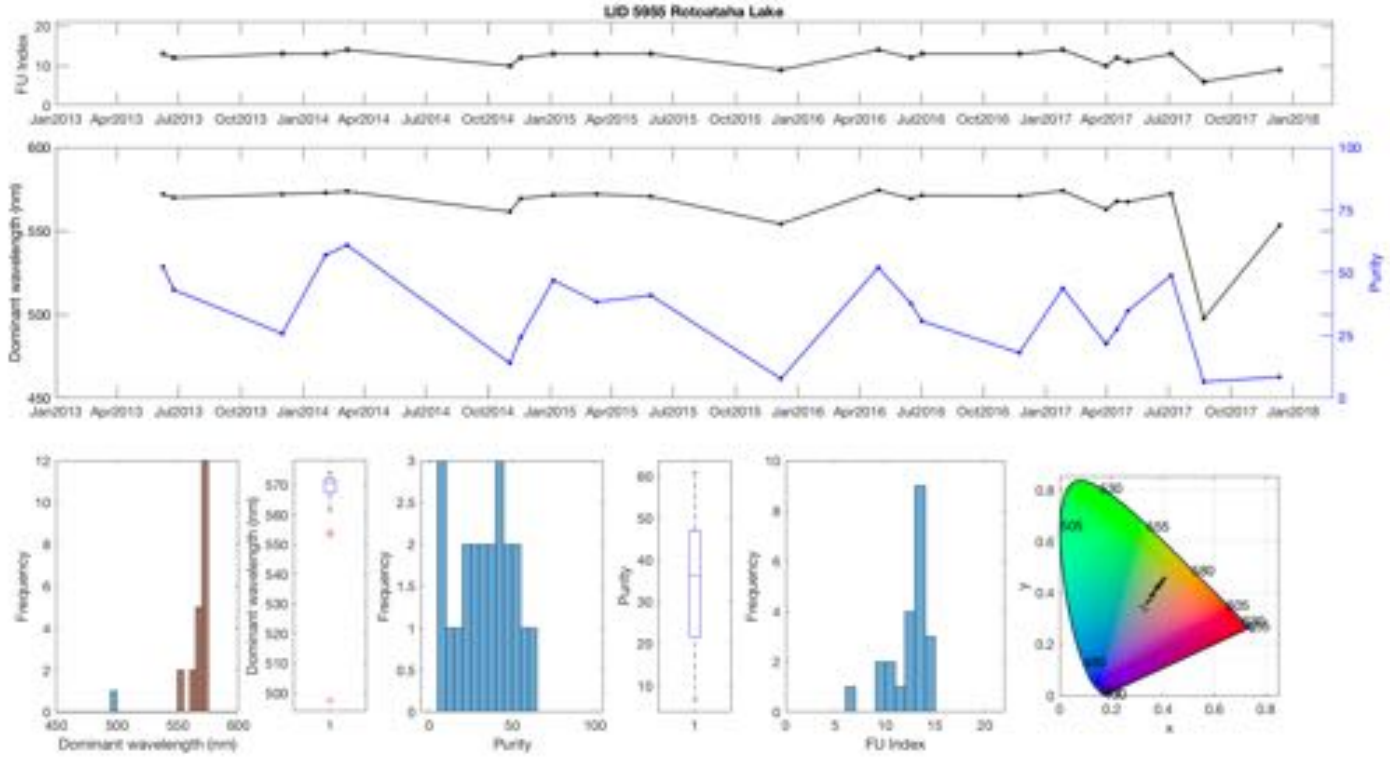
LID 5955 Rotoataha Lake
FU Index
Dominant wavelength (nm)
Purity
Frequency
Dominant wavelength (nm)
Purity
Frequency
Purity
Frequency
FU Index
y
x

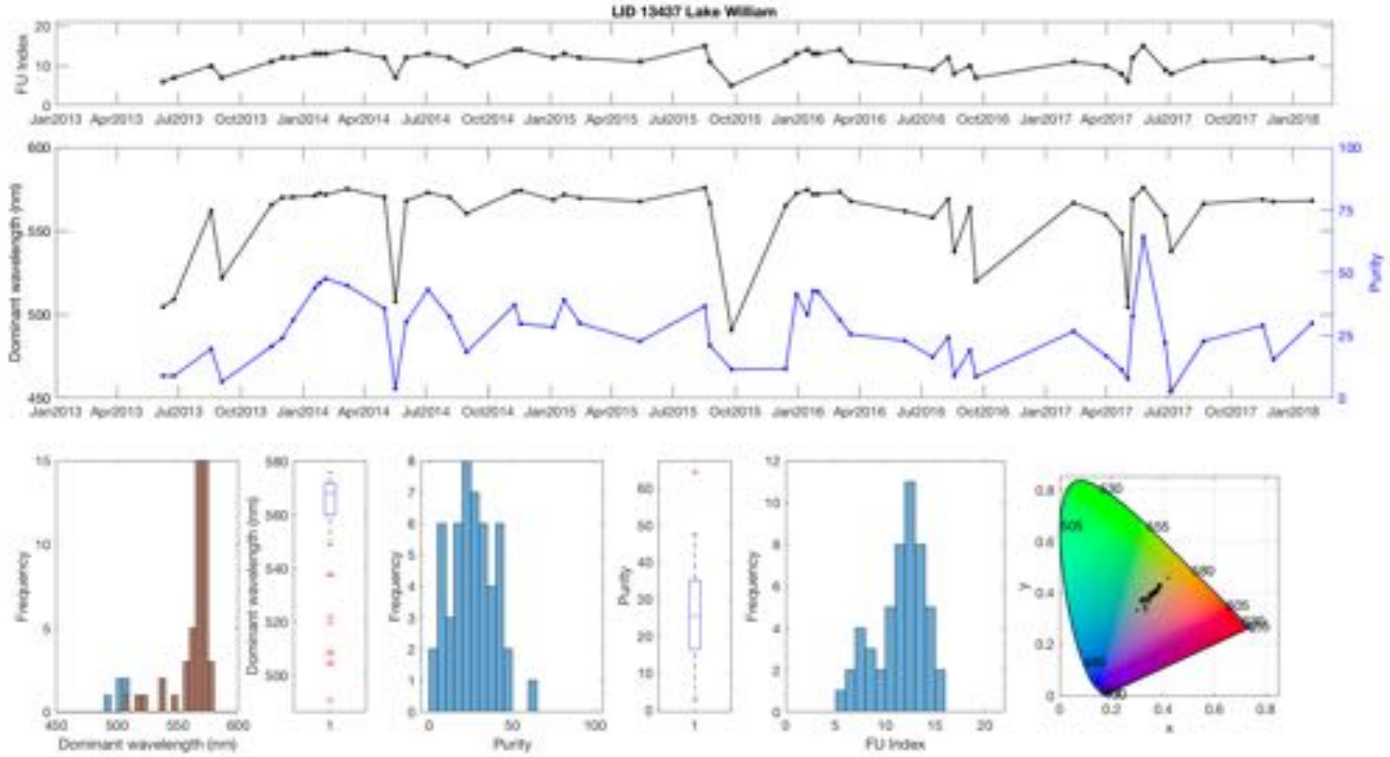
LID 13437 Lake William
FU Index
Dominant wavelength (nm)
Purity
Frequency
Dominant wavelength (nm)
Purity
Frequency
Purity
Frequency
FU Index
y
x

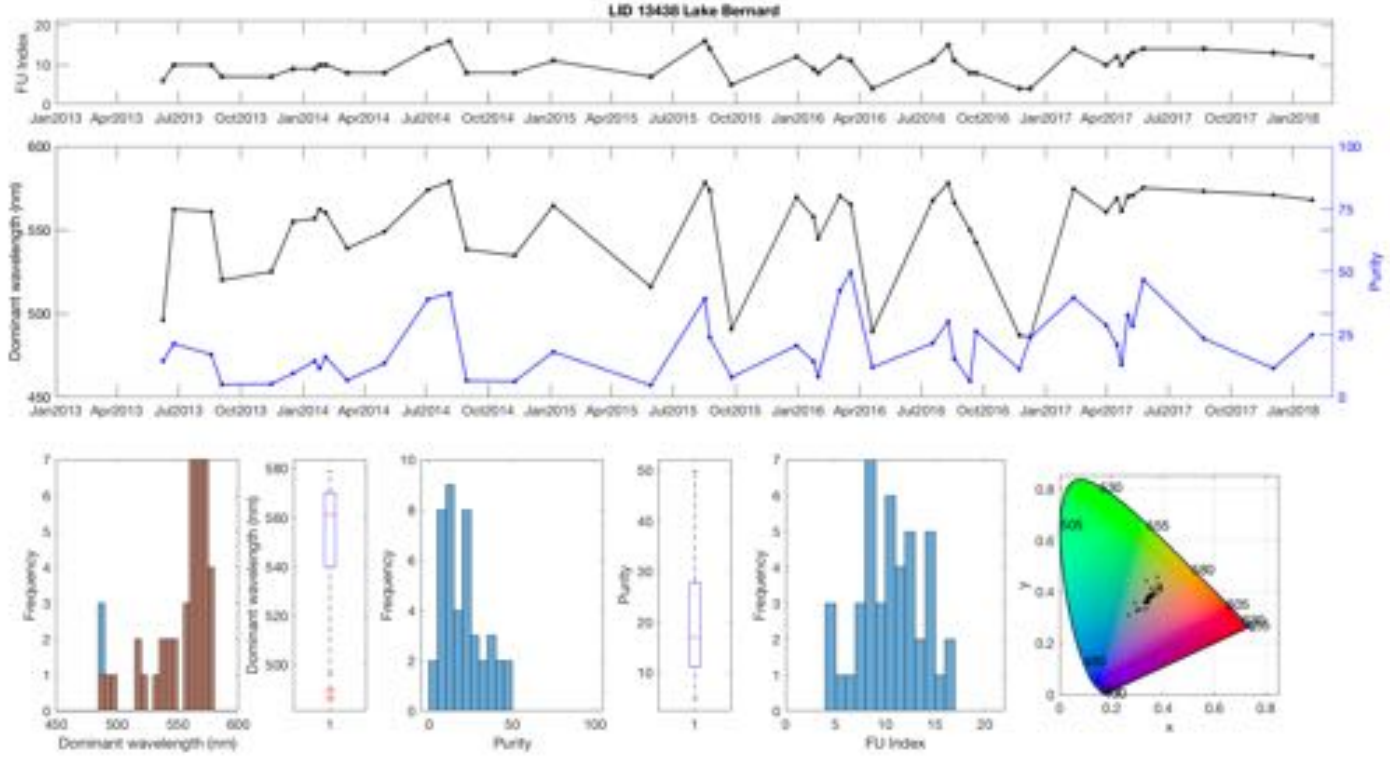
LID 13438 Lake Bernard
FU Index
Dominant wavelength (nm)
Purity
Frequency
Dominant wavelength (nm)
Purity
Frequency
Purity
Frequency
FU Index
y
x

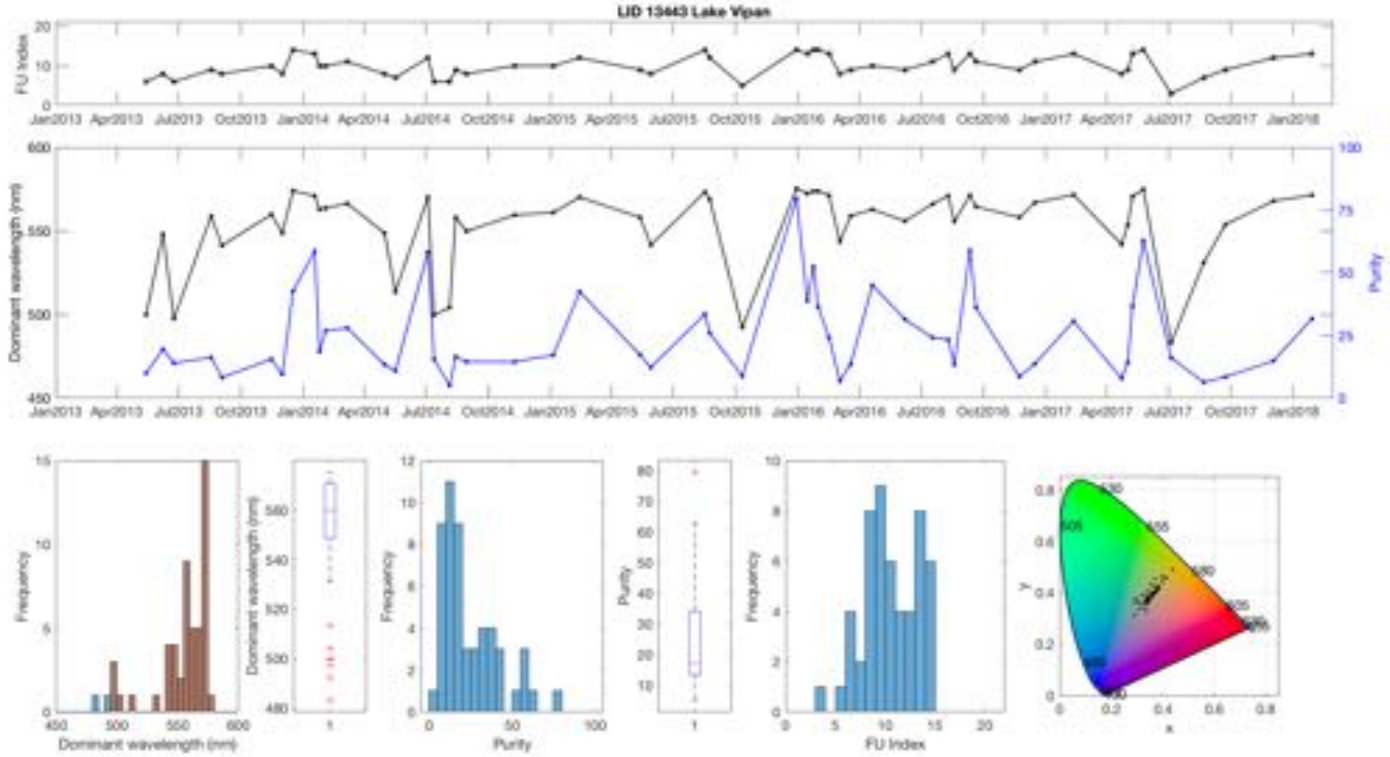
LID 13443 Lake Vpan
FU Index
Dominant wavelength (nm)
Purity
Frequency
Dominant wavelength (nm)
Purity
FU Index
x
y

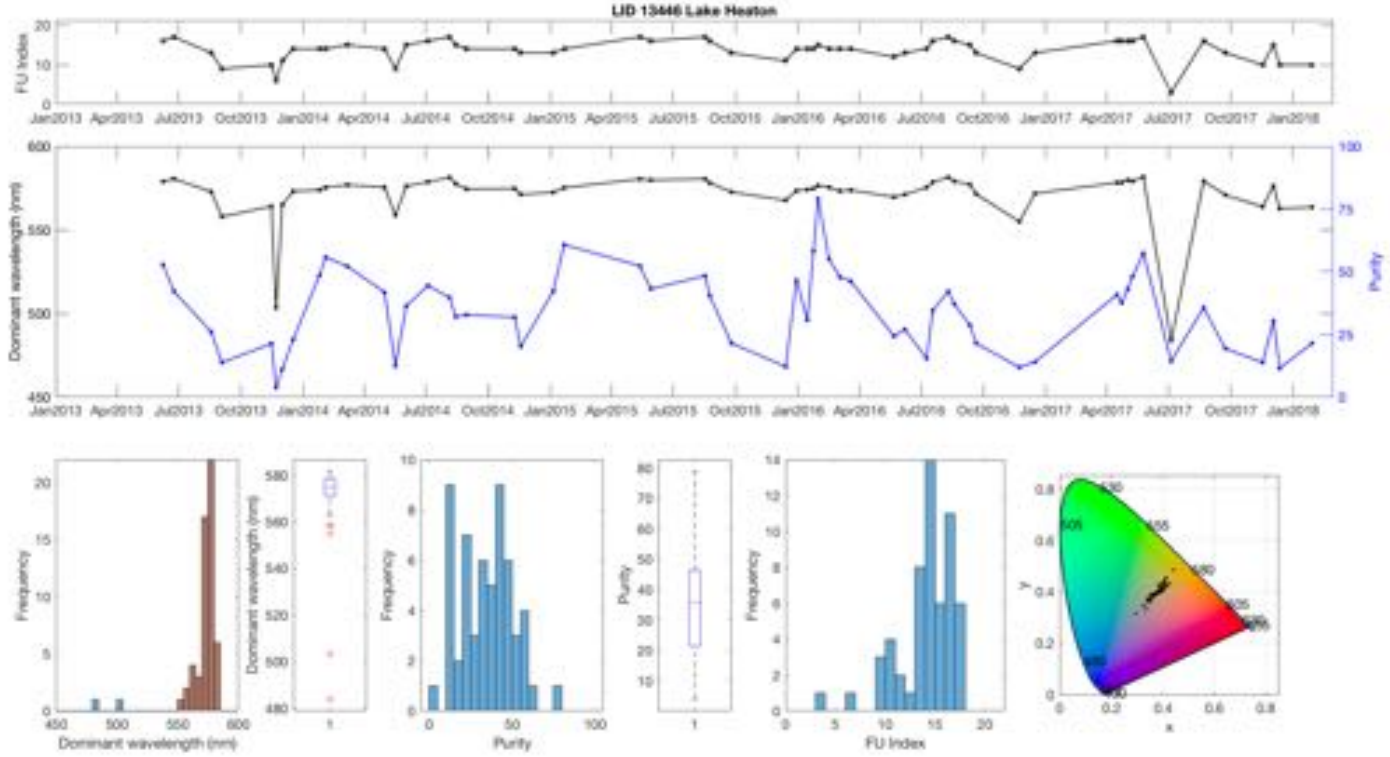
LID 13446 Lake Heaton
FU Index
Dominant wavelength (nm)
Purity
Frequency
Dominant wavelength (nm)
Purity
FU Index
x
y

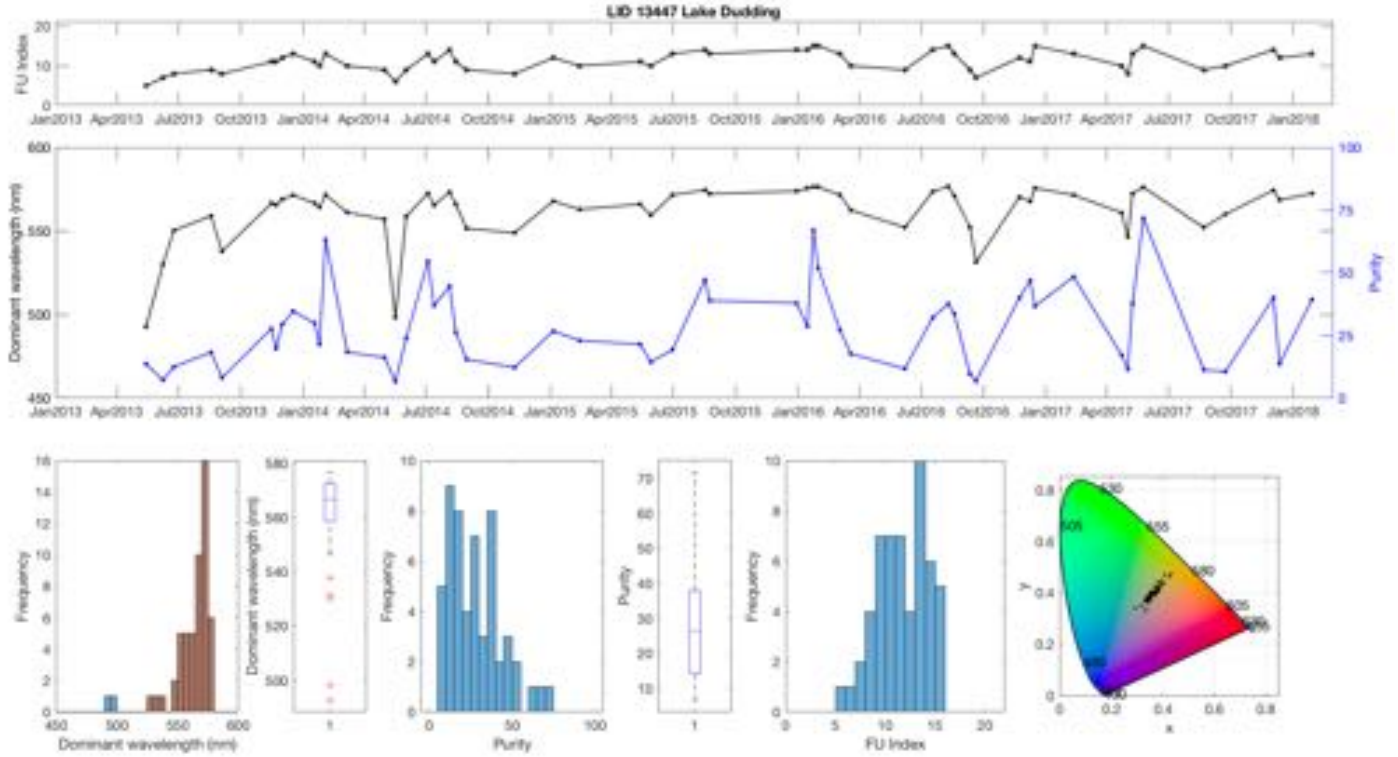
LID 13447 Lake Dudding
FU Index
Dominant wavelength (nm)
Purity
Jan2013 Apr2013 Jul2013 Oct2013 Jan2014 Apr2014 Jul2014 Oct2014 Jan2015 Apr2015 Jul2015 Oct2015 Jan2016 Apr2016 Jul2016 Oct2016 Jan2017 Apr2017 Jul2017 Oct2017 Jan2018
Frequency
Dominant wavelength (nm)
Purity
FU Index
x
y

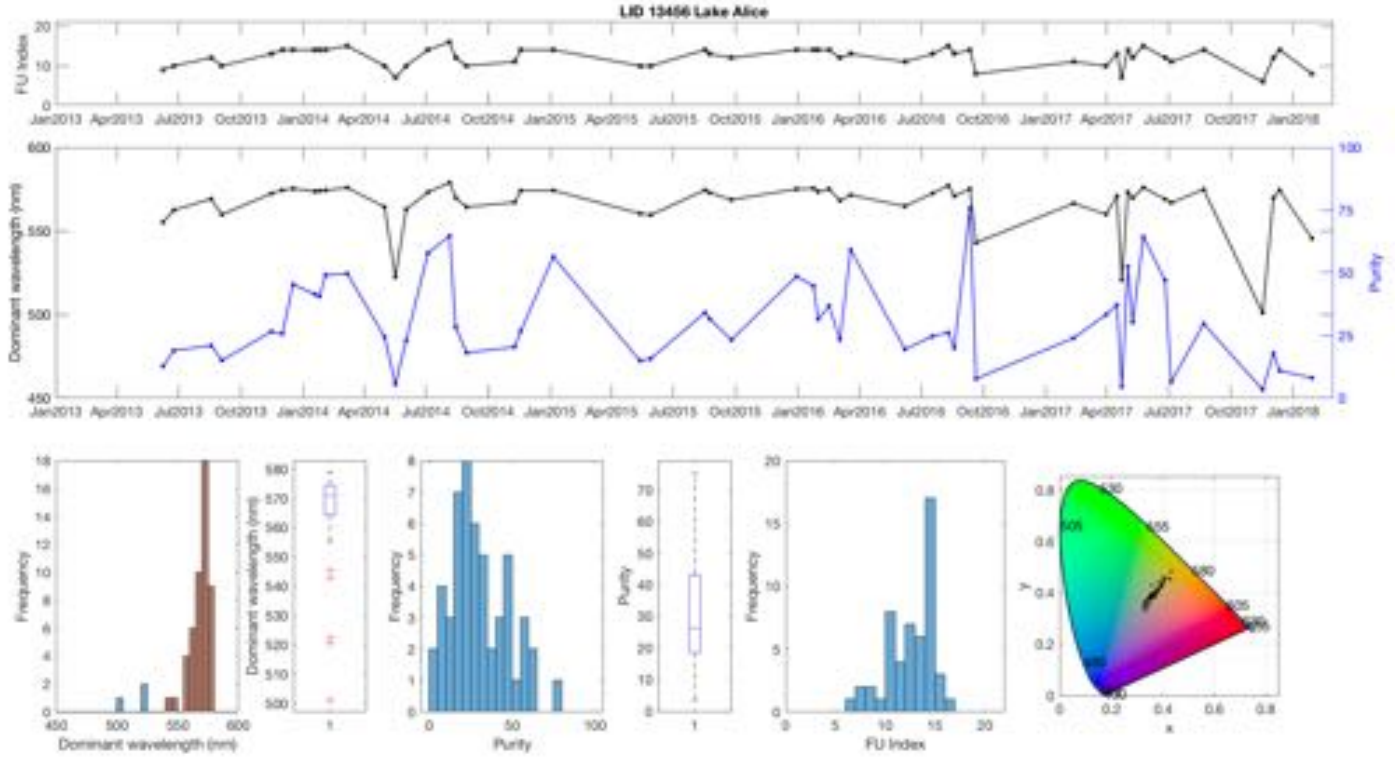
LID 13456 Lake Alice
FU Index
Dominant wavelength (nm)
Purity
Jan2013 Apr2013 Jul2013 Oct2013 Jan2014 Apr2014 Jul2014 Oct2014 Jan2015 Apr2015 Jul2015 Oct2015 Jan2016 Apr2016 Jul2016 Oct2016 Jan2017 Apr2017 Jul2017 Oct2017 Jan2018
Frequency
Dominant wavelength (nm)
Purity
FU Index
x
y

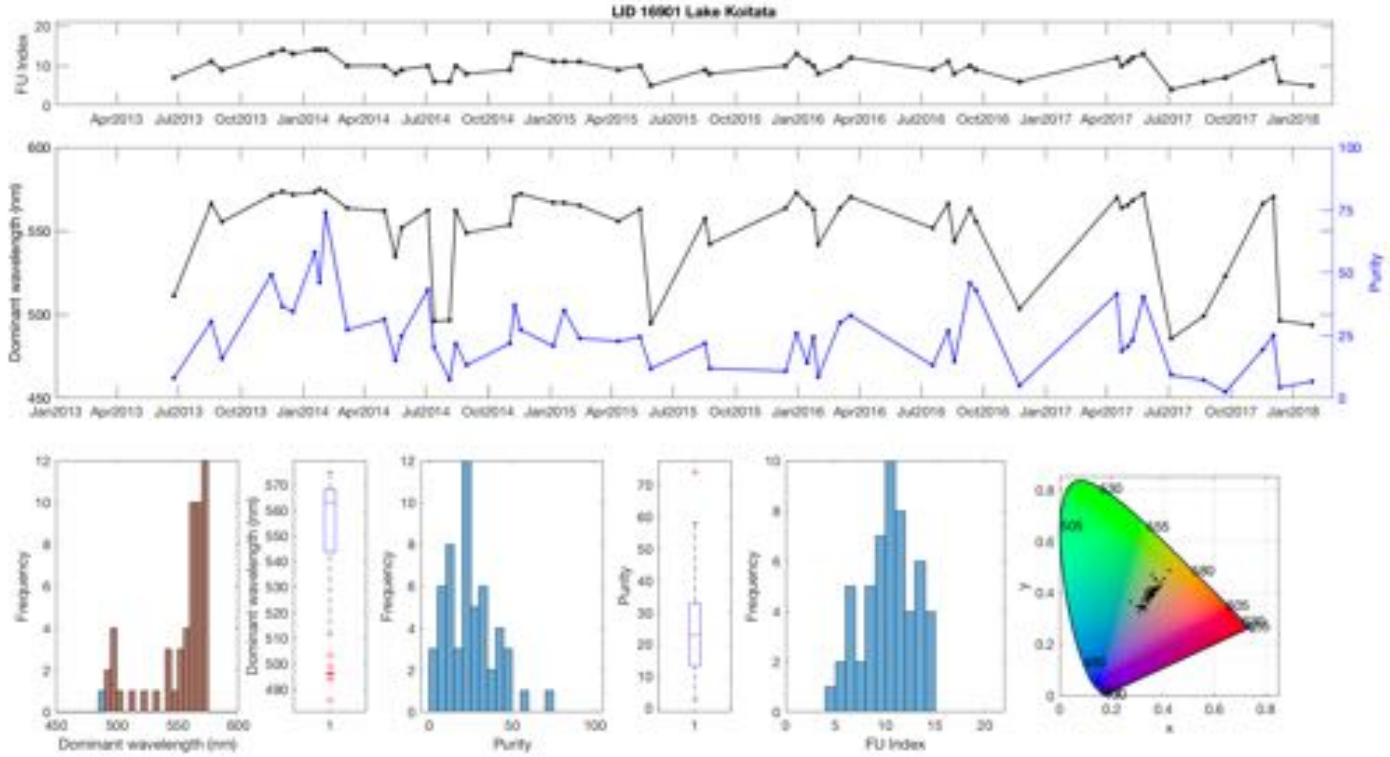
LID 16901 Lake Koitata
FU Index
Dominant wavelength (nm)
Purity
Frequency
Dominant wavelength (nm)
Purity
FU Index
x
y

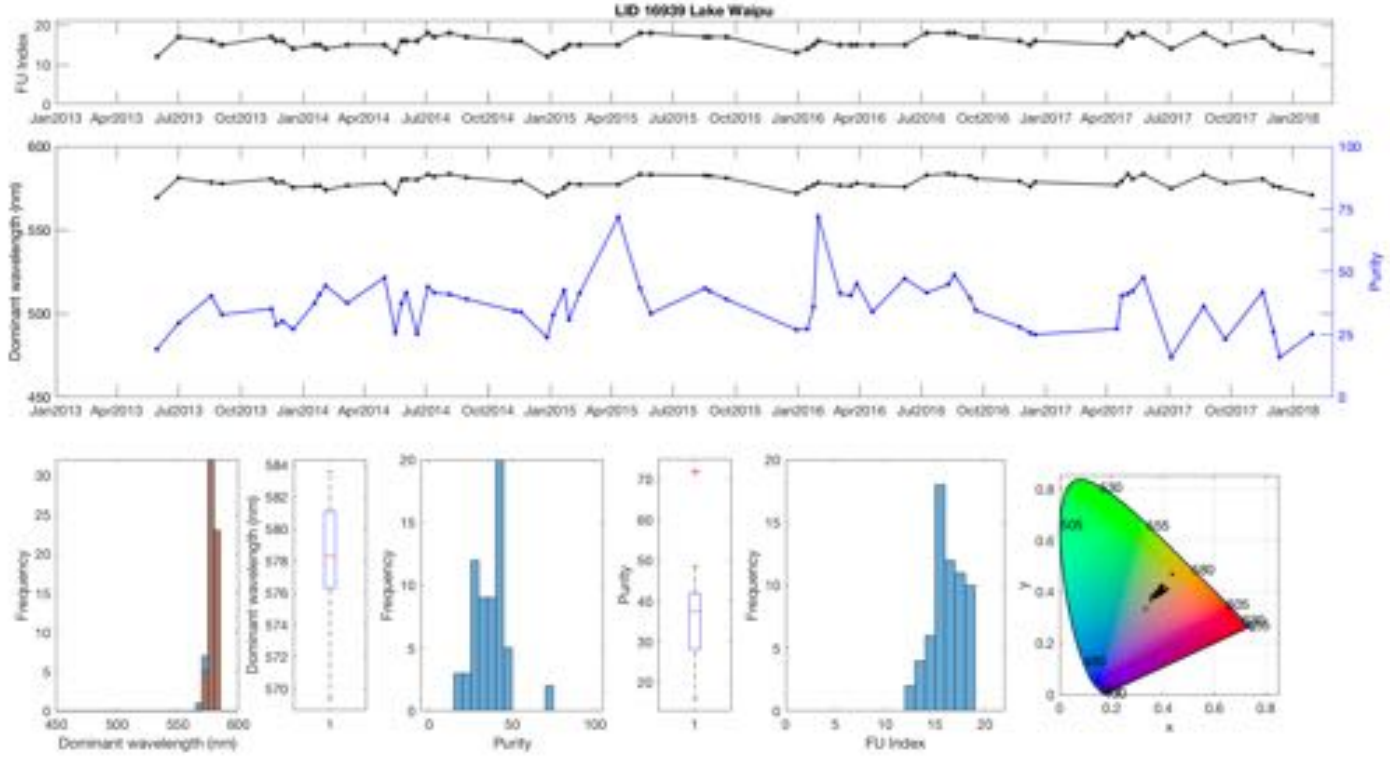
LID 16939 Lake Waipu
FU Index
Dominant wavelength (nm)
Purity
Frequency
Dominant wavelength (nm)
Purity
FU Index
x
y

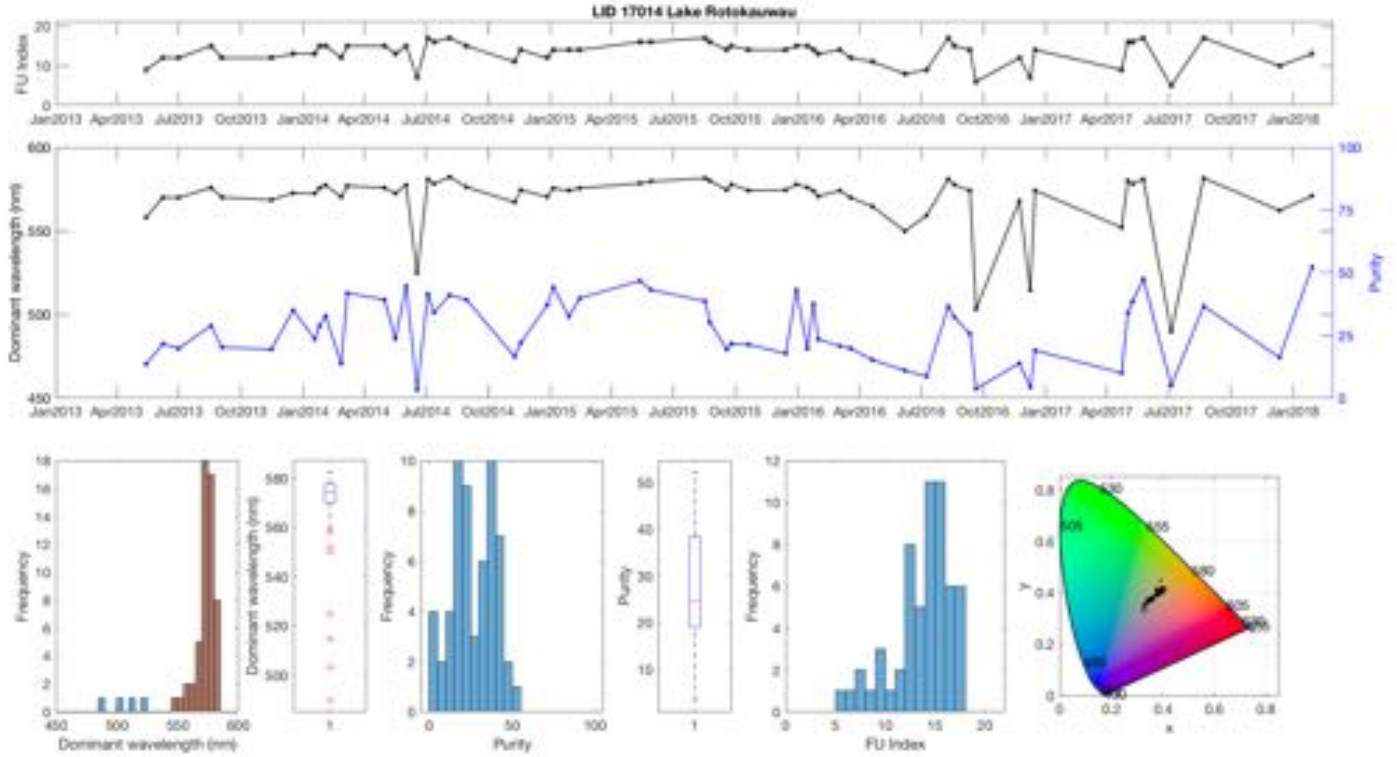
LID 17014 Lake Rotokauwau
FU Index
Dominant wavelength (nm)
Purity
Jan2013 Apr2013 Jul2013 Oct2013 Jan2014 Apr2014 Jul2014 Oct2014 Jan2015 Apr2015 Jul2015 Oct2015 Jan2016 Apr2016 Jul2016 Oct2016 Jan2017 Apr2017 Jul2017 Oct2017 Jan2018
Frequency
Dominant wavelength (nm)
Purity
FU Index
x
y

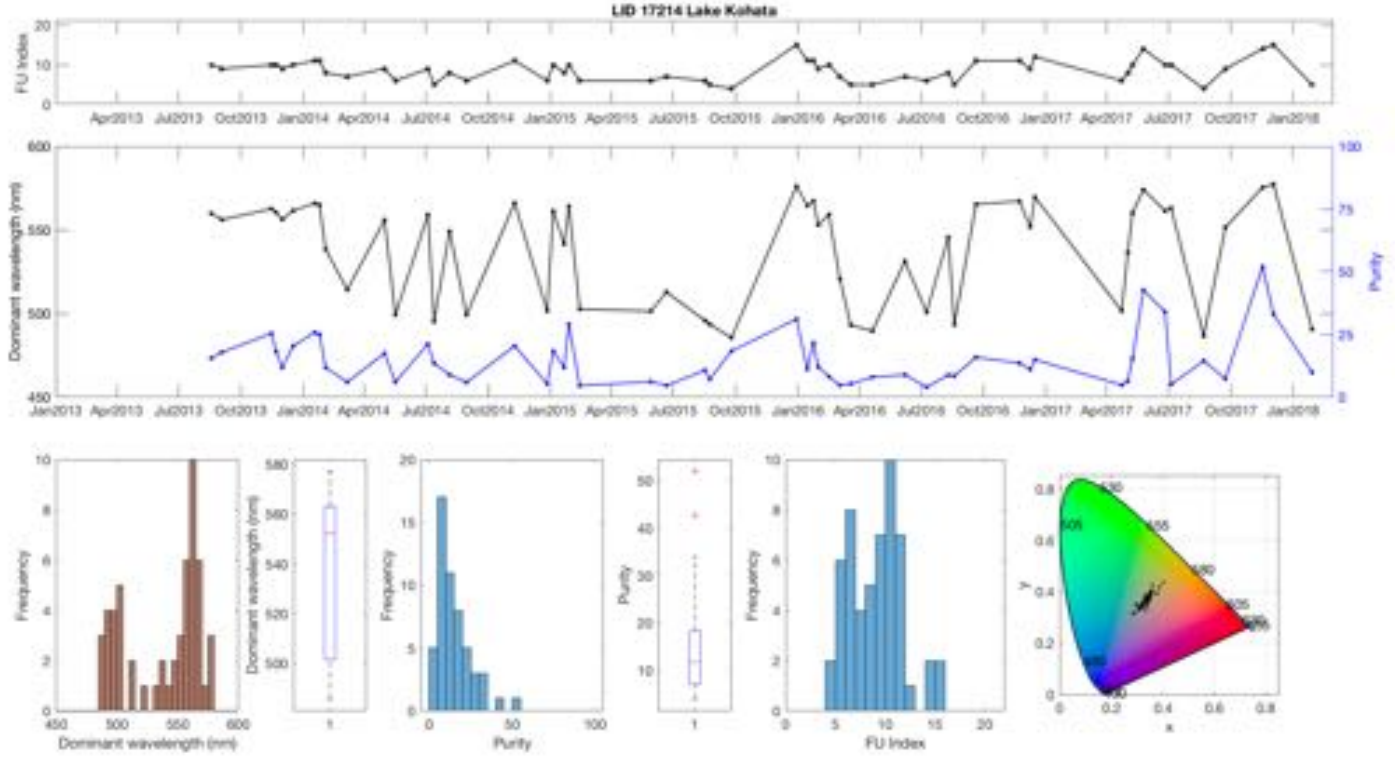
LID 17214 Lake Kohata
FU Index
Dominant wavelength (nm)
Purity
Apr2013 Jul2013 Oct2013 Jan2014 Apr2014 Jul2014 Oct2014 Jan2015 Apr2015 Jul2015 Oct2015 Jan2016 Apr2016 Jul2016 Oct2016 Jan2017 Apr2017 Jul2017 Oct2017 Jan2018
Frequency
Dominant wavelength (nm)
Purity
FU Index
x
y

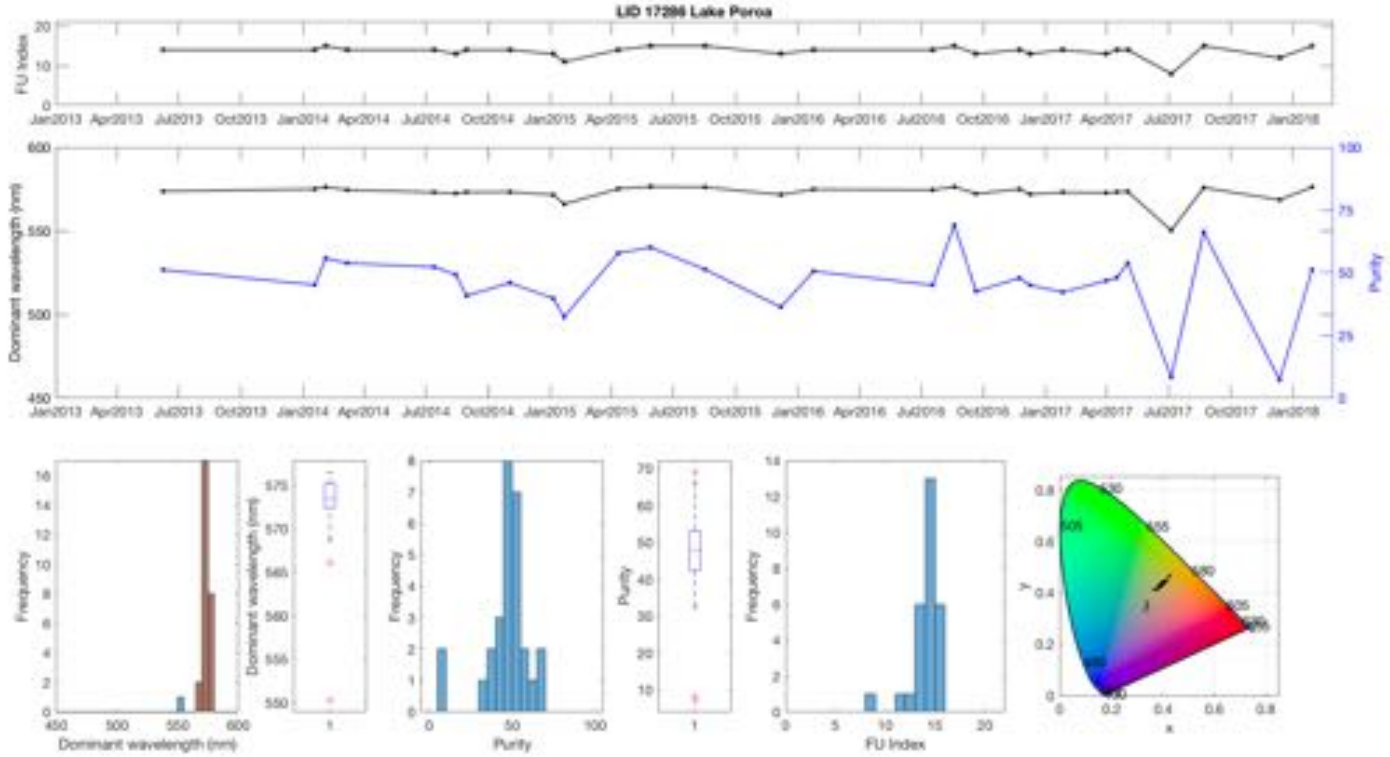
LID 17286 Lake Poroa
FU Index
Dominant wavelength (nm)
Purity
Jan2013 Apr2013 Jul2013 Oct2013 Jan2014 Apr2014 Jul2014 Oct2014 Jan2015 Apr2015 Jul2015 Oct2015 Jan2016 Apr2016 Jul2016 Oct2016 Jan2017 Apr2017 Jul2017 Oct2017 Jan2018
Frequency
Dominant wavelength (nm)
Purity
FU Index
x
y

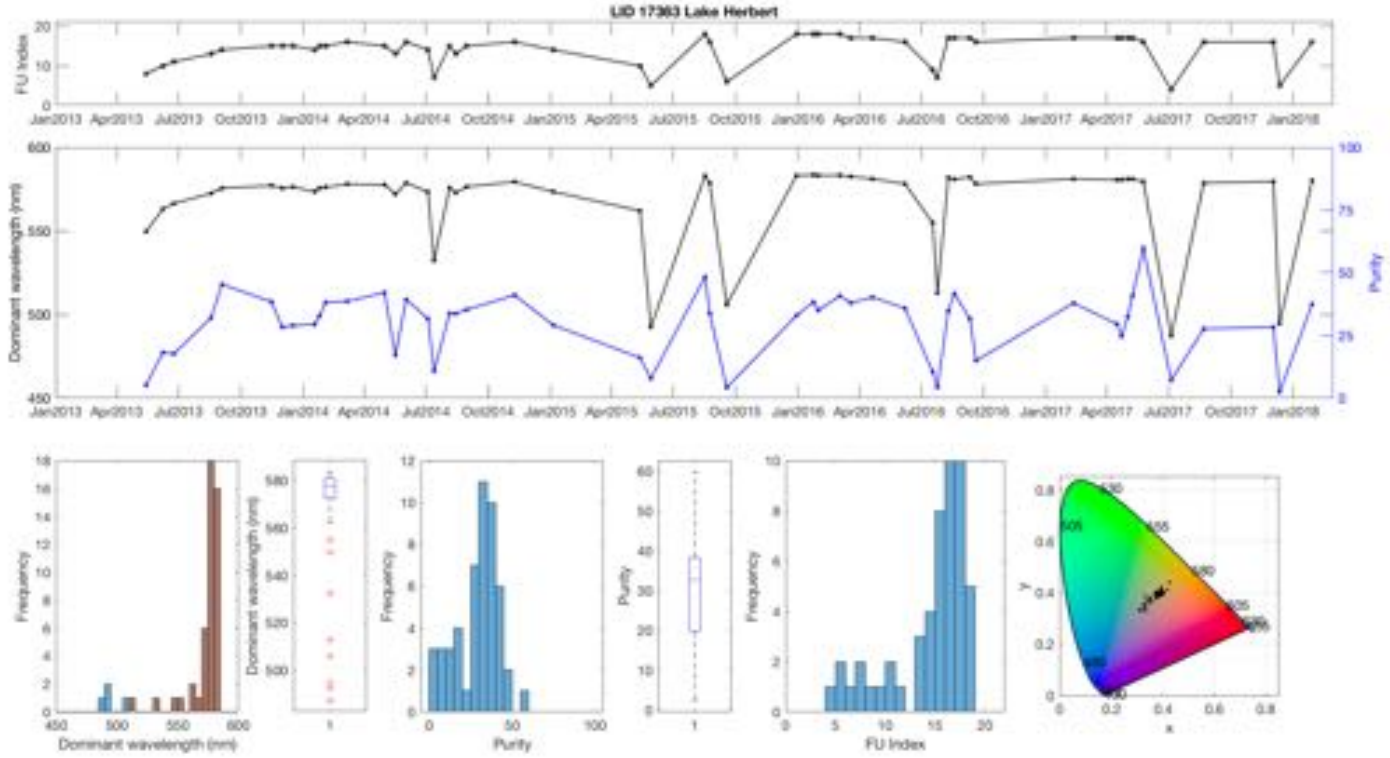
LID 17363 Lake Herbert
FU Index
Dominant wavelength (nm)
Purity
Jan2013 Apr2013 Jul2013 Oct2013 Jan2014 Apr2014 Jul2014 Oct2014 Jan2015 Apr2015 Jul2015 Oct2015 Jan2016 Apr2016 Jul2016 Oct2016 Jan2017 Apr2017 Jul2017 Oct2017 Jan2018
Frequency
Dominant wavelength (nm)
Purity
FU Index
x
y

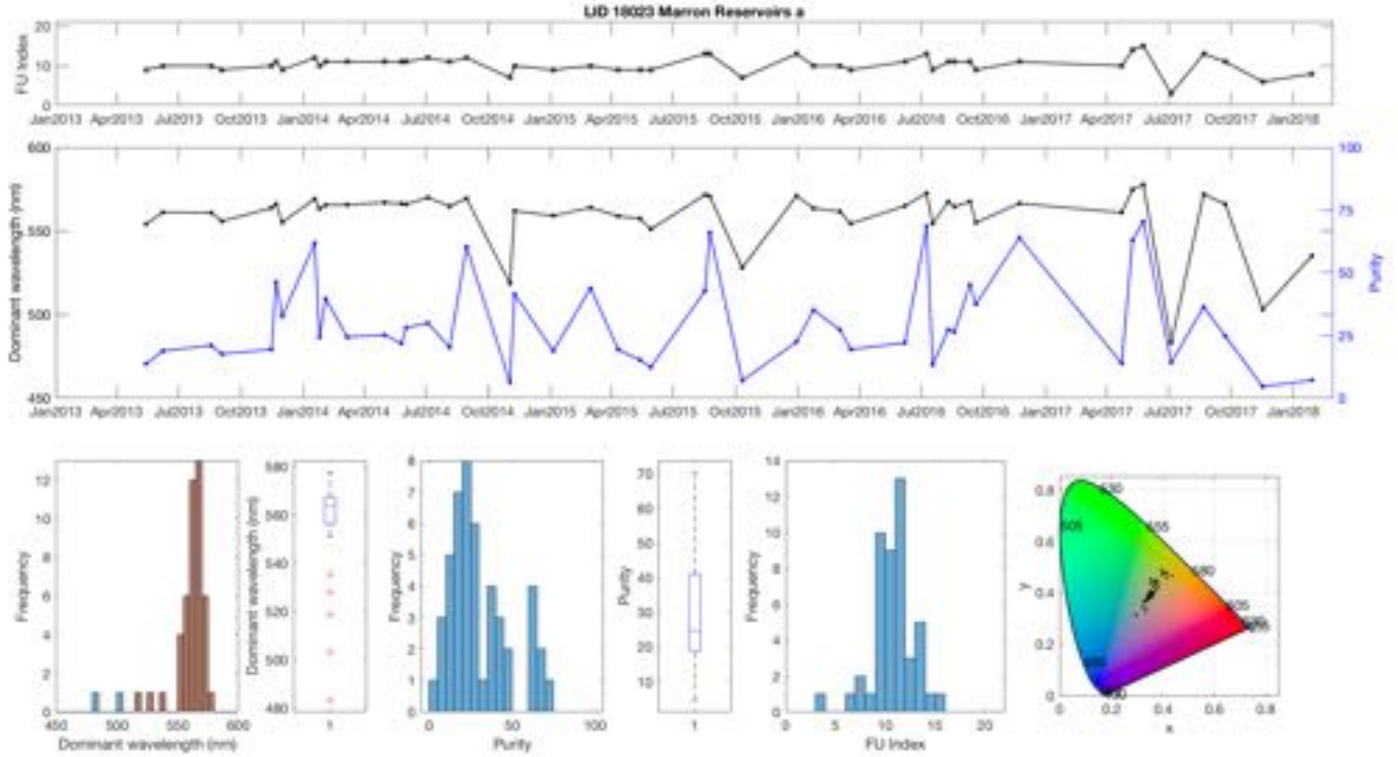
LID 18023 Marron Reservoirs a
FU Index
Dominant wavelength (nm)
Purity
Frequency
Dominant wavelength (nm)
Frequency
Purity
Purity
Frequency
FU Index
x
y

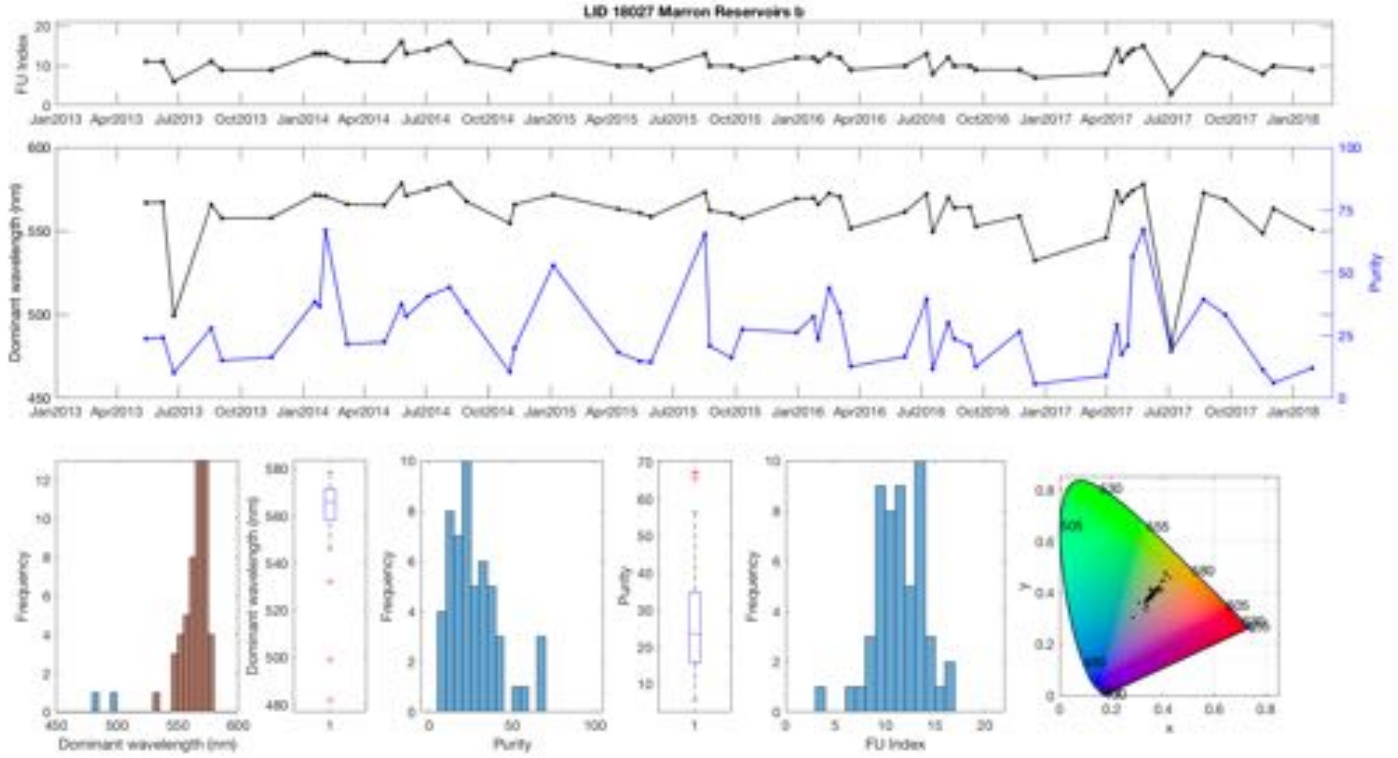
LID 18027 Marron Reservoirs b
FU Index
Dominant wavelength (nm)
Purity
Frequency
Dominant wavelength (nm)
Frequency
Purity
Purity
Frequency
FU Index
x
y

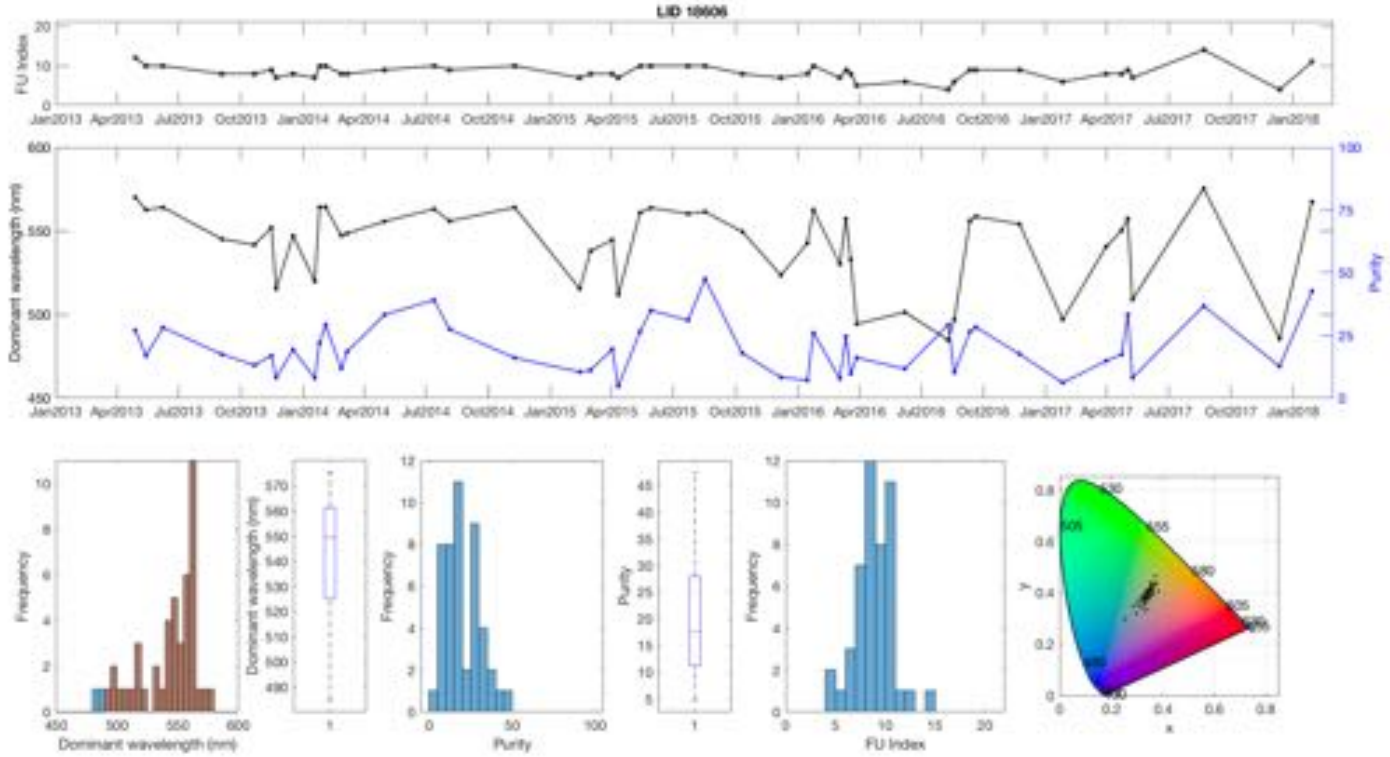
LID 10606
FU Index
Dominant wavelength (nm)
Purity
Frequency
Dominant wavelength (nm)
Purity
FU Index
y
x

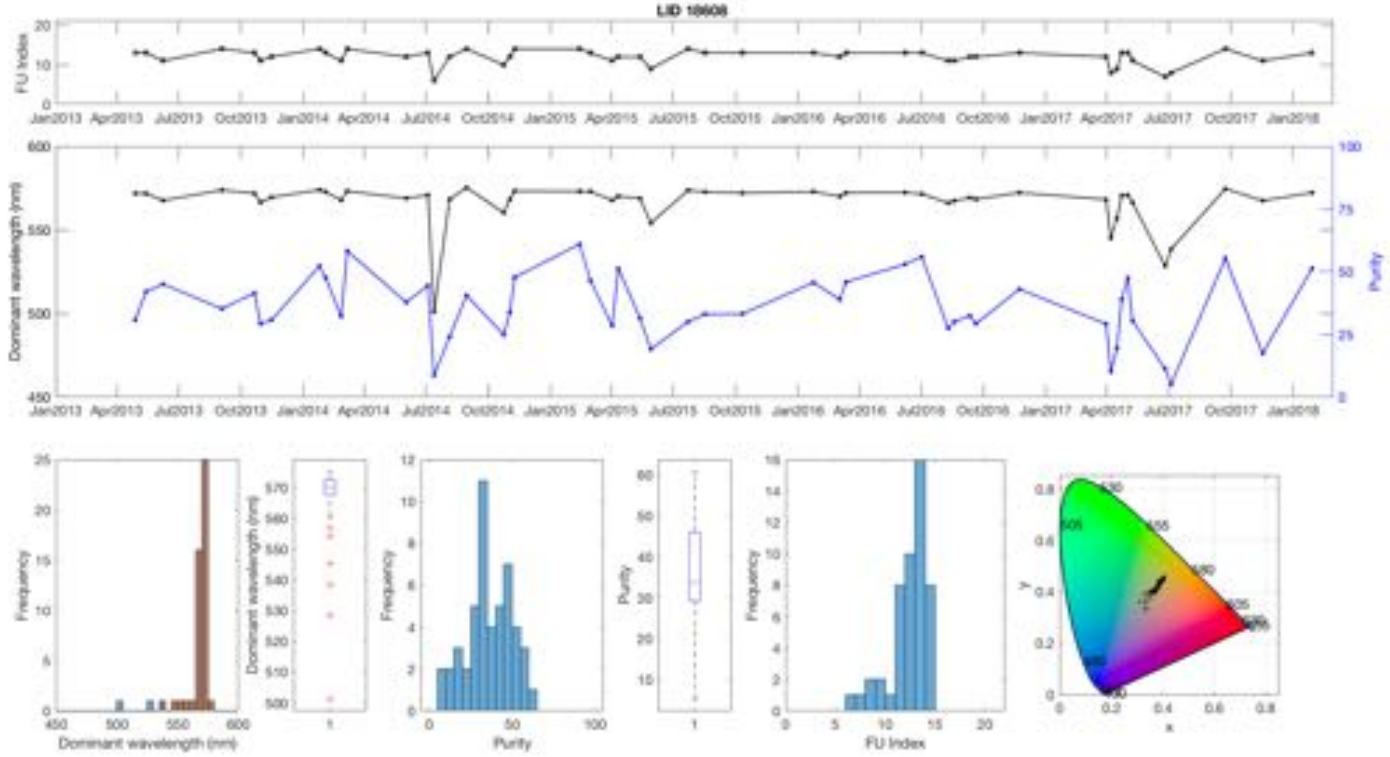
LID 10608
FU Index
Dominant wavelength (nm)
Purity
Frequency
Dominant wavelength (nm)
Purity
FU Index
y
x

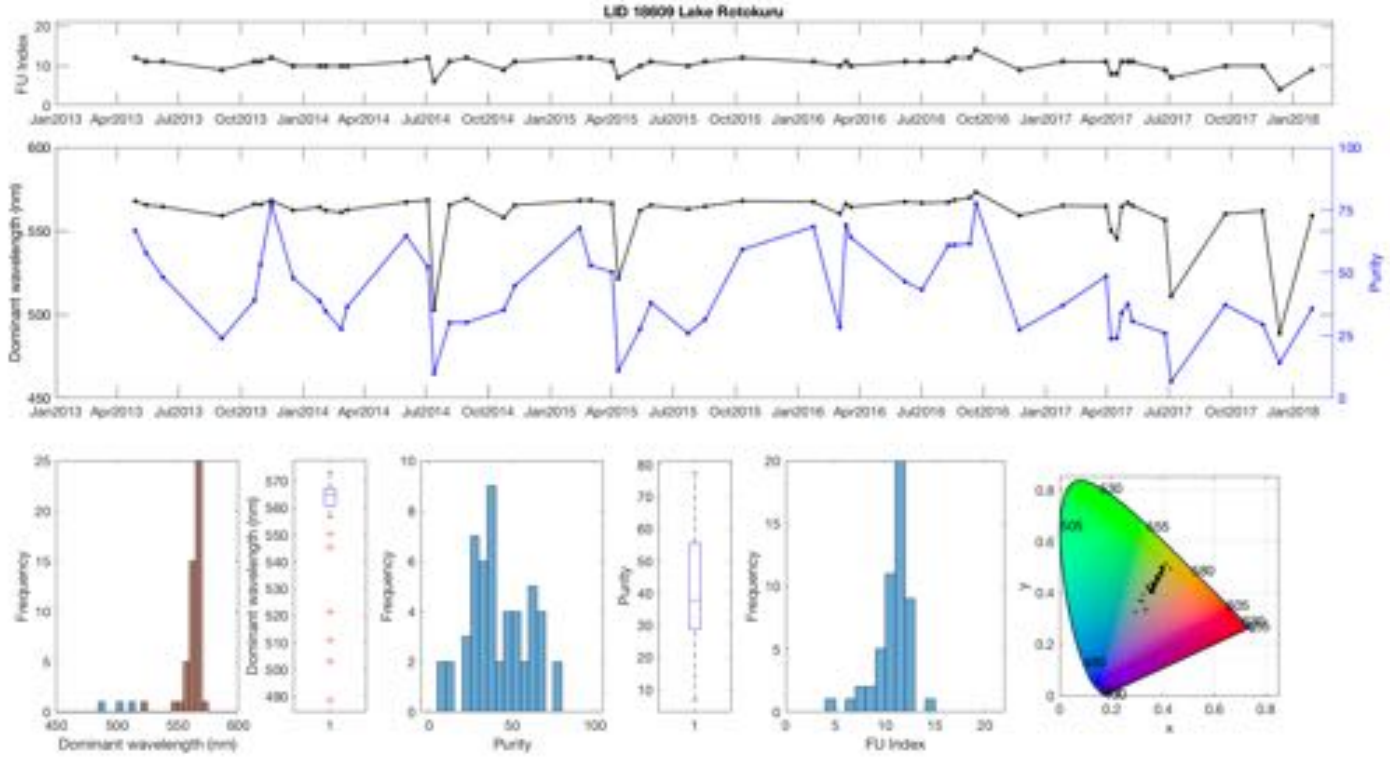
LID 10609 Lake Rotokuru
FU Index
Dominant wavelength (nm)
Purity
Jan2013 Apr2013 Jul2013 Oct2013 Jan2014 Apr2014 Jul2014 Oct2014 Jan2015 Apr2015 Jul2015 Oct2015 Jan2016 Apr2016 Jul2016 Oct2016 Jan2017 Apr2017 Jul2017 Oct2017 Jan2018
Frequency
Dominant wavelength (nm)
Purity
FU Index
x
y

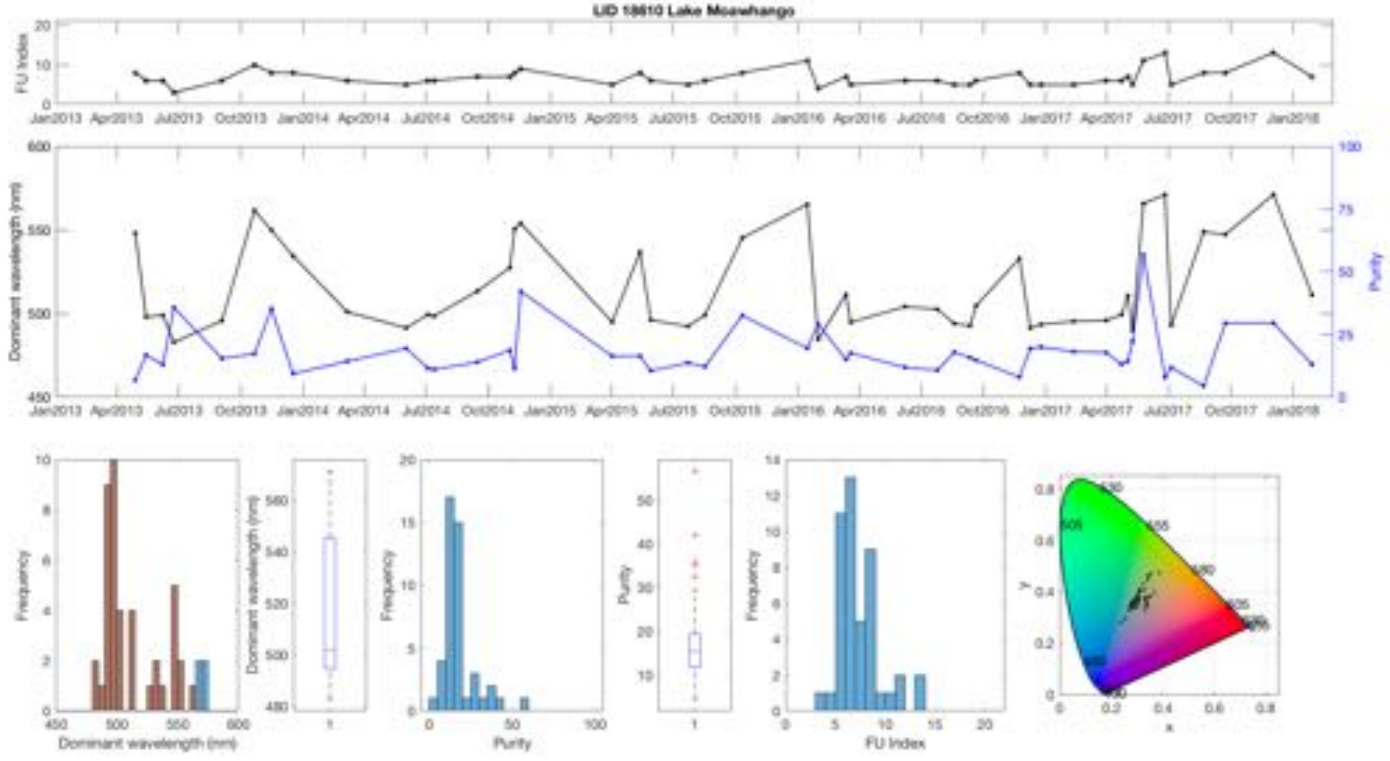
LID 10810 Lake Moawhango
FU Index
Dominant wavelength (nm)
Purity
Jan2013 Apr2013 Jul2013 Oct2013 Jan2014 Apr2014 Jul2014 Oct2014 Jan2015 Apr2015 Jul2015 Oct2015 Jan2016 Apr2016 Jul2016 Oct2016 Jan2017 Apr2017 Jul2017 Oct2017 Jan2018
Frequency
Dominant wavelength (nm)
Purity
FU Index
x
y

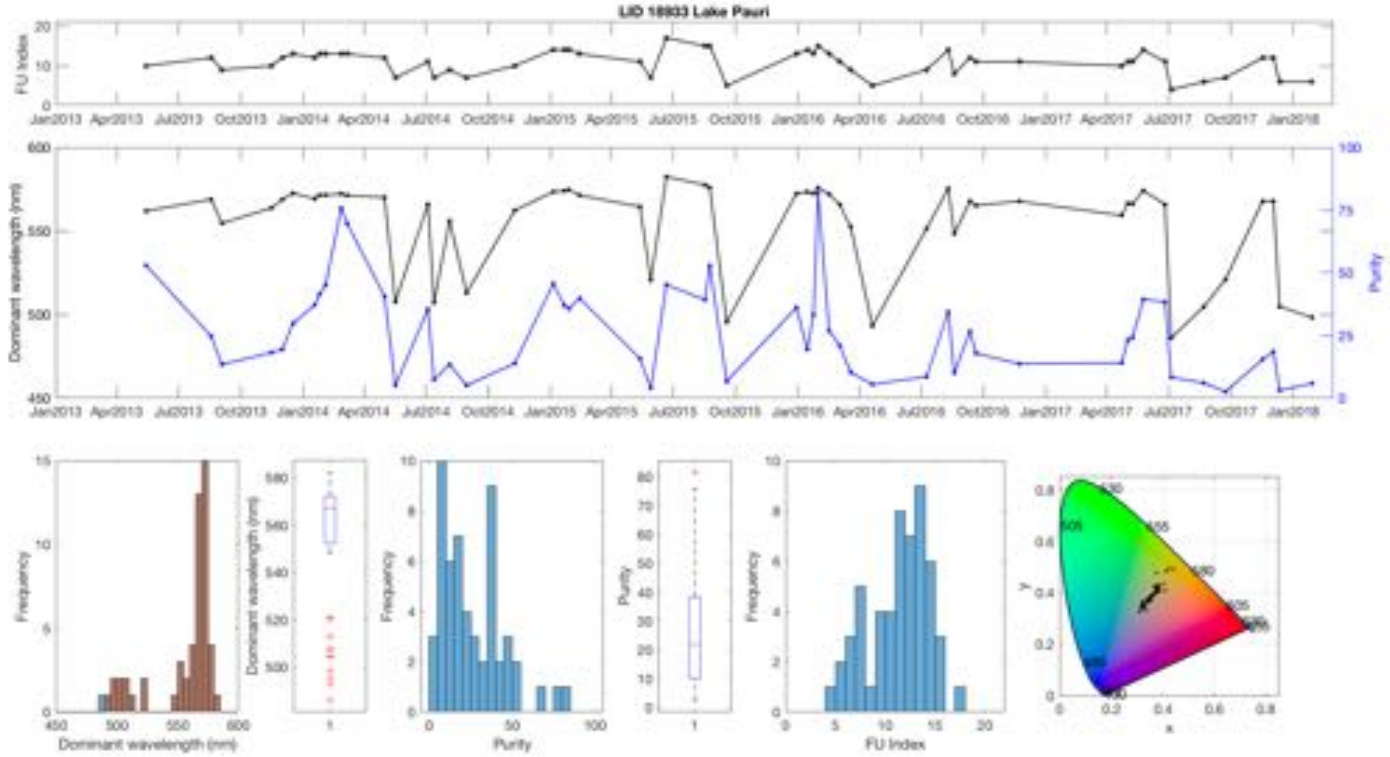
LID 18933 Lake Pauri
FU Index
Dominant wavelength (nm)
Purity
Frequency
Dominant wavelength (nm)
Purity
FU Index
x
y

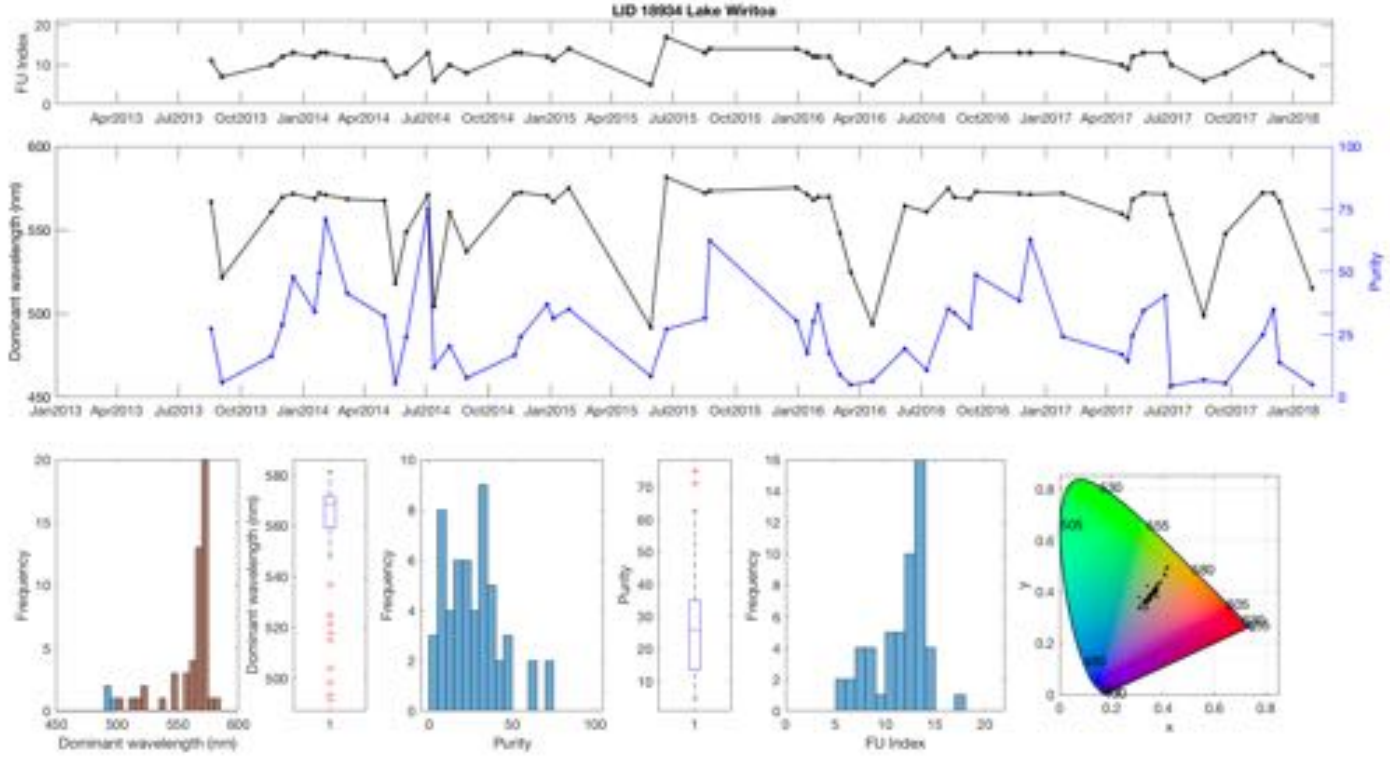
LID 18934 Lake Wiritoa
FU Index
Dominant wavelength (nm)
Purity
Frequency
Dominant wavelength (nm)
Purity
FU Index
x
y

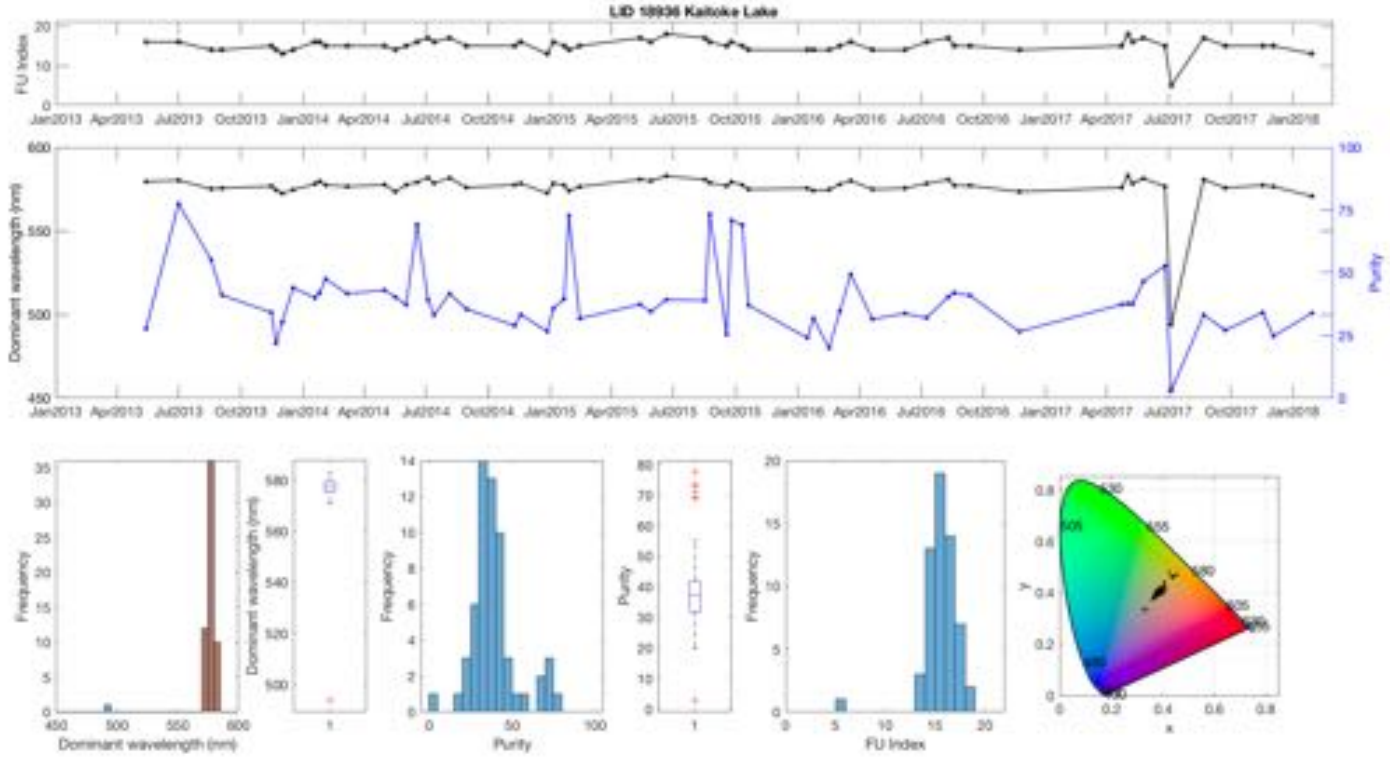
LID 10936 Kaitoke Lake
FU Index
Dominant wavelength (nm)
Purity
Jan2013 Apr2013 Jul2013 Oct2013 Jan2014 Apr2014 Jul2014 Oct2014 Jan2015 Apr2015 Jul2015 Oct2015 Jan2016 Apr2016 Jul2016 Oct2016 Jan2017 Apr2017 Jul2017 Oct2017 Jan2018
Frequency
Dominant wavelength (nm)
Purity
FU Index
x
y

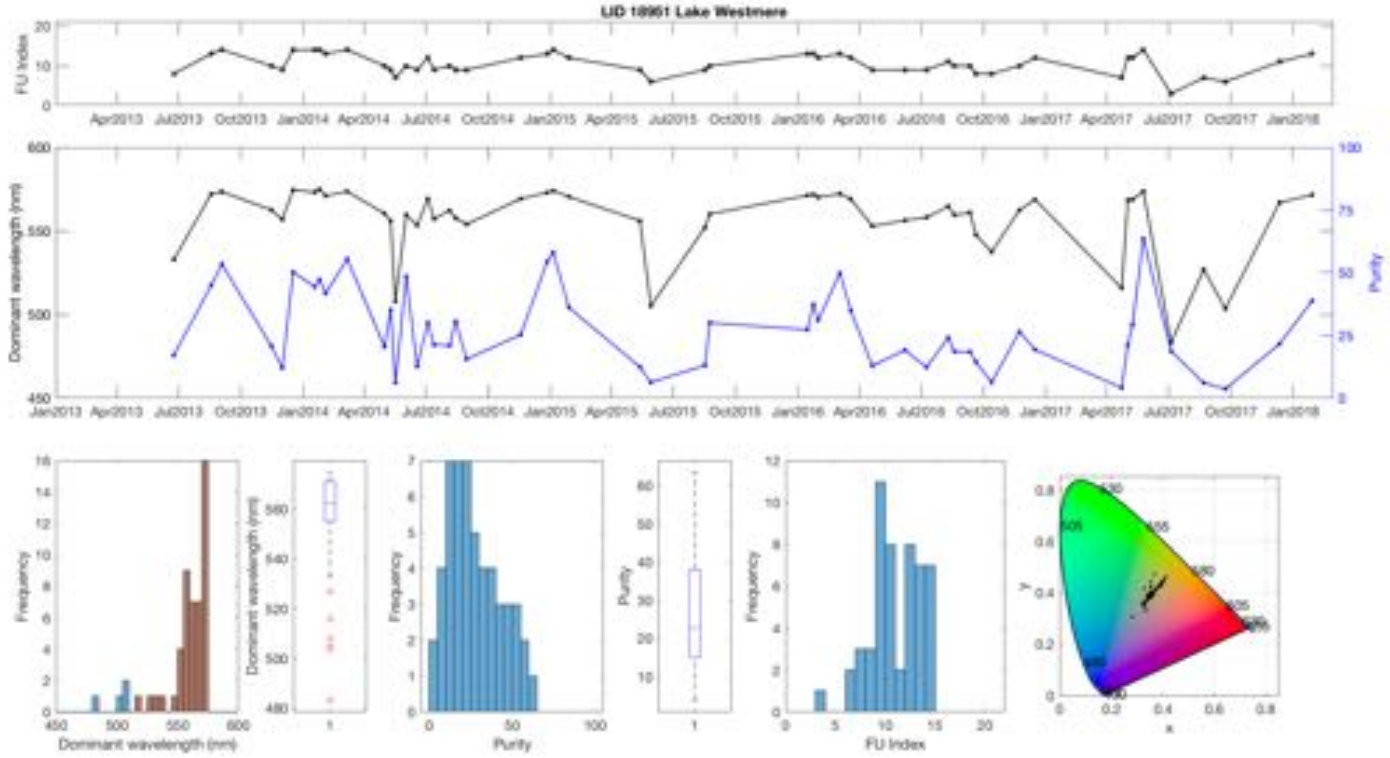
LID 10951 Lake Westmere
FU Index
Dominant wavelength (nm)
Purity
Apr2013 Jul2013 Oct2013 Jan2014 Apr2014 Jul2014 Oct2014 Jan2015 Apr2015 Jul2015 Oct2015 Jan2016 Apr2016 Jul2016 Oct2016 Jan2017 Apr2017 Jul2017 Oct2017 Jan2018
Frequency
Dominant wavelength (nm)
Purity
FU Index
x
y

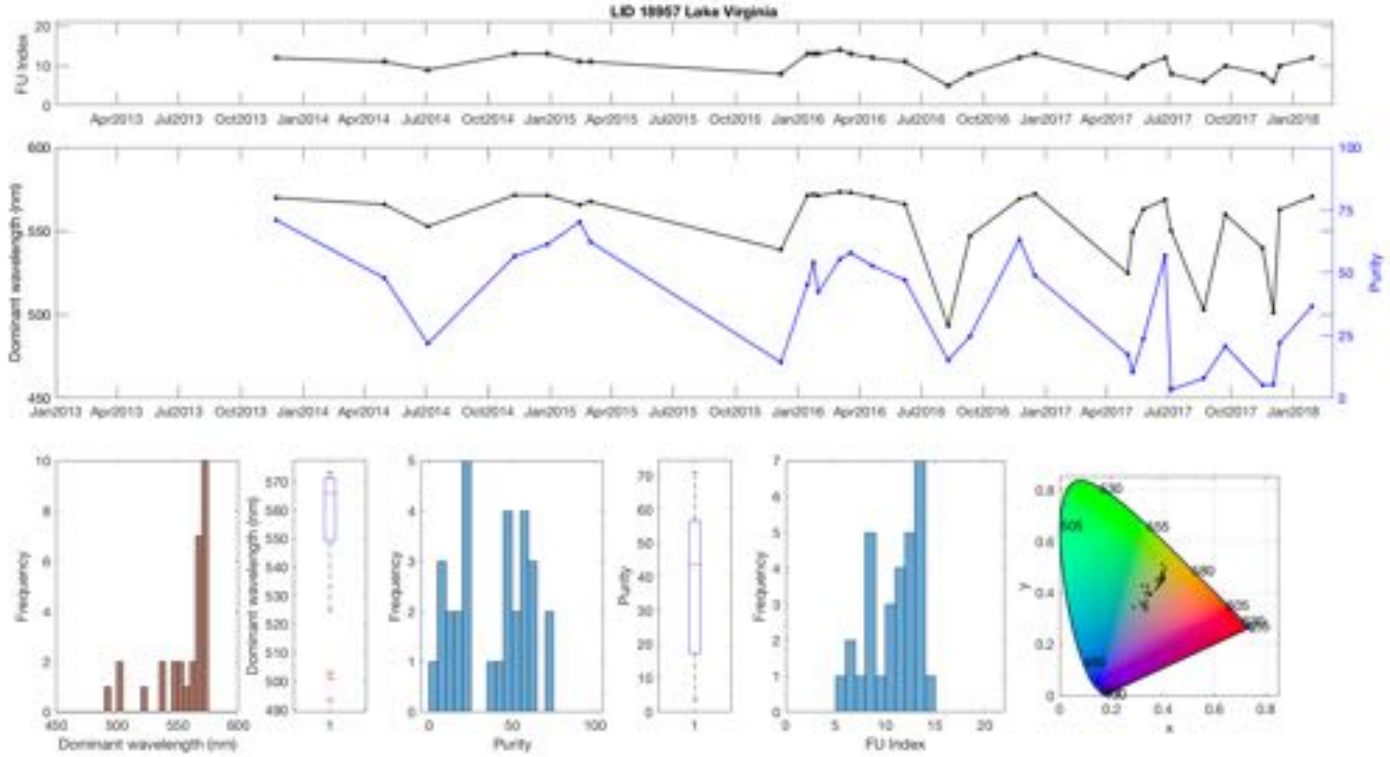
LID 19957 Lake Virginia
FU Index
Dominant wavelength (nm)
Purity
Frequency
Dominant wavelength (nm)
Frequency
Purity
Frequency
FU Index
y
x

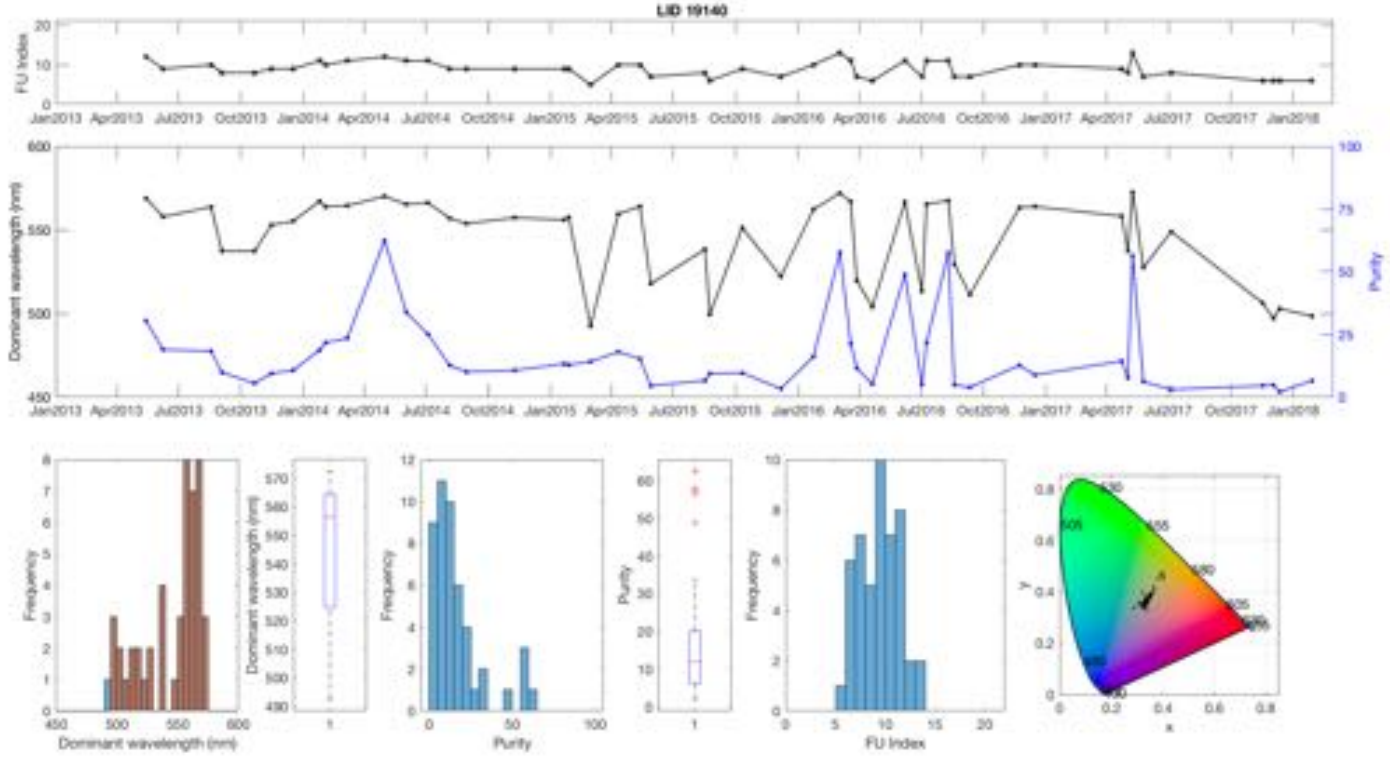
LID 19140
FU Index
Dominant wavelength (nm)
Purity
Frequency
Dominant wavelength (nm)
Frequency
Purity
Frequency
FU Index
y
x

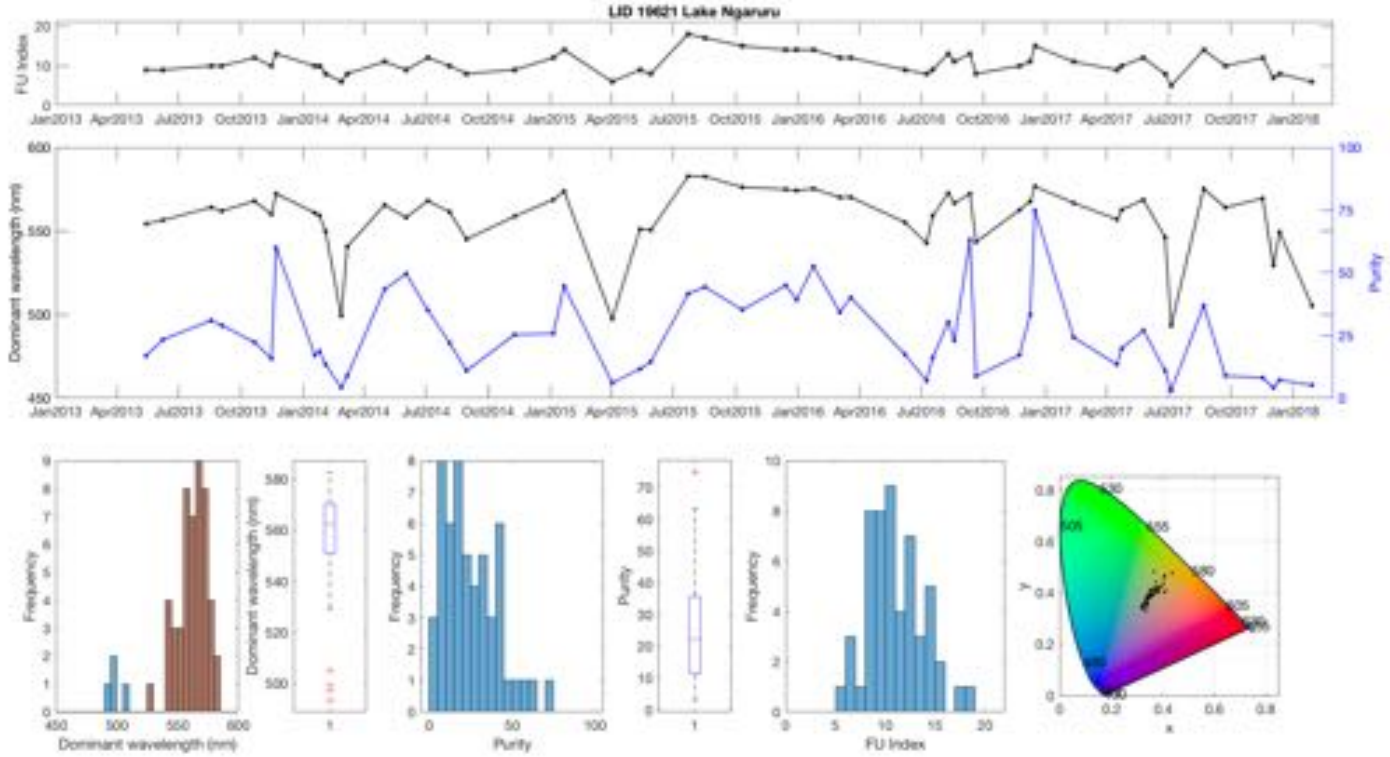
LID 19621 Lake Ngaruru
FU Index
Dominant wavelength (nm)
Purity
Frequency
Dominant wavelength (nm)
Frequency
Purity
Purity
Frequency
FU Index
y
x

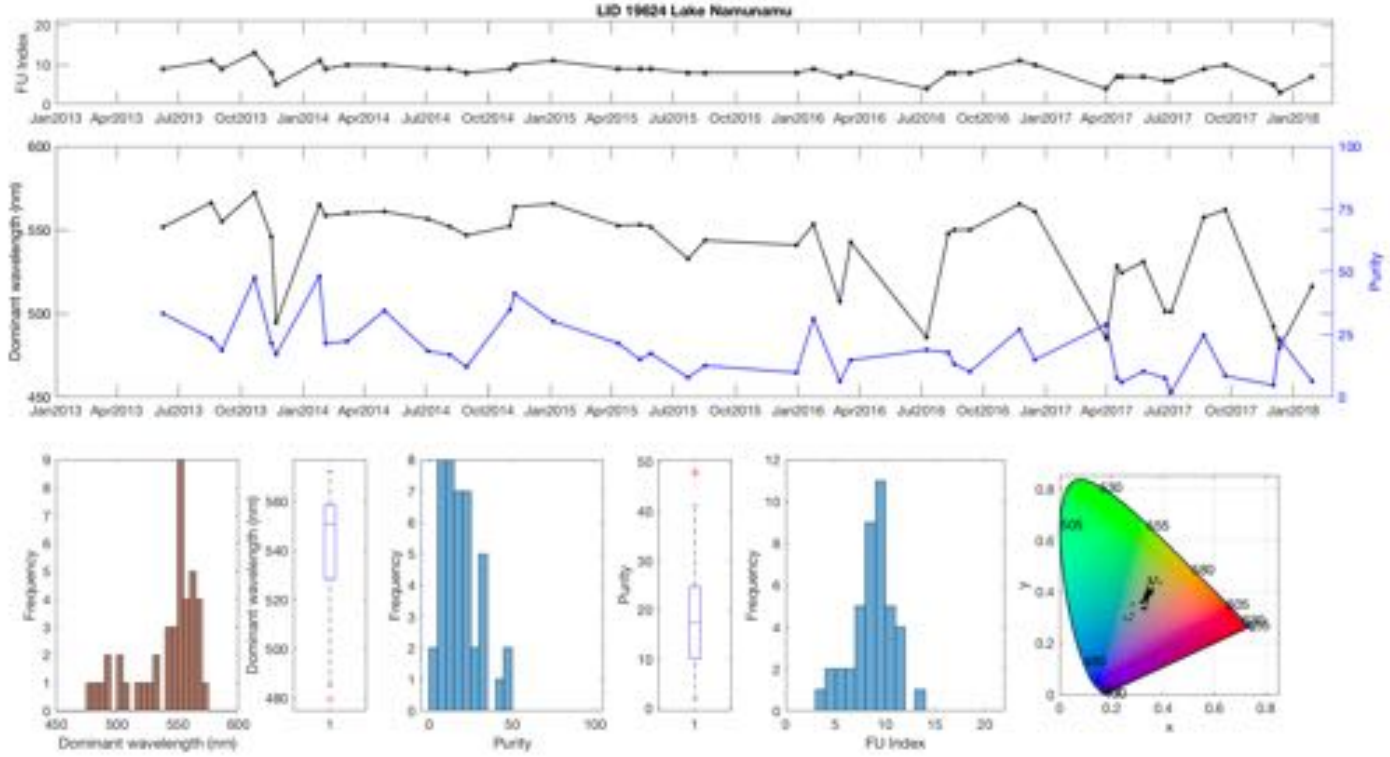
LID 19624 Lake Namunamu
FU Index
Dominant wavelength (nm)
Purity
Frequency
Dominant wavelength (nm)
Frequency
Purity
Purity
Frequency
FU Index
y
x

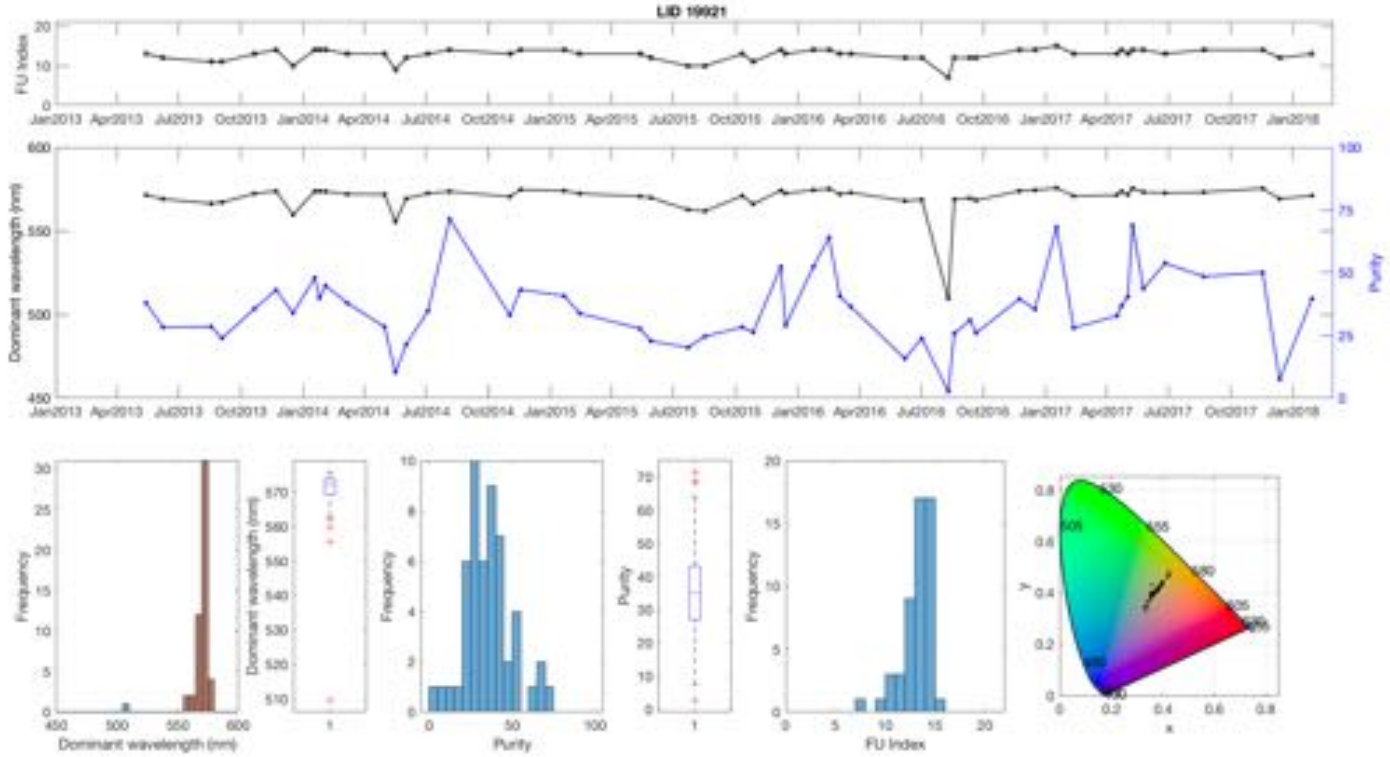
LID 19921
FU Index
Dominant wavelength (nm)
Purity
Frequency
Dominant wavelength (nm)
Purity
Frequency
Purity
Frequency
FU Index
y
x

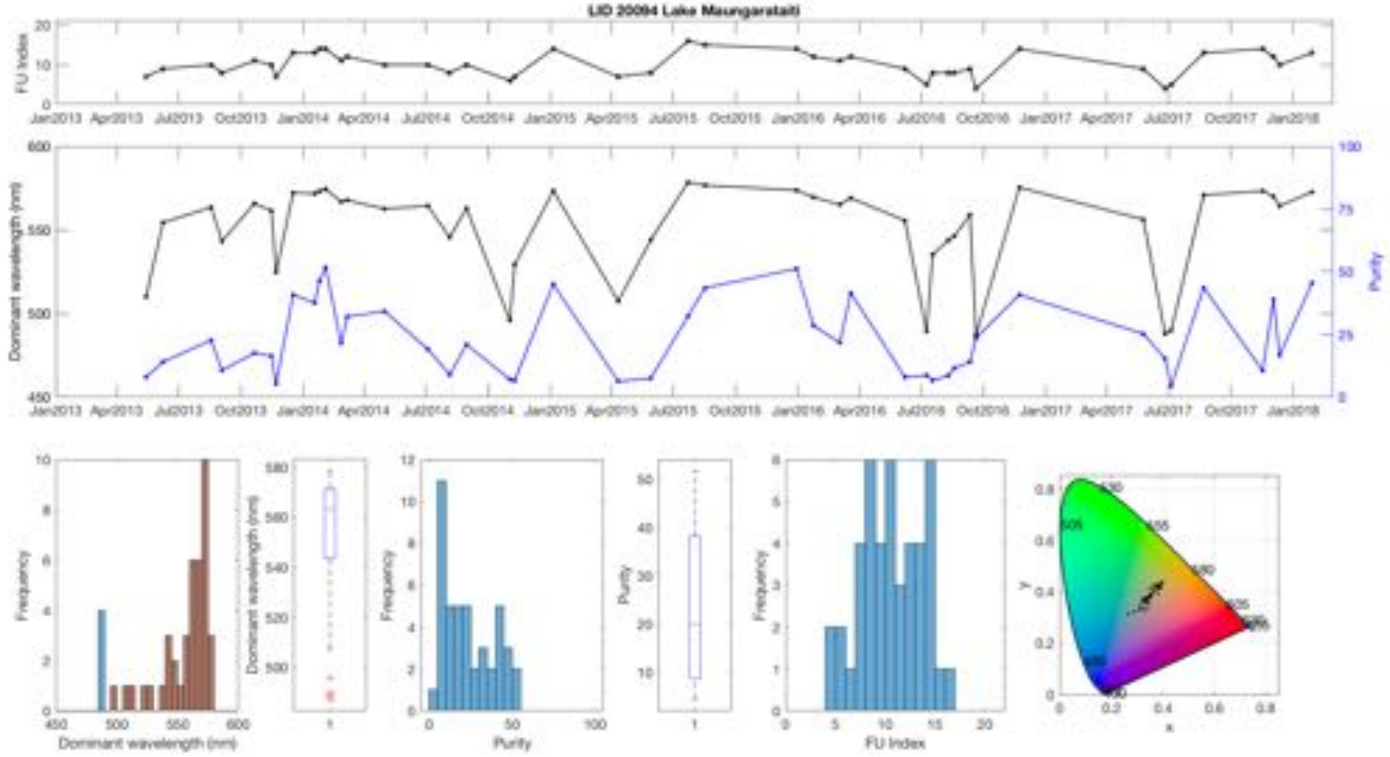
LID 20094 Lake Maungaratiti
FU Index
Dominant wavelength (nm)
Purity
Frequency
Dominant wavelength (nm)
Purity
Frequency
Purity
Frequency
FU Index
y
x

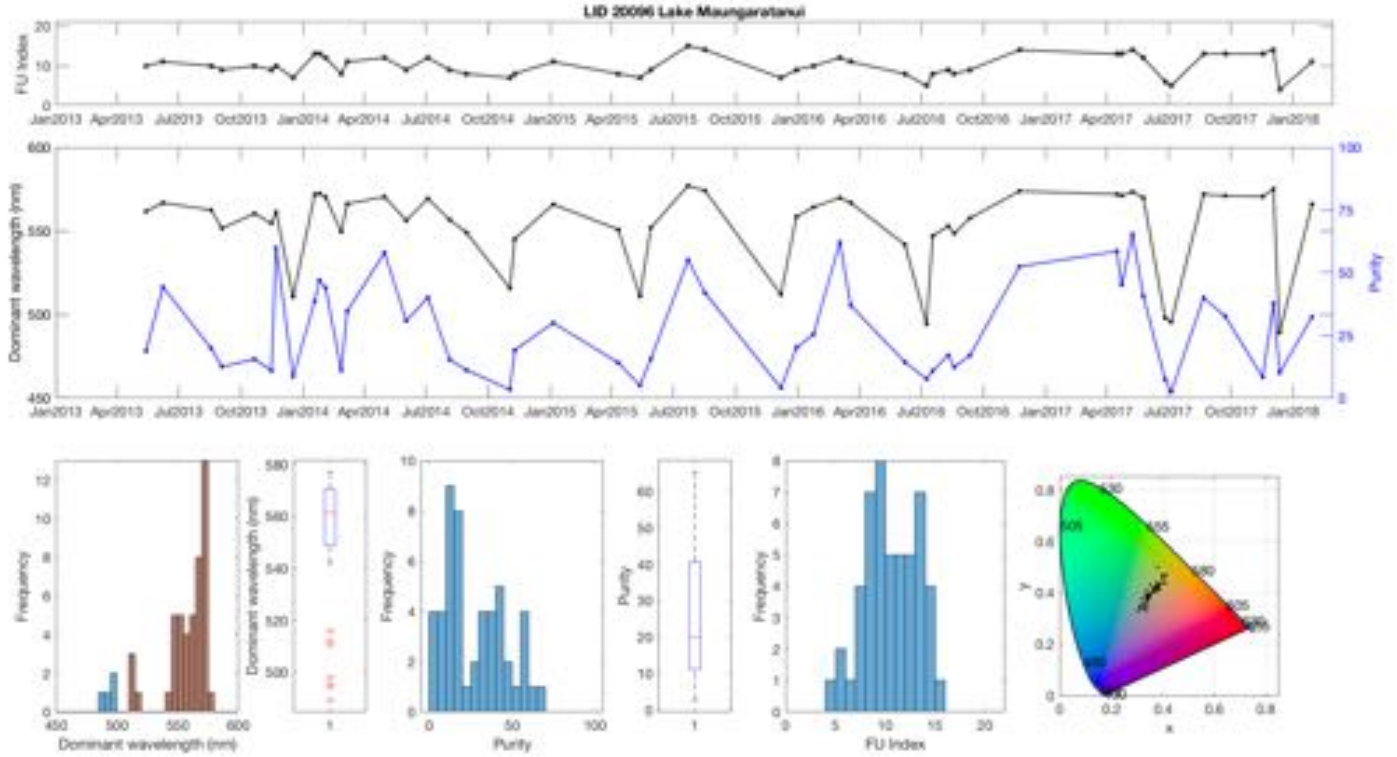
LID 20096 Lake Maungaratanui
FU Index
Dominant wavelength (nm)
Purity
Jan2013 Apr2013 Jul2013 Oct2013 Jan2014 Apr2014 Jul2014 Oct2014 Jan2015 Apr2015 Jul2015 Oct2015 Jan2016 Apr2016 Jul2016 Oct2016 Jan2017 Apr2017 Jul2017 Oct2017 Jan2018
Frequency
Dominant wavelength (nm)
Purity
FU Index
x
y

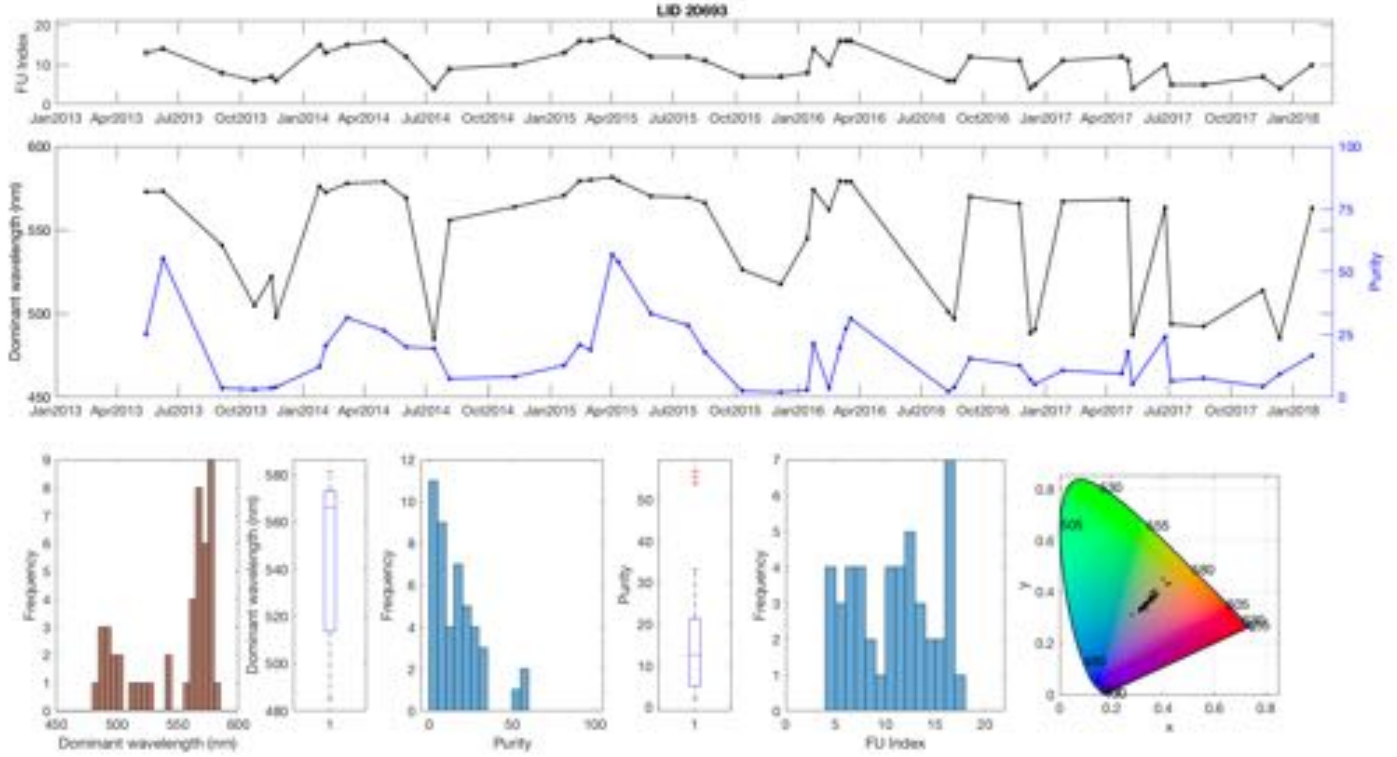
LID 20693
FU Index
Dominant wavelength (nm)
Purity
Jan2013 Apr2013 Jul2013 Oct2013 Jan2014 Apr2014 Jul2014 Oct2014 Jan2015 Apr2015 Jul2015 Oct2015 Jan2016 Apr2016 Jul2016 Oct2016 Jan2017 Apr2017 Jul2017 Oct2017 Jan2018
Frequency
Dominant wavelength (nm)
Purity
FU Index
x
y

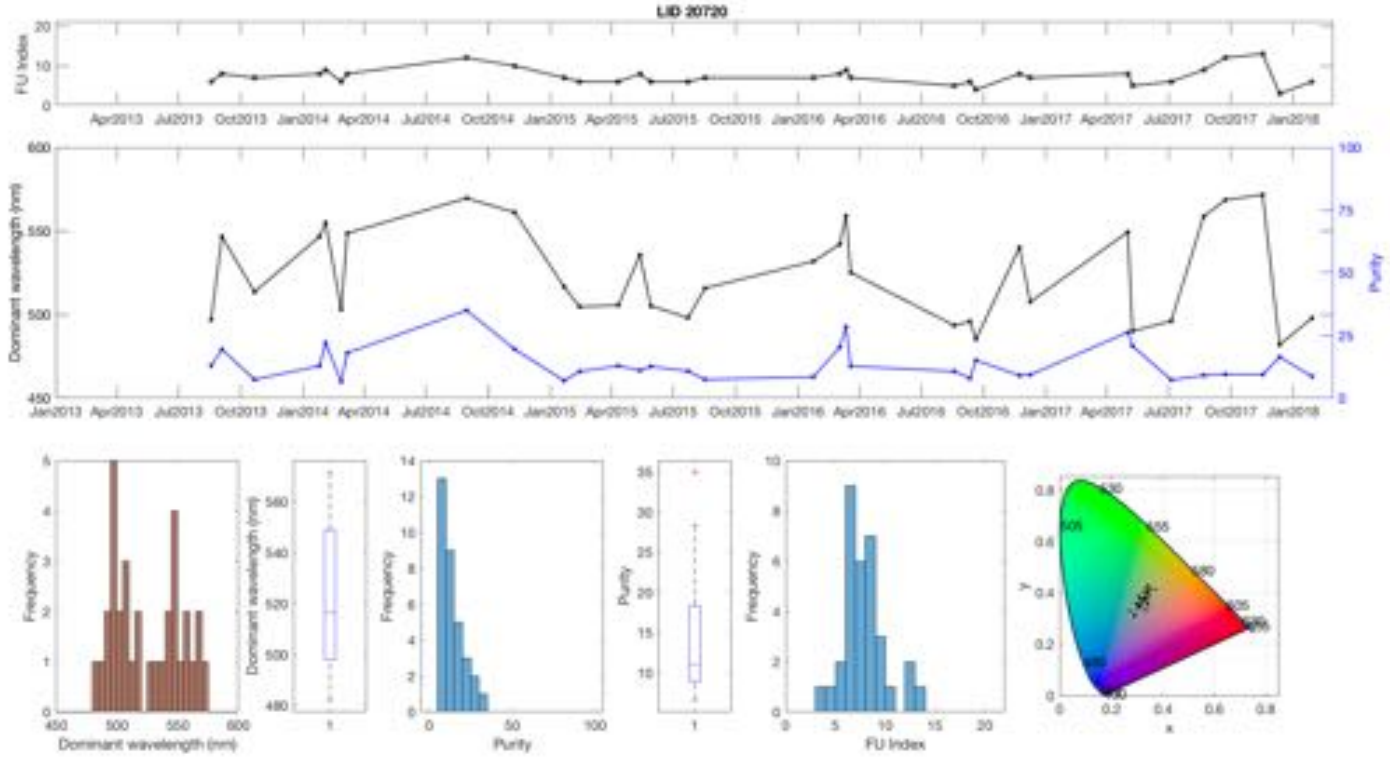
LID 20720
FU Index
Dominant wavelength (nm)
Purity
Frequency
Dominant wavelength (nm)
Purity
FU Index
x
y

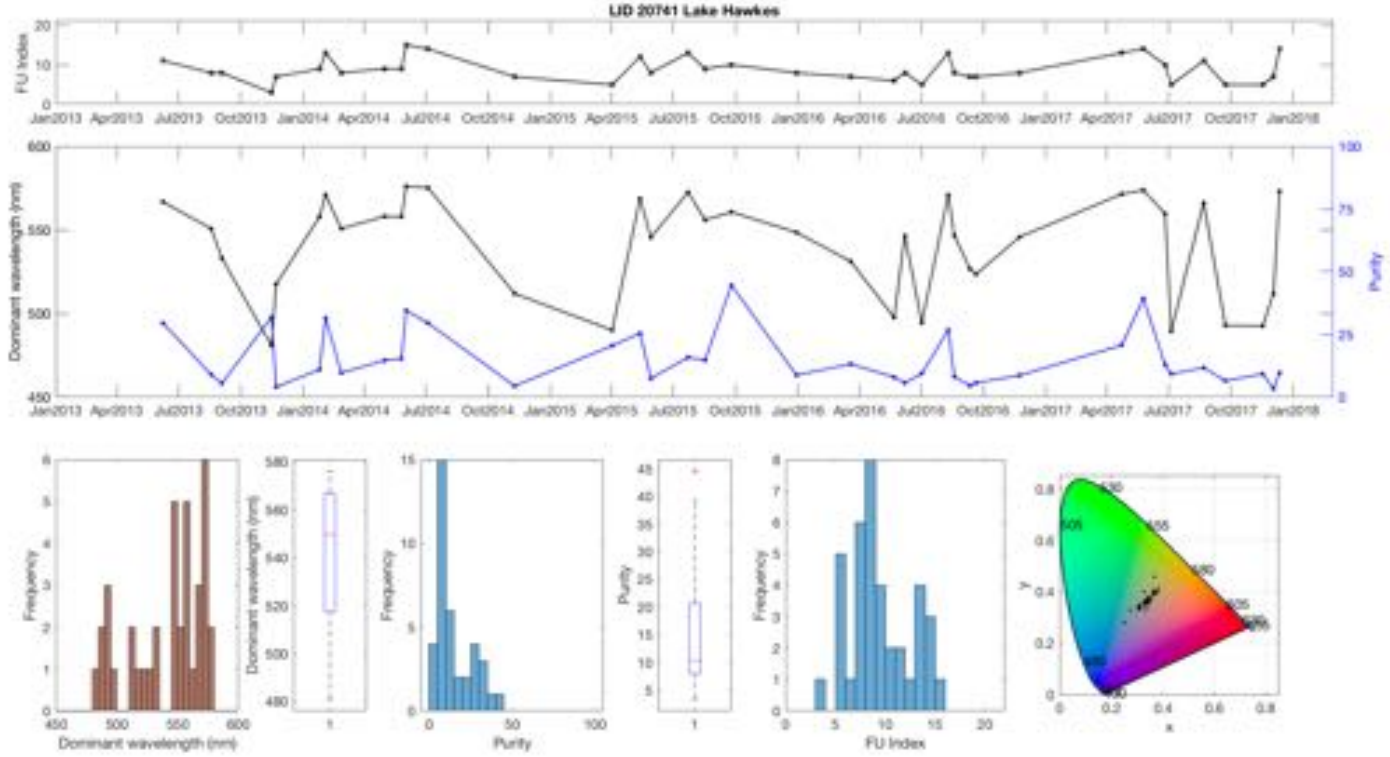
LID 20741 Lake Hawkes
FU Index
Dominant wavelength (nm)
Purity
Frequency
Dominant wavelength (nm)
Purity
FU Index
x
y

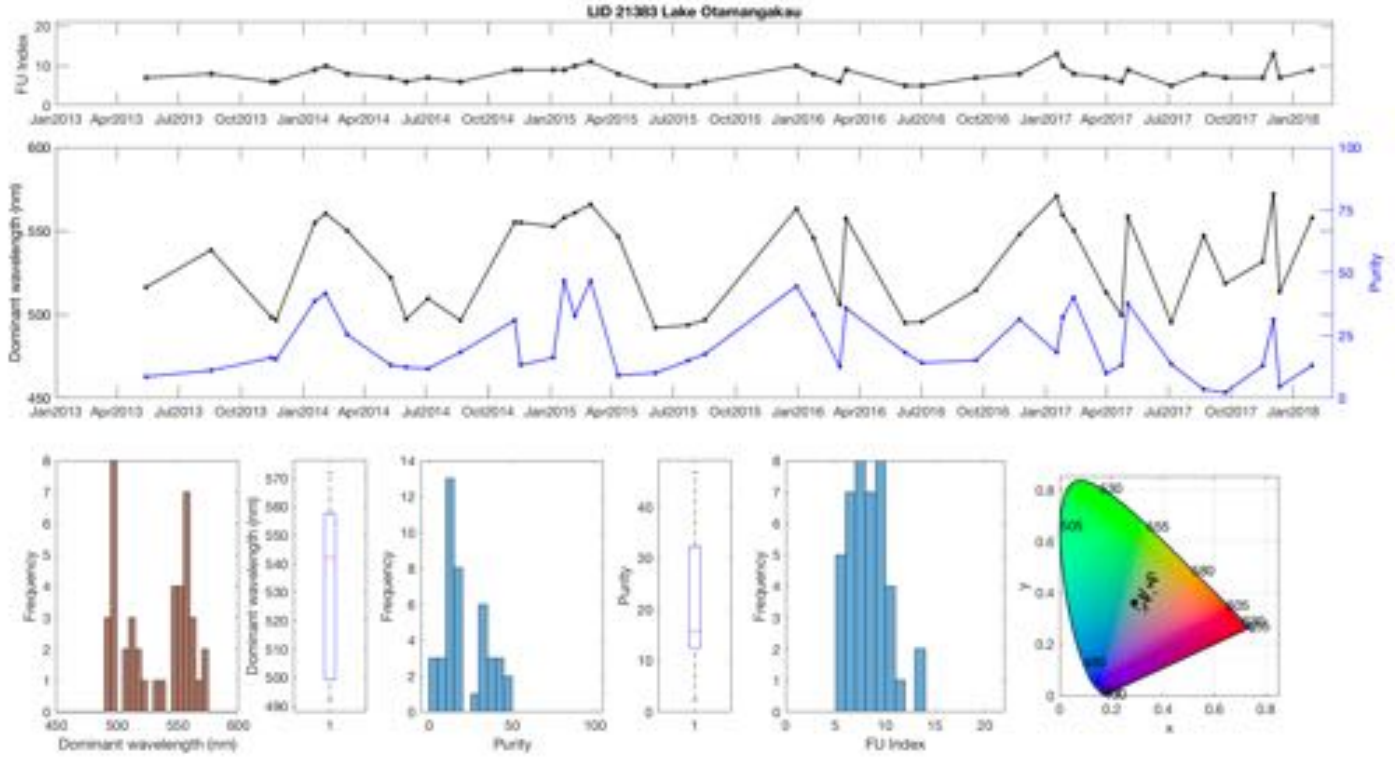
LID 21383 Lake Otamangakau
FU Index
Dominant wavelength (nm)
Purity
Frequency
Dominant wavelength (nm)
Purity
Frequency
Purity
Frequency
FU Index
y
x

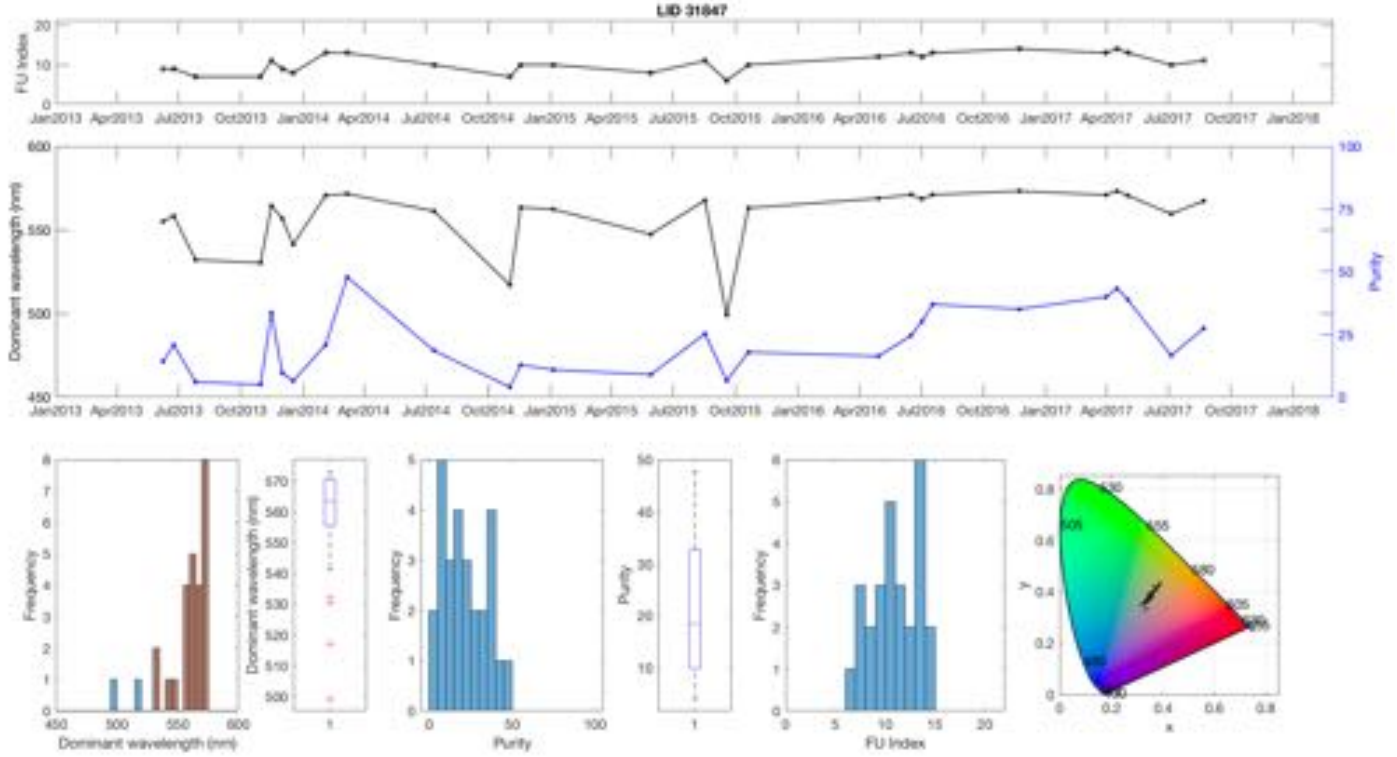
LID 31847
FU Index
Dominant wavelength (nm)
Purity
Frequency
Dominant wavelength (nm)
Purity
Frequency
Purity
Frequency
FU Index
y
x

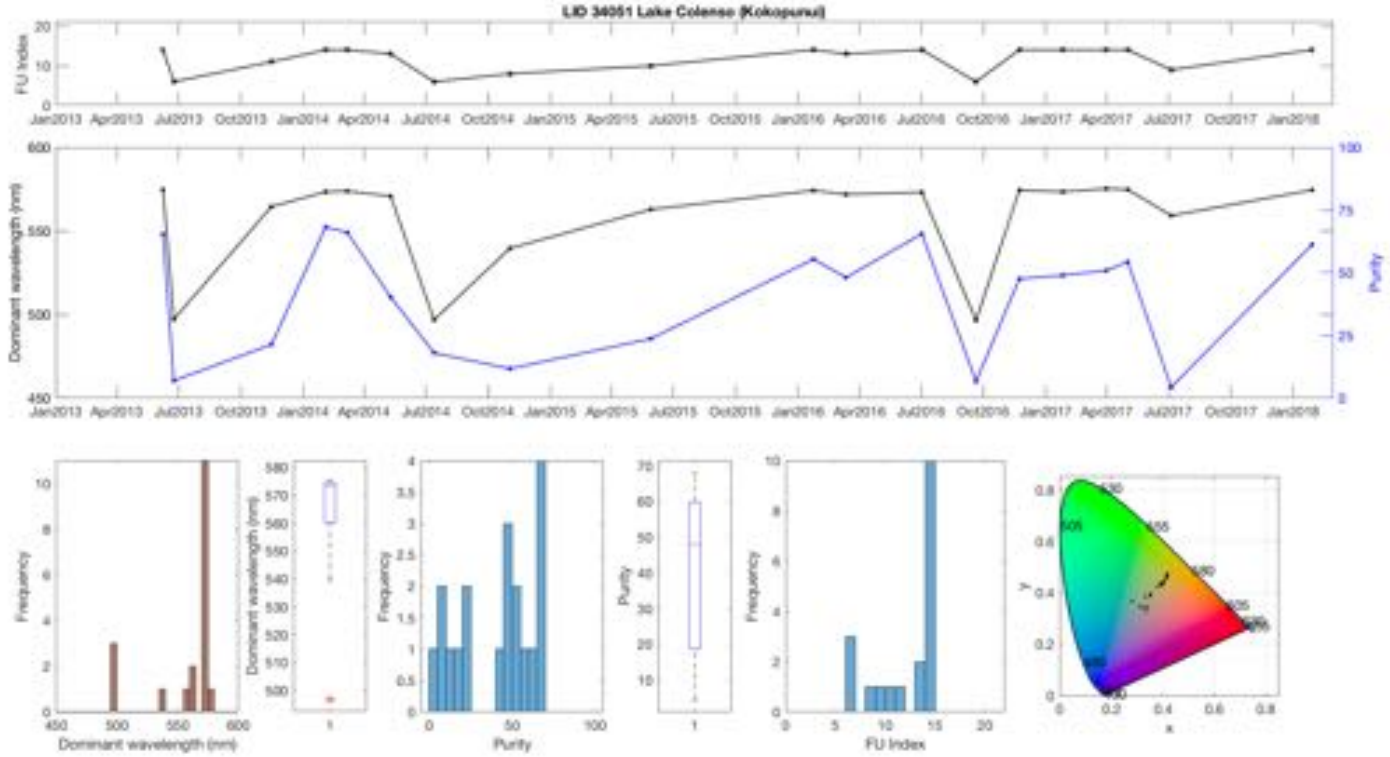
LID 34051 Lake Colenso (Kokopunui)
FU Index
Dominant wavelength (nm)
Purity
Jan2013 Apr2013 Jul2013 Oct2013 Jan2014 Apr2014 Jul2014 Oct2014 Jan2015 Apr2015 Jul2015 Oct2015 Jan2016 Apr2016 Jul2016 Oct2016 Jan2017 Apr2017 Jul2017 Oct2017 Jan2018


Frequency
Dominant wavelength (nm)
Purity
FU Index
x
y